ANALYSIS OF BATTERY THERMAL MANAGEMENT SYSTEM BASED ON FLAT HEAT PIPE FOR LI-ION BATTERY OF ELECTRIC VEHICLES

Thesis Submitted for the Award of the Degree of

DOCTOR OF PHILOSOPHY

in

Mechanical Engineering

By
Manmeet Singh

Registration Number: 42000378

Supervised By
Dr. Sudhanshu Dogra (16900)
Mechanical Engineering (Associate Professor)
Lovely Professional University, Phagwara

LOVELY PROFESSIONAL UNIVERSITY, PUNJAB
2025

DECLARATION

I hereby declared that the presented work in the thesis entitled "Analysis of battery thermal management system based on flat heat pipe for Li-ion battery of electric vehicles" in fulfilment of degree of **Doctor of Philosophy (Ph. D.)** is outcome of research work carried out by me under the supervision of Dr. Sudhanshu Dogra, working as Associate Professor, in the School of Mechanical Engineering of Lovely Professional University, Punjab, India. In keeping with general practice of reporting scientific observations, due acknowledgements have been made whenever work described here has been based on findings of other investigator. This work has not been submitted in part or full to any other University or Institute for the award of any degree.

(Signature of Scholar)

Name of the scholar: Manmeet Singh

Registration No.: 42000378

Department/school: Mechanical Engineering

Lovely Professional University,

Punjab, India

CERTIFICATE

This is to certify that the work reported in the Ph. D. thesis entitled "Analysis of battery thermal management system based on flat heat pipe for Li-ion battery of electric vehicles" submitted in fulfillment of the requirement for the award of degree of **Doctor of Philosophy (Ph.D.)** in the School of Mechanical Engineering, is a research work carried out by Manmeet Singh, 42000378, is bonafide record of his/her original work carried out under my supervision and that no part of thesis has been submitted for any other degree, diploma or equivalent course.

(Signature of Supervisor)

Name of supervisor: Dr. Sudhanshu Dogra

Designation: Associate Professor

Department/school: Mechanical Engineering

University: Lovely Professional University

Abstract

Electrical vehicles (EVs) are emerging as a suitable replacement for conventional IC engine-based automobiles because of their environmental friendliness. An EV is powered by a rechargeable battery pack usually made of Lithium-ion batteries. A battery plays an important role in running electrical vehicles as they store energy during charging period and discharge energy at various C-rates as per requirement of electrical vehicle. For energy storage and release, electrochemical reactions occur inside a battery cell. The electrochemical reactions which occur during the operation cycle results in exothermic reactions and ohmic effect, which further results heat generation inside the battery cells. The heat generated if not removed and extracted out of the system, accumulates inside the cell thereby increasing cell temperature. Excessive heat accumulation inside battery pack can increase battery temperature to such an extent where they can swell, explode, and become hazardous to an EV user and environment. A Li-ion battery cell works better and efficiently in optimum range of temperature between 40ºC to 50ºC. A higher or lower temperature variations from this optimum range can degrade cells beyond repair and reduces their energy storage and conversion efficiency which may further led to failure of cells, electrolyte leakage, release of hazardous gases and explosions. Other than peak temperature, temperature uniformity or homogeneity is also an important factor which affect overall life of battery pack. Non-uniformity of temperature led to some cells being at higher temperature than others which may results in earlier failure and reduced life span of these cells which negatively affect overall operational life cycle of battery pack. The temperature non-uniformity within a battery pack should be ideally limited to 5ºC and acceptable limit may be 7 or 8ºC. The thermal management of batteries is important for their safe operation and optimum lifespan. A battery thermal management system (BTMS) is an essential component of electrical vehicle, and its main function is to control operating temperature of battery cells within ideal operational limits. It should perform two main functions: regulate maximum and minimum temperature within battery pack and maintain temperature uniformity inside the battery pack. It should also allow the pack to work under a good range of climatic conditions and supply ventilation for hazardous gases generated inside battery pack. The operation cycle of battery pack consists of charge and discharge processes. The present research focusses on thermal management of battery pack during discharge process. In present research work, a comparative analysis of temperature homogeneity (uniformity), peak temperature and average temperature of battery pack is conducted for free convection

based BTMS, forced convection based BTMS and heat pipe-based hybrid BTMS. In a battery pack, the cells that are at higher temperature than average temperature of battery pack are more liable to fail earlier as compared to other cells of pack. Present research focuses on finding such critical cells in a battery pack consisting of twelve lithium-ion batteries. Four different type of battery packs consisting of twelve li-ion cells were fabricated for present research: (1) battery pack for free convection with 2 mm interspacing between cells, (2) battery pack for forced convection with 2 mm interspacing between cells, (3) battery pack for forced convection with 4 mm interspacing between cells and (4) battery pack with heat pipe insertions under forced convection with 2 mm interspacing between cells. The lithium-ion cells selected for present research work are Lithium Iron Phosphate cylindrical battery cells. These cells are popularly called 32650 LFP battery cells and they are bigger in size and have higher capacity as compared to conventional 18650 li-ion cells which are popular in Electrical vehicles. High energy density and higher capacity battery cells are an essential requirement of EVs as these factors directly affect driving range of an EV. Li-ion cells come in various shapes and configurations like cylindrical, pouch, prismatic etc. but cylindrical cells are more popular due to their compactness and energy density. An experimental testing facility was developed to test battery thermal management systems at various discharge rates, air inlet velocity and interspacing between cells. The testing facility mainly consists of battery pack, thermocouples, data logger and battery tester. The temperature of each cell is measured at regular intervals during the discharge process by thermocouples installed at various critical locations inside battery pack. The thermocouples fed data to data logger and recorded data from data logger is extracted for analysis of temperature variations inside battery pack. The battery tester selected for present research can charge and discharge battery between 9V to 99 V under varies C-rates setting by varying voltage and current settings. The first objective of present research is to analyse cooling performance of base case without heat pipe (woHP) BTMS. The free convection based BTMS and forced convection based BTMS are considered as base case BTMS-woHP and their performance analysis is conducted for better understanding their operational limits. These cooling systems are designated as without heat pipe (woHP) cooling systems. The free convection based BTMS (BTMS-FR) is tested under three discharge rates (1C,2C and 3C). The results indicate that temperature of battery cells reaches beyond 50ºC limit and although temperature uniformity is maintained with acceptable limit of 8ºC. The battery packs under forced convection are discharged under different combinations discharge rates (1C, 2C and 3C) and air inlet velocities (3.6 m/s, 4.6 m/s, 5.5 m/). The results showed that although peak temperature of cells is reduced in forced convection as compared to free convection but the

temperature non-uniformity within battery pack is increased due to non-uniform cooling pattern of forced convection. The second objective of research work explores if cooling performance in forced convection (BTMS-FO) can be improved by increase interspacing between cells. The performance analysis showed that there no significant improvement any of the three performance parameters i.e. peak temperature, average temperature and temperature uniformity, by increasing interspacing from 2 mm to 4 mm. The variations in temperature of battery cells across battery pack is mainly due to air flow pattern, shape of battery cells, battery pack design and in certain cases inherent disadvantage of BTMS systems, for example: Inherent disadvantage of air and liquid cooling is rise of temperature of coolant when it flows from inlet to outlet. Maintaining temperature homogeneity and restricting peak temperature within ideal range is a challenge. In present research work, the third objective is focussed on development and analysis of novel heat pipe based forced cooling system to overcome limitations of conventional cooling systems. The battery pack of hybrid system is fabricated with flat heat pipe insertions inside the rows of cells within the battery pack. The condenser section of flat heat pipes is inserted inside battery module and evaporator section is cooled by forced air cooling. Fine powder of Silicon Carbide (SiC) is utilized as interface or interspacing filler between each cylindrical surface of battery cell and flat surface of heat pipe. Silicon Carbide is utilized to improve thermal conductivity between cell and flat heat pipe as it increases the contact area and thermal conductivity between battery cell and heat pipe The performance parameters i.e. temperature homogeneity, average temperature of battery pack and peak temperature of cells, is measured while discharging the battery pack at varying discharge rates and air inlet velocity. A comparative analysis of hybrid heat pipe based BTMS is conducted respect to conventional free and forced air cooled battery thermal management system (BTMS-FR and BTMS-FO). The results indicated that Hybrid thermal management system with heat pipe (BTMS-HY) is better in maintaining temperature homogeneity and peak temperature within critical limits. The BTMS-HY can be combined with liquid cooling to increase its cooling performance as heat transfer rate would be higher in liquid as compared to air. The present research work presents a novel design of BTMS based on flat heat pipe. Although performance analysis is conducted and analysis showed that heat pipe based system is better as compared to conventional free and forced convection based system but still analysis in terms of vehicle efficiency, weight and overall performance can be taken as future work. Further improvement in design such as increasing surface area of heat pipe with extended surfaces, better interspacing fillers, improved fan placement may enhance and refine the heat pipe system, and this research work can be taken as future work.

Acknowledgement

I am truly grateful and deeply humbled as I express my heartfelt thanks to all who supported me during my doctoral research at Lovely Professional University, Phagwara. This journey would not have been possible without the encouragement, guidance, and contributions of many individuals.

First and foremost, I extend my sincere gratitude to my supervisor, Dr. Sudhanshu Dogra (Department of Mechanical Engineering, Lovely Professional University, Phagwara, India), for his invaluable guidance, constructive feedback, and continuous motivation throughout this research. His unwavering support and insightful discussions were instrumental in shaping this thesis. I am also deeply thankful to Dr. Ravindra D. Jilte (Associate Professor, Department of Mechanical Engineering, Maulana Azad National Institute of Technology, Bhopal, India), whose mentorship in the early stages of my work provided the inspiration and confidence to embark on this academic journey.

I sincerely acknowledge the contributions of the Doctoral Research End Term Evaluation Committee for their invaluable input and guidance. My heartfelt thanks also go to all the faculty members of the Department of Mechanical Engineering, Lovely Professional University, for their support and encouragement at various stages of my research.

I am especially grateful to Shri Harideesh Kumar B (Director and Executive Head, Institute of Banking Personnel Selection, Mumbai) and Prof. Vipin K. Chilan (Senior Professor & Advisor, Institute of Banking Personnel Selection, Mumbai) for their continuous encouragement and support throughout my academic pursuit. I also extend my thanks to my Heads of Department, Ms. Ayesha Martin and Dr. Dipika Khurana, along with the entire departmental staff, for their motivation and assistance in bringing this journey to fruition. I remain thankful to my organization, the Institute of Banking Personnel Selection, for fostering a research-oriented environment that inspired me to undertake and complete this work.

My deepest gratitude goes to my beloved parents, Smt. Gurmail Kaur and Sh. Amrik Singh, my wife Jyoti Singh, and my brother Sumit Singh, whose love, support, and sacrifices have been my greatest strength. Their constant encouragement has been the foundation of my perseverance and success.

I also extend my heartfelt thanks to my friends and well-wishers, who, though not mentioned individually, have always supported and motivated me. Above all, I bow in gratitude to the Almighty God, whose blessings and guidance have been with me throughout every phase of this journey.

Finally, I thank each and every individual who has directly or indirectly contributed to the successful completion of this research.

(Manmeet Singh)

Table of Contents:

List of Tables:

List of Figures:

List of Appendices

Abbreviations:

EVs	Electrical vehicles
IC	Internal combustion engines
HEV	Hybrid electric vehicles
BEV	Battery Operated Vehicles
PHEVs	Plug-in Hybrid Electrical Vehicles
LFP	Lithium Iron Phosphate
LMO	Lithium Manganese Oxide
LTO	Lithium Titanate
LCO	Lithium Cobalt Oxide
NCA	Lithium Nickel Cobalt Aluminium
NMC	Lithium Nickel Manganese Cobalt
SOC	State of charge
BTMS	Battery thermal management system
PCM	Phase change material
TEG	Thermoelectric generators
TEC	Thermoelectric coolers
CFD	Computational fluid dynamics
woHP	Without heat pipe
BTMS-FR	Battery thermal management system based on free convection
BTMS-FO	Battery thermal management system based on forced convection
BTMS-HP	Hybrid battery thermal management system with heat pipe insertions
PT	Threshold limits of Peak temperature
TU	Threshold limits of Temperature uniformity

Symbols:

T_{max}	Peak or maximum temperature of cells
T_{avg}	Average temperature of battery pack
T_{∞}	Ambient temperature of air
T_i	Inlet air temperature (forced convection)
T_e	Outlet air temperature (forced convection)
T_f	Film temperature of air
T	Temperature
T_m	Arithmetic mean temperature of fluid
$T_{s,avg}$	Average surface temperature of cells
T_s	Surface temperature of cell
ΔT	Temperature uniformity (battery pack)
ΔT_{lm}	Logarithmic mean temperature difference
I	Current
V	Voltage
E	Open circuit voltage
R_i	Internal equivalent resistance of cell
R_p	Resistance of positive collector (cell)
R_n	Resistance of negative collector (cell)
I_p	Current values at positive collector (cell)
I_n	Current value at negative collector (cell)
Q_r	Reversible heat loss
Q_i	Irreversible heat loss
Q_t	Total heat loss

Q_{tg}	Total heat generation
Q_u	Unsteady heat generation
Q_{conv}	Convective heat transfer rate
Re	Reynolds number
Gr	Grashoff number
Ra	Rayleigh number
Pr	Prandtl number
h	Heat transfer coefficient
A_s	Curved surface area of cells
A_f	Cross-sectional area of fan
D	Diameter of cells
L_c	Characteristic length
Ve	Air velocity
m_f	Mass flow rate of air
Nu	Nusselt number
S_T	Transverse pitch between cells in the battery pack
S_L	Longitudinal pitch between cells in the battery pack
k	Thermal conductivity of air
ρ	Density of air
g	Acceleration due to gravity
β	Coefficient of volume expansion
ξ	Curvature parameter of cylindrical cells
ν	Kinematic viscosity of air

Chapter 1 Introduction

The electric powered vehicle (EVs) market is steadily growing over the last decade. In recent years, many innovative technologies were developed and introduced in the automobile market which has revolutionized the electrical vehicle market. The shift of automobile industry to environmentally friendly technologies like electrical power trains, hydrogen driven vehicles, biofuels, regenerative technologies is due to rise in interest and demand of consumers for environment friendly vehicles. The high and fluctuating cost of fossil fuels apart from environment concerns are also major contributors to rise in demand of electrical powertrain-based vehicle as an alternative to conventional internal combustion (IC) engine vehicles. Both environment and economic factors are pushing government of various nations to establish guiding policies for more environment responsible technologies to reduce deterioration of environment. One of the major contributors in the total emissions of greenhouse gases and related environmental effects like climate change and global warming are passenger and transport vehicles. The number of vehicles worldwide is increasing at a rapid rate and may reach about 2 billion by 2050 [1]. India is one of the emerging market and manufacturer of two-wheeler and four-wheeler vehicles. The India's transportation sector contributes about 14% of CO_2 emissions and this is likely to increase further as India's urban population is going to double by 2050 [2]. The transport sector is very crucial to growth and development of India's infrastructure and manufacturing sectors. The objective of achieving climate goals and sustainable growth can be achieved by adoption of low carbon emissions technology in transport sector. Electric vehicles present a better alternative to fossil fuel fired conventional IC engines as by their utilization we can shift emissions to electricity generation sector where they can be reduced effectively by using better technology and renewable energy. Adoption of electrical vehicles is still a challenging task to its acceptance as the ultimate automobile of the future. Some of the challenges that are critical to adoption of EVs at mass level are slow paced charging of electrical vehicles, safe working of battery cells, cost of manufacturing electrical vehicles and limited range of EVs. Hybrid electrical vehicles (HEV) have also gained popularity since they combine the advantages of both IC engines and battery-operated EVs. These hybrid vehicles are costlier, but they overcome the inherent anxiety of EV's small operational range. The development prospects of EVs are extremely high as they present various advantages: environment friendly, high efficiency, sustainable endurance and harmless[3], [4]. An EV consists of an electric motor powered by a module made up

electrochemical batteries. A battery module is nothing, but array of battery cells connected to produce desired output voltage, current, power, and other electrical characteristics. The discharge cycle of battery module run electrical vehicle and determine acceleration of EVs whereas during charging process energy is stored in the batteries. The charging time of batteries is critical factor affecting reliability and energy storage of electrical vehicle. At present, the refuelling of conventional IC engine fuel tanks takes less time as compared to charge time of EVs. The refuelling time (charging time) of EVs can be reduced by utilizing of high charge rates (C-rates) for EV's charging [5]. The charge and discharge rates at which a battery cell operate are limited by heat generated during electrochemical process of battery [6]. Due to extensive research and advancement in technology [5], [7], [8], [9], the battery materials and manufacturing technologies have improved over time, but still further improvements are required in EVs to be able to achieve higher charge and discharge rates without compromising safety. The charge and discharge rates of batteries are affected by battery cell material, configuration, manufacturing quality. One of the most popular types of battery cell configuration used for energy storage in EVs is Lithium-ion cells [7]. Lithium-ion batteries perform better as compared to other rechargeable batteries such as lead-acid, nickel metal hydride (NiMH) in terms of efficiency, energy density, discharge rates, operating cycles, and safety [10]. The battery cells come into varies shapes and sizes. Some of the popular ones are cylindrical, prismatic and pouch [11]. The performance of an EV depends upon the efficiency of their battery pack. Batteries are electrochemical cells which convert chemical energy to electrical energy and vice versa. The operating temperature of battery cells rises due to heat generated during operation cycle of cell. One of the major sources of heat accumulation in the battery cells is irreversible joule heating which is caused due to internal resistance of a cell [12]. Overheating of cells can cause thermal runaway and degradation of cells at elevated temperature which may led to electrolyte explosion and fire hazards [13], [14]. The effective operational temperature range of battery cells is the most prominent factor affecting performance of batteries and ideally it should be maintained between 20°C to 40°C [15], [16]. The temperature of battery cells across the battery module should be as homogenous as possible. The non-homogeneity of temperature in a battery module if any should be maintained within 5°C [15], [17]. The non-uniformity of temperature results in condition when some cells have higher temperature as compared to other cells and this promotes cell imbalance and unequal ageing of cells. These critical cells under high stress may fail earlier as compared to other cells. A battery thermal management system (BTMS) should maintain temperature of battery cells in the range of acceptable operational limits [18], [19]. A BTMS should be able to control the

temperature of the battery cells below upper operational limit when they are heated up during harsh summer conditions and in the same manner it should be able to heat up battery cells under harsh winter conditions. The main objective of present research is to understand performance parameters and limitations of conventional BTMS types and develop a thermal cooling method with utilization of heat pipes, which can overcome limitation, and enhance performance of conventional system. The coming subsections in this chapter provide details about electrical vehicles, battery cells, types of thermal management systems and objective of present research.

1.1. Electrical Vehicles

With increasing awareness about global warming and depletion of oil reserves, demand of electromobility vehicles has increased significantly in recent years. The first electric car was developed by Thomas Davenport in the year 1821 with non-rechargeable batteries. With the invention of rechargeable lead-acid batteries in the year 1860, there have been slow but steady improvement in storage technologies. In the year 2008, Tesla launched "Tesla Roadster" in US market. The "Tesla Roadster" was powered by series connected 6,187 laptop batteries [20]. The rising prices of fossil fuels, government policies and increased focus on sustainable environmentally friendly technologies have renewed the interest of transportation sector in electrical vehicles [21], [22]. The battery operated or electric powered vehicles as an alternative of IC engines have the potential to reduce emission of greenhouse gases as they can be driven by electricity generated from various non-fossil based energy sources like solar, wind, nuclear, hydro which are much cleaner as compared to fossil fuels. The electromobility as given in Figure 1.1 has various environment, technology and economic advantages over conventional fossil fuel based Internal combustion (IC) engines. These advantages of electrical vehicles make them favourable choice for cleaner future choice of mobility. Despite several advantages still electrical vehicle market has not taken over IC engines because of certain limitations: limited distance range of EVs, longer charge time, limited development of charging stations and safety issues with energy storage batteries. However, with advancement in technology, age of fossil fuels will diminish, and innovative technologies will revolutionize the automobile sector.

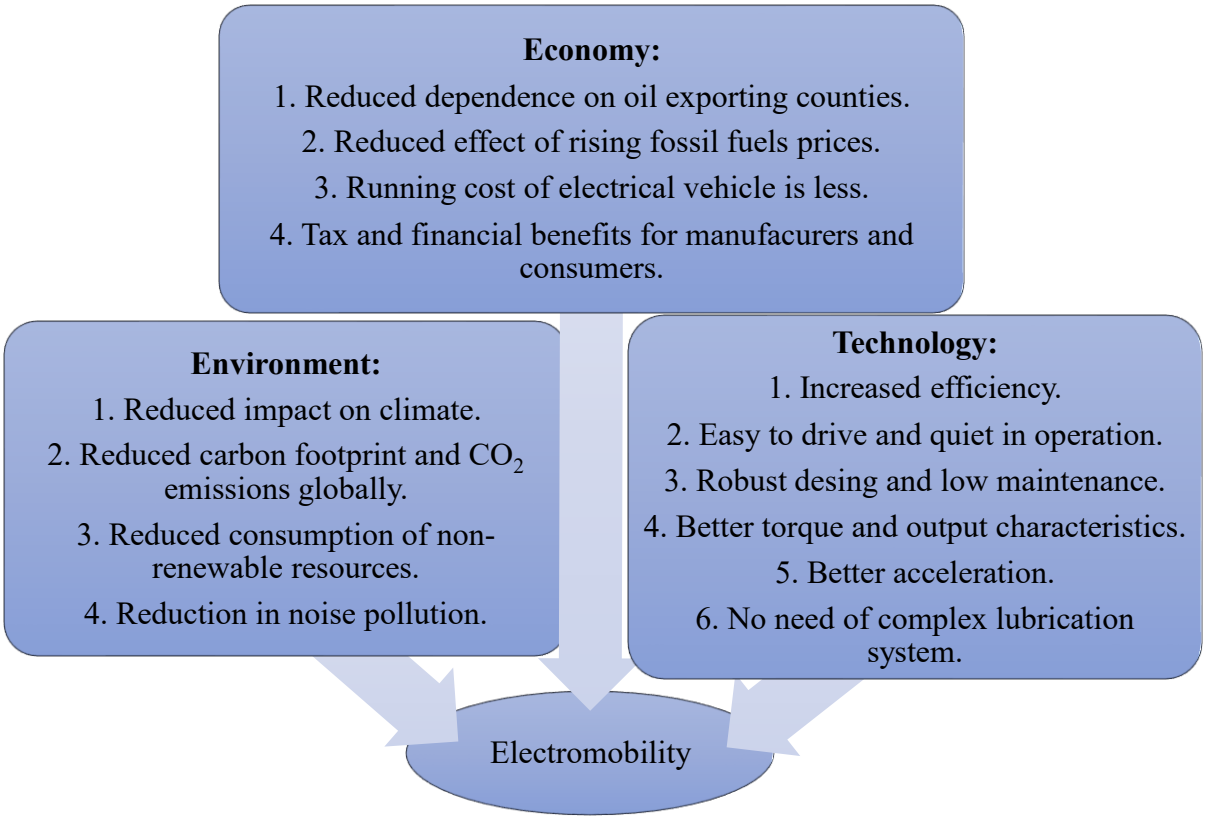

Figure 1.1: Advantages of Electrical Mobility [20], [23]

An electrical vehicle in all sorts can be a dependable alternative to fossil fuel-based engines. The construction of electrical vehicle is much simpler to IC engines. The power source of an EV is the battery packs on-board the vehicle. The electric motors which drive the wheels of an EV are supplied with power from these on-board batteries. There are different control arrangements developed by various automotive manufacturers to effectively control electric power flow from batteries to electric motors [23], [24], [25]. An electrical vehicle consists of following important components Figure 1.2:

1. Electric Motor
2. Transmission
3. Power electronics
4. High voltage lines
5. High Voltage rechargeable battery module/pack
6. Control unit for battery regulation
7. Cooling system
8. Braking system
9. Battery charge unit

10. External power source for battery charging

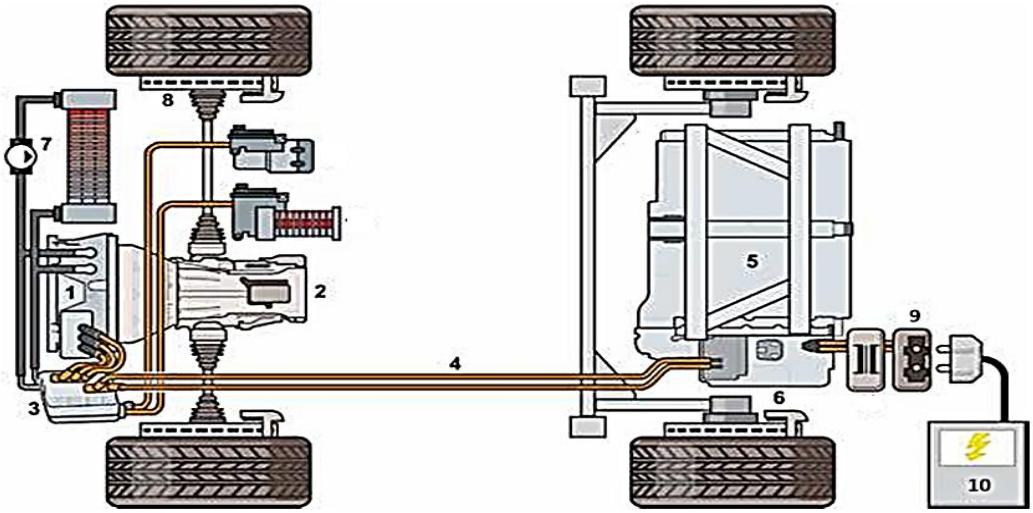

Figure 1.2: Electrical vehicle components [20]

The electrified vehicles which only rely on battery for their working are usually called Battery Operated Vehicles (BEV) or simple Electrical vehicles (EVs). Other than BEVs, Hybrid Electrical Vehicles (HEVs) and Plug-in Hybrid Electrical Vehicles (PHEVs) are two other forms of electric power operated vehicles. A hybrid electrical vehicle apart from batteries as source of energy uses other source of energy such as combustion engine or fuel cell [26], [27]. Ther involve an extra cost of installing combustion engine in the same vehicle. One of the benefit hybrid vehicles is range extender as generator can be operated by combustion engine to recharge the battery. Plug-in hybrids (PEVs) were first introduced in the market in the year 2010 [28]. PEVs batteries can be charged by plugging them into electrical outlets. For short trips PEVs run on electric mode while for long distance travel they can be switched to combustion engine mode. PHEVs as compared to HEVs have more battery storage capacity and can be switched to zero emission mode for longer distances and duration[29]. The components and usual layout of a BEV and HEV are given in Figure 1.3

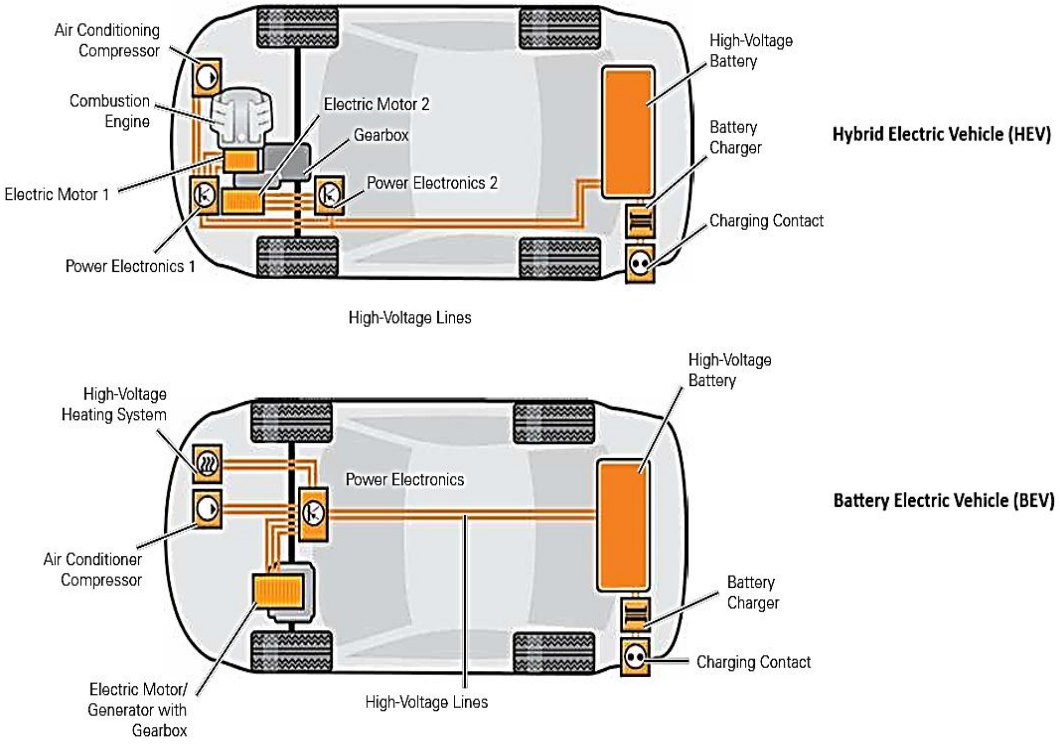

Figure 1.3: Hybrid Electric Vehicle (HEV) and Battery Electric Vehicle (BEV)[20]

1.2. Rechargeable Batteries

An electrical battery is an energy storing device which rely on electrochemical reactions between an anode and a cathode, separated by an electrolyte, to storage and release energy. The discovery of electrostatic effects paved the way for development of electric energy storage devices. First practical approach for maintaining a steady current with electrochemical cell was developed by an Alessandro Volta in 1800s [30]. A. Volta built electrical cells consisting of a copper disk, a zinc disk, and a separator made up of conductive fluid moistened paperboard. Since then, significant advancements have taken place in the field of energy storage devices. Over the period due to different requirements, energy storage devices become separated into two distinct groups: Primary disposable cells and Secondary rechargeable cells. Primary battery cells are based on irreversible chemical reactions, and these batteries are discarded after use as they are not rechargeable. One of the examples of primary cells are zinc-carbon based batteries used in torches, television remotes and other portable electronic devices [31]. Secondary battery cells are based on reversible electrochemical reactions and these batteries can be recharged again after discharge process. The active material in the secondary batteries can be restored by applying current in the reverse direction to discharge current, and therefore

these cells are also known as rechargeable battery [32]. A rechargeable battery is the heart of an electrical vehicle. The fundamental principle of working of a rechargeable battery is an electrochemical cell where spontaneous redox reactions occur between a reductant electrode, and an oxidant electrode, separated by an ionic conductive and electrically insulated electrolyte [33]. The demand to power electronic devices for extended period and reusability, advancement in rechargeable batteries technology resulted in development of various types of rechargeable cells and these cells can be classified based on electrode and electrolyte materials as: Lead Acid cells, Nikel-metal hydride (NiMH) type cells [34] , Nickel–Cadmium (NiCd) type cells [35], lithium-ion type cells (Li-ion) [36] and sodium-ion type cells [37]. Lead-Acid batteries are traditional batteries using lead plates and sulfuric acid as electrolyte. Lead acid-batteries are usually 12 V cells and for electrical vehicles these cells are not well suited as they have many disadvantages: enormous size, short life cycle, frequent maintenance requirements and reduced loading capacity [20]. NiMH and NiCd batteries have memory effect problem, and these batteries are not good at tolerating overcharging and harsh operating conditions[20]. The most popular and promising rechargeable batteries used for energy storage in Electrical vehicles are Lithium-ion batteries [38]. Lithium-ion batteries compared to other batteries have high energy density and low memory effect [20]. Li-ion batteries have advantage of high energy and power densities with ability to withstand for long-life cycles, which makes them ideal for electrical vehicles [39]. Lithium is one of the lightest metals and has density of 0.534 g cm^{-3}. Lithium is an ideal material for batteries as its low density promotes both gravimetric and volumetric energy density [40]. The performance parameters of different types of rechargeable batteries have been studied extensively in terms of energy density, cost, battery life, memory effect, self-discharge rate, energy efficiency and safety. An important parameter affecting selection of batteries for EVs is Energy content of batteries. Specific energy (mass based) (kJ/kg), Specific energy (Volume based) (kJ/L), Specific power (W/kg) and battery efficiency are parameters related with energy content of batteries. These parameters are extensively studied for various types of batteries and as indicated in Table 1.1 and Figure 1.4, Lithium-ion batteries have an edge over other batteries with better specific energy/power values and efficiency. The edge in these energy content related parameters improve range of EV, reduce overall weight and size of battery module thereby further improving energy utilization.

Table 1.1: Energy content of various rechargeable batteries

Type of battery	Specific energy content (kJ/kg)	Specific energy content (kJ/L)	Specific Power (W/kg)	Energy Efficiency (%)	Ref.
Nickel-metal hydride	288	-	-	-	[41]
	-	-	250	85	[42]
Nickel-iron	108-198	216-396	-	-	[43]
Nickel-zinc	216-234	432-468	-	-	[43]
Lead acid	172.8	-	-	-	[43]
	108-180	216-360	-	-	[44]
	-	-	130	65	[42]
Lithium-ion	334.8	410.4	-	-	[45]
	341.3	-	-	-	[46]
	432-468	720-1080	-	-	[41]
	540	1080	-	-	[47]
	540-720	1656-2160	-	-	[48]
	-	-	330	95	[42]

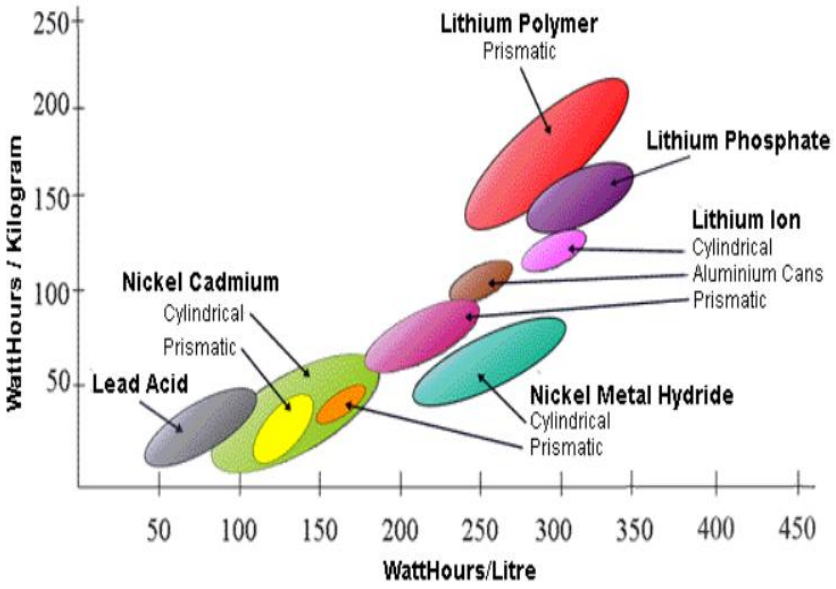

Figure 1.4: Mass and Volumetric energy density of rechargeable batteries[50]

A suitable battery for an electrical vehicle should have long cycle life, no memory effect and low self-discharge rate [20], [49]. The working life cycle of batteries is defined in cycles. For example, if cycle stability of a battery is 1000 cycles it means it can be charged from flat to full up to 1000 times. After that, their capacity starts to reduce as compared to 100% capacity. Memory effect phenomenon is well known in Ni-Cd and NiMH batteries, and it is gradual reduction in capacity of cell owing to repetitive charge and partial discharge cycle of cell [50]. Other parameters such as safe operation, manufacturing and maintenance cost are also important criterion in the selection of batteries for electrical vehicle. A comparison in terms of cost, safety, memory effect, cycle life and self-discharge between several types of rechargeable batteries can be seen in Table 1.2. Overall, at present, Lithium-ion batteries are one of the most popular batteries for electrical vehicles. A SWOT analysis of lithium-ion batteries is presented in Figure 1.5 and it can be seen in the figure that thermal degradation, cost and safety issues are the main concerns related to usage of li-ion batteries. A complete section 1.4 describes the challenges and thermal issues of Lithium-ion batteries in detail.

Table 1.2: A comparison between parameters of rechargeable batteries [42]

Battery type	Cycle life	Self-discharge (%/month)	Memory effect	Safety	Cost
Nickel-metal hydride	300-500	30-35	Yes	High	Medium
Nickel-Cadmium	500-1000	25-30	Yes	High	Low
Lead acid	200-300	5	No	Medium	Low
Lithium-ion	1000	<10	No	Low	High

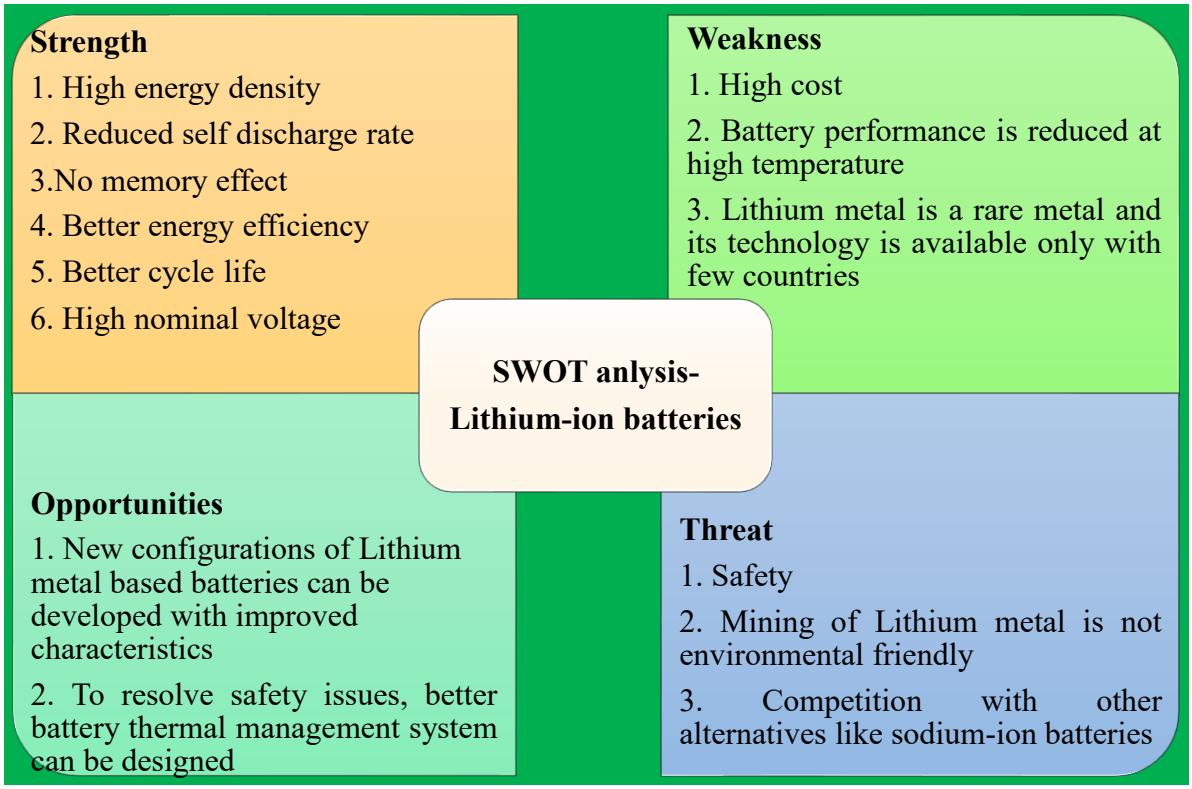

Figure 1.5: Li-ion batteries: SWOT analysis for EVs

1.3. Construction and Working Principle of Lithium-ion Batteries

Lithium-ion cells are new cell chemistries based on "intercalation" mechanism rather than traditional redox reactions. A Li-ion cell, as can be seen in Figure 1.6, mainly consist of six main components: an anode (typically carbon based), a cathode, electrolyte, a separator (also act as thermal fuse), terminals and an enclosure (case) [51]. Anode and Cathode are isolated from each other by separator, thereby preventing any chance of short circuit. Lithium ions are inserted into host electrode's crystalline lattice without affecting crystal structure of electrode. The selection of electrode materials is dependent two important properties: first is the ability of insertion and extraction of ions and the other the acceptance of compensating electrons. With advancement of technology, various chemistry configurations of Lithium-ion cells were developed. Out of these configurations, some of the configurations have particularly good potential to be used for electrical vehicles. The naming convention of Lithium-ion cells is usually based on cathode material used. The chemistry configurations (cathode material) which have good energy storage capacity include Lithium Manganese Oxide, Lithium Iron Phosphate, Lithium-Nickel-Cobalt-Aluminium, Lithium Cobalt Oxide and Lithium Nickel Manganese Cobalt Oxide [52], [53], [54]. Anode material commonly utilised for Li-ion cells is graphite as it has better capacity than other cells (theoretical -372 mAh/g) and high coulombic efficiency

($\eta_c > 95$)is also high, but many other materials are also used like hard carbon, graphene, lithium titanate oxide, lithium germanium, lithium silicide[54], [55]. The electrolyte separates two electrodes, and they do not touch each other. Water cannot be used as electrolyte in Li-ion cells as Lithium react violently with water [56]. An electrolyte function as an interface for li-ions movement between cathode and anode and it is usually a mixture of Lithium salts (non-aqueous) such as Lithium Triflate, and an organic solvents like Ethyl Carbonate or Diethyl Carbonate [51]. Other than organic lithium salt-based electrolyte, many other types of electrolytes are also used and under research. Few examples of such electrolytes are aqueous electrolytes, solid electrolyte, solid polymer electrolyte, gel polymer electrolyte, ionic liquid electrolyte and polyvinylidene fluoride-based electrolyte [57].

Charging and discharging processes constitute one operational cycle of cell, and one is reverse in direction to other. In discharge process, the movement of electrons through the external circuit generate electric current in the cell. At this point, reduction occurs at positive electrode while oxidation takes place at negative electrode. In the discharge process of cell, lithium ions are release by negative electrode, these ions migrate through electrolyte and then intercalated into positive electrode. The direction of reaction and ion movement reverses in the charge process by applying current at the terminals in reverse reaction. A solid electrolyte interphase (SEI) sometimes formed in certain cell configurations at initial phase of reaction may result in capacity loss [56]. Chemical reactions typically occurring during charge/discharge process at positive and negative electrode of Li-ion cell (Eq. 1.1 and Eq. 1.2) [58] and the charge/discharge mechanism of a typical Lithium-ion battery cell is indicated in Figure 1.7 [59].

Reaction- Positive Electrode of cell

$$\mathrm{LiMO_2} \ \rightleftarrows^{\text{charge}}_{\text{discharge}} \ \mathrm{Li_{1-x}MO_2} + \mathrm{xLi^+} + \mathrm{xe^-} \tag{1.1}$$

Reactions- Negative Electrode of cell:

$$\mathrm{C} + \mathrm{xLi^+} + \mathrm{xe^-} + \mathrm{LiMO_2} \rightleftarrows^{\text{charge}}_{\text{discharge}} \ \mathrm{Li_xC} \tag{1.2}$$

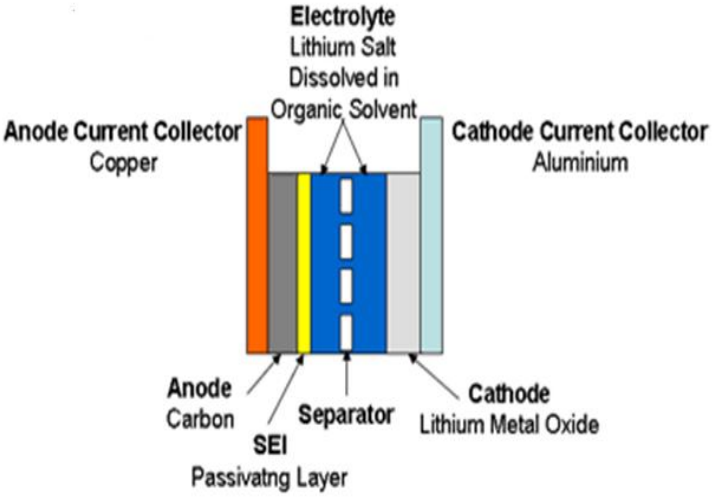

Figure 1.6: Physical structure of Lithium-ion battery cell [50]

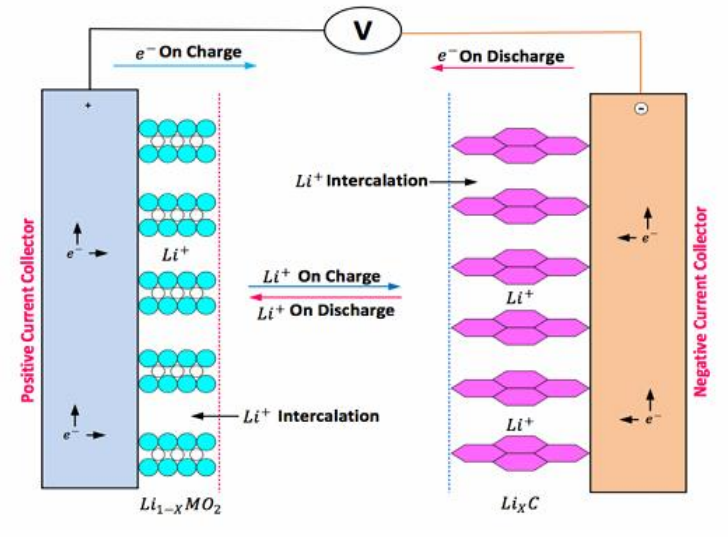

Figure 1.7: Charge and Discharge mechanism in Lithium-ion cell [60]

1.4. Types of Lithium-ion chemistries

A Lithium-ion cell is available in wide variety of cell chemistries and naming convention of these chemistries is usually based on the type of cathode material used. Lithium Iron Phosphate (LFP), Lithium Manganese Oxide (LMO), Lithium Titanate (LTO), Lithium Cobalt Oxide (LCO), Lithium Nickel Cobalt Aluminium (NCA) and Lithium Nickel Manganese Cobalt (NMC) are some of the popular chemistries of Li-ion cell [60]. The different cell chemistries have their own characteristics, benefits, and limitations. The performance characteristics of

most common Lithium-ion cell chemistries are shown in Table 1.3 and a graphical comparative analysis is presented in Figure 1.8. Lithium Iron Phosphate (LFP) are most common chemistries used in automotive industry as it has following advantages: good power density, low self-discharge rate, safe design, high thermal runaway temperature, wide operating temperature range, low cost, and better life cycle than majority of available cell chemistries. Lithium Nickel Manganese Cobalt (NMC) cell chemistry due to its high energy density (higher than LFP) is becoming popular selection for electrical vehicles. The nominal voltage (3.2-3.7 V) of NMC is also high as compared to other battery configurations such as LFP, LTO and NCA. This presents more energy storage capacity per unit weight in the cell and improve volumetric efficiency of battery module. Other cell chemistries LTO, LCO, LMO and NCA are usually not used in EVs, and they are not suitable in automobile applications but very popular in portable electronic equipment and other power applications [60], [61].

Table 1.3: Performance characteristics of most common Lithium-ion chemistries

Parameter	Lithium Iron Phosphate	Lithium Titanate	Lithium Cobalt Oxide	Lithium Nickel Cobalt Aluminium	Lithium Nickel Manganese Cobalt	Lithium Manganese Oxide	Ref.
Cathode Material	LFP	LTO	LCO	NCA	NMC	LMO	[61]
Nominal Voltage (V)	3.2-3.3	2.2-2.3	3.6-3.8	3.6	3.6-3.7	3.8	[61]
Specific Energy (Wh/kg)	80-130 90-120	70 -	120-150 150-190	80-220 -	140-180 140-180	105-120 100-135	[61] [63], [64], [65]
Energy Density (Wh/L)	220-250	130	250-450	210-600	325	250-265	[61]
Self-Discharge rate (%/month)	<1%	2-10%	1-5%	2-10%	1%	5%	[61]
Operating temperature range (°C)	-20 to +60	-40 to +55	-20 to +60	-20 to +60	-20 to +55	-20 to +60	[61]
Thermal runaway (°C)	270	-	150	-	210	250	[63], [64], [65]
Cost per kWh (in $)	400 - 1200	600-2000	250-450	600-1000	500-900	400-900	[61]
Safety	High	-	Medium	-	Safer than LCO	Medium	[63], [64], [65]

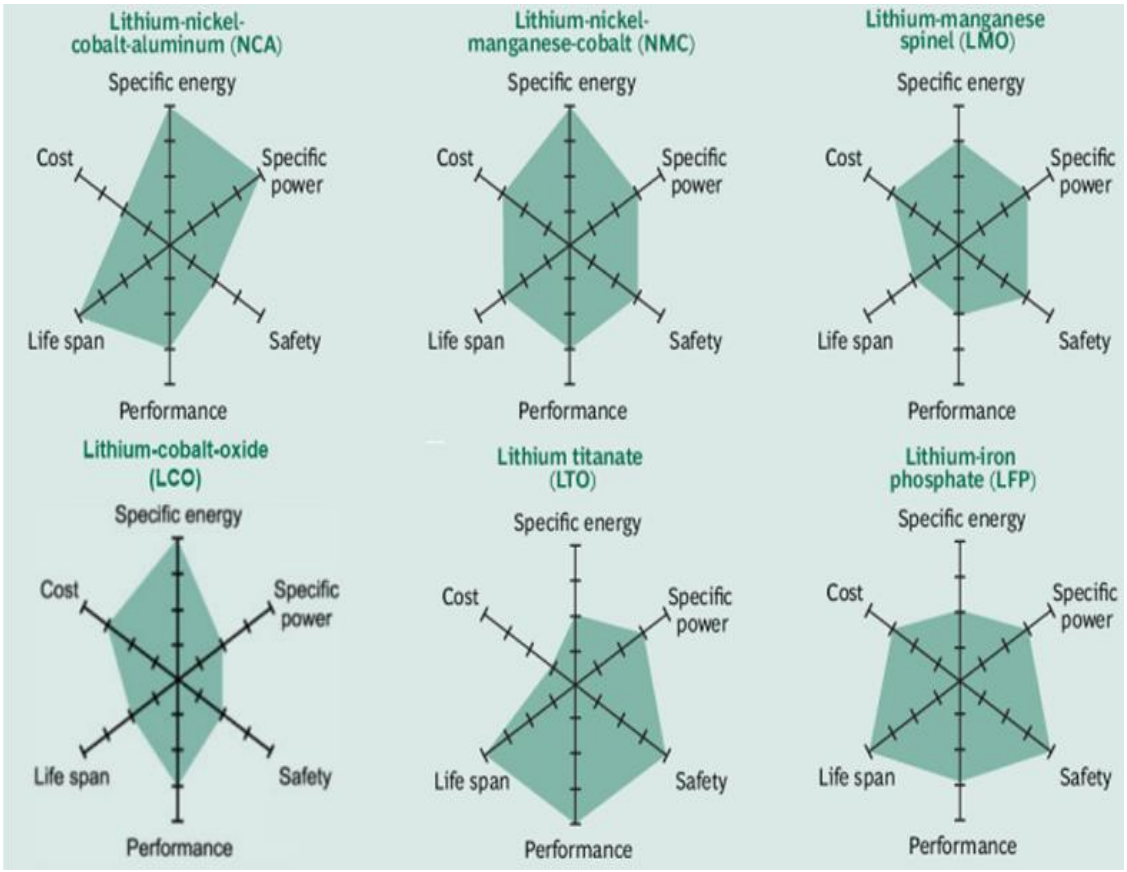

Figure 1.8: Lithium-ion batteries comparative analysis [62]

1.5. Lithium-ion Battery Type and Sizes

Lithium-ion cells are available in various sizes and shapes. The four main types of cell shapes are coin, cylindrical, pouch and prismatic and their internal structure is shown in Figure 1.9. Cylindrical cells are used by Tesla S models while Pouch type batteries are used by Nissan Leaf and Chevrolet Volt [62], [63]. The shape of battery selected is based on design of electric vehicle by automotive manufacturer. The manufacturing process of cylindrical cells is comparatively easy as compared to other shapes and the cylindrical shape enhance their mechanical stability. 18650 cylindrical Li-ion cells, at present, is by far the most popular cell configuration in production because of their low manufacturing cost per kWh [60]. Other popular cylindrical cell types include 20700, 21700, 22700, 26660 and 32650. These cells present more energy capacity as compared to 18650 cylindrical cells with significant improvement in volumetric capacity. For example, 21700 cells have double capacity of 6000 mAh as compared to 18650 cells (3000 mAh) with only 50% increase in volume of cell [61]. Prismatic cells offer greater space utilization as compared to cylindrical cells, but they lack

rigidity in structure and there are chances in swelling in the cell [64]. Prismatic cells offer better space utilization and flexibility in designing but these cells are more costly to manufacture and have low energy density as compared to cylindrical cells. The capacity of a prismatic cell is more than cylindrical cell, so for a required capacity battery pack, fewer number of prismatic cells are required as compared to cylindrical cells thereby increasing system stability and reducing complexities [65]. Larger cells present greater safety risk and thereby affect the reliability of system. The increasing order of safety risk for three main configurations is: cylindrical < pouch < prismatic [66]. A battery pack or module consists of array of cells (hundreds to thousands) connected in series, parallel or combination of series-parallel arrangement to obtain required voltage and capacity. For example, 7000 cylindrical cells are used in Tesla EV to produce 400 V and 85 kWh capacity [67].

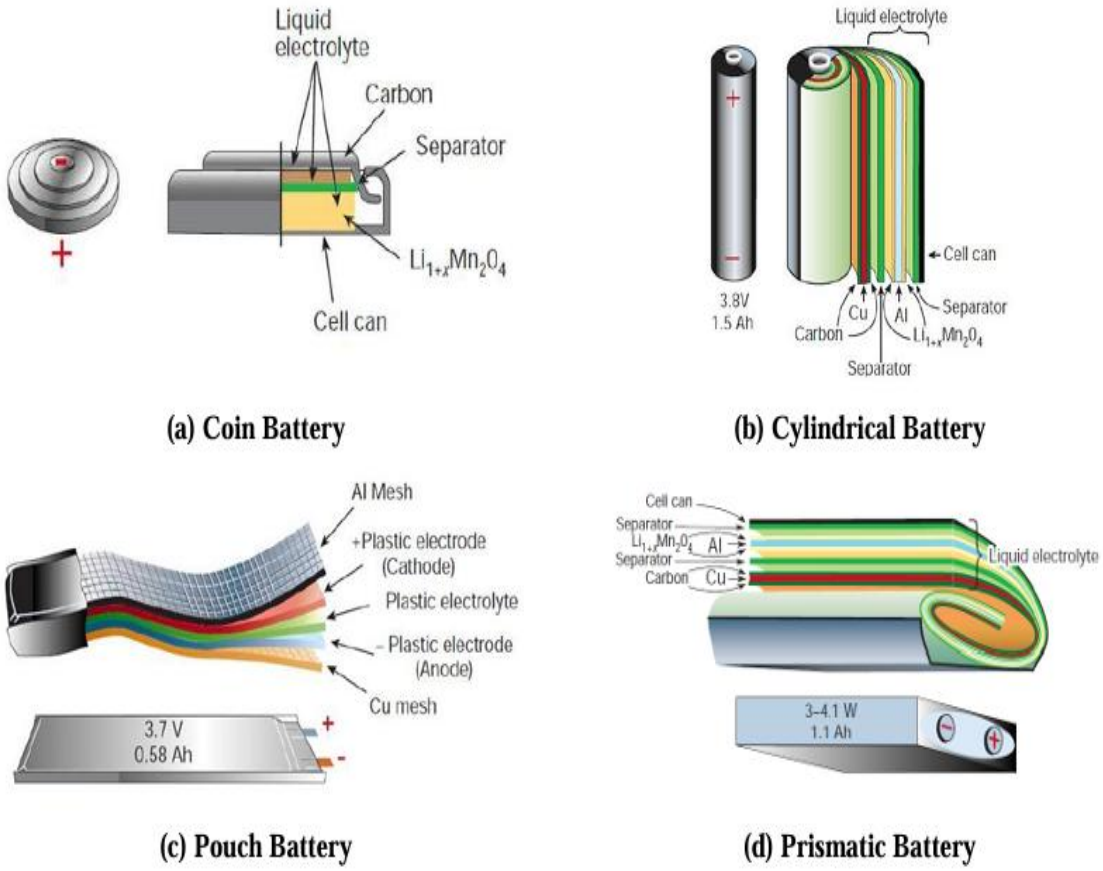

Figure 1.9: Internal structure of different Lithium-ion cells [68]

1.6. Temperature rise and Thermal issues in lithium-ion batteries

Lithium-ion batteries store chemical energy and the electrochemical reactions occurring inside battery are exothermic in nature. The reactions generate heat while converting chemical energy to electrical or vice versa. When current flow through a circuit, due to cell's internal resistance, heat is generated because of Ohmic or Joule heating effect, also called as resistive heating. Mainly three different processes can be mainly responsible for heat generation within the Li-ion cell: 1) Joule or Ohmic heating effect; 2) Entropy change due to electrochemical reactions; and 3) Overcharging of cell (usually neglected and can be controlled) [68]. The heat generated during operation cycle of cell can be reversible and irreversible in nature. The heat generated due to movement of electrons/ions i.e. Joule heating, at current collector, electrode, electrolyte and separator can be regarded as irreversible heat generation. The irreversible heat is exothermic which accounts for about 70% of total heat generated during the process, and it is directly depended on charge/discharge rates (C-rate) [69], [70]. The experimental analysis carried out by Balasundaram M. et al at 1C, 2C and 5C to study heat generation distribution for an 18650 $LiFePO_4$ with graphite anode is shown in Figure 1.10. The intercalation as well as de-intercalation of Lithium-ions at anode and cathode produce reversible entropy changes during electrochemical process [71]. The reversible reactions can be endothermic and exothermic because of negative or positive change in entropy of electrode during various states of charge/discharge process [72]. The heat loss distribution in a typical Lithium-ion cell is presented in Figure 1.11. The summation of reversible heat loss (Q_r) and irreversible heat loss (Q_i) gives total heat loss (Q_t) by the cell given by Eq. 1.3.

$$Q_t = Q_r + Q_i \tag{1.3}$$

The total heat generated (Q_{tg}) inside a Li-ion cell may be determined from the Eq.1.4 [73], [74], [75].

$$Q_{tg} = I(E - V) - I\left[T\left(\frac{dE}{dT}\right)\right] \tag{1.4}$$

Where:

Q_{tg} = Total heat generation (W)

I = Current (A), + in discharge and − in charge

E = Open-circuit voltage (OCV) (V)

V = Cell voltage (V)

T = Temperature (K)

(dE/dT) = Temperature coefficient or entropic heat coefficient (V/K)

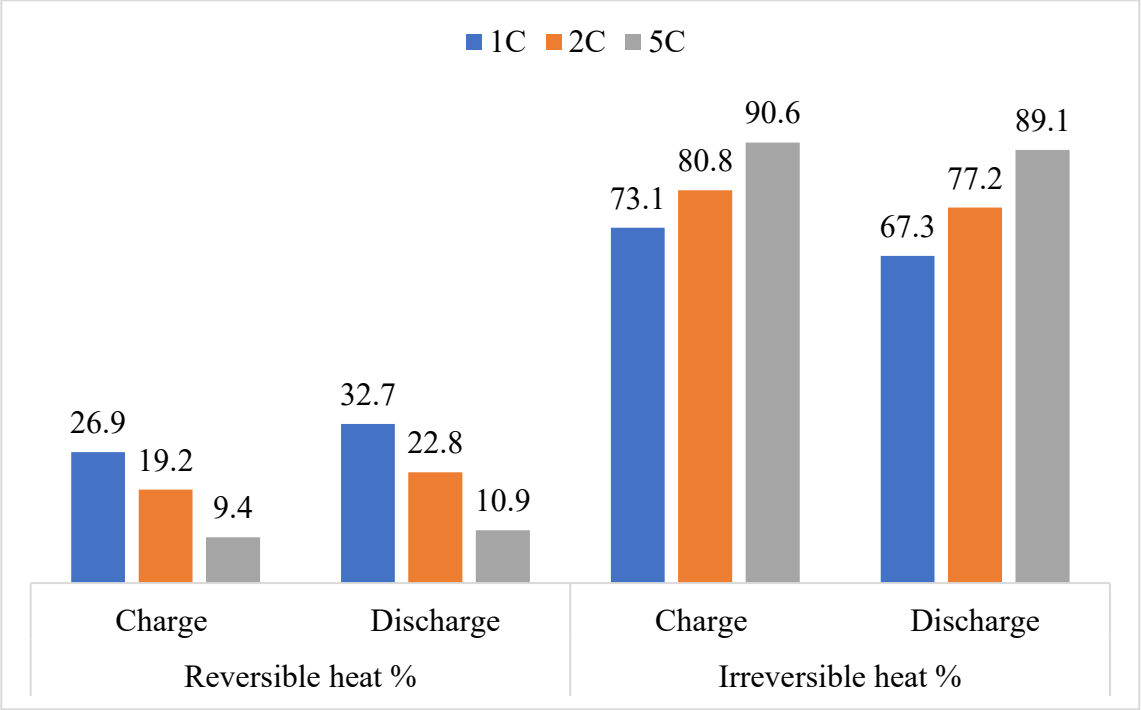

Figure 1.10: Heat contribution at various C rates in 18650- LFP cell [75]

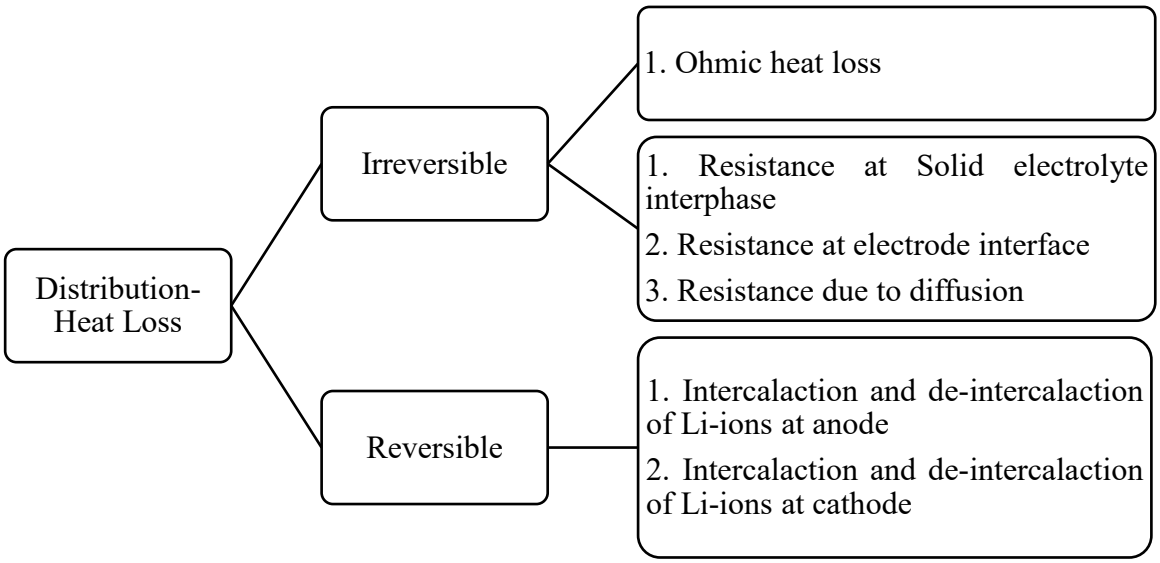

Figure 1.11: Heat distribution in Lithium-ion cell [74], [78]

In the Eq. 1.4, the term, I(E-V) is irreversible heat generated due to ohmic effects. It determines the irreversible heat generated at anode, cathode, electrolyte, separator and current collector. The second term, $I\left[T\left(\frac{dE}{dT}\right)\right]$, is reversible heat generation (Q_r) due to entropy changes in the cell components. The term, $\left(\frac{dE}{dT}\right)$, in the equation is dependent on state of charge (SOC) of cell and its value at various SOC levels is given in Table 1.4. The value of entropic coefficient can be positive and negative at different stages of SOC levels as it is dependent on Open-circuit voltage (OCV) of cell. The entropy heat loss (reversible heat loss) determined by the second term of Eq. 1.4 is small as compared to irreversible losses, and it is neglected for EV and HEV applications [76]. The irreversible heat (Q_i) as given by term I(E-V) determines the heat generated at anode, cathode, electrolyte and separator. It is mainly dependent on internal equivalent resistance (R_i) as given by Eq. 1.5.

$$Q_i = I(E - V) = I^2 R_i \tag{1.5}$$

The internal equivalent resistance (R_i) is combination of capacitive, resistive and inductive resistances of cell and can be determined by Eq. 1.6 [77], where cell temperature (T) is single parameter used for calculation of R_i.

$$R_i = -0.0001\,T^3 + 0.0134\,T^2 - 0.534\,T + 12.407 \tag{1.6}$$

Gu W. e al. [78] developed equation, to account for resistance at current collectors. The modified equations is written as given in Eq.1.7.

$$Q = -I\left[T\left(\frac{dE}{dT}\right)\right] + I(E - V) + A_p R_p {I_p}^2 + A_n R_n {I_n}^2 \tag{1.7}$$

Where area of negative and positive collector are denoted as A_n and A_p respectively, R_n and R_p denote the resistance of negative and positive collector respectively, and I_n and I_p are current values at negative and positive collectors.

Table 1.4: Entropic heat coefficient at different SOC levels of Li-ion cell (LFP) [79]

SOC	0	0.2	0.4	0.6	0.8	1	>1
$\left(\frac{dE}{dT}\right)$	-0.310	-0.130	0.005	0.020	0.032	-0.059	0

The heat generated during charge and discharge processes should be removed, otherwise this accumulated heat in the battery pack, starts a chain of additional exothermic reactions thereby producing more heat [80], [81], [82]. This results in a positive feedback exponential increase in temperature of batteries which results in thermal runaway, complete degradation of batteries and even release of explosive gases may occur. Operating cells at elevated temperatures significantly affect their capacity thereby reducing their efficiency, cycle life and overall reliability of cell [66], [83]. The most common issues of Li-ion batteries are capacity fading, self-discharge, electrical imbalance in battery pack, cold and elevated temperature performance degradation, and thermal runway at elevated temperatures [84], [85]. As can be seen in Figure 1.13, the operating temperature of battery plays a significant role among the several factors which affect life span (cycle life). Other than life span, super-fast charging, performance driving and extended range are important parameters in design of an EV [86], [87]. The battery capacity, its energy density and size of cell significantly affect the heat generation and temperature of cell [88]. The range of an EV can be extended by choosing higher capacity and energy density cells. But before switching to higher capacity cells like cylindrical 32650 and 21700 instead of popular 18650 cylindrical cells, a better system of heat removal and temperature needs to be developed. Higher capacity cells like 32650 and 21700 cylindrical although when compared to popular 18650 cells have lower energy densities, but they have about 50% more energy capacity as compared to 18650 [89]. A major challenge presented by high energy capacity batteries is their higher heat generation rates. When these high capacity and energy density cells are discharged at high C-rates to achieve better drive performance of EV, chances of overheating increases which results in premature degradation of batteries, cell imbalance inside battery pack or unequal ageing of cells, fire, and explosion hazards [90]. In the present study, 32650 $LiFePO_4$ (LPF) cells are selected due to their safe nature of operation and characteristics like more popular 18650 Li-ion cells. Batteries are electrochemical cells and there is strong correlation between charge/discharge rates (C-rates) with temperature of battery [91]. A battery pack must operate under extreme cold and hot climates at high C-rates [92]. At lower working temperature, high rate charging pose challenge as lithium plating can occur which cause safety concerns and shortens battery life [93], [94]. The capacity of Li-ion cells is strongly affected by temperature and a study conducted on 18650 cells showed that after 800 cycles capacity loss was 36% at 45°C, but capacity loss increased to 70% after just 490 cycles at 55°C [83]. Temperature above 70°C can cause thermal run away of batteries where they generate excessive heat due to exothermic reactions. For every one degree rise between 30°C and 40°C operational range, the lifespan of cell is affected, and they age

prematurely [95]. The cell performance also drops at low temperature, and it reduces significantly of temperature is dropped to freezing temperature. The availability of energy of 18650 cell drops to 60% at -20°C as compared to normal ambient temperature [96]. The research conducted at extreme cold temperatures of -40°C showed that 18650 cells can only deliver about 1.25% and 5% of their initial power capacity and energy capacity respectively [8]. The most prominent factor which affect performance and efficiency of batteries is temperature which must be controlled in a narrow range of 20-40°C [16], [97], [98]. As shown in Figure 1.12 [99], the power generated by battery would be maximum when its working within the range of 20-40°C. The optimum temperature range of 20-40°C is very narrow but battery cell can give maximum cycle life in this narrow range only. Below 10°C, anode plating kicks off and beyond 60°C, electrode material breakdown starts thereby reducing life of battery. A more relaxed threshold of peak temperature for modern batteries can be 50°C [100]. Based on operating temperature, three levels of performance of batteries can be considered: optimal limit, acceptable limit, and safety limit. The optimal limit, acceptable limit, and safety limit of peak temperature (T_{max}) for a battery pack can be kept at 40°C, 50°C and 60°C respectively [101]. Another important factor other than operating temperature is temperature uniformity or homogeneity that must be ensured in the battery pack. Temperature uniformity (ΔT) means the difference between cell-to-cell temperature. A higher temperature difference creates electrochemical imbalance that causes deterioration of the whole battery pack. The electrical imbalance caused by non-homogeneity of temperature in the battery pack affect SOC of cells thereby reducing the performance of batteries [102]. There is 30% and 50% degradation of battery module with temperature variations of 10°C and 15°C respectively [103]. Temperature difference across battery module can occur under stressful operating conditions but must be maintained below 5°C [89], [103], [104]. The need for a thermal management system for batteries arises because of the issue concerning dependence of Li-ion batteries performance on temperature. Maintaining temperature homogeneity and restricting peak temperature within ideal range is a challenge.

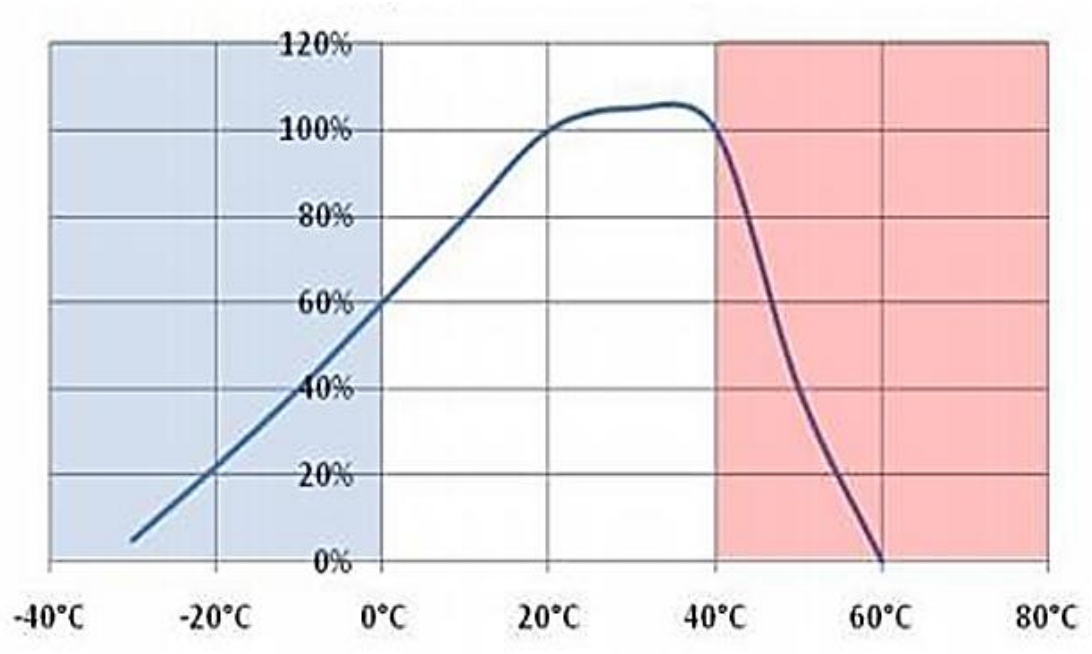

Figure 1.12: Battery Power versus Temperature [104]

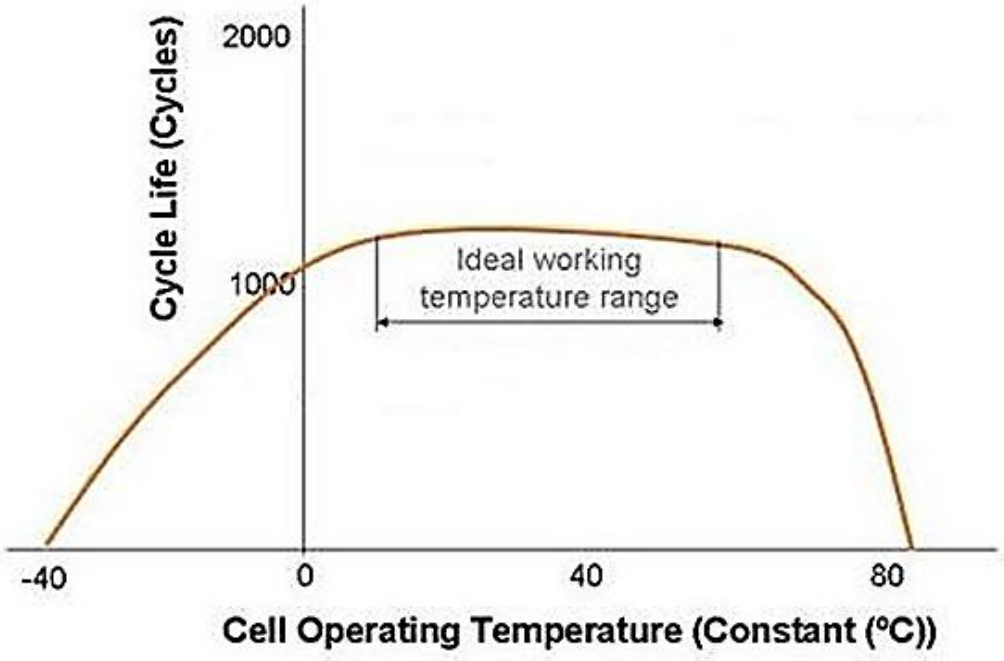

Figure 1.13: Battery life cycle versus Operating temperature[50]

A thermal management system of batteries should control the temperature of each battery cell and battery pack within ideal operational limits of temperature. The best results and performance can be achieved with Li-ion batteries, if the maximum temperature of cells and

temperature homogeneity of pack is maintained within optimum operating range by BTMS [105]. A good BTMS should also satisfactorily work under varying hot and cold climates at various C-rates, consuming low power, while keeping cost and complexity to minimum [106]. There are mainly two types of BTMS: Active and Passive, as indicated Figure 1.14. Passive BTMS do not consume any energy while operational and they are generally based on free convection. The incorporation of heat pipes and phase change materials as an additional heat extraction mechanism in various thermal and electronic systems has become an area of interest for enhancing performance of passive cooling systems. Active systems are usually based on forced convective and have components like fan, blower, or pump. Liquid cooling and air cooling are nowadays the most widely used active cooling system adopted in EVs. Both active and passive systems can also be combined to form hybrid BTMS for better control of temperature uniformity and maximum temperature within battery pack. An air cooling BTMS are simpler in constructive and less costly as compared to liquid cooling arrangements. However, air cooling is not dependable under extreme and stressful conditions of high charge or discharge rates and high ambient temperature [107]. Liquid cooling systems are more promising methods of battery cooling, but they are bulky and complex in construction. Moreover, there are chances of leakage, and they require proper seal layer and packaging [108]. Air cooled BTMS can be applied to lower power density vehicles with short operating durations. To enhance the performance of air-cooled systems, several research studies have been conducted numerically and experimentally on parameters that affect performance of air cooled BTMS such as cell arrangement, air flow pattern and inlet air velocity [109], [110], [111], [112]. The research by Fan et al. [113] showed that the best air-cooling performance is achieved in neatly arranged battery cells where power consumption for air cooling was 23% lower as compared to staggered and cross arrangement. When comprehensive cost is considered, a 5×5 cubic arrangement of cells has best cooling capacity [111]. The width of inlet and outlet channels in air cooling play significant role in cooling performance and power consumption and research has shown that by optimization of width, the power consumption can be reduced by 32% in forced air-cooling system [114]. Even after various optimizations, the air-cooling system lacks the performance offered by liquid cooling systems. One of the limitations which air-cooling systems has been its low heat transfer coefficient of air. The utilization of high heat transfer devices such as heat pipes and PCMs are proved to be effective in improving the efficiency of traditional air-cooling systems [115], [116], [117], [118]. The two passive system of heat transfer which gained lot of attention in recent years are heat pipe and PCM [119], [120], [121], [122]. Heat pipes are high conductivity devices which can be

manufactured in various geometries such as circular, flat, plate and L-shape. Heat pipes are best in controlling temperature rise in pouch and prismatic li-ion batteries. However, the effective use of heat pipes for cylindrical is still a challenge as these cells present low effective contact area for heat transfer [123]. Heat pipes when inserted through core of cylindrical cells and through critical zone of cylindrical cells-based battery module can effectively control temperature rise of cells and prevent overheating [124], [125], [126]. The effective use of heat pipes as cooling medium for battery thermal management require an effective thermal contact design. A cooling system for thermal management with embedded heat pipes designed by Gan et al. [127] effectively enhanced the cooling performance of traditional cooling system. In the designed cooling system, the contact between cell and heat pipes was improved using a conduction element. Behi et al. [128] developed and analysed the performance of a heat pipe assisted air cooled hybrid thermal management system. The main idea of their research was to enhance contact area between cylindrical cell and flat surface of heat pipe by using a heat pipe copper sheet design (HPCS). Dan et al. [107] presented a design which used micro heat pipe array arrangement, and the results showed that the numerically designed thermal cooling system was able to provide quick response under varying charge/discharge conditions. It has been investigated, and results have indicated that a heat pipe assisted BTMS can improve peak temperatures and temperature uniformity of EV's battery module [129]. Flat and ultra-thin heat pipe designs are flexible and suitable for various practical applications [17], [130]. Trade-offs based on operating conditions, power requirements, and various other factors needs to be made of while selecting a BTMS type for an EV. A brief description of various BTMS technologies, their advantages and disadvantages are discussed in section 1.8.

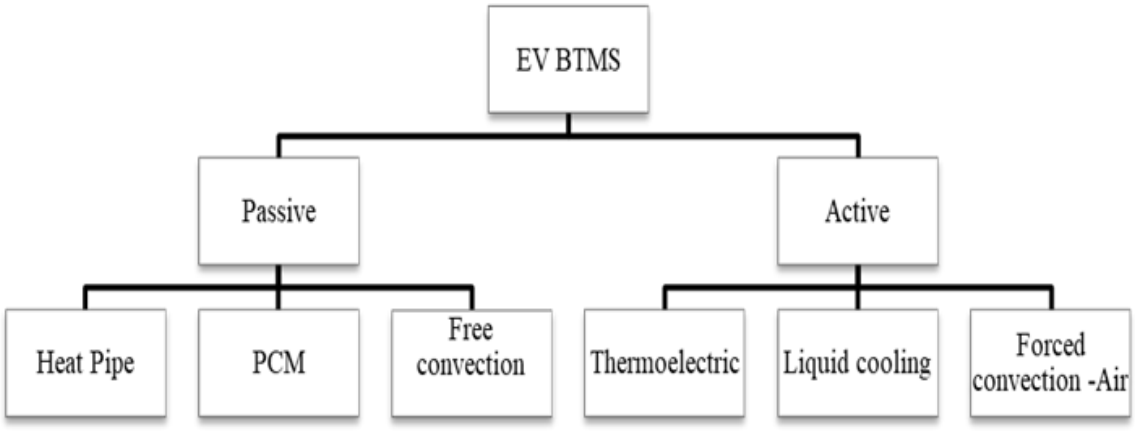

Figure 1.14: Battery thermal management systems of EVs

1.7. BTMS technologies

A battery thermal management system (BTMS) of an EV perform four main important functions as per requirements: 1) Cooling, 2) Heating, 3) Ventilation, 4) Insulation[131]. The function of cooling and heating systems is to keep temperature of battery pack within optimum temperature range. The ventilation system provides an escape to gases generated due to reactions occurring inside the batteries. This system can also be combined with active air-cooling and heating systems. The insulation is provided by BTMS so that to reduce heat loss or gain from surrounding. Also, the insulation provide protection to an EV batter pack from harsh environmental conditions. A brief description of various types of BTMS is given in next sub-sections.

1.7.1. Air-cooling and heating systems

Air cooling is one of the simplest and low-cost cooling/heating used in EVs. Air cooling can be free (natural) i.e. passive or forced convection (active) system. Free convection-based battery cooling system are not efficient and not used in automobiles. Forced air cooling systems work by taking air directly from atmosphere (ambient air) as shown in Figure 1.15 or from cabin of vehicle (see Figure 1.16). The use of ambient air require that proper filtration system should be installed before forcing air through battery pack. When utilising cabin air, the air again cannot be reused as it may get contaminated due to release of toxic gases from battery pack [132]. The air-cooling based system provide ventilation, cooling and heating in one system and there is no need for separate system for each. A schematic diagram of air-cooling system in Toyota Highlander using cabin air for cooling is shown in Figure 1.17. It uses a refrigerant circuit to cool cabin air which is then used to extract heat from battery system. The air-based cooling systems are simpler, but they have certain disadvantages: low performance, noise, concerns of fouling smell, safety concerns of toxic gases mixing and non-uniformity in temperature distribution in the battery pack [132], [133].

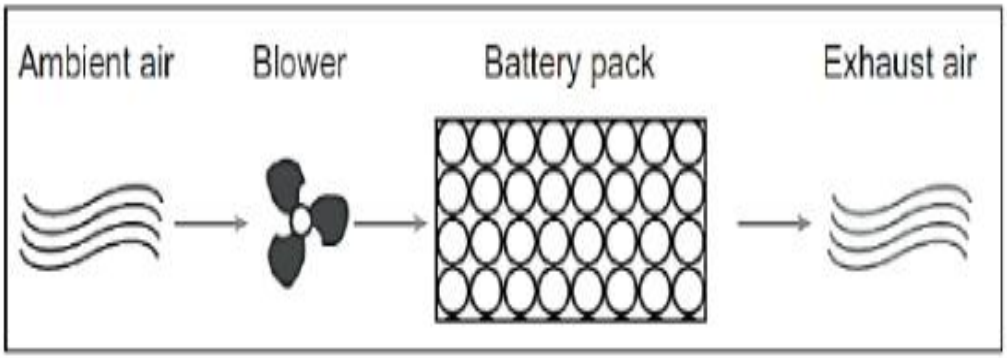

Figure 1.15: Ambient air-based battery cooling system[139]

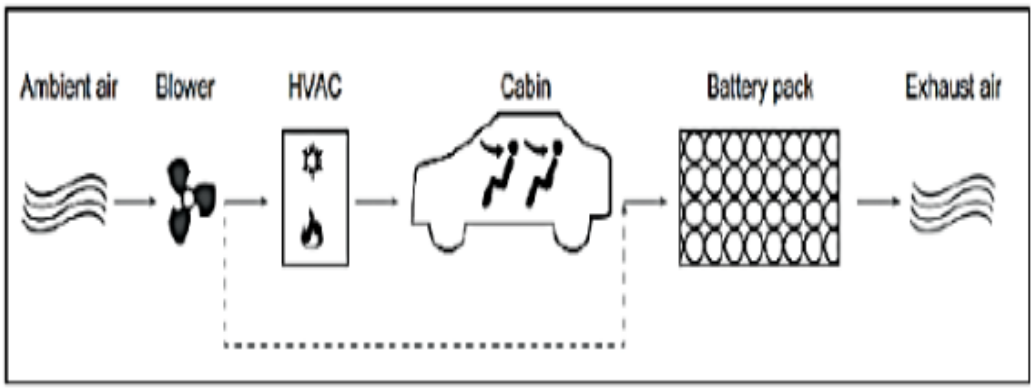

Figure 1.16: Pre-conditioned cabin air-based battery cooling system[139]

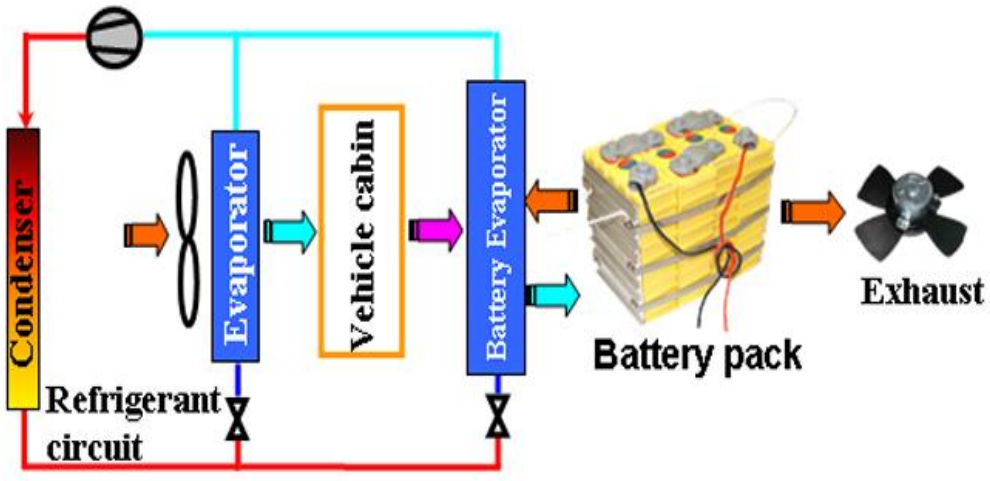

Figure 1.17: Independent air-cooling system of Toyota Highlander [140]

1.7.2. Liquid cooling and heating system

Liquid cooling technologies are much more complex than conventional air-cooling systems, but they offer better performance and cooling capacity than air cooling. The better performance is due to higher heat transfer coefficient and heat capacity of liquid as compared to air [131]. Based on liquid flow pattern, a liquid cooling system can either be a direct contact type or indirect contact type [134] (see Figure 1.18). In direct contact type liquid cooling system, batteries are immersed in a dielectric or non-conductive media such as mineral oil [135]. Non-conductive median must be used to avoid short circuit as coolant remains in contact with the battery directly direct liquid cooling system [136]. Sometimes to utilise latent heat change of coolant, phase change process is used for heat extraction. If coolant change phase during cooling process, then direct cooling is called as double phase cooling otherwise when there is no phase change involved in the process it is single phase direct cooling process. Indirect cooling system essentially use two methods of cooling. First method is by flow of liquid inside discrete pipes, plates or jackets surrounding the batteries or affixed to battery surface as shown in Figure 1.19. The second method used liquid cooled fins affixed to surface battery cells. The use of extended fins to cool battery is shown in Figure 1.20. Discrete tubes and jackets are usually used with cylindrical cells while cold plates are better suited with prismatic and pouch type Li-ion batteries [136]. The most popular cooling system used in EVs is indirect contact liquid cooling system usually using water and glycol mixture as cooling medium mixture. Although direct cooling is more promising as compared to indirect cooling because of its several advantages: compact design, better cooling performance, temperature uniformity, better safety and no need of complex flow path design, but still, it is not as popular as indirect cooling [136], [137].

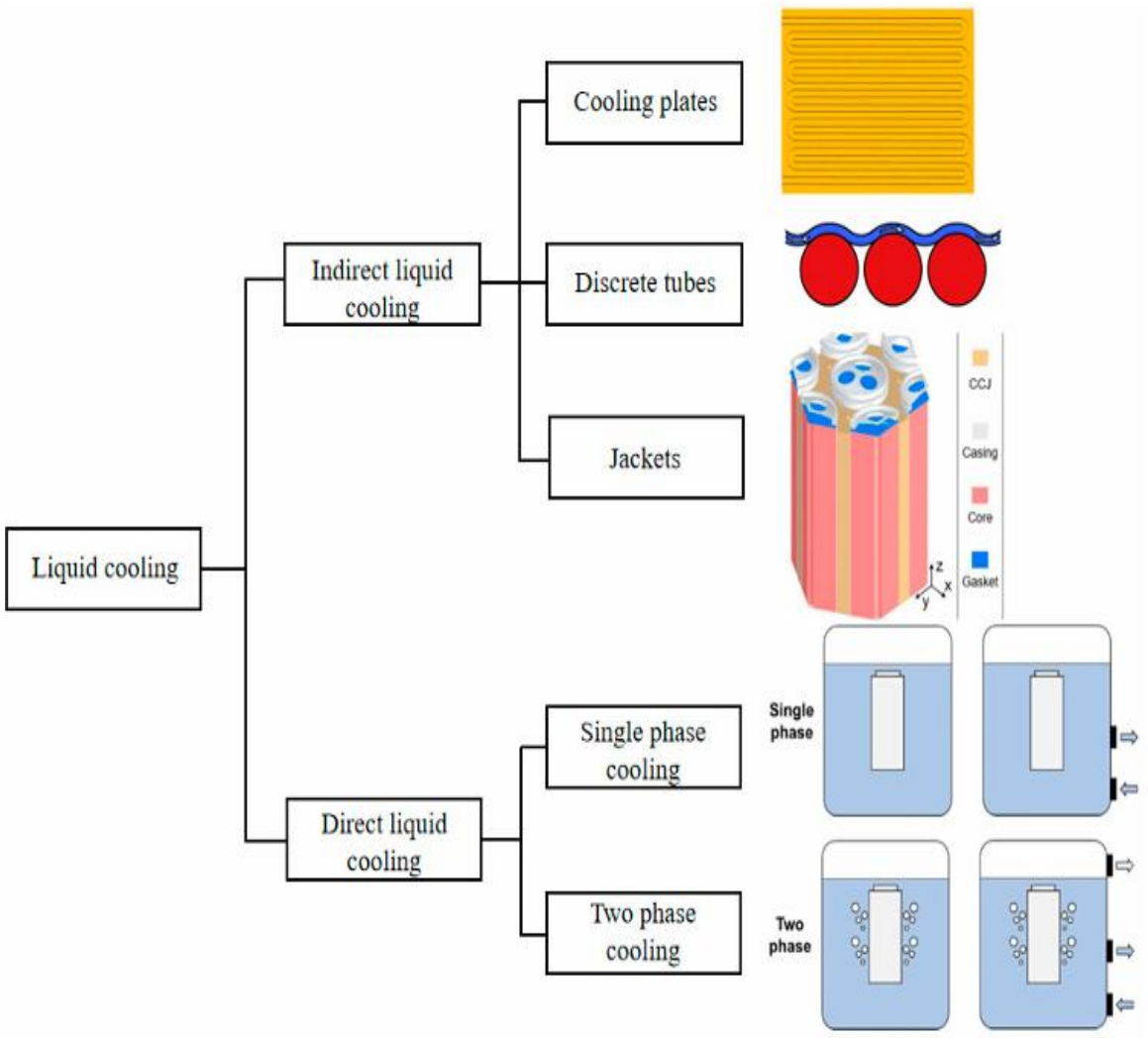

Figure 1.18: Types of liquid cooling systems[143]

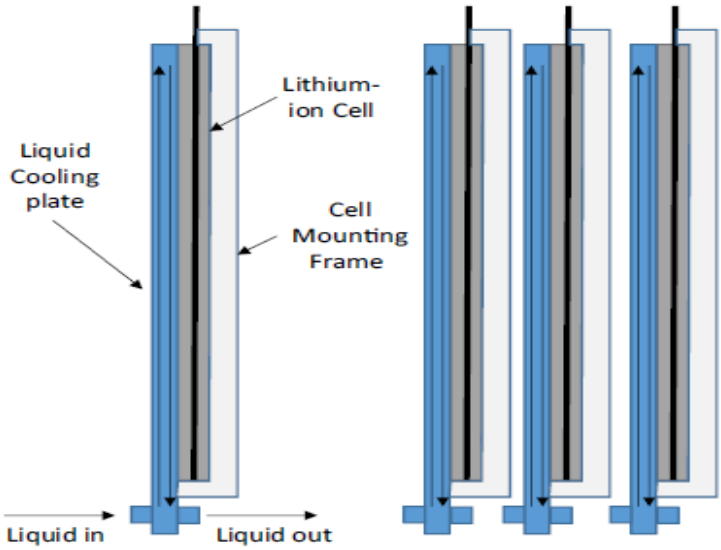

Figure 1.19: Plate liquid cooling [141]

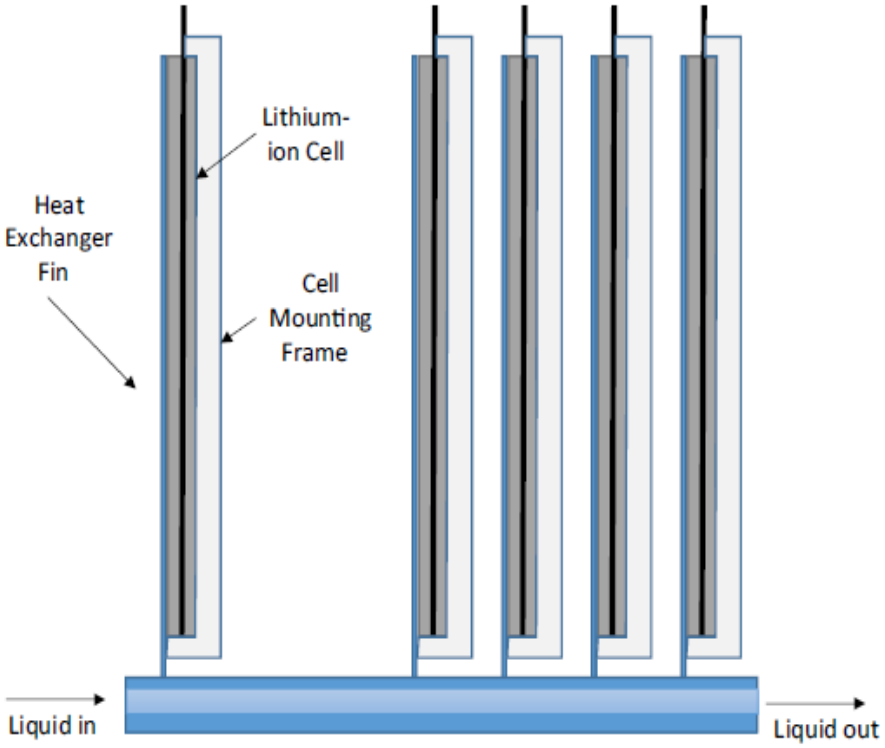

Figure 1.20: Use of fin in liquid cooling [141]

1.7.3. Phase change materials (PCM)

Phase change materials are latent heat storage material, and they are well suited for temperature control of batteries. PCMs usually extract heat from batteries by their phase change latent heat. The latent heat of phase change material directly related to heat extraction capability of PCM cooling that keep the temperature rise under control. The stored energy during phase change once released, and when temperature fall below phase transition point, PCM again changes to solid [138]. PCMs are passive system of thermal management and can be used with any other active or passive heat extraction mechanism to enhance thermal management efficiency of cooling systems. The properties of PCMs such as their lightweight, better efficiency in heat storage, simple operation and ability to provide better temperature homogeneity makes them a good thermal management system [139]. Some of the properties which a PCM should have to be utilized in thermal management of an EV are high latent heat value, required melting point, good thermal and chemical stability, light weight, goof thermal conductivity and low cost [140], [141]. PCMs can broadly classified as Organic, Inorganic and Eutectics (see Figure 1.21). Paraffins, Molten salts, Alcohols, Salt hydrates and Glycol are some of the commonly studied PCMs for use in thermal management systems [138]. Each type of PCM material has its own

advantages and disadvantages. Paraffins have high latent enthalpy, but low thermal conductivity and can aggravate fire as they are flammable. Alcohols have high biocompatibility but low latent enthalpy and low thermal conductivity [138], [139]. The overall selection of PCM is based on operating and heating conditions, safety requirements and design and type of battery used. A PCM enhanced battery pack by V. Johnson et al. is shown in Figure 1.22, where cylindrical cells are embedded in PCM to improve temperature uniformity and lower the peak temperature of high-power Li-ion batteries[142].

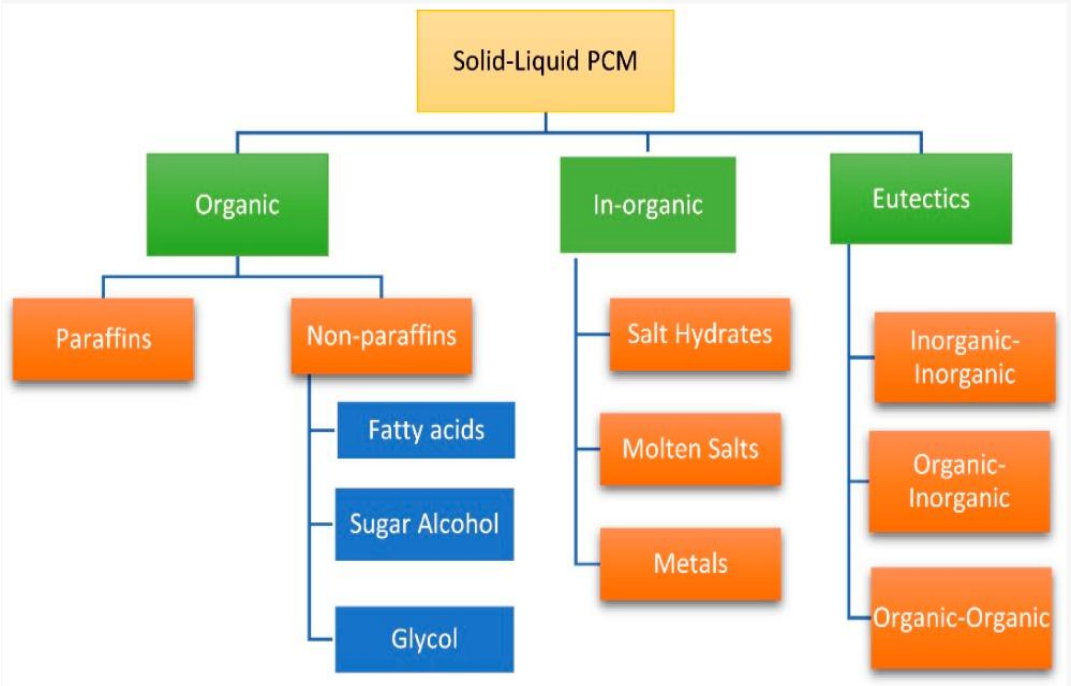

Figure 1.21: Classification of phase change materials [145], [147]

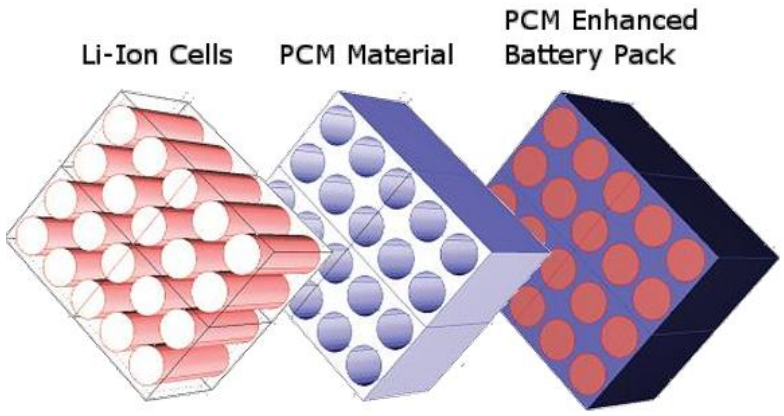

Figure 1.22: PCM enhanced Li-ion battery pack [149]

1.7.4. Thermo-electric system

Thermo-electric systems can be based on See beck effect or Peltier effect. Those based on See beck effect are called thermoelectric generators (TEG) and they convert waste heat into electricity [143]. The systems working of Peltier effect are used for cooling and they convert electricity into heat. These systems are called Thermoelectric coolers (TEC) [144], [145]. The TEG is used for cooling while TEC is a heating system. At present, these systems are still development stage and lot of research is still required for their utilization in any form of cooling system. Low efficiency and high cost of material are major limitations of thermoelectric systems[146].

1.7.5. Heat Pipes

A heat pipes is passive, single construction, high thermal conductivity heat exchange element working on the principle of evaporation and condensation or phase change. Ther high heat transfer rates make them one of the most attractive options for heat transfer and cooling systems [147]. In 1944, a lightweight very basic first of its kind, a heat transfer device like heat pipe was patented by Gauler [148]. But at that time complex phase change heat transfer devices are not required and as such not much attention was given to it until 1960s. Trefethen in 1962 first suggested this technology [149] and then in 1963, Wyatt [150] patent application revived attention to phase change-based energy transfer systems. While working with cooling system of space craft's nuclear cells, George and other members of team reinvented two phase heat transfer device and they named it "heat pipe"[151]. Since then, heat pipes have been used in many applications such as aerospace, electronics, military, buildings, energy storage, metallurgy [152], [153], [154]. Their popularity comes from the fact that heat pipes use latent energy and vaporization to transfer heat rather temperature gradient which makes them fastest heat conducting element. A basic heat pipe is a hermetically sealed container containing a working fluid (see Figure 1.23). A wick structure is lined on its inner walls which helps in capillary action and its type and structure determine how efficiently a heat pipe can transfer heat from one end to other. The working fluid in a heat basically continuously circulates between evaporator and condenser section in a cyclic process [155]. So basically, a standard heat pipe is very simple in construction consisting of only three main components:

1) The container or outer shell
2) The wick structures

3) The working fluid

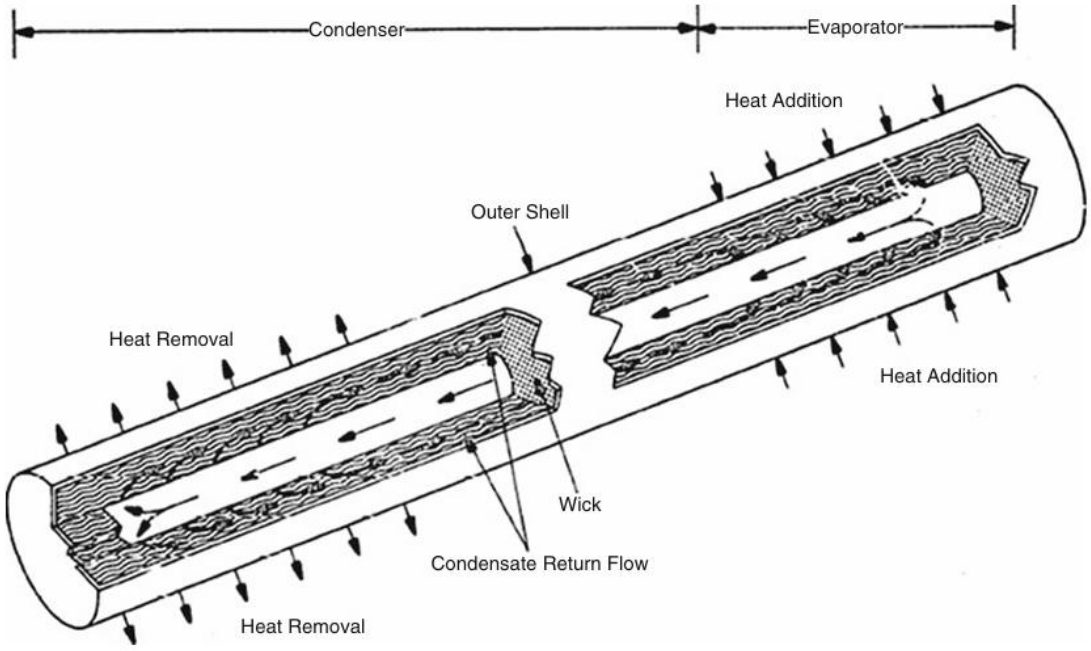

Figure 1.23: Parts of a heat and their functions[163]

The container is made from high thermal conductivity material such as copper or aluminium to ensure that there very less thermal resistance between the source of heat and the wick element [151], [156]. The design and material of container should be selected to ensure that vessel remain leakproof, non-porous, and have high strength to weight ratio[156]. The fluid of heat pipe, based on working temperature range and application, can be divided into two categories: Low temperature fluid with working range of -70°C to 270°C and Cryogenic fluid operating below -70°C [155]. Freon refrigerants, Methanol, Ethanol, Acetone, Water, Toluene, Propane, Ammonia are usually used for low temperature applications such as in pharmaceutical, biotechnical, medical, chemical and food processing industries [155]. Helium, Hydrogen, Methane, Oxygen, Nitrogen, Argon, Neon, Ethane are some of the working fluids which work in cryogenic temperature range [155]. A heat pipe can work efficiently if it has high thermal stability, high latent heat and thermal conductivity, good wettability, and good compatibility with wick material. Other than these a low freezing point and vapor pressure also affect the performance of heat pipes [155], [156]. The wick material of heat pipe is a porous structure usually fabricated using felts and metal forms of high conductivity material like aluminium, copper etc. Some other material like ceramics have also been used but their small pore size presents a challenge to their effective use [156]. The wick structure of heat pipe is available is

various materials, shapes and geometries. Some of the common types of wick structures which are used in heat pipes are given in Figure 1.24. Sintered powder metal, Grooved tube and Wire screen mesh are commonly used structures in heat pipes.

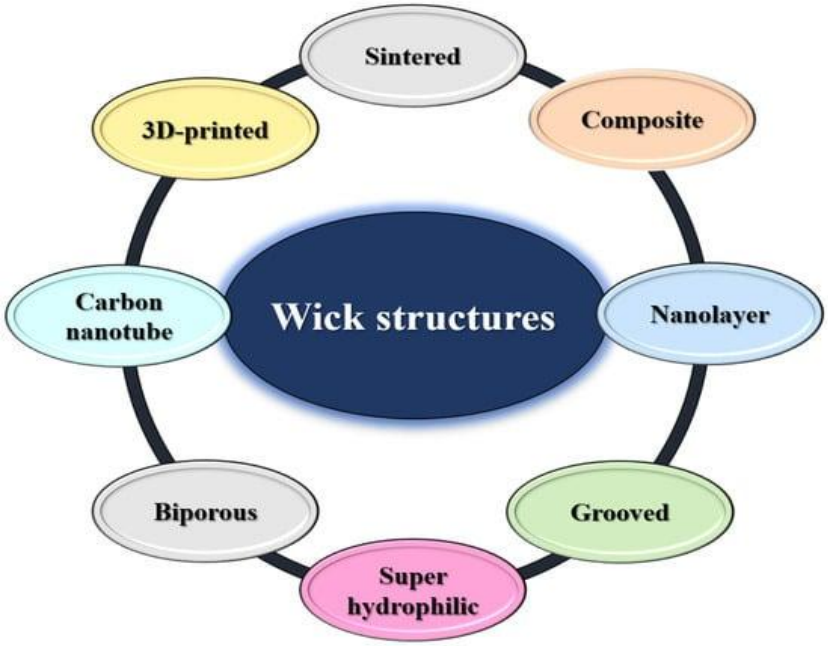

Figure 1.24: Common types of wicks [164]

The basic working principle of a standard heat pipe is based on evaporation, condensation, capillary action and pressure difference. When the heat to be removed from any system is added to working fluid in the evaporator side of heat pipe through conduction from the outer shell, the added heat evaporates the liquid working fluid to vapour state. The vapours then flows towards the condenser section of heat pipe due to increase in vapour pressure and density difference between vapour and liquid. These vapours are again cooled down at condenser section by heat extraction thereby condensing the vapours to liquid state. The condensed liquid again flows back to evaporator section of heat pipe by capillary action through the wick structure [156]. The basic operation of heat pipe is shown Figure 1.25. Other than capillary action (wick) which is usually used to return condensate in standard heat pipe, other condensate return methods are gravity, centripetal force, bubble pump force, magnetic volume force, electrostatic volume force and osmotic force [157]. The energy transfer in heat pipe consumes no power and working fluid remains inside the system in closed circuit thereby making heat pipes one of the stable and reliable heat conductors. The heat transfer rate of a heat pipe is mainly affected by rate of evaporation, the rate at which liquid gets transferred from condenser

to evaporator via the wick structure, the vapor flow and pressure differential [156]. The selection of heat pipe construction, design and working medium depends on various parameters. These include [158]:

(a) Heat transfer rate requirements
(b) The range of working temperature
(c) Materials properties required: stability, strength, weight, cost etc.
(d) Type of environment and other operating conditions

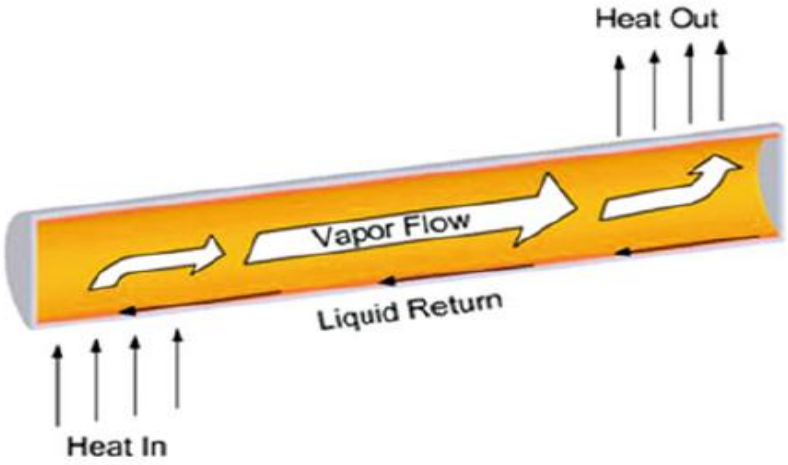

Figure 1.25: Basic operation of heat pipe[163]

Heat pipes have emerged as an attractive heat transfer mechanism because of its several advantages:

1) High thermal conductivity which is many times better than most conductive metals such as copper and silver [156], [157].
2) Flexibility of heat pipe to work and installed at any arbitrary angle from vertical to horizontal position[156].
3) The flexibility in construction and selection of various heat pipe geometries. Heat pipes are available in various geometries like circular pipes, plate type, flat thin pipes and various other geometries [159].
4) Heat pipes require no power for their working. They are passive heat transfer system[160].
5) The cost of maintenance of heat pipe is less as compared many other cooling systems like liquid cooling and air cooling[160].
6) The ability of heat pipes to operate in zero gravity conditions [151], [156].

7) The ability of heat pipes to transfer heat over long distances [156].
8) Better life and leak proof system.
9) Ease of integrating with other cooling systems.

Heat pipes have been used since 1960s and their application can be found in various fields such as aerospace, electronics cooling, solar collectors, photovoltaic devices, energy storage devices, datacentres, naval antennas, radar systems, nuclear systems, building comports, geothermal systems, waste heat recovery systems, and many other various applications. This has proven that these devices are very effective in cooling and heating purposes [149], [160]. Although heat pipes have found significant market penetration in various fields but still their effective implementation in automotive and battery thermal management systems is under development and research [161]. One of the challenges with heat pipe when using cylindrical cells is lack of proper contact between heat pipe and cylindrical surface [3]. Other limitation is at high temperature all liquid is converted to vapor and sufficient liquid is not present at evaporator section for evaporation. This generally happen when heat extraction system at condenser section is not much efficient, and system runs out of working fluid in liquid state [156]. Selection of liquid filling, channel size, material, heat pipe geometry and design affect the performance of cooling which heat pipe may provide, and these crucial parameters if not selected properly, heat pipe will not produce the desired results [146]. Heat pipes standalone when applied to cooling cannot prevent thermal runaway of battery therefore generally hybrid systems are developed [162]. Therefore, heat pipes are usually used with other cooling systems to enhance their efficiency and overcome their drawbacks.

1.9. Hybrid systems

With advancement of technology and increasing requirements to enhance the capacity, range, power and performance of electric vehicles, the demand of better and highly efficient cooling systems have increased. When a single cooling method is used, it has its own limitations and drawbacks. A comparison, in terms of benefits and drawbacks, of four popular cooling methods used for automobiles BTMS is given in Table 1.5. The choice of thermal management systems selected depends on various factors like battery capacity, heat generation, operating conditions, power requirements, type of battery selected, operating cost, initial cost, automobile complexity and various other factors [131], [163], [164], [165], [166]. The drawbacks of various cooling methods and specific operating requirements of manufacturers and consumers

is pushing towards development of hybrid cooling systems. Various combination of cooling systems developed as hybrid systems can be seen in Figure 1.26. These systems when combined overcome each other drawbacks to some extent, although all combinations are not equally successful. The right choice depends on the requirements. For example, liquid cooling when combined with heat pipe can reduced the power consumption and was also successful in restricting temperature of batteries to below 50°C [162].

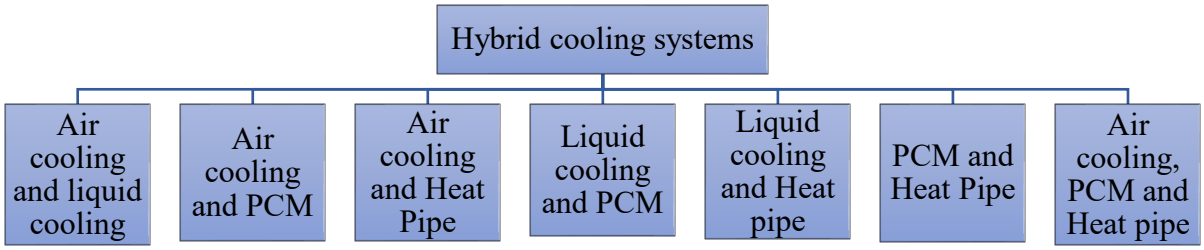

Figure 1.26: Hybrid battery thermal management system[170]

Table 1.5: Comparison of four main types of single cooling methods[166], [167], [168], [169]

Cooling method	Dominance	Problems
Air-cooling	Ease of use, simple design and structure, low initial cost, low annual cost, ease of maintenance, better life and proven commercial use	Uneven temperature, low efficiency, low temperature drop, high thermal resistance and inability to work under heat dissipation conditions
Liquid cooling	High efficiency, better temperature homogeneity, large temperature drops and high thermal conductivity	Leakage problems, high initial and operational cost, high maintenance cost, difficulty in maintenance and complex structure
PCM	High latent heat, low cost, passive system, low cost of operational, ease in	Leakage problems, large volume change requirements, complex design

	maintenance, large temperature drop, high efficiency, better life and better temperature uniformity	
Heat Pipe	Simple and compact, long life, low weight, high thermal conductivity, high efficiency, no power consumption, large temperature drop, better temperature uniformity and low maintenance cost	High initial cost, small contact area and small capacity

The heat pipes in any of the cooling applications are rarely used alone. Usually, heat pipes are always combined with other cooling technologies to make hybrid systems. A good example of hybrid cooling is electronic cooling systems where heat pipes are combined with forced air cooling to enhance cooling rate[170]. As shown in Figure 1.26, various hybrid systems which are developed using heat pipe (HP) are [162] :

A) HP assisted air cooling
B) HP assisted liquid cooling
C) HP and PCM assisted air cooling
D) HP combined with PCM passive cooling
E) HP and PCM assisted liquid cooling

These hybrid systems based of heat can also be called as heat pipe assisted cooling system. Research studies have proved that heat pipes assisted BTMS can significantly reduce peak temperatures and control temperature homogeneity battery module within operational limits [129]. Heat pipes embedded design as proposed by Saha et al. [171] can effectively prevent or delay thermal runway of batteries. A heat pipe assisted liquid cooling proposed by Yuan et al. [172] can be seen in Figure 1.27. In the cooling mechanism developed, the heat pipes are attached to liquid cooled cold plate. The developed system met the requirements of heat dissipation in continuous cycle of operation, and the peak temperature and temperature homogeneity were respectively observed under 35°C and 1°C [172].

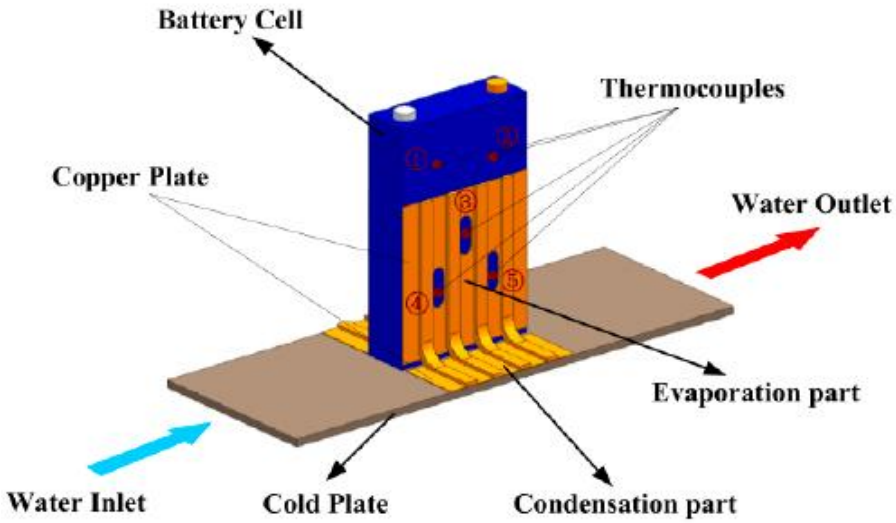

Figure 1.27: Liquid coolant based heat pipe assisted cooling system [178]

The heat pipe assisted cooling or heating systems are still under research and their practical application in automotive has not gained momentum. The heat pipe technology has a proven record and if their effective use can be found out in battery thermal management system of EVs, higher capacity and higher energy density batteries can be used without compromising the safety.

Chapter 2 Review of Literature

The chapter presents an overall overview of research studies related to energy source and thermal management of electrical vehicles. The different kinds of thermal management used in electrical vehicles, their working and operational requirements of li-ion batteries, their advantages and limitations were already discussed in chapter one. This chapter is mainly focussed on heat pipe assisted thermal management systems. Important studies or research work which have essential criterions that may be used for development a better and efficient thermal management mechanism of batteries were discussed, and their significant contribution is summarized at the end of the chapter.

2.1 Literature Review

Strumpf H et al. [173] (1982) presented a conceptual for heat recovery system for industrial furnace exhaust gases. Conventional heat exchangers due to metal temperature limitation have a working temperature range of 760°C to 820°C. To work with hotter gases above 840°C, a recuperator ceramic coated heat pipe-based system with radial fins was presented in the paper (see Figure 2.1). The heat pipes were used to form bank of tubes, like conventional recuperator heat exchanger and but both flue gases and inlet air (combustion air) were passed over bank of heat pipes separated by partition. The results were concluded by presenting an economic analysis of heat pipe system. Saving in fuel cost, total set-up cost of new system and its payback period were discussed. The saving in fuel cost were 40-50% with payback period range of about 6 months.

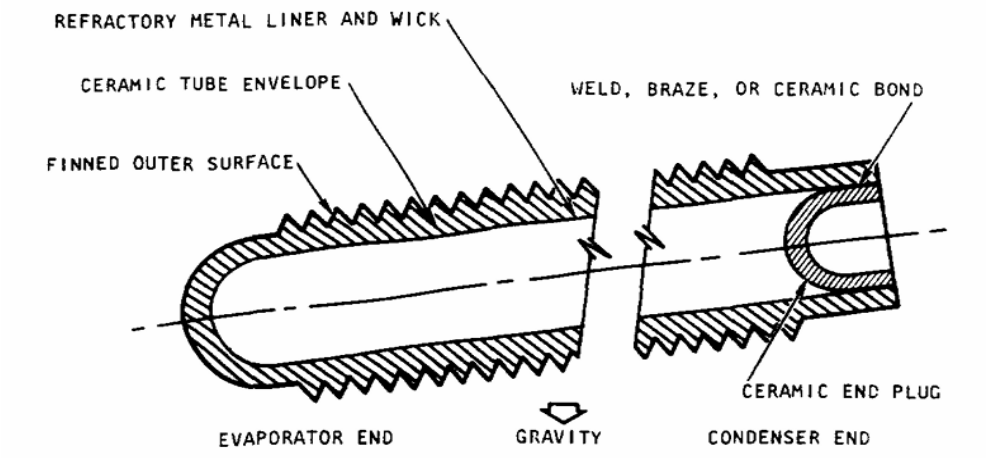

Figure 2.1: Schematic of finned ceramic heat pipe[179]

M. Broussely et al. [9] (1997) built an electrochemical cell of 100 Ah capacity by using graphite and $LiNiO_2$. A 220 V and 20 kWh assembly was built, and results showed that full discharge of cell can fulfil requirements of electrical vehicles. It was concluded that a battery must fulfil two important parameters to be suitable for electrical vehicles: (i) safety, and (ii) low manufacturing, maintenance and operational cost which include reliability and better cycle life.

Chau K et al. [43] (1999) presented an overview of EVs advantages and energy sources. Various positive aspects of EVs discussed in their research were:

1. Higher overall energy conversion efficiency of electrical vehicles as compared to gasoline engine. It was 12.5% and 9.3% respectively for EV and gasoline engine.
2. Increasing the range of EV by up to 15% with regenerative braking.
3. The inherent benefit of energy diversification presented by EVs. Energy generated from thermal, hydro, nuclear, solar or any other method can be used to power an EV.
4. The benefits of environment protection, noise and air pollution reduction presented by EVs offer them an edge over conventional IC engines.

In their research, various potential energy sources of electrical vehicles were reviewed. The Figure 2.2 shows various types of batteries that were discussed in the paper. Although no battery type satisfied all the criteria of selection, but li-ion batteries emerged as potential battery of EV application.

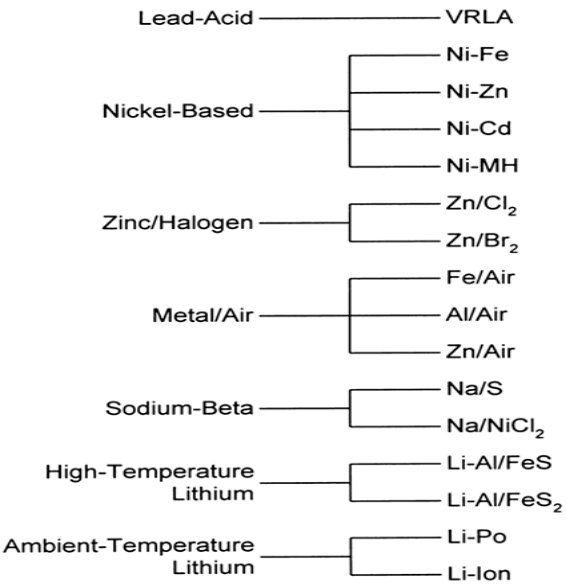

Figure 2.2: Classification of batteries[44]

Ramadass P et al. [174] (2002) carried out capacity fade analysis at elevated temperatures for li-ion Sony 18650 type cylindrical cells with rated capacity of 1.8 Ah. Cells were discharged at varying discharge rates from C/9 to 1C for number of cycles: 150, 300 and 800 and at three temperature values :45°C, 50°C and 60°C. Analysis was carried out for both fresh cells and recharged cells with CC-CV protocol. Three important capacity losses were discussed in the research: rated capacity loss, active material degradation and primary active material loss. Results showed that secondary loss of secondary material was the dominating factor for capacity fading of cells. At elevated temperatures, high-capacity losses were due to formation of film over anode surface resulting in lithium loss and increased resistance of negative electrode.

Yimin Xuan et al. [175] (2004) performed theoretical and experimental performance analysis of a flat geometry heat pipe under different orientations, heat fluxes and at varying quantities of working fluid. A porous sintered layer copper powder was applied to heat pipe and result showed that evaporation process and boiling rates were enhanced by porous layer application. A theoretical model was developed to predict dynamic behaviour of flat heat pipe. The thermal simulation results were validated by experimental results. The experimental facility as shown in Figure 2.3 consisted of heater, axial fan, flat heat pipe, thermocouples, and data acquisition devices. The results showed that performance of flat heat pipe is affected by orientation, working fluid amount and geometrical parameters of heat pipe. Potential application of thin flat heat pipe in cooling of electronic components was investigated by comparing performance with heat sink.

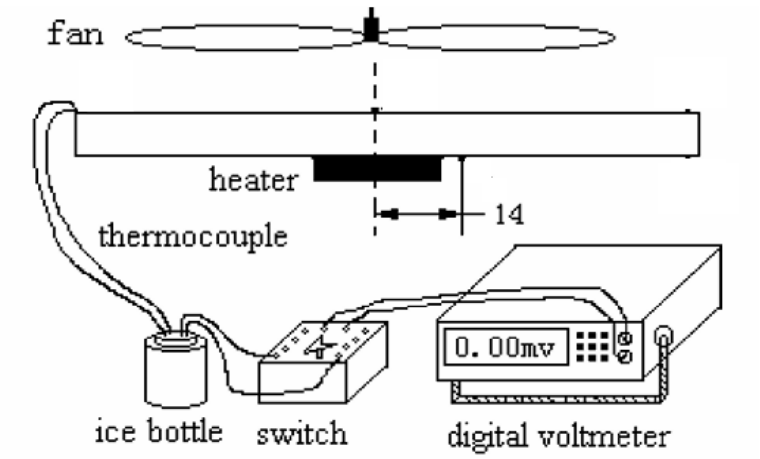

Figure 2.3: Experimental facility for analysis of flat heat pipe [181]

Amine K et al. [176] (2005) study on prismatic Lithium Iron Phosphate (LFP) batteries was focussed on capacity fading and cycling characteristics of battery at high temperature. Battery was charged and discharged at C/3 rate for number of cycles and capacity of cell was recorded. LFP cells with carbon coated electrodes were investigated and XRD patterns were used to compare results before and after carbon coating. The results showed significant drop in capacity with increasing number of cycles at 55°C and 37°C as compared to 25°C. The capacity fading was the result of iron ions release from electrode into the electrolyte at high temperature. The capacity fading was reduced by replacing the electrolyte with lithium bis-oxalatoborate salt.

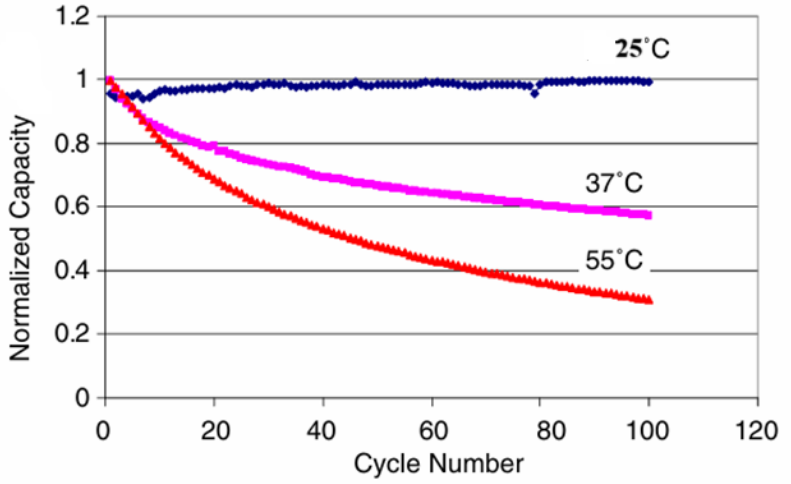

Figure 2.4: Capacity fading of LFP cells at high temperature[182]

Kong et al. [177] (2005) investigated the gas generation behaviour of three different 18650 cell chemistries viz. LiCoO2, $LiMn_2O_4$, and $LiFePO_4$. The gas generated in the batteries results in swelling of cells and certain gases may also result in hazardous conditions such as explosions etc. It can be observed from their research work that cathode material does not significantly affect gas generation under normal charge and discharge conditions. While when cells are overcharged, cathode material started significantly affecting the type and amount of gas generation. More C_2H_2 is produced by $LiFePO_4$ while more CO_2 is produced by $LiCoCO_2$ cell chemistry. Overcharging significantly affects the oxidation ability of cathode material, and $LiCoCO_2$ has the highest and $LiFePO_4$ has the lowest oxidation ability among the three cell chemistries.

Inui Y et al. [65] (2007) developed 2D and 3D simulation model for li-ion cylindrical cell under discharge condition to study temperature distribution in transient conditions. 2D model utilized

symmetry of cell and was based on cylindrical coordinates while 3D model considered radius and height of cells. The temperature distribution as obtained by numerical simulation can be seen in Figure 2.5. The numerical results were validated by experimental results and results indicated that temperature distribution is dependent on shape of battery. It was concluded that under similar conditions, capacity and volume of cell, laminated cylindrical cells perform better than prismatic cells. The developed numerical simulation model may also be used to measure temperature distribution of large battery cells under transient conditions.

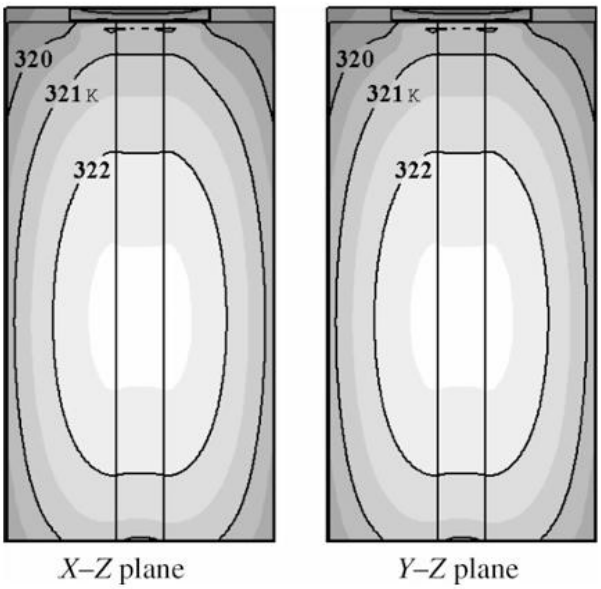

Figure 2.5:Numerical obtained temperature distribution of cylindrical cell [70]

Robak C et al. [178] (2011) experimentally analysed the possibility of using heat pipes and fins for improving results with latent heat storage materials (PCM). The PCM material used was paraffin with purity of 99%. The experimental facility developed is shown in Figure 2.6 and it consisted of two heat exchangers, thermocouples and data acquisition system, constant temperature bath, heat pipes or fins and PCM. The heat pipe with PCM while under charge and discharge conditions performed better than fins. Results showed that by heat pipe inclusion, PCM melting rates increased by 60% and during solidification process heat transfer was doubled between PCM and cooling fluid as compared to non-heat pipe configuration.

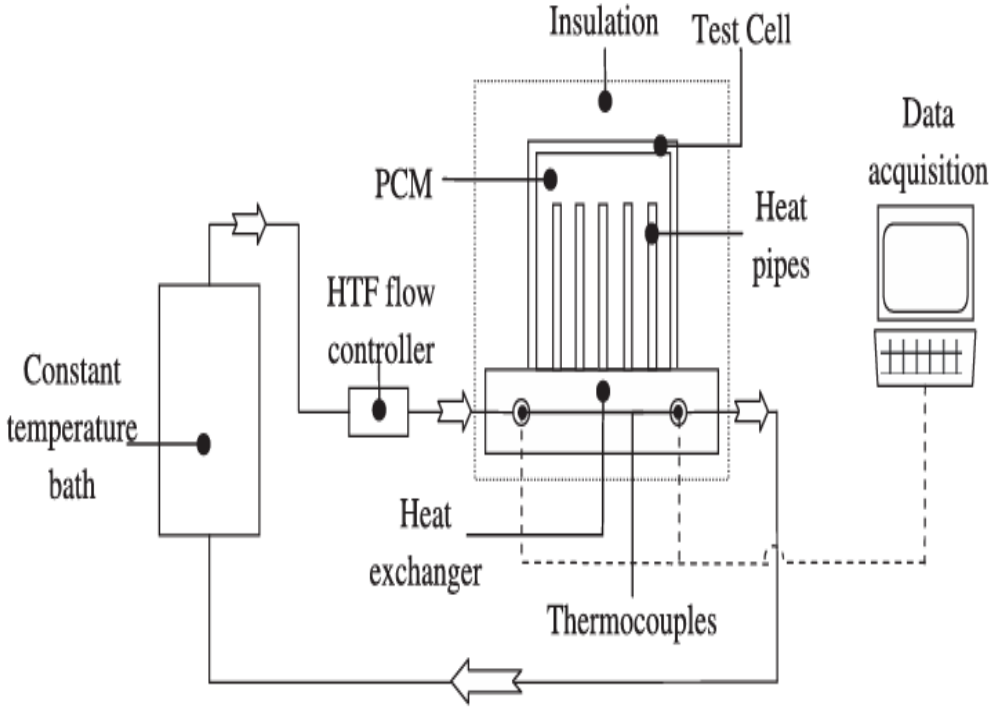

Figure 2.6: Experimental facility for testing heat pipe embedded latent system [184]

Ying-Che Weng et al. [170] (2011) proposed a hybrid cooling system utilizing a round heat pipe (HP) and PCM for cooling of electronic components (see Figure 2.7). They used PCM filling to cover adiabatic part of heat pipe. The performance of heat extraction arrangement was experimentally analysed under charge and discharge conditions at various PCM volumes, fan speed, and heat generation rate. It can be observed from the results that heat pipe combined with PCM can save 46% power consumption as compared to conventional heat pipe cooling system. Three different strategies to improve cooling performance were tested. First method utilized doubling the number of fins at condenser section, second method increased contact area of heat pipe by increasing diameter of heat pipe and third method was based on utilizing higher conductivity PCM material.

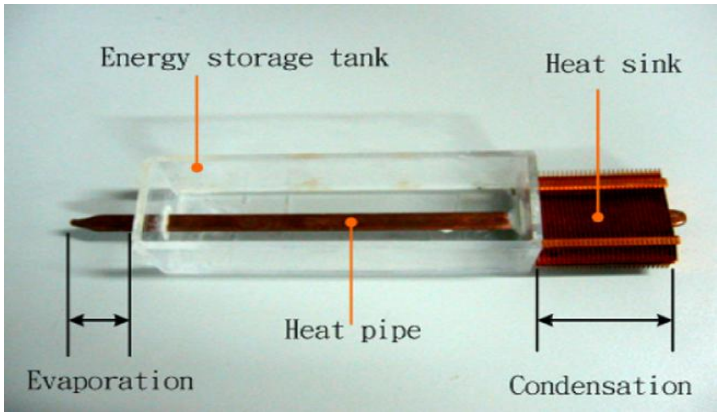

Figure 2.7: Heat pipe with adiabatic section covered with PCM energy storage tank [176]

Rao et al. [120] (2013) designed a BTMS for EVs which utilized a heat pipe for heat extraction. The objective of their research was to reduce cost of EVs by increasing the cycle life of batteries. The proposed design consisted of four heat pipes and thermal silica was used as interface material between cell and heat pipe. The heat pipes were copper made with flattened evaporator section and outside diameter 5 mm. The schematic of experimental facility can be seen in Figure 2.8. Heat pipes were tested during start-up process between 10 W to 50 W heat input. To simulate the unsteady non-continuous operating conditions of electrical vehicles, heat pipes were tested at input power of 30W and randomly varying heating time of 542, 458, 650 and 600 seconds. From their results it can be observed that heat pipes provided desired performance of controlling maximum temperature within 50°C.

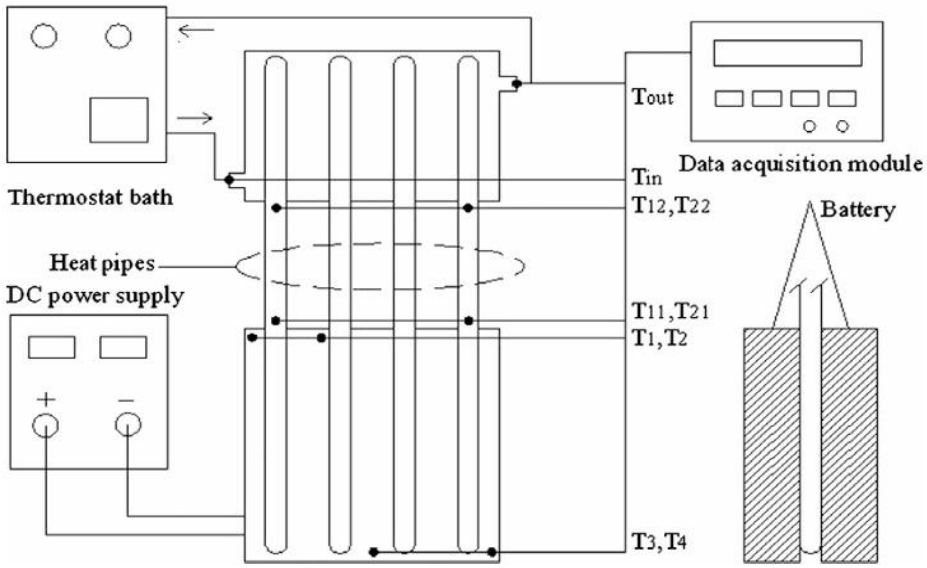

Figure 2.8: Experimental facility [125]

Tran et al. [104] (2014) investigated usability of flat heat pipe assisted system as compared to conventional method where heat sinks were used for cooling hybrid electrical vehicles. The selected batteries were cylindrical with 7Ah capacity as a reference for heat load. The nominal heat flux and transient heat flux generated by batteries were simulated by a flat heater and induction heater respectively. The proposed design of battery module consisted of batteries packed in a non-conductive resin matrix (see Figure 2.9). The utilization of heat pipes reduced heat sink resistance to heat flow by 30% in natural free convective currents, and 20% in low windy situations. When heat pipes were tested under various inclination angles, the results showed that they can be useful at inclination angle from 0° to 90° orientation. The proposed cooling method successfully controlled the temperature below 50 °C. It can be concluded from their work that flat heat pipes have large flexibility in terms of space utilization, road, and operating conditions.

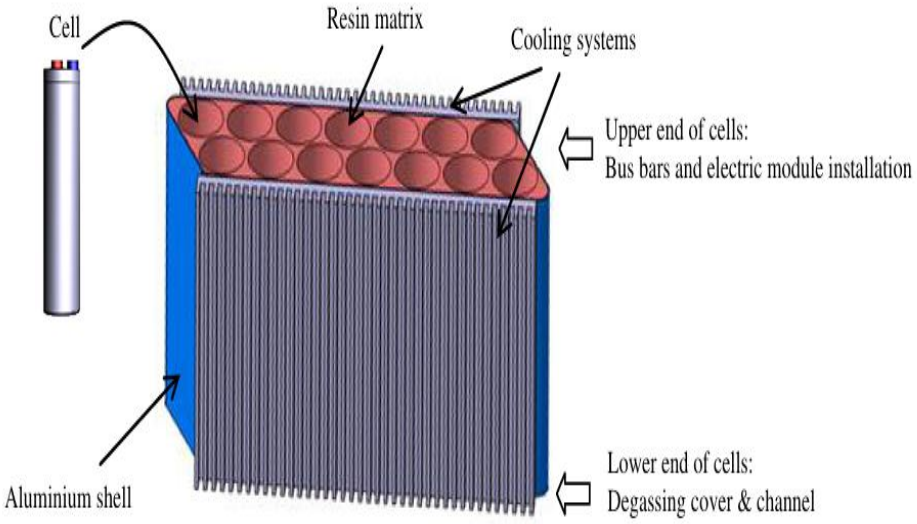

Figure 2.9: Battery model with non-conductive resin matrix[109]

Wang et al. [111] (2014) investigated the performance of rectangular, hexagonal and circular cell arrangement. The different cell arrangements investigated were three rectangular arrangements: 1×24, 3×8, 5×5 –,a hexagonal with 19 cells and a circular arrangement with 28 cells. The cooling performance of various air-cooling strategies with varying fan installation position as shown in Figure 2.10 were also investigated for better temperature uniformity. CFD analysis and lumped method applied for single cell were used to obtain temperature distribution at varying cell arrangement, fan locations and intercell spacing. Temperature distribution for rectangular arrangement is shown in Figure 2.11, where middle cells are at higher temperature

as compared to other surrounding cells under free convection. The conclusion drawn are: 1) fan at top arrangement gave best cooling performance, 2) cubic structure is most cost effective and gave best cooling performance, 3) hexagonal cell arrangement has better space utilization.

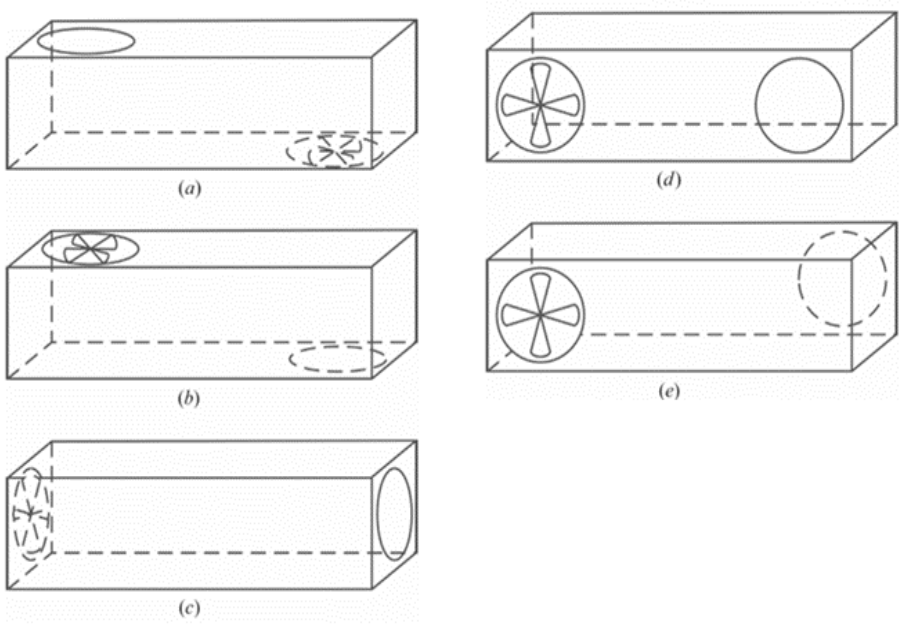

Figure 2.10: Various cooling strategies based on fan position[116]

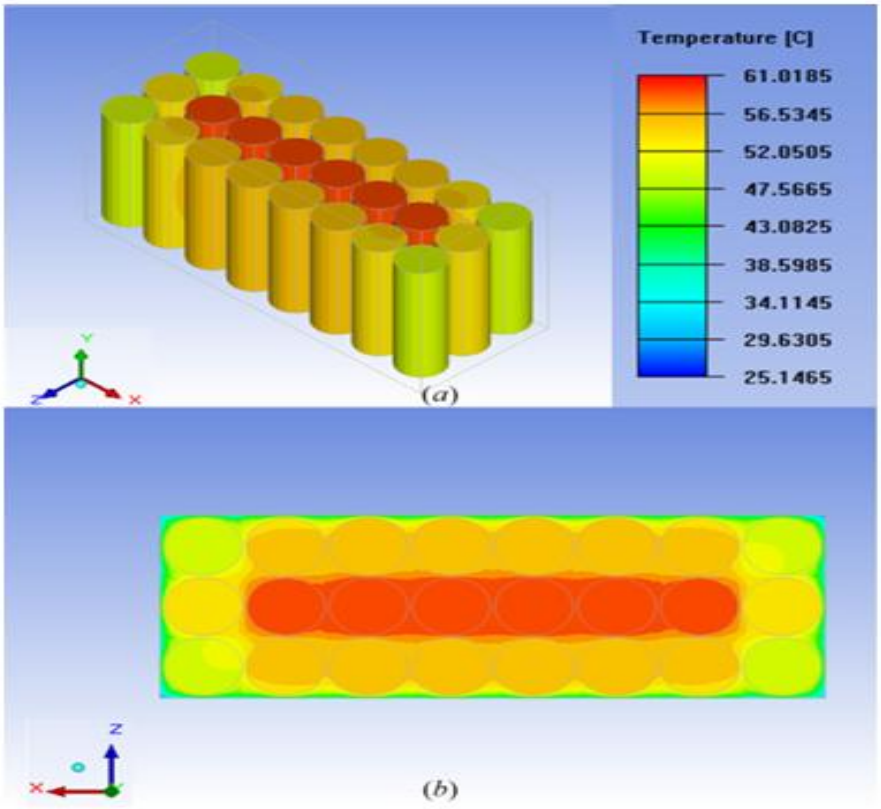

Figure 2.11: Temperature uniformity in rectangular arrangement without air flow[116]

Greaco A et al. [179] (2014) proposed a simplified computational model for prismatic li-ion battery utilizing thermal circuit model. A sandwiched model of prismatic battery and heat pipes was developed. The proposed computational model treats battery and heat pipe separately. Conservative chi model was used to calculate heat thermal resistance of heat pipe evaporator section. Three separate approaches: 1D model, 3D CFD model, and analytical solution, were used and results were nearly same. It was concluded that 1D model can be used in conservative cases to predict temperature distribution when batteries were used with heat pipes. The results confirmed that heat pipes produce better results as compared to forced convection owing to their higher surface area and it was concluded that heat pipes can be used in confined spaces and are effective as thermal management system.

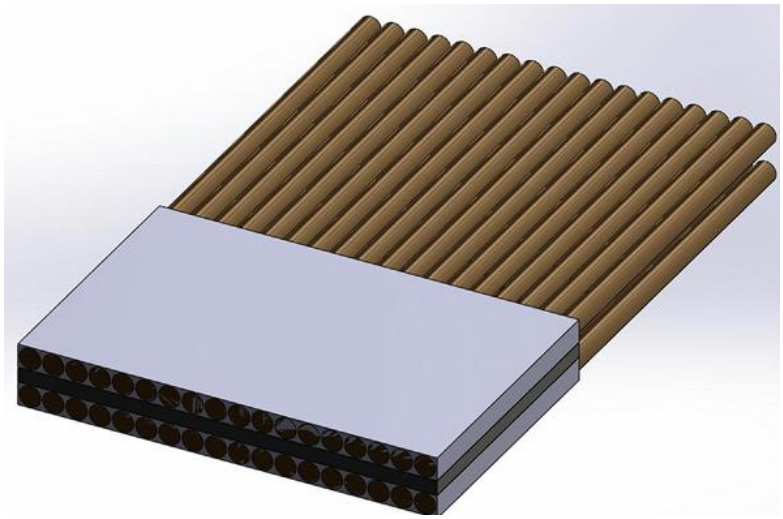

Figure 2.12: Prismatic battery cell sandwiched between heat pipes [185]

Zhao et al. [180] (2015) proposed a BTMS for thermal surge conditions of li-ion batteries that utilized ultrathin heat pipes and wet cooling. Two different pouch batteries of capacity 3Ah and 8 Ah and sandwiched heat pipe arrangement as shown in Figure 2.13 were studied under free convection cooling, forced air cooling, and wet cooling. Maximum charge and discharge rates used were 5C and 25C respectively and tests were conducted to control battery temperature between 20°C and 60°C. Various cooling strategies invested were free convection, vertical heat pipe air cooling, horizontal heat pipe air cooling, and water bath heat pipe cooling. The comparative results related to heat pipe angle of placement between vertical and horizontal showed that performance of system is not significantly affected by angle of placement of heat pipe. A combination of free, forced convection and wet cooling with intermittent water sprays

proposed was able to maintain temperature uniformity and peak temperature within optimum operating conditions.

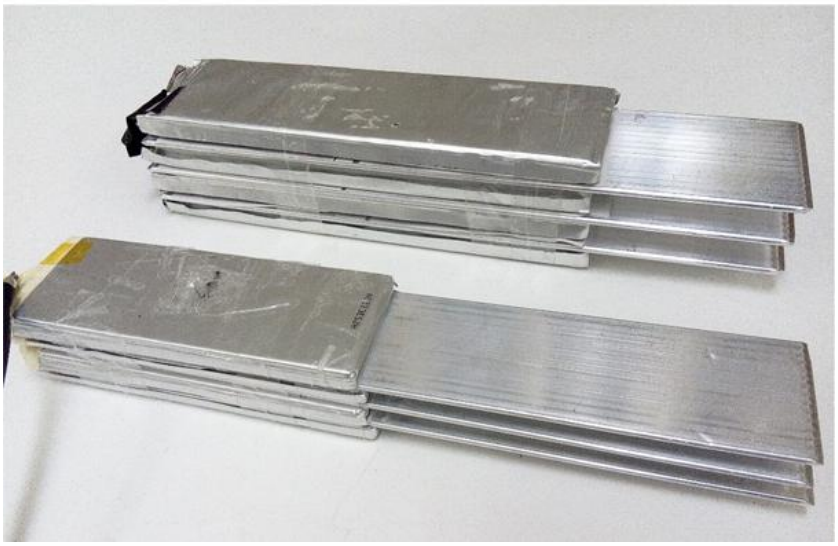

Figure 2.13: 8 Ah (top) and 3 Ah (bottom) batteries with heat pipe insertions[186]

Zhao et al. [91] (2015) reviewed the methods of improving the thermal performance of lithium-ion cells. The two methods mainly discussed were based on electrode modification of cell and utilization of thermal management system. It was concluded that temperature rise of batteries has strong relation with charge/discharge rate. Although thermal management system increases about 10% to 20% cost of electrical vehicles but by its utilization more energy dense batteries can be utilized. For their review, it can be said that thermal management is extremely important for safe functioning of batteries without thermal runaway and occurrence of other hazardous conditions. Lithium-ion cells are highly susceptible to deterioration at high temperature due to self-heat and thermal management can improve SOC, capacity and cycle life of cells.

Yuan et al. [181] (2016), as can be seen Figure 2.14, investigated a self-designed heat pipe-assisted BTMS and its utilization in electrical vehicles. The cooling module is integrated with commercially available Lithium Iron Phosphate ($LiFePO_4$) having capacity of 10 Ah. The condenser section cooling fins contacted cell while evaporator section of heat pipe consisted of aluminium heat collection plate. The evaluated results validated the use of dual heat pipe structure is advantageous and preferably should be used with forced convection. The cooling mechanism controlled the temperature within optimum range of maximum and minimum temperature (32.2°C and 27.6°C respectively). They showed that surface temperature of cell in contact with heat pipe was at lower temperature as compared to other locations of cells.

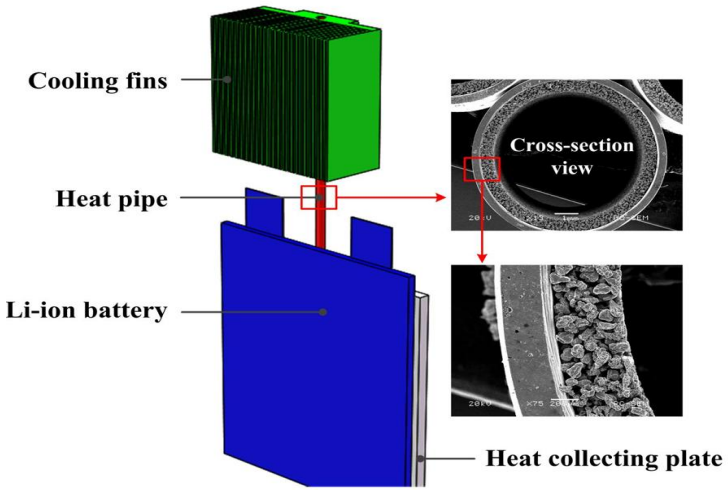

Figure 2.14: Self-designed heat pipe assisted thermal management system[187]

Putra et al. [182] (2016) conduced experimental analysis of "flat plate loop heat pipe (FPLHP)" system to investigate its performance as a heat exchanger for electric vehicle (see Figure 2.15). The experimental setup consisted of 400 W aluminium made cartridge heater (heat source) simulating heat generation by batteries. The three different working fluids investigated for performance were distilled water, acetone, and alcohol, at 60% fill ratio. The acetone gave better performance at 50°C evaporator temperature than other two with heat flux load and thermal resistance of 1.61W/cm^2 and 0.22 W/°C respectively. Acetone and alcohol both were able to maintain temperature within operating range of lithium-ion batteries.

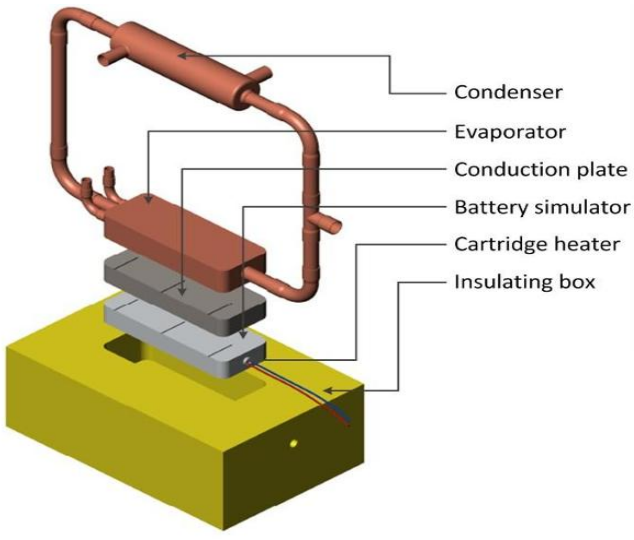

Figure 2.15: Schematic diagram of FPLHP

Y. Ye et al. [152] (2016) proposed a cooling system utilizing heat pipe (HPTMS) for fast charging of prismatic type li-ion batteries. The HPTMS was tested different values of C-rates and results indicated that improved design with fins added to condenser section was able to

handle twice the heat generated at 8 C charging rate (see Figure 2.16). Methanol and water performed better as working fluids of heat pipe with less chances of dry out. They concluded that precooling of batteries to below 15°C is detrimental to batteries as lithium plating is promoted at low temperatures. They proposed a "quench strategy" to improve cooling system performance by cooling battery pack at 25°C with coolant at 15°C. Their improved design was able to maintain battery pack with optimum range of 25°C - 40°C.

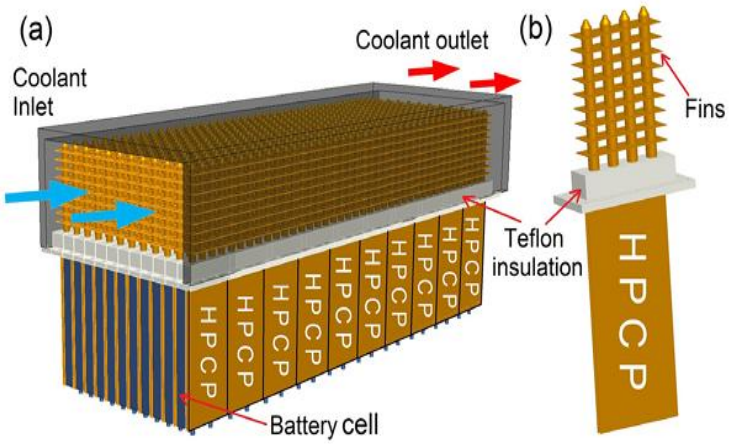

Figure 2.16: Heat pipe with fins added to condenser section[159]

Shah et al. [126] (2016) investigated use of an annular channel centrally placed parallel to the axis of the cell for cooling Lithium-ion cells. Two different approaches were studied: air cooling by air through the annular section and heat pipe insertion in the channel and cooling heat pipe tip with air flow. The paper demonstrated the fabrication of a thermal test cell of dimensions equivalent to 26650 li-ion cells. The fabricated test cell was able to generate heat through joule heating corresponding to varying discharge rates with facility to measure internal temperature of cell with the heal of embedded thermocouples. The testing facility with heat pipe insertion in the annular region, test cell and air cooling can be seen in Figure 2.17. Experiment results showed that with heat pipe insertion there is 18-20°C drop in core temperature of cell. Heat pipe was successful in preventing thermal runaway and short-circuiting under stress conditions. The energy density loss due to annular channel was also studied and results indicated that 2 mm diameter only results in 2% energy density loss. But increase in diameter drastically reduce energy density and that should be accounted for while using annular channel concept.

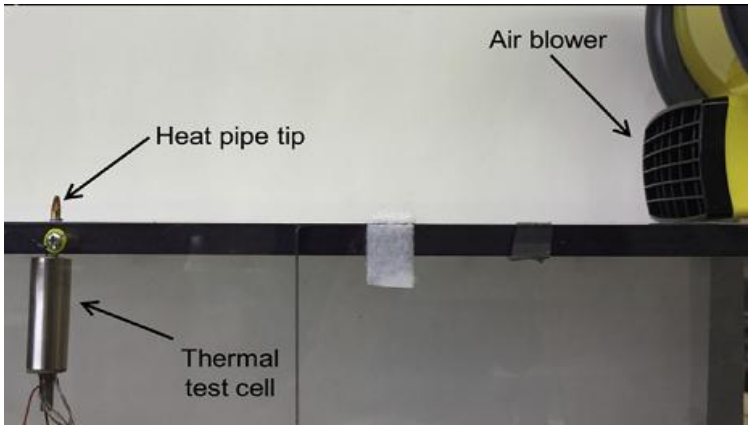

Figure 2.17: Heat pipe insertion in the annular region of cell [131]

Chen et al. [183] (2017) optimized the cell spacing of air-cooled BTMS with the aim to minimize temperature rise of battery cells. The battery pack and air-cooled TMS developed is shown in Figure 2.18. The optimization strategy proposed was utilizing "flow resistance network model" and "heat transfer model". Their optimization technique used increased the spacing around the cells with highest temperature while spacing around the cells with lowest temperature was reduced. Results showed that after optimization temperature uniformity improved by 29% with slight reduction in maximum temperature was observed with no significant increment in pressure drop.

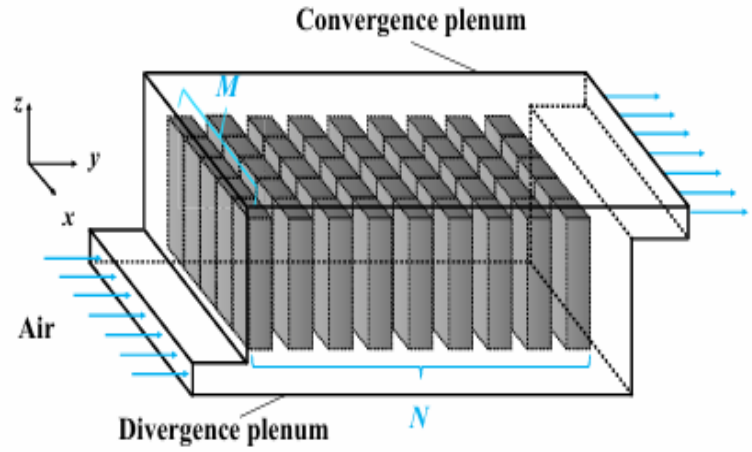

Figure 2.18: Schematic of air-cooled thermal management[189]

Worwood et al. [125] (2017) presented an approach for heat extraction management of cylindrical lithium-ion cells. The cylindrical cells were cooled internally rather than conventional surface cooling methods. Heat pipe was utilized and placed inside the mandrel of cylindrical battery cell. Heat spreader disc of thickness 2 mm and 3mm were connected to evaporator and condenser side of heat pipe which was cooled by active cooling system. Two

different cell types were used in the research:18650 and 32113 li-ion cells. Results from the work indicated that heat pipe successfully increased the heat transfer rate. But addition of spreader disc to the cylindrical cell reduced energy density and increased the mass of cells. Addition of spreader disc of 2 mm and 3 mm reduced the energy density of 18650 cell by 5.8% and 11.7% respectively. For 32113 cells the energy density for 2 mm and 3 mm thickness were recorded as 6.0% and 10.0% respectively. The degree of cooling can be increased by using forced liquid cooling application to evaporator section of heat pipe.

Smith et al. [184] (2018) proposed a BTMS for high heat load (up to 400 W) with heat pipe as heat extraction medium. The module was fabricated of eight prismatic high-power batteries. The proposed design consisted of cooling plates, interface plate, heat pipe and liquid cooled plate (see Figure 2.19). The plates connected to heat pipe are inserted between prismatic batteries cooled the cells and transferred heat to interface plate. The remote heat pipes connected interface plate with liquid cooled heat dissipation plate. The proposed BTMS controlled the temperature below 55°C with 1 litre/minute of coolant flow at 25°C inlet temperature. They cooling system was successful in maintaining temperature uniformity within prismatic module to below 5°C. They concluded that the proposed system could provide high performance cooling and safety with simple design solution for automotive industry.

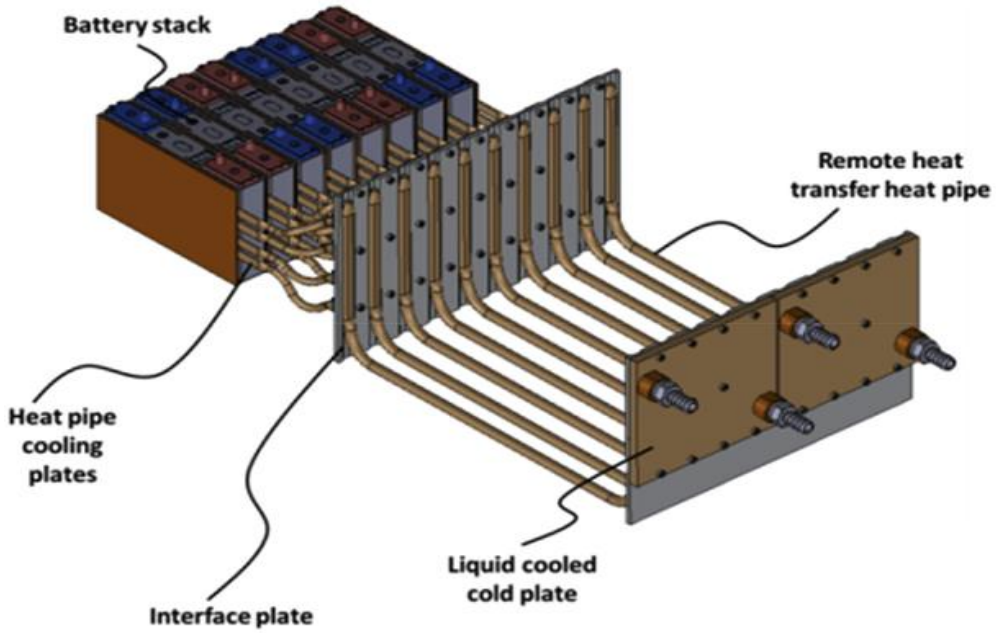

Figure 2.19: : Heat pipe-based battery thermal management system with heat pipe cooling plates [190]

Hong et al. [185] (2018) in their paper presented a method to improve performance of commonly used air cooling using secondary air vent. The effected of vent position and its size were investigated through numerical case with results indicating that performance is strongly affected by position of vent. In their study, a model to calculate unsteady heat generation (Q_u) for Lithium Iron Phosphate battery of 2.2Ah capacity as given by Eq. 2.1 was presented. Cell internal resistance was calculated using state of charge (SOC) and measured cell temperature (T_{cell}).

$$Q_u = \frac{I^2 R}{V} \tag{2.1}$$

Where $R = 27.54 - 27.68 \times e^{(-1.91\backslash T_{cell})} + \frac{223.71}{1+21.61\times SOC} - 225.06 \times \frac{e^{(-1.91\backslash T_{cell})}}{1+21.61\times SOC}$

Mathematical analysis of presented in research showed that that maximum temperature and temperature uniformity in an EV are not affected by air inlet temperature rather they are strongly correlated with heat generation rate. It can be concluded from their study that proper selection of air vent position and air flow velocity are important to improve cooling rate of air-cooled thermal management systems. There was 60% reduction in maximum temperature by use of vents under same working conditions and results are improved as secondary vent size is increased.

Liang J et al. [186] (2018) in their research investigated the effects of coolant inlet temperature and mass flow rate, the temperature of ambient air, and time of start-up on the performance heat-pipe based BTMS. Their experimental facility consisted of a circulating bath for cooling and heating, a power supply to simulate heat generation of battery, data acquisition system, a pump, valve, and a flow meter. The results showed that the thermal performance improved at reduced coolant temperature and increased coolant flow rate. The intermittent cooling proposed was able to keep temperature uniformity and peak temperature under control with only slight performance difference as compared to continuous cooling. The intermittent cooling was successful in achieving nearly same performance with significant reduction in power consumption.

Amin M et al. [187] (2018) proposed a BTMS using L-type heat pipe (HP) and phase PCM for heat management of li-ion batteries. In the developed cooling system, the heat pipe served as

heat transfer device while PCM was used as a hint sink. Equipment use for fabrication of hybrid cooling system are shown in Figure 2.20. The PCM used was beeswax having melting point of 62.28 °C and 141.49 kJ/kg latent heat. The main objective of study was to evaluate the performance of hybrid cooling system at 50°C temperature at varying heat load from 20 W to 50 W and at air velocity 2.4 m/s. There was significant drop in maximum temperature observed for batteries in case heat pipe and PCM based hybrid cooling.

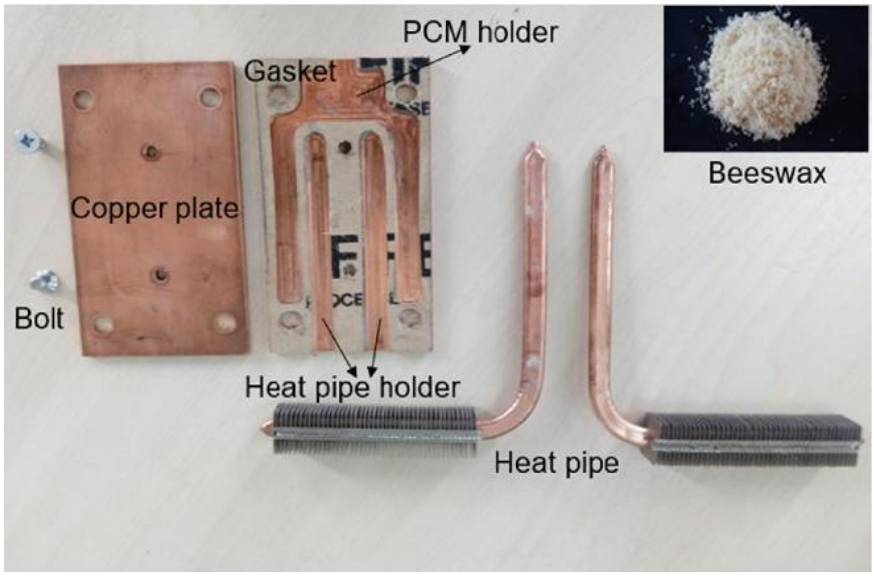

Figure 2.20: Equipment used for fabrication of hybrid heat pipe and PCM based thermal management system[193]

Jiang et al. [188] (2019) proposed a BTMS based on heat pipe and PCM as heat extraction units. The developed sandwiched design can be seen in Figure 2.21. In their research, a lumped thermal model validated by experimental data was proposed for cooling structure. The effect of various environmental conditions, thickness ratio of PCM and cell and heat transfer coefficient at heat rejection site i.e. heat pipe condenser section on performance of proposed coupling mechanism was revealed. The coupling of PCM with heat pipe ensured that latent heat of PCM is recovered after every charge/discharge cycle. It can be concluded from their results that to ensure proper functioning of battery within optimum temperature range and to ensure long cycle life of cells, the PCM solid to liquid phase change temperature should be 3°C above environmental temperature with thickness ratio and phase change ratio of 0.17 and 0.55 respectively. The heat pipe condenser section heat transfer coefficient recommended in the research were between 30W/m^2 to 60 W/m^2. Their proposed lumped thermal model can be used for battery packs consisting of hundreds or thousands of cells.

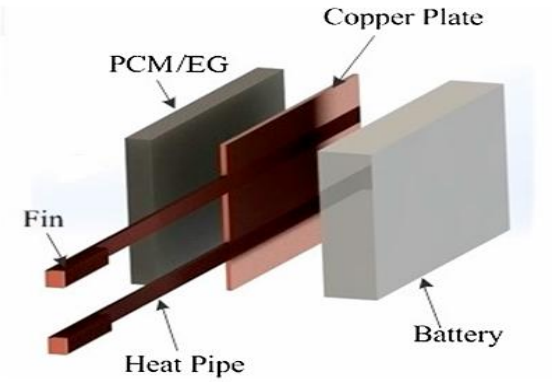

Figure 2.21: Sandwiched design of thermal management module[194]

Wei et al.[189] (2019) developed and experimentally tested "oscillating heat pipe (OHP)" based thermal management of electrical vehicle. The experimental facility mainly consisted of sandwiched OHPs between heating, cooling and data acquisition system. The OHPs were tested at different proportions of water to ethanol mixing ratio (MR) ranging from 1:1 to 4:1 and at three different volumetric fill ratios (FR): 30%, 40% and 50%. For reference, OHPs were first tested under three different conditions: zero filling ratio, pure water filling and pure ethanol filling. The performance of OHPs were affected by both fill ratio (FR) and mixing ratio (MR). The mixtures showed better results, especially at MR of 1:1 and FR 30%, as compared to pure water and ethanol. The "sandwich" designed developed using OHP for battery can be seen in Figure 2.22. The results showed that the "novel plug-in OHP" was able to control temperature below 46.5°C with improved temperature uniformity of 1-2°C.

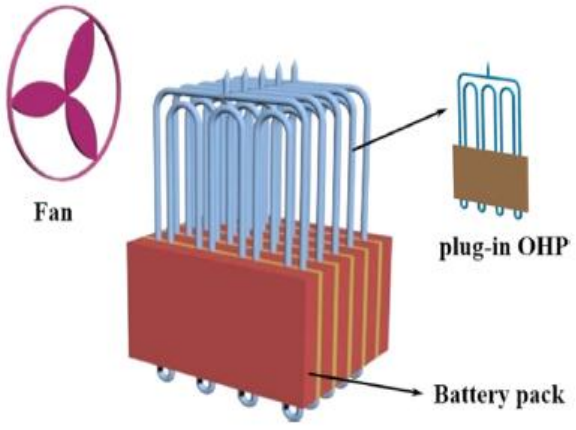

Figure 2.22: Schematic diagram of plug-in OHPs (oscillating heat pipes) based BTMS[195]

Wang J et al. [190] (2019) proposed a heat pipe assisted system for cylindrical li-ion cells. The selected li-ion cells were 18650 cells with nominal voltage of 3.7 V and capacity of 1.96 Ah. CFD model was developed using ANSYS Fluent software to investigate influential factors and

their sensitivity with temperature distribution of cells. The CFD model was validation with experimental results (see Figure 2.23). The cell spacing, circumference contact angle between cell and heat pipe conduction element, height and thickness of conduction element were selected as influential factors and their effects on cooling performance were investigated at 3C and 5C rates. Numerical analysis was carried out for only one conduction element, and it was assumed that cylindrical cells are isotropic, heat pipe has high thermal conductivity, there is no relative slip between fluid and solid surface, water is incompressible ideal fluid. The results from their study showed that most sensitive parameter effecting temperature and uniformity of EV was conduction element height, then second most sensitive was circumference contact angle, while thickness of conduction element and cell spacing were least sensitive and produced minimal effect.

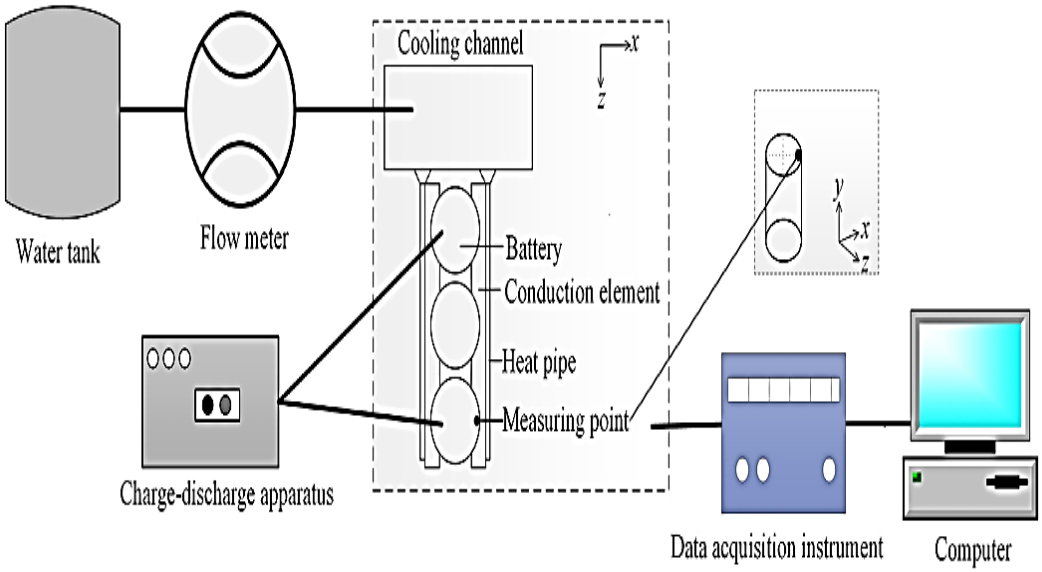

Figure 2.23: The experimental setup[196]

Behi et al. [124] (2020) identified critical zones in a single battery cell during heat generation. Their analysis showed that one heat pipe if mounted on critical region can sufficiently work for heat management of cell as it provided up to 29.1% of the required cooling load (see Figure 2.24). Three different cooling strategies were evaluated for thermal management of prismatic battery: natural convective (air), liquid cooling, and liquid cooling assisted by heat pipe (LCHP). The LCHP provided better results as compared to natural cooling and liquid cooling. The maximum temperature as compared to natural air cooling was respectively 32.6% and 29.9% lower in LCHP and liquid cooling.

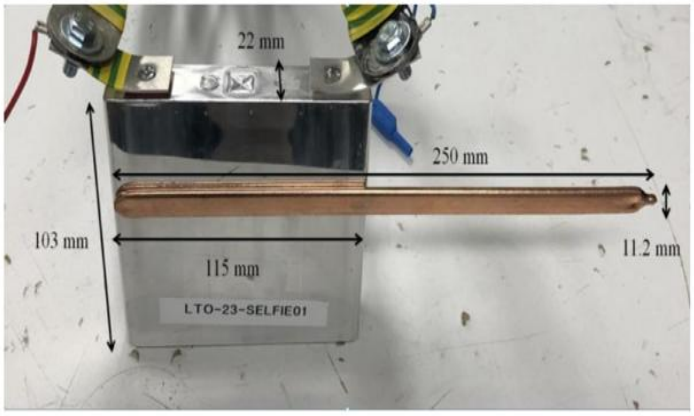

Figure 2.24: Single heat pipe installed at critical region of prismatic cell[129]

Gan et al.[127] (2020) developed a copper made heat pipe for thermal management of cylindrical batteries as shown in Figure 2.25. To improve contact area, aluminium made conduction elements were placed between cylindrical cell and condenser part of heat pipe. The model used thermal grease of about 0.3 mm to increase thermal conduction between cell and conduction element. Effect of discharge rate, air velocity and coolant temperature on the cooling performance of proposed BTMS were experimentally investigated and results showed that cell temperature when compared with natural convection was reduced by 14 °C at 5 C-rate. For development of temperature control strategies, real prediction and analysis of battery packs, a “thermal equivalent circuit” was proposed in the research.

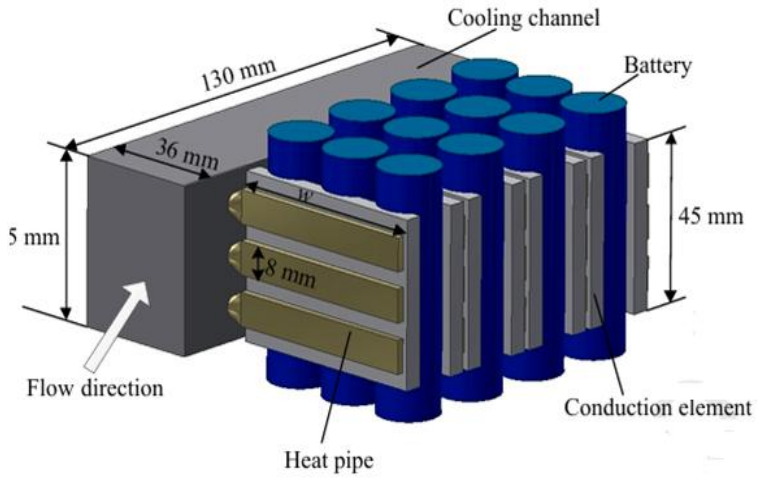

Figure 2.25: Schematic of heat pipe based thermal management system for cylindrical batteries [132]

Behi et al. [128] (2020) presented the concept of improved BTMS with air-cooling and heat pipe. Their proposed design consisted of copper sheet as interface medium between cells and heat pipe. This design was called “Heat Pipe Copper Sheet (HPCS) model”, and it is shown in Figure 2.26. The mathematical and thermal modelling of battery pack having 24 cylindrical 18650 li-ion cells was conducted and four convective cooling mechanism: natural or free, forced, L-shaped heat pipe and HPCS were analysed for performance. Three different test scenarios were presented in the research paper. In the first scenario, natural and forced air cooling were examined for peak temperature. Second scenario was related with forced air cooling at varying cell spacing, ambient temperature and air velocity to achieve better temperature uniformity. In the third scenario comparative analysis of the peak temperature of cells and temperature uniformity of pack in natural convection, forced convection, L-shaped heat pipe and HPSC model. The results showed that there was about 73%, 66% and 39% reduction in temperature difference and 43%, 42%, and 34% reduction in maximum temperature in HPCS, L-shape heat pipe and forced air-cooling as compared to natural convection.

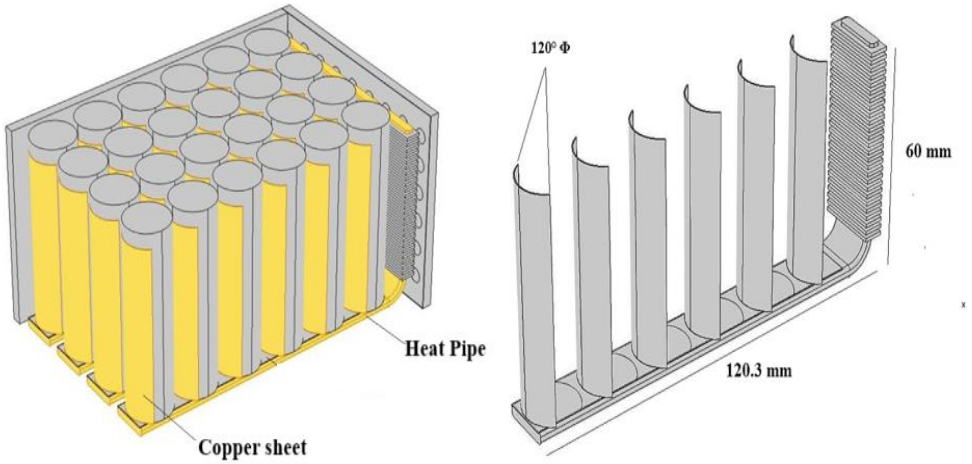

Figure 2.26: Heat Pipe Copper Sheet (HPCS) based thermal management model[133]

Lei S et al. [191] (2020) analysed a thermal management system with heat pipe. Two Lithium Iron Phosphate batteries were used in parallel connection for experimental study. The flattened evaporator part of heat pipe sintered with copper powder was sandwiched between batteries while the condenser cylindrical section was cooled in a spray tank. The cooling performance was investigated at different inlet air velocities, relative humidity values and spraying frequencies. The main objectives of their research were to investigate feasibility, thermal characteristics of li-ion battery and effectiveness of proposed heat-pipe based BTMS. The

batteries were discharged at two different rates: 1C and 1.92C. The developed model used air cooling and water spray as cooling mechanism. The water spray was used in an intermittent manner, and it is only activated after battery temperature reached temperature of 40°C. Results showed that insertion of heat pipe improved the cooling performance. The difference in temperature inside pack and peak temperature were reduced by 8.0°C and 29.2°C respectively in comparison to conventional cooling system. Their research showed that heat pipes are reliable and their application in battery thermal system can improve battery life and performance of cooling systems.

Waldmann T et al. [89] (2020) carried out comparative analysis of popular li-ion 18650 cells and new geometry li-ion 21700 cells in terms of thermal, electrochemical, geometrical properties, effect of electrode curvature and cyclic ageing. The new 21700 cells were made from same electrode, electrolyte, and separated material as was used for 18650 cells. The voltage curves at discharge process indicated similarity of both cells at low discharge rates 0.1C and 0.5 C but due to increased polarization of 18650 cells, curves deviate at high discharge rates. The discharge capacity of 21700 cells was observed to be about 50% higher than 18650 cells between 0.5C and 3.75C discharge rates. It has observed in the results that the extension of diameter in 21700 cells positively affect energy density of cells with about 6% increase as compared to 18650 cells. The energy density or specific capacity in there was about 6% higher for 21700 cells as compared to 18650 cells. The effect of increased cell diameter was evaluated for larger cells like 30700 were also estimated. Increased diameter showed a positive impact of energy density of cell.

Patil et al. [192] (2021) presented in their research a direct immersion cooling technology which was assisted by forced air tab cooling (see Figure 2.27). They used dielectric fluid as cooling media and Lithium-ion pouch batteries are directly immersed in dielectric. When the performance of dielectric immersion cooling with assisted forced air tab cooling was compared at discharge rate of 3C with natural cooling, the results showed 46.8% reduction in maximum temperature at the positive tab. Their proposed dielectric direct cooling method achieved better control of maximum temperature having 9.3% lower value than conventional indirect cooling. The results showed that direct tab cooling can prevent thermal run away of battery pack under internal short circuit condition when temperature was as high as 341.7°C. The investigated direct dielectric cooling technology with assisted forced air tab cooling can be used as battery

thermal management technology for high capacity and high-density battery cells of electric vehicles.

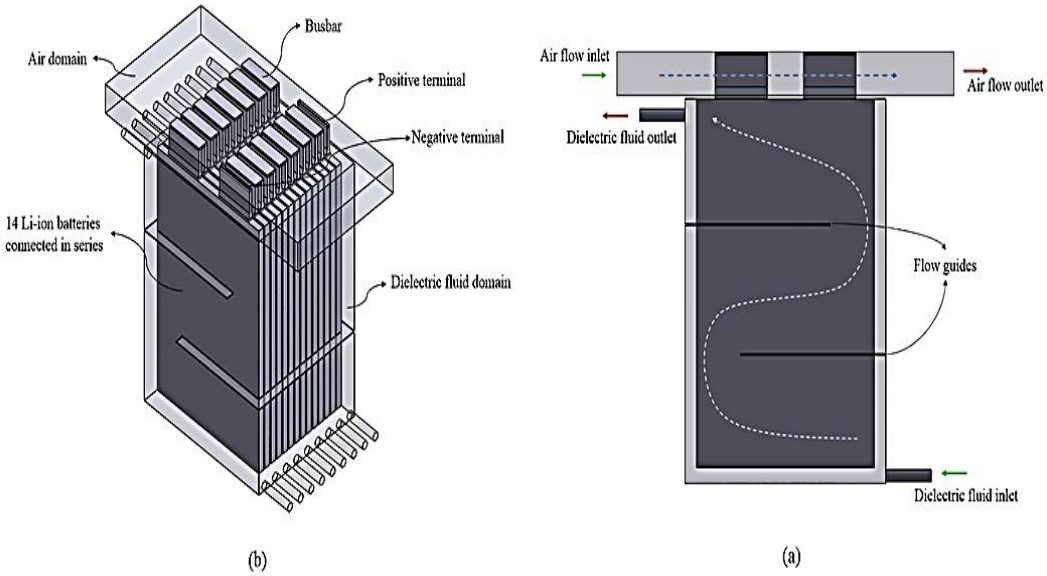

Figure 2.27: Dielectric fluid immersion technology[198]

Milan Vachhani et al. [193] (2023) developed and investigated the performance of a novel "Single Evaporator Loop Heat Pipe (SE-LHP)" based BTMS. As compared to traditional heat pipe, LHP are more efficient and capable of transferring heat over large distances. The battery module developed had twelve 18650 type cells and it was tested under 1C, 1.5C and 2C charge/discharge conditions. The testing was performed at different ambient temperature between 30°C to 45°C showed that SE-LHP thermal management system was able to lower the maximum temperature of cells as compared to without BTMS case. The drop in temperature at 35°C ambient temperature FOR 1C, 1.5C and 2C discharge rate were 15%, 16.4% and 16.29% respectively. The results indicated that SE-LHP BTMS also improved discharge capacity of cells with 2% and 3% increase in state of charge (SOC) at 1.5C and 2C discharge rates. Temperature uniformity improvement was also recorded, and results indicated improvement in evenness of temperature across battery module. The temperature difference measured across battery module was maximum 2.43°C and 3.38°C for all charge and discharge rates respectively.

Burkitbay A et al. [194] numerically investigated the performance of a novel hybrid cooling system utilizing a heat-pipe in vertical orientation at varying discharge rates up to 8C. A staggered arrangement of gravity assisted heat pipes was used to improve performance of

forced convection (see Figure 2.28). The design allowed maximizing the heat flow rate and was proposed to overcome lack of perfect contact between cylindrical cells and round heat pipe. The tests were performed at varying discharge rates of 4C and 8C, and at varying coolant temperature of 15°C, 20°C and 25°C. The proposed hybrid cooling system while working with coolant at temperature 25 °C, maintained the surface temperature of cell and temperature difference within battery pack at about 64 °C and 2.5 °C respectively.

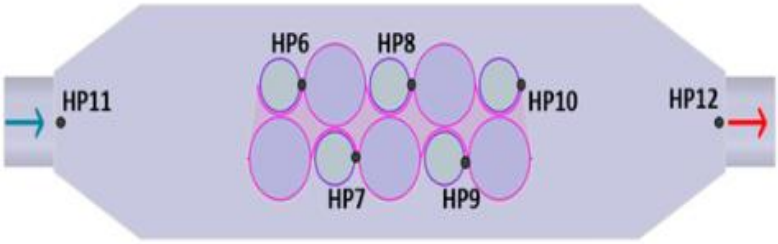

Figure 2.28: Staggered arrangement of gravity assisted heat pipes

Shengshi Wang et al. [195] (2024) proposed a L-shaped heat pipe as a combination with air cooling and investigated cooling performance of system under varying discharge rates between 1C and 3.5C. A CFD model of pack was developed with NTGK method. The two phase heat transfer mechanism in heat pipe and Volume of fluid (VOF) method was used to simulate heat transfer mechanism. The temperature difference between electrode and cell surface was also investigate. The analysis revealed that once after reaching dynamic equilibrium, the heat transfer coefficient values reached up to 4000 W/m^2K. Their approach to utilize of cold air of air conditioning system was successful in achieving ideal temperature control and minimized temperature difference across battery module. The heat generation at various C-rates and air inlet velocity as calculated during investigated is given in Table 2.1.

Table 2.1: Discharge rate, heat generation and inlet air velocity [195]

Discharge rate	Heat generation (W)	Inlet velocity of air (m/s)
1C	8.4	0.9
1.5C	19.9	0.9
2C	36.1	2.2
2.5C	57.1	2.2
3C	82.9	3.7
3.5C	113.6	3.7

Patil S et al. [196] (2024) conducted a CFD-based study and investigated the role of cylindrical heat pipes in BTMS under varying heat loads of 30W, 45W, 60W and 80W. The results showed that the heat pipes performed better as battery heat generation rises (see Figure 2.29), since the working fluid reaches the required phase-change temperature and enhances heat removal efficiency. The lowest and highest temperature of 35°C and 78°C respectively were obtained in a 30 W system with a star-shaped heat pipe and at 80 W without any heat pipe. Their findings emphasized that battery systems producing 80 W or more must not operate without heat pipe integration, as this leads to overheating, potential shell damage, and system failure. The study concluded that heat pipes are indispensable for ensuring safe and reliable operation in high-power applications, with conductance that adapts to increasing thermal loads. Furthermore, it highlighted the importance of continuous development of heat pipe designs and configurations to optimize temperature regulation in electric vehicle battery packs, thereby extending operational life and preventing catastrophic failures.

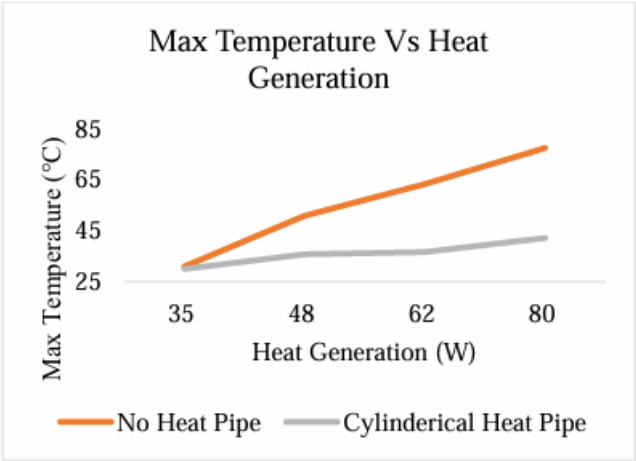

Figure 2.29: Temperature profile vs Heat generation[196]

Zhu F et al. [197] (2024) In their work, studied the performance of flat heat pipe (FHP)-based BTMS under discharge rates of 1C, 2C, and 3C, with the operating conditions set at an initial temperature of 20 °C, an SOC of 0.9, and 80% depth of discharge. A coupled thermo-electrical model was developed to link the heat generated during electrochemical reactions with the heat transfer characteristics of the FHP, and its accuracy was validated through experimental testing. The findings demonstrated that incorporating flat heat pipes significantly lowered the maximum battery temperature while improving both temperature uniformity and SOC balance across the module. It was further observed that a reduction in vapor chamber thickness increased vapor thermal resistance, leading to higher maximum temperatures, larger

temperature gradients, and non-uniform internal resistance, which in turn produced uneven current distribution. To overcome these limitations, the study introduced an optimization approach that considered vapor chamber thickness, overall thickness, and heat pipe length as key design parameters. With this optimization, the modified FHP system achieved a 6.4% reduction in maximum temperature, an 18.4% reduction in maximum temperature difference, and a 16.3% reduction in SOC variation compared to the baseline design, thereby confirming the potential of optimized FHP structures to enhance the thermal and electrochemical performance of EV battery packs.

Lu H et al. [198] (2024) experimentally evaluated a hybrid BTMS combining oscillating heat pipe (OHP) technology with liquid cooling, achieving superior thermal regulation compared to conventional systems. A filling ratio of 26.1% was found optimal, with acetone providing effective heat transfer at low loads and acetone–ethanol mixtures reducing temperature fluctuations. The ⊥-shaped OHP improved heat dissipation under high loads, extending the system's heat transfer capacity from below 100 W to over 280 W. Compared with liquid-only BTMS, the hybrid reduced ΔTmax and RBTMS by 19.1% and 8.06% at 280 W, while graphene nanofluid further enhanced performance, lowering ΔTmax by 32.7% and RBTMS by 20.1%. These results highlight the hybrid BTMS as a reliable solution for high-power battery applications, with future research needed on large-scale designs and long-term operational stability.

Maalej S et al. [199] (2025) study on battery thermal management systems (BTMS) combining heat pipes and cold plates have demonstrated their ability to dissipate heat loads up to 40 W while keeping cell temperatures below the safety threshold of 60°C. Their experimental findings showed that the maximum heat transport capacity increases with rising heat input, accompanied by a reduction in thermal resistance until the capillary limit is reached. Heat pipes exhibit significantly higher thermal conductance of up to 4.6 times that of copper rods. The CFD simulations and infrared (IR) measurements showed strong agreement with experimental data, confirming both the accuracy of modelling approaches and the practical suitability of heat pipes for battery cooling applications.

2.2 Summary of literature review

Table 2.2: Summary: Literature review

Sr. No.	Author	Year	Remarks
1	Strumpf H et al.	1982	Bank of tubes using heat pipes were used for furnace heat recovery system. It was observed that by use of heat pipes in heat recovery system, the saving in fuel cost is about 40% to 50%.
2	M. Broussely et al.	1991	Concluded that a battery must fulfil two important parameters to be suitable for electrical vehicles: (i) safety, and (ii) low manufacturing, maintenance and operational cost which include reliability and better cycle life.
3	Chau K et al.	1999	Reviewed various potential energy sources of electrical vehicles. Although no battery type satisfied all the criteria of selection, but li-ion batteries emerged as potential battery of EV application.
4	Ramadass P et al.	2002	Capacity fade analysis during discharge process at elevated temperatures for Sony 18650 Li-ion cylindrical cells were carried out at rates from C/9 to 1C at three different temperatures :45°C, 50°C and 60°C. At elevated temperatures, high-capacity losses were observed due to formation of film over anode surface resulting in lithium loss and increased resistance of negative electrode.
5	Yimin Xuan et al.	2004	A flat plate heat pipe performance was investigated experimentally and theoretically under different orientations, heat fluxes and amount of heat pipe working fluid. The results showed that performance of flat heat pipe is affected by orientation, working fluid amount and geometrical parameters of heat pipe.
6	Amine K et al.	2005	Research was focussed on capacity fading and cycling characteristics of prismatic Lithium Iron Phosphate (LFP) batteries at high temperature. Battery was charged and discharged at C/3 rate for number of cycles and results showed

			significant drop in capacity with increasing number of cycles at 55°C and 37°C as compared to 25°C.
7	Kong et al.	2005	The gas generation behaviour and swelling of three different 18650 cell chemistries viz. LiCoO2, $LiMn_2O_4$, and $LiFePO_4$ were investigated. The results indicated that cathode material has no significant effect on gas generation under normal charge and discharge conditions. While when cells are overcharged, cathode material started significantly affecting the type and amount of gas generation.
8	Inui Y et al.	2007	To study temperature distribution under transient discharge conditions, 2D and 3D simulation models for li-ion cylindrical cell were developed. The results showed that under similar conditions, capacity and volume of cell, laminated cylindrical cells perform better than prismatic cells.
9	Robak C et al.	2011	The possibility of utilizing heat pipes and fins for improvement of latent heat storage materials (PCM) was investigated. The performance of heat pipe while charging and discharging of PCM was better as compared to fins. Results showed that by heat pipe inclusion, PCM melting rates increased by 60% and during solidification process heat transfer was doubled between PCM and cooling fluid as compared to non-heat pipe configuration.
10	Ying-Che Weng et al.	2011	A hybrid electronic cooling system based of heat pipe and phase change material was developed. Three different strategies to improve cooling performance were tested. First method utilized doubling the number of fins at condenser section, second method increased contact area of heat pipe by increasing diameter of heat pipe and third method was based on utilizing higher conductivity PCM material.
11	Rao et al.	2013	A thermal management system for EVs was proposed which consisted of four heat pipes and thermal silica as interface material between cell and heat pipe. desired performance of controlling maximum temperature within 50°C.

12	Tran et al.	2014	A flattened heat pipe based thermal management system was compared to conventional heat sink cooling method for hybrid electrical vehicles was investigated. The proposed design consisted of batteries packed in a non-conductive resin matrix. The results indicated that by utilization of heat pipes, heat sink thermal resistance reduced by 30% in free convection, and 20% in low velocity (windy conditions), and temperature was controlled below 50 °C. It was shown that heat pipes can be used at various inclination angle from horizontal to vertical.
13	Wang et al.	2014	The thermal performance of three different cell arrangements: rectangular, hexagonal and circular, was investigated at varying fan installation position. Middle cells were at higher temperature as compared to other surrounding cells under free convection in rectangular arrangement. Their results indicated that: 1) fan at top arrangement gave best cooling performance, 2) cubic structure is most cost effective and gave best cooling performance, 3) hexagonal cell arrangement has better space utilization.
14	Greaco A et al.	2014	A simplified computational model for prismatic li-ion battery based on thermal circuit model was proposed. A sandwiched model of prismatic battery and heat pipes was developed. The results showed that heat pipes produce better results as compared to forced convection owing to their higher surface area and it was concluded that heat pipes can be used in confined spaces and are effective as thermal management system.
15	Zhao et al.	2015	A BTMS utilizing ultrathin heat pipes was developed for thermal surge conditions of li-ion batteries. Heat pipes were sandwiched between batteries and study was carried out under free convection cooling, forced air cooling, and wet cooling conditions. A combination of free, forced convection and wet cooling with intermittent water sprays proposed was able to maintain temperature uniformity and peak temperature within optimum operating conditions.

16	Zhao et al.	2015	Two methods of improving thermal performance of li-ion batteries were discussed. One was based on electrode modification of cell and other was utilization of thermal management system. It was concluded that temperature rise of batteries has strong relation with charge/discharge rate. Although thermal management system increases about 10% to 20% cost of electrical vehicles but by its utilization more energy dense batteries can be utilized.
17	Yuan et al.	2016	Thermal analysis of a self-designed heat pipe assisted BTMS was investigated. The cooling module is integrated with commercially available Lithium Iron Phosphate ($LiFePO_4$) having capacity of 10 Ah. The cooling method was able to control temperature with optimum temperature between 32.2°C and 27.6°C respectively. The results showed that surface temperature of cell in contact with heat pipe was at lower temperature as compared to other locations of cells.
18	Putra et al.	2016	A performance analysis of a "flat plate loop heat pipe (FPLHP)" based system was experimentally investigated. The performance of three different working fluids: distilled water, acetone, and alcohol, at 60% fill ratio. The results indicated that acetone gave better performance with heat flux load of 1.61 W/cm^2 and thermal resistance of 0.22 W/°C at 50°C evaporator side temperature.
19	Y. Ye et al.	2016	An optimized BTMS for fast charging of prismatic lithium-ion battery cell/pack was proposed. The HPTMS developed was tested at various C-rates and results showed that improved design with fins added to condenser section was able to handle twice the heat generated at 8 C charging rate. They proposed a "quench strategy" to improve cooling system performance by cooling battery pack at 25°C with coolant at 15°C. Their improved design was able to maintain battery pack with optimum range of 25°C to 40°C.

20	Shah et al.	2016	Two different approaches were studied for cooling of lithium-ion batteries: (i) air cooling by air flow through the annular channel, and (ii) insertion of heat pipe in the channel and cooling heat pipe tip with air flow. Experiment results showed that with heat pipe insertion there is 18-20°C drop in core temperature of cell. Heat pipe was successful in preventing thermal runaway and short-circuiting under stress conditions.
21	Chen et al.	2017	The cell spacing of air-cooled BTMS was optimized with aim of restricting maximum temperature rise of battery cells. The proposed optimization strategy increased spacing around the cells with highest temperature while spacing around the cells with lowest temperature was reduced. Results showed that after optimization temperature uniformity improved by 29% with slight reduction in maximum temperature was observed with no significant increment in pressure drop.
22	Worwood et al.	2017	A novel approach to cool cylindrical cells internally rather than conventional surface cooling methods was presented. Heat pipe was utilized and placed inside the mandrel of cylindrical battery cell. Two different cell types were used in the research:18650 and 32113 li-ion cells. Results showed that heat pipe successfully increased the heat transfer rate, and the degree of cooling can be increased by using forced liquid cooling application to evaporator section of heat pipe.
23	Smith et al.	2018	The proposed design consisted of heat pipe cooling plates inserted between prismatic batteries. The proposed BTMS was able to keep maximum temperature below 55°C with 1 litre/minute of coolant flow at 25°C inlet temperature. They cooling system was successful in maintaining temperature uniformity within prismatic module to below 5°C. They concluded that heat pipe-based thermal management system can provide high performance cooling and safety with simple design solution for automotive industry.

24	Hong et al.	2018	A method to improve the performance of commonly used air cooling using secondary air vent was presented. Results indicated that the performance of air cooling is strongly affected by vent position and its size. Mathematical analysis conducted in the research work proved that the maximum temperature and temperature difference in battery module are not affected by air inlet temperature rather they are strongly correlated with heat generation rate. There was 60% reduction in maximum temperature by use of vents under same working conditions and results are improved as secondary vent size is increased.
25	Liang J et al.	2018	The effects of various parameters mass flow rate and temperature of coolant, ambient temperature, and time of start-up, on the performance heat-pipe based BTMS was investigated. The results showed that the thermal performance improved at reduced coolant temperature and increased coolant mass flow rate. The intermittent cooling was proposed, and it was able to keep temperature uniformity and peak temperature under control with only slight performance difference as compared to continuous cooling.
26	Amin M et al.	2018	A hybrid cooling system using L-type heat pipe (HP) and PCM for li-ion batteries was proposed. In the developed cooling system, the heat pipe served as heat transfer device while PCM was used as a hint sink. As observed from results, the use of heat pipe and PCM kept the surface temperature of cell below 50 °C, at heat load range of 20 - 50 W. There was drop in peak temperature of batteries in case heat pipe and PCM based hybrid cooling. The paper proposed use of heat pipe and PCM as alternative cooling system for battery thermal management.
27	Jiang et al.	2019	A battery thermal management system based on heat pipe and phase change material (PCM) as heat extraction units was proposed. The effect of various environmental conditions, thickness ratio of PCM and heat transfer coefficient at heat rejection site was revealed. It can be concluded from their results

			that to ensure proper functioning of battery within optimum temperature range and to ensure long cycle life of cells, the PCM melting temperature should be 3°C above environmental temperature with thickness ratio and phase change ratio of 0.17 and 0.55 respectively. The heat pipe condenser section heat transfer coefficient recommended in the research were between 30W/m^2 to 60 W/m^2.
28	Wei et al.	2019	A "oscillating heat pipe (OHP)" based thermal management of electrical vehicle was developed and experimentally tested. The experimental facility mainly consisted of sandwiched OHPs between heating unit, a cooling unit, and data measurement system. The OHPs were tested at different proportions of water to ethanol mixing ratio (MR) ranging from 1:1 to 4:1 and at three different volumetric fill ratios (FR): 30%, 40% and 50%. The results showed that the "novel plug-in OHP" was able to control maximum temperature below 46.5°C with improved temperature uniformity of 1-2°C.
29	Wang J et al.	2019	A heat pipe based thermal management system for cylindrical li-ion cells was proposed. The selected li-ion cells were 18650 cells with nominal voltage of 3.7 V and capacity of 1.96 Ah. The cell spacing, circumference contact angle between cell and heat pipe conduction element, height and thickness of conduction element were selected as influential factors and their effects on cooling performance were investigated at 3C and 5C discharge rates. The results from their study showed that most sensitive parameter effecting maximum temperature and temperature uniformity of battery module was conduction element height, then second most sensitive was circumference contact angle, while thickness of conduction element and cell spacing were least sensitive and produced minimal effect.
30	Behi et al.	2020	An analysis was conducted for li-ion cell to identify the most critical zone under stress in terms of heat generation was conducted. Their analysis allowed them to maximize heat

			dissipation with only one heat pipe mounted on the vital region. Three different cooling strategies were evaluated for thermal management of prismatic battery: natural air cooling, liquid cooling, and heat pipe embedded liquid cooling. The heat pipe assisted liquid system (LCHP) provided better results as compared to natural cooling and liquid cooling.
31	Gan et al.	2020	A copper heat pipe based thermal management system for cylindrical batteries was developed. To improve contact area, aluminium made conduction elements were placed between cylindrical cell and condenser section of heat pipe. The model used thermal grease of about 0.3 mm to reduce thermal resistance between cell and conduction element.
32	Behi et al.	2020	A hybrid BTMS based on air-cooling and heat pipe was presented which consisted of copper sheet made interface medium placed between battery cell and heat pipe. The mathematical and thermal modelling of battery pack consisting of 24 cylindrical li-ion cells of type 18650 was done to investigate the performance of four cooling mechanism: natural convection, forced convection, L-shaped heat pipe and HPCS. The results showed that there was about 73%, 66% and 39% reduction in temperature difference and 43%, 42%, and 34% reduction in maximum temperature in HPCS, L-shape heat pipe and air-cooled forced convection as compared to natural convection.
33	Lei S et al.	2020	Two Lithium Iron Phosphate batteries were used in parallel connection for experimental study. The flattened evaporator section of heat pipe sintered with copper powder was sandwiched between batteries while the condenser cylindrical section was cooled in a spray tank. The main objectives of their research were to investigate feasibility, thermal characteristics of li-ion battery and effectiveness of proposed heat-pipe based BTMS. The batteries were discharged at two different rates: 1C and 1.92C. Results showed that insertion of heat pipe improved the performance of thermal management system. The maximum

			temperature difference and maximum temperature were reduced by 8.0°C and 29.2°C in comparison to conventional cooling system.
34	Waldmann T et al.	2020	A comparative analysis was carried out of popular li-ion 18650 cells and new geometry li-ion 21700 cells in terms of thermal, electrochemical, geometrical properties, effect of electrode curvature and cyclic ageing. The discharge capacity of 21700 cells was observed to be about 50% higher than 18650 cells between 0.5C and 3.75C discharge rates. It has observed in the results that the extension of diameter in 21700 cells positively affect energy density of cells with about 6% increase as compared to 18650 cells. The effect of increased cell diameter was evaluated for larger cells like 30700 were also estimated. Increased diameter showed a positive impact of energy density of cell.
35	Patil et al.	2021	A direct immersion cooling technology using dielectric fluid as cooling media was proposed in which lithium-ion pouch batteries were directly immersed. Their proposed dielectric direct cooling method achieved better control of maximum temperature having 9.3% lower value than conventional indirect cooling. The results showed that direct tab cooling can prevent thermal run away of battery pack under internal short circuit condition when temperature was as high as 341.7°C. The investigated direct dielectric cooling technology with assisted forced air tab cooling can be used as battery thermal management technology for high capacity and high-density battery cells of electric vehicles.
36	Milan Vachhani et al.	2023	A novel “Single Evaporator Loop Heat Pipe (SE-LHP)” based BTMS was investigated. The module with twelve 18650 type li-ion cells was tested at 1C, 1.5C and 2C rates under charge and discharge processes. The testing performed at varying ambient temperature between 30°C to 45°C showed that SE-LHP thermal management system was able to lower the maximum temperature of cells as compared to without BTMS case. The drop in

			temperature at 35°C ambient temperature for 1C, 1.5C and 2C discharge rate were 15%, 16.4% and 16.29% respectively. Temperature uniformity improvement was also recorded, and results indicated improvement in evenness of temperature across battery module.
37	Burkitbay A et al	2023	Numerical analysis was conducted to evaluate the performance of a novel hybrid cooling battery thermal management system utilizing a heat-pipe in vertical orientation at varying discharge rates up to 8C. A staggered arrangement of gravity assisted heat pipes was used to improve performance of forced convection. The tests were performed at varying discharge rates of 4C and 8C, and at varying coolant temperature of 15°C, 20°C and 25°C. The hybrid cooling system was able to maintain surface temperature of battery and homogeneity within battery pack at about 64 °C and 2.5 °C respectively at coolant temperature of 25 °C.
38	Shengshi Wang et al.	2024	A L-shaped heat pipe coupled with air cooling was proposed and performance was investigated at varying discharge rates between 1C and 3.5C. The temperature difference between electrode and cell surface was also investigate. The analysis revealed that once after reaching dynamic equilibrium, the heat transfer coefficient of heat pipe reached up to 4000 W/m^2K. Their approach to utilize of cold air of air conditioning system was successful in achieving ideal temperature control and minimized temperature difference across battery module.
39	Patil S et al.	2024	Their study showed that heat pipes enhance performance as heat generation increases, due to phase-change activation of the working fluid. The Lowest temperature recorded: 35 °C at 30 W with a star-shaped heat pipe. Battery systems at 80 W or higher must not operate without heat pipe integration to avoid overheating, shell damage, and system failure.
40	Zhu F et al.	2024	The study showed that flat heat pipe (FHP)-based BTMS reduces battery maximum temperature, improves temperature uniformity

			and SOC balance. Optimization of FHP parameters further lowered Tmax by 6.4%, ΔT by 18.4%, and SOC variation by 16.3%, enhancing EV battery thermal and electrochemical performance.
41	Lu H et al.	2024	The study demonstrated that a hybrid BTMS integrating OHP and liquid cooling significantly improves battery thermal regulation. An optimal 26.1% filling ratio enhanced performance, with acetone effective at low loads and acetone–ethanol mixtures stabilizing temperatures. The system extended heat transfer capacity beyond 280 W, while graphene nanofluid reduced ΔTmax and RBTMS by 32.7% and 20.1%. Overall, the hybrid BTMS proved highly suitable for high-power battery applications.
42	Maalej S et al.	2025	Studies on BTMS with heat pipes and cold plates showed that the safety threshold was taken as 60 °C, with the system dissipating heat loads up to 40 W. The heat pipe exhibited about 4.6 times higher conductance than copper rods, and in single-cell setups, loads up to 20 W were managed while keeping the maximum temperature below 40 °C. Simulations and IR measurements agreed well with experiments, confirming the reliability of numerical modelling.

2.3 Chapter summary:

In future, the BTMS should be further miniaturized, and heat pipes can play an effective role in reducing the size and complexity of thermal management systems while maintaining safety and efficiency. Air cooling systems are among the simplest and lightest approaches, making them attractive for compact battery designs, but their performance is limited by the inherently low heat capacity and thermal conductivity of air. This restricts their applicability in high-power electric vehicles where large heat fluxes must be dissipated quickly. Indirect liquid cooling systems, such as those using water or dielectric fluids, are considered more effective because of their higher heat transfer coefficients, and they are widely implemented in commercial electric vehicles. However, liquid cooling is an active method, requiring

circulation pumps, pipelines, and additional control, which not only adds to system complexity but also consumes a portion of the battery's stored energy, thereby reducing vehicle range.

Several studies have highlighted the potential of heat pipes (HPs) to overcome these limitations by providing a passive and energy-free method of thermal control. Shah et al. [126] demonstrated that inserting heat pipes into a cylindrical cell arrangement reduced the core temperature by nearly 20°C compared to natural air convection, while Lei S et al. [191], [192] showed that a flattened HP system could suppress maximum cell temperature by as much as 29.2°C. These findings reinforce that HPs, through phase-change-driven heat transport, can significantly enhance temperature uniformity and prevent localized hot spots that accelerate degradation or trigger thermal runaway. Nevertheless, research outcomes are not always consistent. Patil et al. [192], for example, reported that a direct immersion liquid cooling system achieved a 9.3% better temperature control than a heat-pipe-based system, suggesting that under extreme heat generation scenarios, liquid systems can still outperform HPs, particularly when the prevention of thermal runaway is critical. Similarly, optimized air and liquid approaches, such as vent-augmented airflow designs (Hong et al. [185]) or intermittent liquid circulation (Liang et al. [186]), have been shown to deliver comparable temperature uniformity to HP-based systems, questioning whether HPs always provide the best standalone solution.

Another consideration is the integration of heat pipes into practical modules. Some studies, such as Worwood et al. [125], observed that internal HP embedding reduced energy density by 6–12% due to the addition of spreader discs, while others, such as Shah et al. [126], achieved significant cooling benefits with minimal volumetric penalties by optimizing geometry. Furthermore, orientation effects remain a debated factor: while Xuan et al. [175] highlighted a strong dependency of performance on gravitational alignment and working fluid charge, Zhao et al. [180]showed that ultrathin flat HPs were nearly insensitive to orientation, indicating that design parameters strongly influence outcomes.

Hybrid thermal management strategies often deliver the most promising results. HPs combined with phase change materials (PCM) accelerate PCM melting and double heat transfer rates during solidification (Robak et al. [178]). At the same time, direct immersion liquid cooling with forced air convection (Patil et al. [192]) can rival or even surpass such hybrids in managing high transient loads. Therefore, while HPs are excellent for passive, compact, and energy-

efficient operation, they should be viewed as part of a broader design palette rather than a one-size-fits-all solution.

Overall, heat pipes offer clear advantages in terms of energy-free operation, compactness, and thermal uniformity, especially for low-to-moderate power applications or where passive safety mechanisms are prioritized. However, their effectiveness depends heavily on factors such as orientation, working fluid selection, structural design, and most importantly, the thermal contact between the HP surface and the battery cells. If direct contact cannot be ensured, the choice of interface medium with high thermal conductivity becomes critical. Future research is increasingly focused on developing hybrid configurations and advanced integration methods that exploit the passive benefits of heat pipes while addressing their limitations. In this context, the present study aims to design a heat-pipe-based BTMS that not only keeps the battery temperature within the safe operating range but also minimizes the temperature gradient across the battery pack, thereby enhancing both safety and cycle life.

2.4 Research Gap

1. Cell Geometry and Material Gap:

Although extensive studies have been carried out on conventional 18650 Li-ion cells for electric vehicle applications, other cell geometries remain comparatively underexplored. In particular, larger 32650 Lithium Iron Phosphate (LFP) cylindrical cells have received very limited attention, despite their demonstrated advantages such as higher safety margin and greater capacity over 18650 cells. This lack of systematic research creates a significant knowledge gap regarding the thermal and electrochemical behaviour of 32650 LFP cells under realistic operating conditions.

2. Cooling Strategy Gap for Cylindrical Cells:

Most of the available literature has concentrated on liquid and air-cooled BTMS for cylindrical cells. However, passive thermal management approaches, such as those utilizing phase change materials (PCM) or heat pipes, remain largely under-investigated. One of the primary reasons is the inherent design challenge associated with the curved surface of cylindrical cells, which complicates effective integration of heat pipes. This design limitation has restricted progress, leaving the need for improved configurations that can make passive cooling systems both practical and efficient.

3. Thermal Interface Material Gap:

In electronic cooling applications, thermal interface materials (TIMs) are routinely used to overcome the imperfect thermal contact between surfaces. The same challenge exists in cylindrical battery packs, where the contact between cells and heat pipes is often suboptimal, leading to increased thermal resistance. Although thermal gels and pastes have been employed as interface materials, their effectiveness remains limited. The present work addresses this gap by proposing the use of fine powdered silicon carbide as a novel interface material to improve heat transfer performance by better filling the interfacial voids between cylindrical cells and heat pipes.

2.5 Research Objectives

1. To analyse the effect of temperature distribution inside Li-ion battery pack at varying discharging rates for base case BTMS-woHP (convection air cooling without heat pipe).
2. To study the effect of interspacing between battery cells on cooling performance of the base case BTMS-woHP at different operating conditions.
3. To evaluate the effect of heat pipe insertion and cooling performance of hybrid BTMS (heat pipe + air cooling) at varying discharging rates and airflow rates.

Chapter 3 Experimental Facility and Methodology

3.1 Introduction

This chapter provides detailed description about research methodology adopted for the research, the layout of experimental facility and its fabrication process along with brief description of each equipment used. The detail of design of experiments, related variables and measured parameters and their uncertainty analysis is also included in this chapter.

3.2 Research Methodology

The main objectives of the present research have already been discussed in Chapter 2. The need of this research work arises from the limitations of conventional battery thermal management systems and identified research gaps. The present research involves experimental work, and it is achieved through step by step approach starting from literature review and fabrication of experimental facility (see Figure 3.1). After problem identification, relevant literature review was started and it was mainly related to fabrication of test facility, development of battery pack and BTMS, selection of variables, design of experiments and analysis of results. Before fabrication of experimental testing facility, necessary instruments were procured. The detail of procured items is given in Table 3.2. Fabrication of test facility and battery pack was done in-house. The main components of experimental facility are battery tester, LFP cells battery pack, cooling arrangement (BTMS), data logger and thermocouples arrangement. Mainly three different types of cooling strategies (BTMS) i.e. free convection, forced convection and heat pipe assisted forced convection, were studied for heat extraction and cooling performance during discharge process of battery pack. To evaluate the performance of these three types of BTMS, discharge rate (C rate), air inlet velocity and interspacing between cells were selected as independent variables. Peak temperature of battery pack, Average temperature of battery pack and Temperature uniformity of battery pack were selected as performance parameters and four different types of battery pack and BTMS arrangement were fabricated based on the BTMS type and interspacing. These are:

1) Free convection cooled battery pack with 2 mm interspacing between cells

2) Forced convection cooled battery pack with 2 mm interspacing between cells
3) Forced convection cooled battery pack with 4 mm interspacing between cells
4) Hybrid heat pipe assisted forced convection cooled battery pack with 2 mm interspacing between cells.

The detail process of fabrication and brief of selected instruments is further discussed in sub-sections of this chapter. Before stating experimentation, a design of experiments table was developed based on variable combinations i.e. discharge rate, air inlet velocity and interspacing (Table 3.1). The selection of discharge rates, airflow velocities, and inter-cell spacing in this study was guided by literature, battery safety constraints, and applicability to real-world electric vehicle (EV) use cases. Discharge rate (C-rate) is a direct indicator of the load on a battery. The selected levels: 1C, 2C, and 3C—were chosen based on:

- 1C: Represents nominal operation or regular driving conditions.
- 2C: Simulates moderate acceleration or medium load demand.
- 3C: Represents high-stress operating scenarios such as rapid acceleration, regenerative braking, or fast charging.

These values fall within the safe operational range of the $LiFePO_4$ cells used and are consistent with existing studies (e.g. [152], [191]), which analyse battery behaviour under dynamic EV operating conditions.

The airflow velocity was selected to represent a range of realistic cooling intensities:

- Free convection: Passive system used as a baseline comparison.
- 3.6 m/s to 5.5 m/s: Represents increasing levels of forced convection, like fan speeds used in automotive battery modules.

These values were derived from prior works (e.g., [111], [185]), where airflow between 3–6 m/s demonstrated measurable improvements in convective heat transfer while remaining within practical power constraints for on-board cooling fans. The data collected for comparative analysis was temperature of each cell during discharge process, air inlet and outlet temperature, temperature of heat pipe condenser section and air velocity. The results were validated with available correlations and details of correlation used for free and forced convection is discussed in this chapter. An analysis of uncertainty in measurement and calculation is also presented in this chapter. After validation of standard process, comparative analysis was done with the help of suitable graphs and tables. Results and conclusion are presented and discussed in the Chapter 4.

Table 3.1: Design of experiments

Factors	Levels
Discharge rate (C)	1C
	2C
	3C
Air flow rates (m/sec)	FR = Free convection
	Ve1 = 3.6 m/s
	Ve2 = 4.6 m/s
	Ve3 = 5.5 m/s
Interspacing between cells (in mm) (X)	X1 = 2 mm
	X2 = 4 mm
BTMS type	Free convection [FR]
	Forced convection [FO]
	Heat pipe assisted forced convection [HP]

Factorial: [3 levels of discharge rate, 3 levels of air inlet velocity, 2 levels of interspacing, 3 levels of BTMS type]

DOE =

Free convection (FR)	Forced convection (FO)	Heat pipe assisted forced convection-hybrid (HP)
1C X1 FR	1C Ve1 X1 FO	1C Ve1 X1 HP
2C X1 FR	1C Ve2 X1 FO	1C Ve2 X1 HP
3C X1 FR	1C Ve3 X1 FO	1C Ve3 X1 HP
	2C Ve1 X1 FO	2C Ve1 X1 HP
	2C Ve2 X1 FO	2C Ve2 X1 HP
	2C Ve3 X1 FO	2C Ve3 X1 HP
	3C Ve1 X1 FO	3C Ve1 X1 HP
	3C Ve2 X1 FO	3C Ve2 X1 HP
	3C Ve3 X1 FO	3C Ve3 X1 HP
	3C Ve2 X2 FO	
	3C Ve3 X2 FO	

Table 3.2: Details of equipment

Sr. No.	Name of Equipment	Details
1.	Heat pipe – flat type	Material – Aluminum,300 W
2.	Data Logger	16 channels
3.	Battery tester- Charger/Discharger	Working range : 9 V to 99 V
4.	Thermocouples	k–type
5.	Battery Cell	Li-$FePO_4$- 32650
6.	Acrylic Transparent Box	
7.	Fan	3 speed steps
8.	Silicon Carbide powder	
9.	Anemometer	Vane type
10.	Multi-meter	
11.	Soldering kit and Spot Welding Machine	
12.	Spacers	2 mm

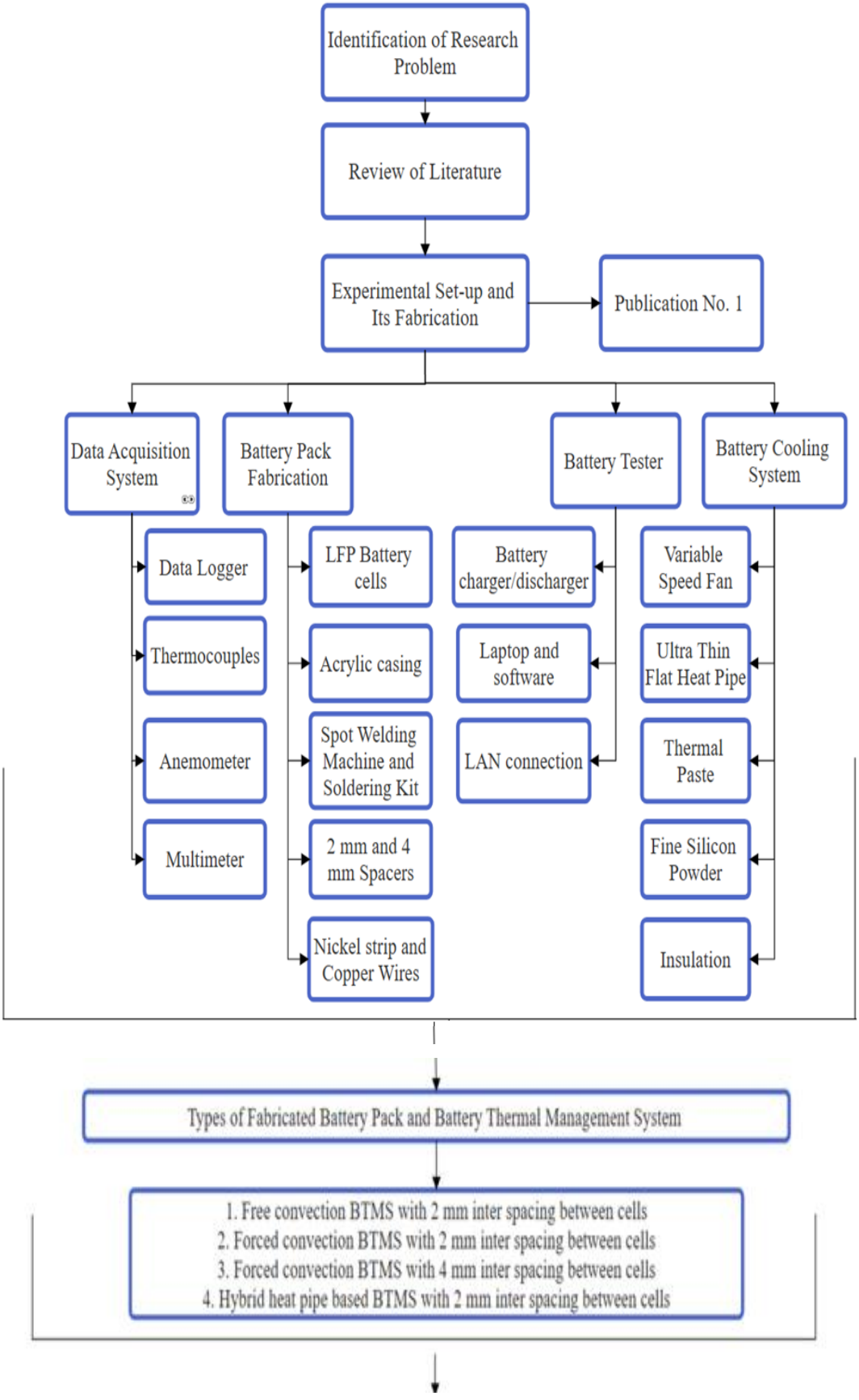
Identification of Research Problem
Review of Literature
Experimental Set-up and Its Fabrication
Publication No. 1
Data Acquisition System
Battery Pack Fabrication
Battery Tester
Battery Cooling System
Data Logger
Thermocouples
Anemometer
Multimeter
LFP Battery cells
Acrylic casing
Spot Welding Machine and Soldering Kit
2 mm and 4 mm Spacers
Nickel strip and Copper Wires
Battery charger/discharger
Laptop and software
LAN connection
Variable Speed Fan
Ultra Thin Flat Heat Pipe
Thermal Paste
Fine Silicon Powder
Insulation
Types of Fabricated Battery Pack and Battery Thermal Management System
1. Free convection BTMS with 2 mm inter spacing between cells
2. Forced convection BTMS with 2 mm inter spacing between cells
3. Forced convection BTMS with 4 mm inter spacing between cells
4. Hybrid heat pipe based BTMS with 2 mm inter spacing between cells

Figure 3.1: Research Methodology

3.3 Experimental facility

The experimental facility was fabricated in-house, and it mainly consists of a battery pack of lithium iron phosphate (LFP) cells, a battery thermal management system, data acquisition system and a battery tester with LAN connection to laptop (see Figure 3.2). Other instruments

which aided in fabrication include a spot welding machine, a multimeter and spacers. The data acquisition system mainly consists of thermocouples, data logger and anemometer. The battery pack consists of twelve Lithium Iron Phosphate (LFP) cells connected in series arrangement. The heat generated inside cells during discharge process raise the temperature of cells. The battery pack was cooled by free convection, forced convection and heat pipe assisted forced convection. The effectiveness of these cooling strategies is evaluated by measuring the rise of surface temperature of cells during discharge process. A cooling strategy is better at heat extraction if the temperature rise is low at same C-rate as compared to other strategies. The surface temperature of cells was measured by K-type thermocouples fixed at middle critical region of each cell. The selected thermocouples have upper and lower temperature limits as 350˚C and 0˚C respectively. A thermal paste and adhesive tapes were applied to sensor of thermocouple to ensure proper cell-sensor contact. The temperature measured during testing were recorded by a 16-channel data logger having resolution of 1˚C. The data logger selected can measure temperature at various variable time intervals, minimum being 1 second. Three cooling systems were tested experimentally: free convection, forced convection (air cooled) and hybrid cooling based on heat pipe and forced air cooling. A vane type anemometer was used to measure air inlet and outlet velocity in forced and heat pipe assisted hybrid cooling systems. The rise in temperature of air is an indication of heat carried away by air while cooling the battery cells. The air inlet and outlet temperature were measured by K-type thermocouples installed at inlet and outlet section of battery pack. The battery tester selected in the present study can charge and discharge batteries at various C-rates by adjusting the value of current and capacity to be discharged. Three different discharge rates are selected for testing: 1C, 2C and 3C, and respective current, capacity discharged, and discharge time are given Table 3.3. As a safety precaution and operating limitation of cells, the cut-voltage where the discharge process will stop irrespective of capacity discharged was predefined in the battery tester as 22 V. So, in each case, the discharge process was stopped when battery pack voltage reached or fall below this value of 22 V. A brief description of each component of experimental facility is presented in this chapter in the following sub-sections.

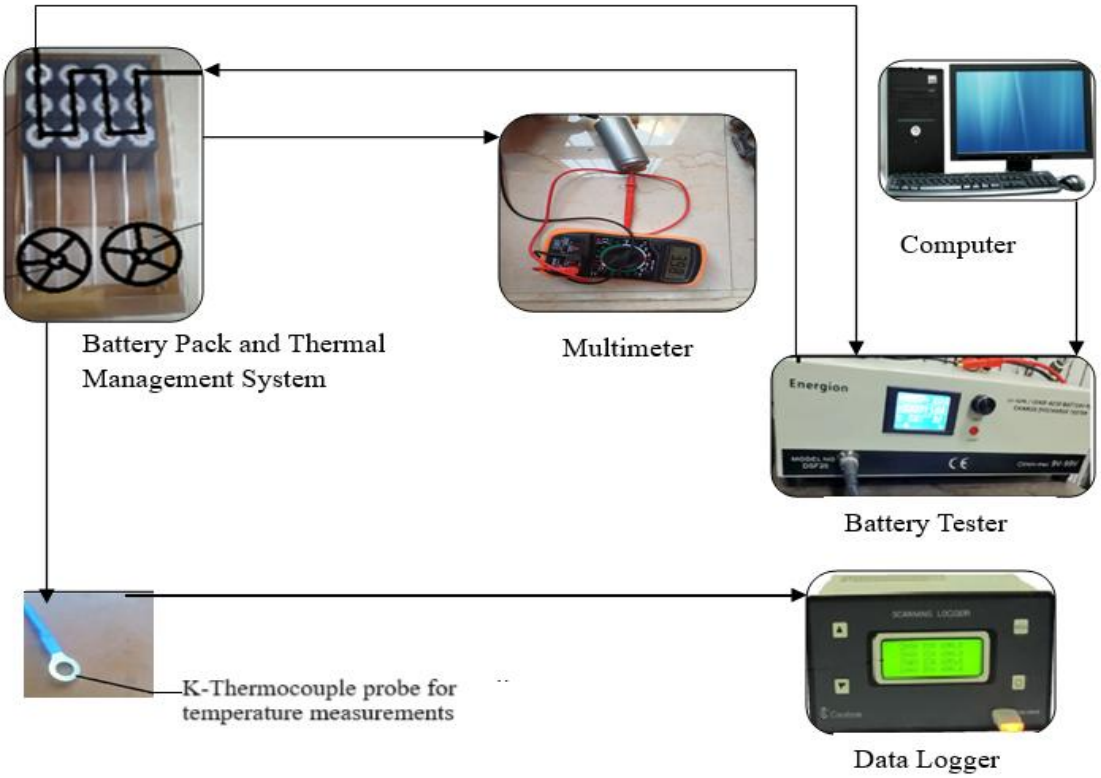

Figure 3.2: Experimental facility

Table 3.3: Current and Capacity settings for C-rates

Discharge rate (C-rate)	Current (A)	Capacity discharged (Ah)	Discharge time (min.)
1C	6	6	60
2C	12	6	30
3C	18	6	20

3.3.1 Description of Battery cells

Batterie are the key component and most expensive part of electrical vehicles. EVs can be powered by several types of batteries. The main characteristics which a battery should have to be suitable for an EV are: high energy storage capacity or battery capacity usually expressed in Ah or Wh, high energy density usually expressed as energy supplied by battery per unit volume (Wh/L), high specific energy which is usually expressed as energy supplied by battery per unit mass (Wh/kg), high specific power (W/kg), better lifespan and charge cycles, low internal resistance of battery as it affect charging time and heat generation in batteries, low cost,

ease of storage, reliability and safety from fire, hazardous gas release and explosions [200]. One of the most popular batteries used for EVs are Lithium-ion batteries due to their high energy density and better cycle life as compared to other available batteries in the market today. (see figure1). The Lithium-ion cells are available in different shapes, sizes, and cathode-anode configurations. Carbon (graphite) is one of the most popular anode materials for commercially available lithium-ion batteries while other materials like lithium titanium oxide (LTO) and silicon are also used in some battery configurations [201]. A comparative analysis related to popular cathode materials configurations of li-ion batteries is presented in Figure 3.4 and Figure 3.5. LFP cell was selected based on literature review as these cells have higher thermal stability, safety and battery cycle life as compared to other cell configurations. The selected Lithium Iron Phosphate cylindrical cells are cylindrical type 32650 cells (see Figure 3.3). These cells have diameter and total length of about 32 mm and 65 mm, respectively. The specifications of 32650 cells as provided by manufacturer are given in Table 3.4. The cathode of these LFP cells is $LiFePO_4$, and anode material is graphite (carbon). The selection of cylindrical shape was made based on the popularity and adoption of these cells in EVs. Due to their high surface to volume ratio, these cells present larger surface for cooling and because of better cooling they can be more energy efficient.

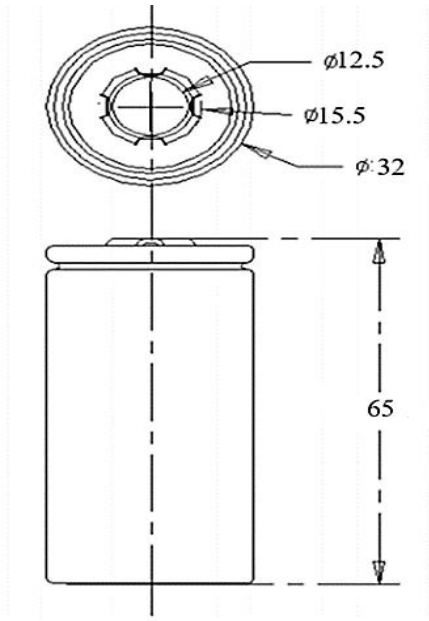

Figure 3.3: Lithium Iron Phosphate cell -32650

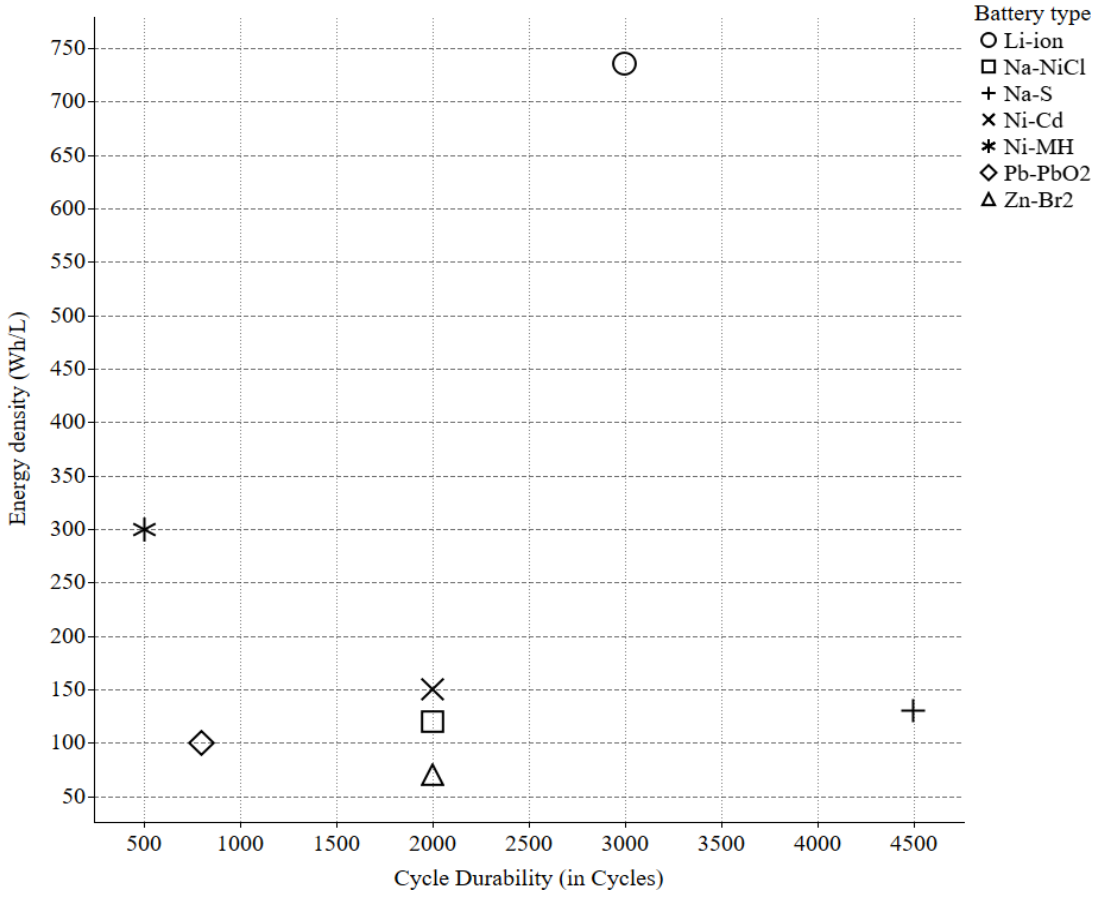

Figure 3.4: Comparative analysis of popular cathode configurations of li-ion cells

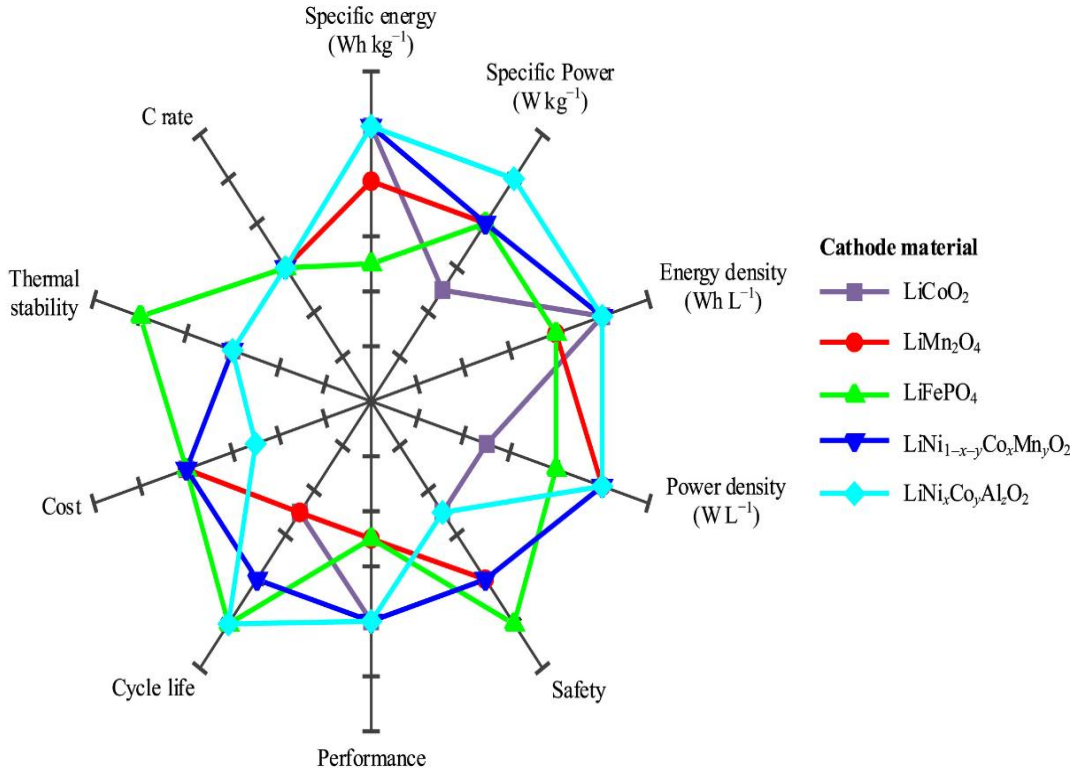

Figure 3.5: Comparison of lithium-ion batteries based on their cathode material[204]

Table 3.4: Specification Lithium Iron Phosphate cells

Parameter	Value
Battery type	$LiFePO_4$
Capacity	6000 mAh
Output voltage	3.2 V
Discharge voltage (cut-off)	2 V
Charging voltage (cut-off)	3.65 V
Maximum continuous charge rate	0.5C to 1C
Maximum continuous discharge rate	3C
Operating temperature	Charging: 0°C to 45°C Discharging: 20°C to 60°C
Cycle life	More than 2000 cycles

3.3.2 Description of Heat Pipes

The hybrid battery thermal management system proposed in the present research utilize flat heat pipes. The heat pipes selected are ultra-thin heat pipes with 2 mm thickness and has width and length of 40 mm and 250 mm respectively (see Figure 3.6). These ultra-thin heat pipes are extremely popular in electronic cooling. The use of aluminium instead of traditional copper make these heat pipes light weight although there may be some performance reduction as compared to copper heat pipes. The selected heat pipe's internal wick structure is groove type, and the working fluid is acetone. General specifications of selected heat pipe as provided by manufactured are given in Table 3.5.

Table 3.5: Specification flat heat pipe

Item	Description
Material of container	Aluminium 1070
Wick Structure and Working Fluid	Groove; Acetone
Dimensions (Thickness, Width, Length)	2 mm, 40 mm, 250 mm
Maximum heat transfer rate– horizontal and vertical	45 W; 175 W at 50°C
Typical thermal resistance	<0.3 °C/W (average)

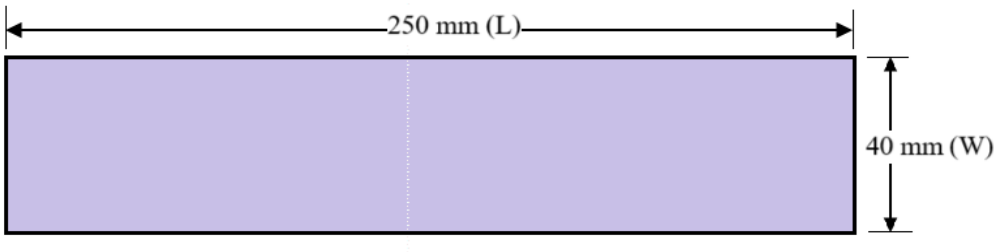

Figure 3.6: Flat heat pipe

3.3.3 Description of Battery pack

EVs battery module/pack consists of several battery cells usually Li-ion connected in either series or parallel connection or combination of both configurations. The present work is based on Lithium Iron Phosphate (LFP) batteries connected in series to form battery pack of twelve cells. The LFP 32650 cells are arranged in rectangular configuration of 3×4 arrangement. The cathode material of these cells is $LiFePO_4$ while anode material is carbon. Each cell has nominal voltage of 3.2 V and capacity of 6 Ah. The specifications LPF battery pack can be seen in Table 3.4. The process of charging/discharging a cell is exothermic and the heat generated (q) inside battery can be calculated from simplified Eq. (3.1) [202] where first and second term represents joule heating and entropy heat generation, respectively.

$$q=I(U-V)-I\,(T\,dU/dT) \tag{3.1}$$

Table 3.6:Battery pack parameters

Arrangement of cells	Total Capacity of battery pack (Ah)	Discharge method	Cut-off discharge voltage (V)
Twelve cells in series	6	Constant current	22 V

Four different pack layouts are fabricated in present study:

1. Battery pack for free convection with 2 mm interspacing between cells (Figure 3.7)
2. Battery pack for forced convection with 2 mm interspacing between cells (Figure 3.7)
3. Battery pack for forced convection with 4 mm interspacing between cells
4. Battery pack with heat pipe insertions (hybrid) with 2 mm interspacing between cells (Figure 3.8 and Figure 3.9)

The LFP cells were placed in acrylic case and the interspacing between cells was initially kept at 2 mm. To study the effect of interspacing on cooling performance of forced convection based BTMS, the interspacing between cells was changed to 4 mm by using modified spacers. The acrylic case was left open from all sides for free convection based BTMS, so every side of a cell were exposed to free convection expect bottom face of the cells. In forced convection based BTMS, a variable speed fan was installed at inlet section of acrylic casing which forced ambient air through the battery pack. In hybrid BTMS, the heat pipes were inserted in between rows of LFP cells such that evaporator section of heat pipe was inserted inside the battery pack while condenser section was air cooled by forced convection. Specifications of flat heat selected for present research are given in Table 3.5. A perfect surface contact is desired between cells and heat pipe for efficient heat transfer, but it is difficult to achieve due to cylindrical shape of cells. To overcome this difficulty, fine silicon carbide powder was used to fill gap between cells and heat pipes. Silicon carbide was used to facilitate the transfer of heat from cylindrical surface of cells to flat surface of heat pipe. The cells in each of the battery pack were numbered 1 to 12 such that these cells got unique identification according to their position in the pack.

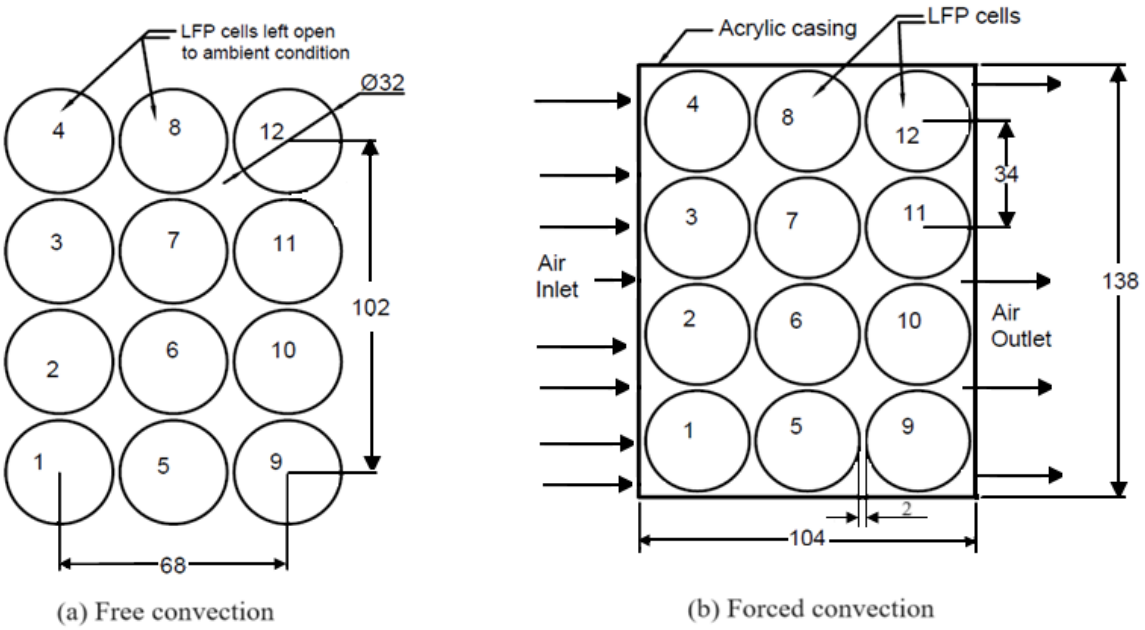

Figure 3.7: (a) Free convection battery pack and (b) forced convection battery pack (dimensions are in mm)

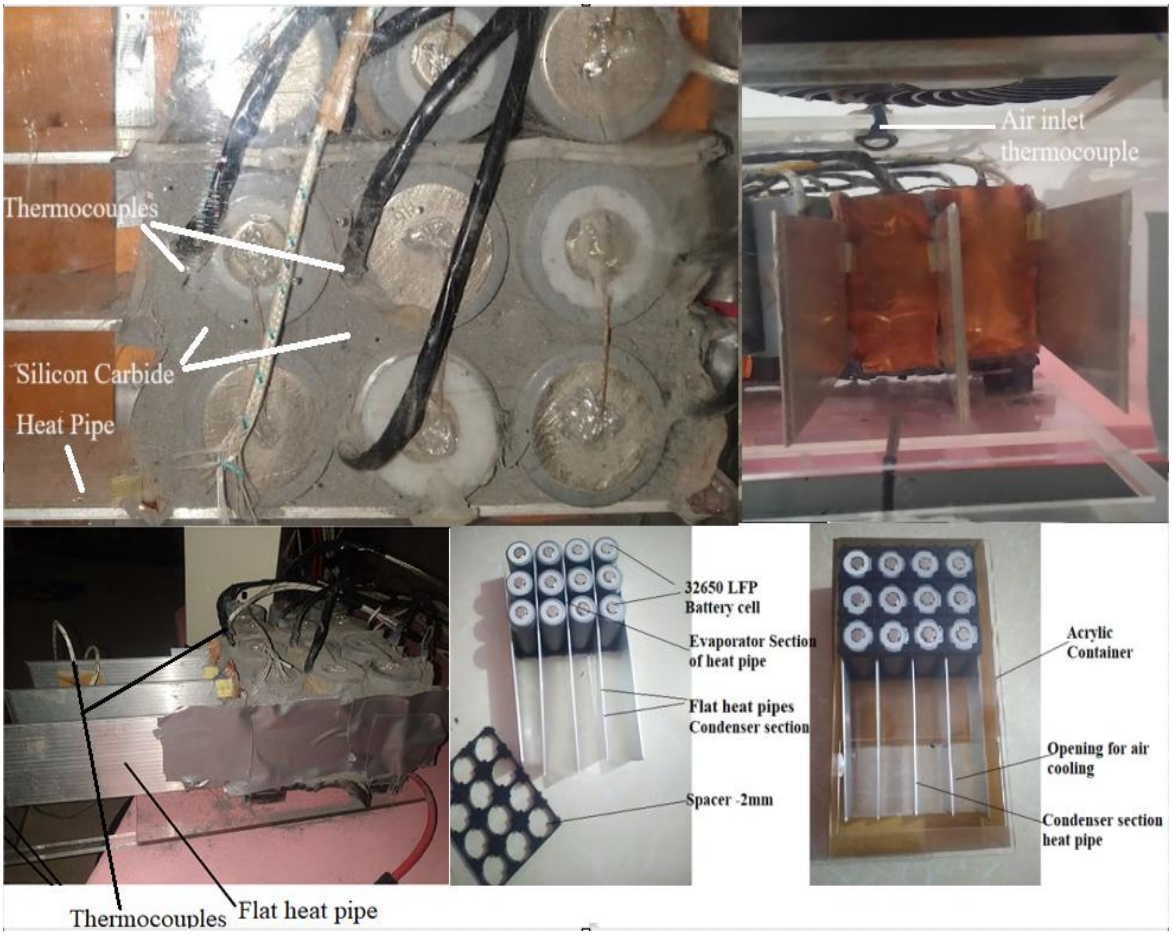

Figure 3.8: Heat pipe insertion in battery pack

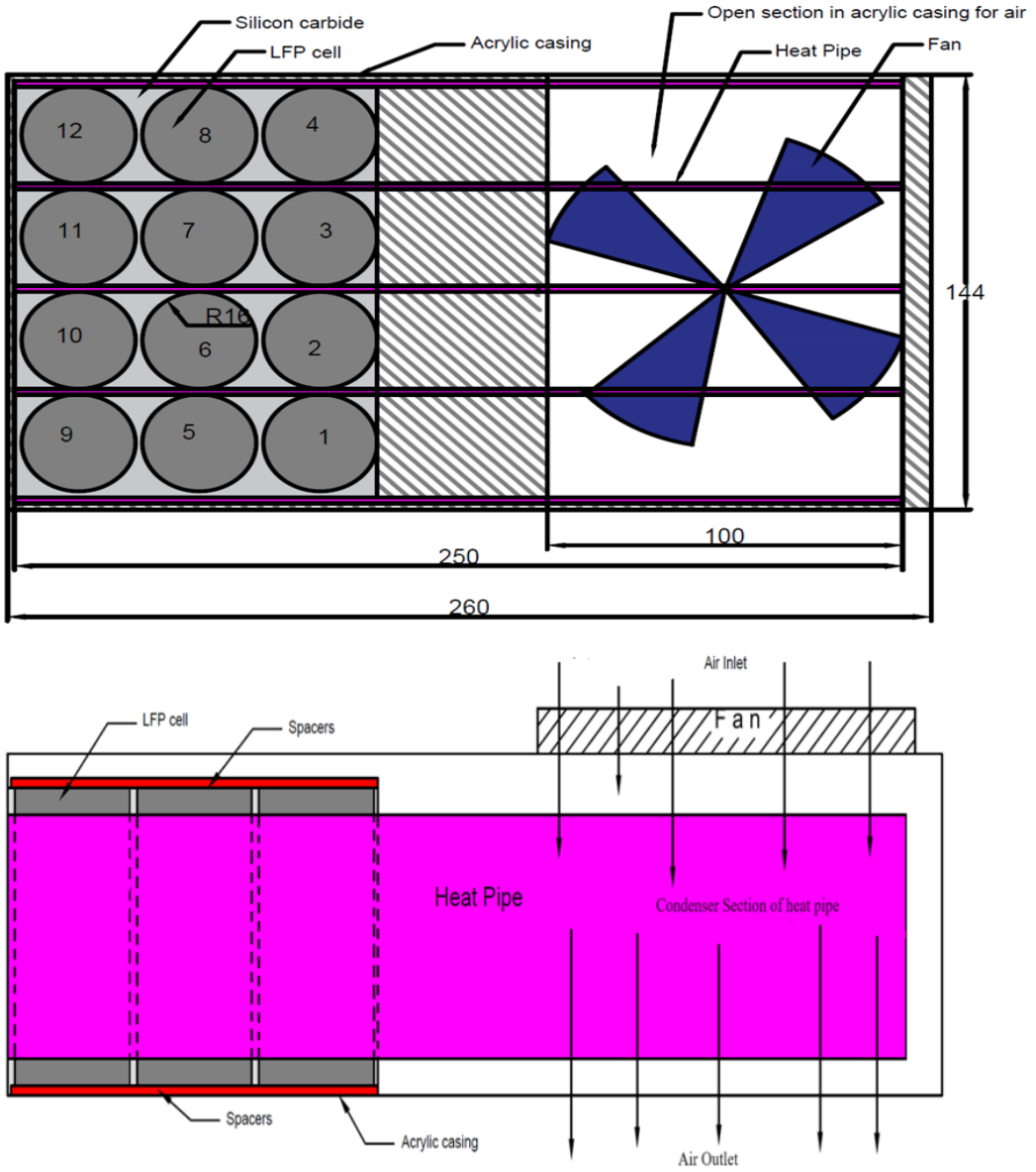

Figure 3.9: Heat pipe assisted forced convection based hybrid battery pack

3.3.4 Description of data acquisition system

The main components of data acquisition system were thermocouples and data logger. K-type thermocouples were selected for cell's surface, inlet air and outlet air temperature measurements. The selected temperature sensors conform to IEC 584 standard. These sensors have rugged design, and their connecting wires are insulated with glass fibre surrounded by stainless stell braid. The probe is made from stainless steel flat disc of external diameter 6 mm (see Figure 3.10). These probes are designed to measure surface temperature and provide fast response time. The specification of selected k-type thermocouple can be seen in Table 3.8. A

16-channel data logger with data storage capability was used to store temperature rise data during discharge process of battery pack. Out of the 16 channels, first 12 are connected to k-type thermocouples mounted on each cell of battery pack (see Figure 3.11) and one each is connected to thermocouples placed in air inlet and outlet section in forced convection. The specifications of data logger are given in Table 3.7.

Figure 3.10: (a) Thermocouple (b) Data logger

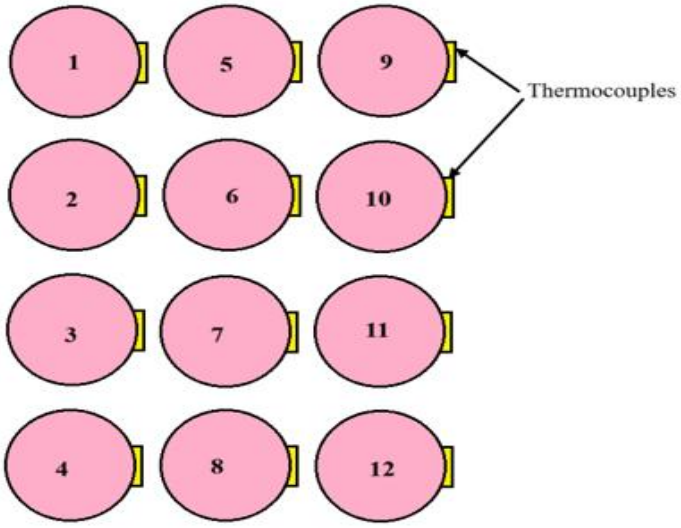

Figure 3.11: Position of thermocouples on cells (top view of battery pack

Table 3.7: Specification of data logger

Number of usable channels	16
Data storage	USB pen drive
Temperature sensors supported	J/K/R thermocouples and PT 100 temperature sensors
Rate of logging	1 second to 99 minute 59 seconds

Accuracy	±1°C

Table 3.8: Specification of thermocouple

Range of measurement	0°C to 350°C
Accuracy	± 1.5°C
Response time	0.7s
Probe diameter	6 mm
Sheath material	Glass fibre
Probe material	Stainless steel
Insulation	PVC
Certification	IEC 584

3.3.5 Battery tester

Testing BTMS at various charging and discharging rates is very important as it simulate nearly real life situation where battery pack must work under various operating conditions. The battery tester provides the facility to charge and discharge battery pack at different C-rates. Technical parameters of battery tester selected for experimental facility is given in Table 3.9. These parameters are selected based on total capacity of battery pack and C-rates to be obtained.

Table 3.9: Battery tester specifications

Parameter	
Input Voltage and Maximum Power:	AC 220V±10%, 50Hz/60Hz, 900W
Charging Method:	Constant current & constant voltage charge
Discharging Method:	Constant current discharge
Charging/Discharging- Current and Voltage:	0.5-20A adjustable, 9V-99V adjustable

3.3.6 Anemometer

A vane type anemometer was used to measure air inlet velocity for mass flow rate measurements in conventional forced convection and heat pipe assisted forced convection cooling. The specifications of anemometer as provided by manufacturer are given in Table *3.10*. The air velocity varies across the cross-section of fan and therefore average air velocity values are used for all calculation purposes. The air readings were taken at four locations (A,

B, C and D) around the cross-section of fan as indicated in Figure 3.12, and average velocity values were used to find mass flow rates required to measure heat carried away by cooling systems. The air density values were taken at temperature of inlet air as recorded by K-type thermocouple.

Table 3.10: Specification of anemometer

Precision	± 5%- air speed
Measuring range	0 m/s to 30 m/sec
Resolution	0.1 m/sec

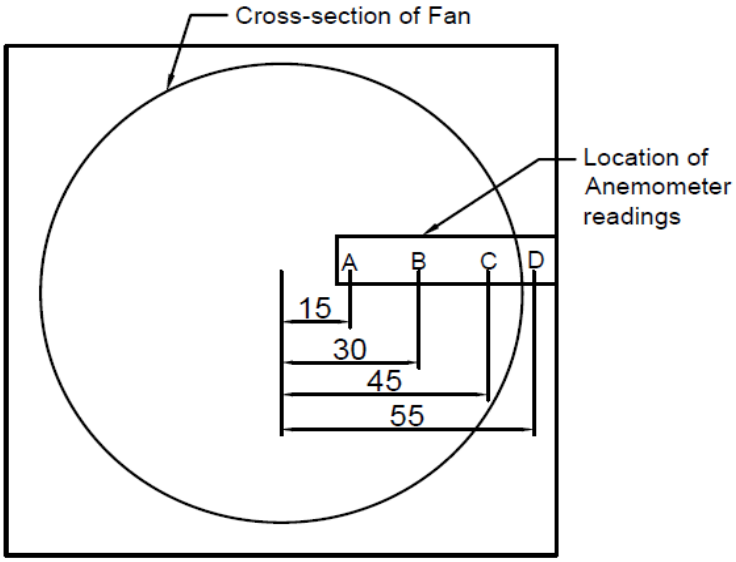

Figure 3.12: Location of anemometer readings on the cross-section of fan

3.3.7 Description of other data acquisition and testing facility fabrication instruments

(i) Multimeter

A multimeter was used to check voltage of each cell before battery pack fabrication and compared with battery pack total voltage after fabrication. Before starting discharge process, the voltage of battery pack was checked and if any variations are there due to defective cell, then it is rectified by replacing the damaged cell.

(ii) Interspacing filler material

Silicon carbide fine powder of mesh size 220 and 63 µm was filled in the interspacing between cells and heat pipe. The thermal conductivity of compressed silicon carbine powder is usually between 120 to 170 W/m-K. High thermal conductivity improves heat transfer rate between cell and heat pipe. A thermal paste layer is also applied to the surface of the cells to improve thermal contact.

(iii) Other instruments

Spot welding machine was used to weld each cell to the nickel strip and fabrication of battery pack. Spacers were of 2mm, and modified spacers of 4 mm were used to keep uniform interspacing between cells. Nickel strips were used to make connection between cells. Soldering kit was used to make wiring connections and adhesive take was used to joints. Figure 3.13 shows various equipment used in the fabrication process.

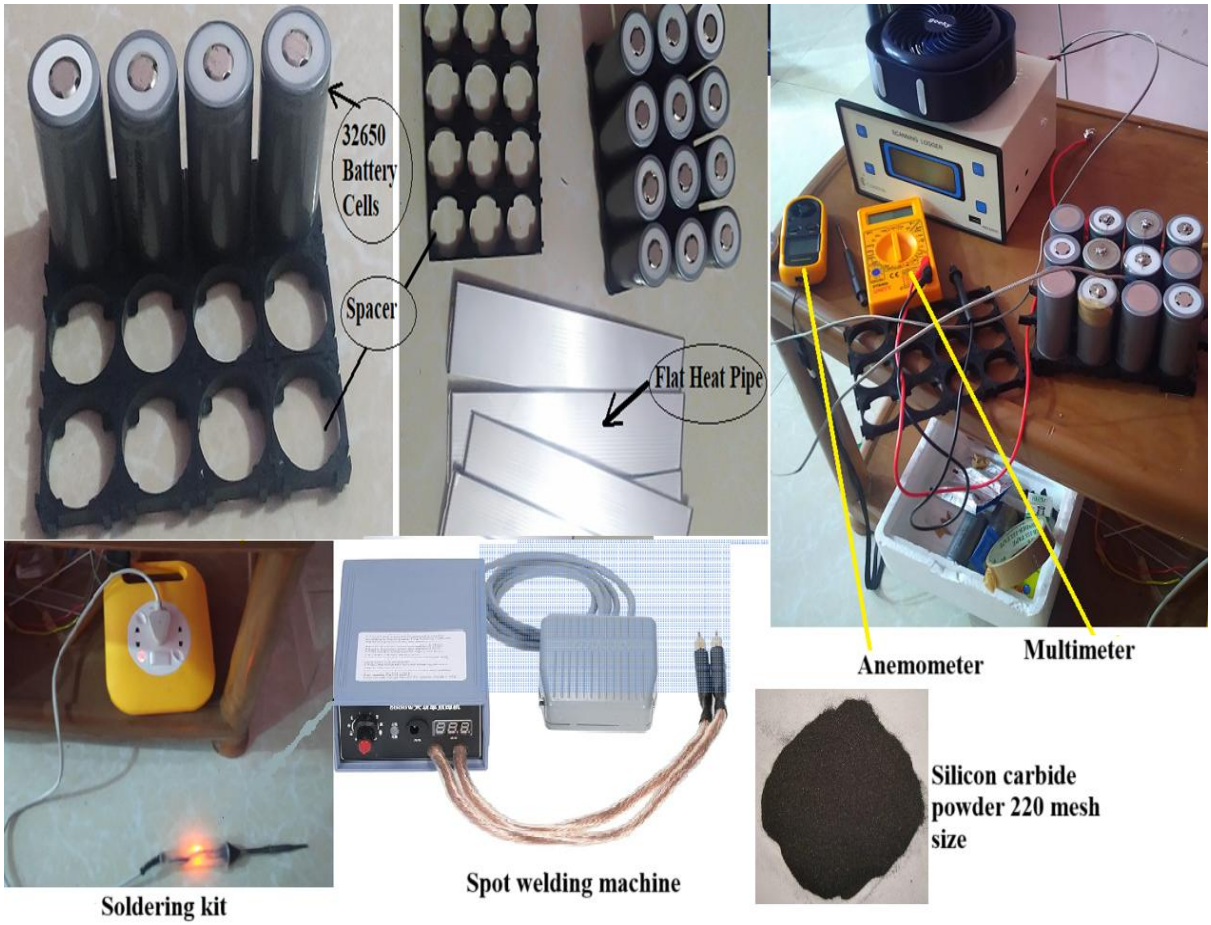

Figure 3.13: Equipment used in fabrication of battery pack and testing facility

3.4 Performance Parameters, Correlations used and Uncertainty analysis

The main parameters which were measured or calculated under experimental investigation are:

1. Average temperature of battery pack (T_{avg}).
2. Peak surface temperature battery cells (T_{max}).
3. Temperature uniformity or homogeneity inside battery pack (ΔT).
4. Mass flow rate (m_f)
5. Grashof number and Rayleigh number
6. Reynolds number
7. Nusselt number
8. Heat transfer rate

The accuracy of measuring instruments affects overall accuracy of results. The parameters as indicated above either directly or indirectly dependent on measured values by different instruments. An uncertainty analysis related to measured values and related calculated values is presented in this section. Uncertainty of measured values in experimental analysis were calculated based on accuracy of each measuring instrument. The method used for calculation uncertainty was based on Moffat [203]. The result (R) in an experiment determined from set of measured values is determined by Eq. 3.2.

$$R = R(X_1, X_2, X_3, \ldots\ldots, X_n) \tag{3.2}$$

Where X_1, X_2, …,X_n are measurements taken during experimentation. Before calculating overall uncertainty, uncertainty in each measurement and variable have been estimated. Each measurement can be described in standard form $X_i + \delta X_i$,where δX_i represent uncertainty. Uncertainty analysis of each parameter is presented in subsections.

3.4.1 Average surface temperature of battery cells

Increase in average temperature of battery during operating cycle is indicative of performance of BTMS. It takes into consideration the overall temperature of the battery pack. If the difference between peak temperature and average temperature is large, this indicates that some cells are under thermal stress. Average temperature should not exceed safe limit of battery cells i.e. 50˚C. The average temperature measured values were used to compare the performance of

battery thermal management systems under various discharge rates and air inlet velocities. The average temperature of battery pack was calculated as given by Eq. 3.3.

$$T_{avg} = \frac{\sum T_s}{N} \tag{3.3}$$

Where T_s represent surface temperature of each cell in the battery pack and N is total number of cells in the battery pack. The k-type thermocouples have accuracy of ±1.5°C. The system disturbance fixed error which may be caused due to exposed wire of thermocouple to coolant was considered negligible as wires are glass fibre coated. The glass fibre coating ensures that there is negligible chance of junction cooling by exposed wires of thermocouples. The data logger has a resolution (accuracy) of ±1°C. To calculate average temperature, mean of twelve different measurements from each cell of battery pack was calculated. Each measurement uncertainty (ΔT) was calculated considering thermocouple uncertainty (ΔX) and data logger uncertainty (ΔY) by root mean square (Eq.3.4).

$$\delta T = \sqrt{\Delta X^2 + \Delta Y^2} \tag{3.4}$$

The overall uncertainty (ΔT_{avg}) in measured value of battery pack average temperature was calculated from Eq. 3.5.

$$\frac{\delta T_{avg}}{T_{avg}} = \pm \frac{1}{\sqrt{12}} \left\{ \left(\frac{\delta T_1}{T_1}\right)^2 + \left(\frac{\delta T_2}{T_2}\right)^2 + \left(\frac{\delta T_3}{T_3}\right)^2 + \cdots \ldots + \left(\frac{\delta T_{12}}{T_{12}}\right)^2 \right\}^{1/2} \tag{3.5}$$

The uncertainty values calculated at different average temperature of battery at 1C, 2C and 3C discharge rates. The range of uncertainty in percentage was ±3% to ±6%. Higher percentage uncertainty was observed at lower temperature values.

3.4.2 Peak temperature of battery pack

The performance of cells is strongly affected by the peak temperature generated during operating cycle. The internal temperature of a cell is higher than the surface temperature measured. Ideally peak temperature should not exceed 40˚C [204]. The threshold of ideal temperature can be further increased owing to improvement in cell technology. A more relaxed acceptable threshold may be set at 50˚C [100]. Peak temperature recorded in case free convection based BTMS, forced convection based BTMS and heat pipe-based hybrid BTMS are indicative of the overall performance of cooling systems. The peak temperature of the battery pack was the based on the cell in the battery pack that has higher surface temperature.

The uncertainty in measurement of peak temperature is equivalent to inaccuracy (uncertainty) of thermocouple and data logger in absolute terms i.e. ±1.5°C and (±1°C) respectively. In terms of percentage, uncertainty calculated was between ±3% to ±4%, with higher values observed at lower peak temperatures. Uncertainty values were higher for lower discharge rate as peak temperature value was lower at 1C rates as compared to 2C and 3C rates.

3.4.3 Temperature homogeneity in the battery pack

Temperature homogeneity (uniformity) is a measure of difference between temperature of cells in a battery pack/module. Ideally, the temperature difference between cells should not be allowed to increase beyond 5˚C [89], [103]. The threshold of 5˚C is mainly based on studies conducted on high energy dense 18650 Li-ion cells as temperature non-uniformity greater than 5°C accelerates imbalance and capacity fade. However, in the case of 32650 $LiFePO_4$ cells (LFP) which are selected for present study, the cell chemistry of LFP cells offers significantly higher thermal stability and lower heat release. This makes them inherently safer against localized heating. The LFP cells exhibit more stable degradation even under high temperature variations. Therefore, LFP 32650 cells, the permissible temperature non-uniformity can be relaxed. In present research, a more relaxed acceptable value of ΔT at 8˚C was used. The acceptable was relaxed to study the effect of relaxation on acceptability of cooling type. Overall better temperature uniformity in a battery pack promotes cell balancing and uniformity in charge/discharge cycle of Li-ion batteries. The temperature homogeneity (ΔT) is measured as the difference between maximum and minimum temperature across the battery pack (Eq. 3.6). The overall uncertainty, $\delta(\Delta T)$,was calculated by taking root mean square of uncertainty values of maximum temperature and minimum temperature (Eq.7).

$$\Delta T = T_{max} - T_{min} \tag{3.6}$$

$$\delta(\Delta T) = \sqrt{\delta T_{max}{}^2 + \delta T_{min}{}^2} \tag{3.7}$$

Where δT_{max} and δT_{min} are equal to root mean square of thermocouple and data logger uncertainties $i.e.\sqrt{1.5^2 + 1^2}$. The total overall uncertainty in measured value of temperature homogeneity in absolute terms is ±2.55°C.

3.4.4 Mass flow rate of inlet air

The mass flow rate was measured based on anemometer readings. The accuracy of anemometer was ±5% (air speed). It was observed the air velocity was varying across the cross section of fan from inner to outer circumference of fan. For mass flow rate calculation, average air velocity was calculated from four different reading across the fan cross-section as shown in Figure 3.12. Uncertainty of each measurement was calculated, and overall uncertainty in air velocity measurement (ΔVe) was calculated from Eq.3.8.

$$\Delta V_e = \pm\frac{1}{\sqrt{4}}\{\Delta Ve1^2 + \Delta Ve2^2 + \Delta Ve3^2 + \Delta Ve4^2\}^{1/2} \quad (3.8)$$

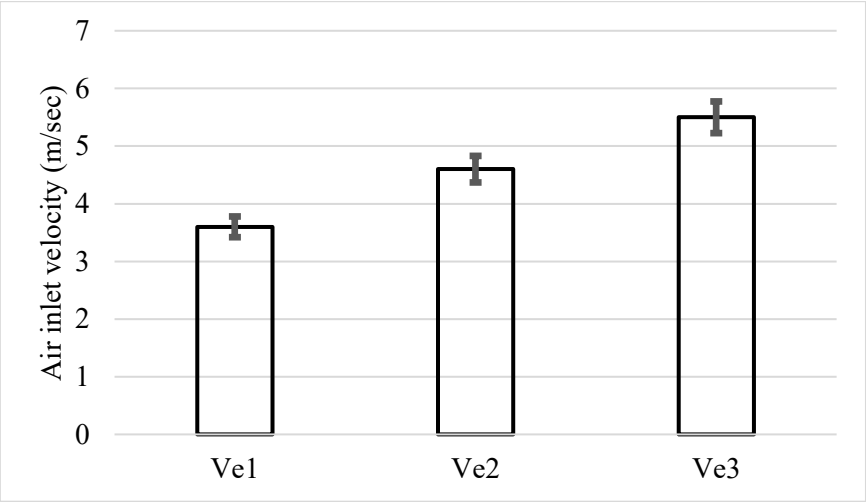

Figure 3.14: Uncertainty in air velocity measurement

The calculated uncertainty at Ve1 (3.6 m/s), Ve2 (4.6 m/s) and Ve3 (5.5 m/s) are ±0.18 m/s, ±0.23 m/s and ±0.275 m/s respectively which is equivalent to ±5% for each case. The mass flow rate was calculated from Eq.3.9. The density values were taken from standard table corresponding to temperature, so there is negligible chance of uncertainty in air density values. The area for all mass flow rate was based on span of fan blades. The diameter of the fan is preciously measured, and it is same for all calculations, so variations are assumed negligible.

Mass flow rate, $m_f = \rho A_f Ve$ (3.9)

As per Eq.3.9 , the uncertainty which mainly affect mass flow is due to air velocity. As calculated, it is equivalent to ±0.18 m/s, ±0.23 m/s and ±0.275 m/s at Ve1, Ve2 and Ve3 respectively.

3.4.5 Grashof number

Grashof number is an important parameter in determination of Nusselt number and convective heat transfer by free convection. It is calculated by Eq.3.10.

$$Gr = \frac{g\beta\,(T_s - T_\infty)L_c^{\,3}}{\nu^2} \tag{3.10}$$

Where g is acceleration due to gravity in m/sec, β is coefficient of volume expansion, T_s is surface temperature, T_∞ is ambient temperature, L_c is characteristic length and ν is kinematic viscosity. While calculating Grashof number, the value of g is taken as 9.81 m/s^2 and kinematic viscosity values are taken from air property tables corresponding to temperature measured temperature of air. The characteristic length is equivalent to height of cell i.e. 65 mm and coefficient of volume expansion is calculated by assuming ideal conditions i.e. $\beta = 1/T_f$. Where T_f is film temperature and calculated by Eq.3.11.

$$T_f = \frac{T_s + T_\infty}{2} \tag{3.11}$$

Where T_s and T_∞ are respectively the surface temperature of cells and ambient temperature of air away from cells. The uncertainty in Grashof number mainly depends on the measured values of T_∞ and T_s as all other values are either taken from standard tables or constant. The percentage uncertainty was calculated from Eq.3.12. The maximum value of uncertainty in free and forced convections was about ±8.5%.

$$\Delta Gr = \pm\sqrt{\Delta T_s^{\,2} + \Delta T_\infty^{\,2}} \tag{3.12}$$

3.4.6 Nusselt number

Nusselt number calculated in free and forced convection is tested for uncertainty. The Eq. 3.14 was used to calculate Nusselt number in free convection. The Eq. 3.14 [205] developed for isothermal vertical cylinder by Cebeci [206] is valid for Prandtl number and Curvature parameter (ξ) of 0:01 to 100 and 0 to 5 respectively. The curvature parameter of cylinder cells was calculated by Eq. 3.13, and it is within the range of 0 to 5.

$$\xi = \frac{4L}{D}\left(\frac{Gr_L}{4}\right)^{-1/4} \tag{3.13}$$

$$Nu_L = Nu_{L.fp} \times \left\{1 + 0.3 \times \left[32^{0.5} Gr_L^{\,-0.25}\frac{L}{D}\right]^{0.909}\right\} \tag{3.14}$$

Where $Nu_{L.fp}$ is the Nusselt number calculated for isothermal flat plate taken from correlation given by Churchill and Chu (Eq.)[205], [207].

$$Nu_{L,fp} = 0.68 + \frac{0.67\ Ra_L{}^{1/4}}{[1+(0.492/Pr)^{9/16}]^{4/9}} \quad (3.15)$$

From the given equations, in free convection, Nusselt number is function of Rayleigh number (Ra_L) and Prandtl number (Pr) (Eq.3.16). The uncertainty in the calculations of these values will affect the calculated value of Nusselt number.

$$Nu_{L,fp} = f\ (Ra_L, Pr) \quad (3.16)$$

In forced convection, the cell arrangement is considered as a case of flow across tube banks. The arrangement of cells is inline where each row consists of four cells and total number of rows are three in number. The correlation as given in Eq. 3.17 , developed by Zukauskas [208] for tube bundles is used to evaluate Nusselt number and this correlation considers wide range of Reynolds number and property variations.

$$Nu_D = F\ C\ Re_{D,max}{}^{m}\ Pr^{n}\ (Pr/Pr_s)^{0.25} \quad (3.17)$$

Where $Re_{D,max}$ is Reynolds number defined on the basis on maximum velocity which occurs within the tube bank at the minimum cross-section, Pr is Prandtl number determined at arithmetic mean temperature of fluid (T_m) and Pr_s is Prandtl number determined at surface temperature of cells. The value of C, m and n is taken based on range of Reynolds number as provided in Table 3.11. The F is the correction factor to be used when number of rows are less than 16. The value of correction factor is taken as 0.86 as indicated in the Table 3.12. The uncertainty in the calculated values of Nusselt number from Eq. 17 can be ±15 percent [209].

Table 3.11: Values of C, m and n in Nusselt number correlation (17) for cross flow over tube banks for N>15 and 0.7< Prandtl number <500 [208], [209]

Range of Reynolds number	C	m	n
0-100	0.9	0.4	0.36
100-1000	0.52	0..5	0.36
10^3 to 2×10^5	0.27	0.63	0.36

2×10^5 to 2×10^6	0.033	0.80	0.4

Table 3.12: Correction factor (F) for Nusselt number in Eq. 17 when number of rows are less than 16 [208], [209]

Number of rows , N_L	1	2	3	4	5	7	10	13
In-line arrangement	0.70	0.80	0.86	0.90	0.93	0.96	0.98	0.99

In the battery pack, the cells arrangement is the assumed as the case of inline tube arrangement with transverse pitch (S_T) and longitudinal pitch (S_L), and two cases are evaluated for interspacing, where first interspacing between cells is kept such that $S_T = S_L$= 2mm and then interspacing is increased to $S_T = S_L$= 4mm (see Figure 3.15) . The Reynolds number ($Re_{D,max}$) have been calculated at minimum cross-section area (A_T) with the tube banks. Based on mass of conservation,

$$\rho A_1 Ve = \rho A_T Ve_{max} \tag{3.18}$$

$$Ve_{max} = A_1 Ve/A_T \tag{3.19}$$

where Ve is the approach velocity at area A_1, Ve_{max} is the maximum velocity within tube bank at area A_T. The Ve_{max} calculated in Eq. 3.19 can be simply calculated from values of S_T (interspacing between cells) and diameter, D of cells by Eq. 3.20.

$$Ve_{max} = S_T Ve / (S_T - D) \tag{3.20}$$

The value $Re_{D,max}$ is calculated from Ve_{max} as given by Eq.3.21.

$$Re_{D,max} = \rho\, Ve_{max}\, D/ \mu \tag{3.21}$$

Where density of air (ρ) and dynamic viscosity of air (μ) are evaluated at arithmetic mean temperature of fluid (T_m) calculated by Eq. 3.22.

$$T_m = (T_i + T_e)/ 2 \tag{3.22}$$

Where T_i and T_e are the inlet and exit fluid (air) temperatures.

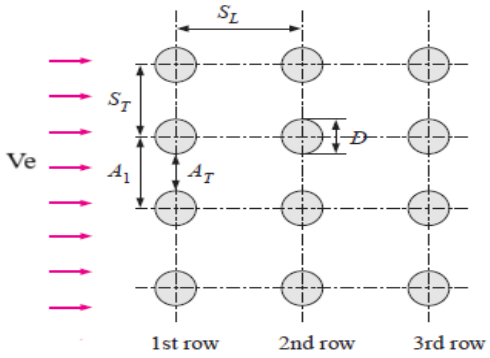

Figure 3.15: Battery cell arrangement as the case of tube inline arrangement in cross flow [212]

3.4.7 Heat transfer

The heat transfer rate by convection was calculated for free and forced convection. In forced convection, the amount of heat absorbed by air is calculated from Eq. 3.23. The overall uncertainty in calculated value by Eq. 3.23 in forced convection heat transfer is based on mass flow rate (m_f), specific heat of air (c_p) and temperature rise of air from inlet to outlet. The uncertainty in specific heat (c_p) is negligible as values are taken from standard table. The uncertainty related to (T_e - T_i) was calculated as ±0.51% from Eq.3.24.

$$Q_{conv,} = m_f c_p (T_e - T_i) \tag{3.23}$$

$$\delta(T_e - T_i) = \sqrt{\delta T_e{}^2 + \delta T_i{}^2} \tag{3.24}$$

Where uncertainties δT_e and δT_i were calculated from RMS based on thermocouple and data logger uncertainties. The uncertainty in heat transfer calculation (δQ_{conv}) was calculated by Eq.3.25. The percentage relative overall uncertainty in heat transfer rate was 5.02%.

$$\frac{\delta Q_{conv}}{Q_{conv}} = \sqrt{\left(\frac{\delta m_f}{m_f}\right)^2 + \left(\frac{\delta(T_e - T_i)}{(T_e - T_i)}\right)^2} \tag{3.25}$$

The convective heat transfer form surface of battery cell to air was also calculated based on correlations as given in section 3.4.6. The heat transfer coefficient (h) is first calculated from Nusselt number (Eq.3.17), and then convective heat transfer is calculated by Newton's law of cooling (Eq. 3.26).

$$Q_{conv} = N h A_s (\Delta T_{lm}) \tag{3.26}$$

Where N is total number of cells, h is heat transfer coefficient, A_s is curved surface area of each cell and ΔT_{lm} is logarithmic mean temperature difference is determined by Eq.27 from average surface temperature of cells ($T_{s,avg}$), inlet temperature of air (T_i) and exit temperature of air from the battery pack (T_e).

$$\Delta T_{lm} = \frac{(T_{s,avg} - T_e) - (T_{s,avg} - T_i)}{\ln[(T_{s,avg} - T_e)/(T_{s,avg} - T_i)]} \quad (3.27)$$

The comparative results of both heat transfer rate as calculated by Eq.3.23 and Eq. 3.26 are evaluated and presented in results (Chapter 4).

The heat transfer rate in free convection based BTMS was evaluated by assuming the case of vertical isothermal cylinder The heat transfer coefficient in free convection based BTMS is evaluated from Eq.3.28 by using Nusselt number (Nu_L) value calculated from correlation as given in Eq. 3.14.

$$h = \frac{Nu_L k}{L_C} \quad (3.28)$$

where L_c is the characteristic length and k is the thermal conductivity of air at film temperature (T_f). The film temperature is calculated by Eq. 3.29.

$$T_f = \frac{T_{s,avg} + T_{amb}}{2} \quad (3.29)$$

Where $T_{s,avg}$ is average surface temperature of cells and T_∞ is ambient temperature of air. All properties if air is taken at film temperature in Eq. 3.14 and Eq.3.15. The heat transfer rate is calculated by Newton's law of cooling (Eq. 3.30).

$$Q_{\text{free convection}} = h\, A_s\, (T_{s,avg} - T_\infty) \quad (3.30)$$

3.4.8 Threshold values of performance parameters

The surface temperature profiles of twelve (12) cells of battery pack were monitored and recorded by K-type thermocouple during discharge process. The time taken to discharge battery pack at various selected discharge rate was less as compared to ideal discharge rate as battery pack reached the cut-off voltage. For analysis of performance of BTMS, three major performance parameters were obtained from recorded data: Peak Temperature, Temperature uniformity and Average temperature. The average temperature at the end of discharge process is the average of peak temperature of each cell, and so mainly threshold is selected for peak

temperature and temperature uniformity only. The experimentation tests are divided into two types of thresholds, ideal threshold (I) and acceptable threshold (A). The combinations of ideal (I) and acceptable threshold (A) were made to evaluate failure and success of systems under various operating conditions. The ideal and acceptable threshold values for peak temperature and temperature uniformity are given in Table 3.13. These values are used in comparative analysis of cooling performance of battery thermal management system.

Table 3.13: Threshold values of performance parameters

(PT) Threshold limits of Peak temperature		(TU) Threshold limits of Temperature uniformity	
Ideal (I)	Acceptable (A)	Ideal (I)	Acceptable (A)
(T ≤40˚C)	(T ≤ 50˚C)	(ΔT ≤ 5˚C)	(ΔT ≤ 8˚C)

3.5 Validation of Experimental Results

The validation of experimental facility was carried out by comparative analysis of Nusselt number in forced convection BTMS at 1C and 2C discharge rate at varying Reynolds number. The variation of Nusselt number calculated from experimentally measured values is analysed and compared with respect to Nusselt number calculated from correlation (Eq.3.17) for cross flow across tubes by Zukauskas A [208]. The experimental Nusselt number ($Nu_{L,exp}$) (Eq.3.32) was calculated from heat transfer coefficient (h) obtained from energy balance equation (Eq.3.31).

$$m_f c_p (T_e - T_i) = N h A_s (\Delta T_{lm}) \tag{3.31}$$

$$Nu_{L,exp} = \frac{L_c}{k}\left[\frac{m_f c_p (T_e - T_i)}{N A_s (\Delta T_{lm})}\right] \tag{3.32}$$

The Nusselt number values are calculated at 1C and 2C rates at varying air inlet velocity. At every air inlet velocity two Reynolds value are taken as density of air changes with air temperature. The comparative results between correlations based Nusselt number and Nusselt number based on experimental data for 1C and 2C discharge rates can be seen in Figure 3.16 and Figure 3.17 respectively. The variation in experimental Nusselt number with Reynolds follows the same trend as correlation based Nusselt value. The difference between empirical and experimental Nusselt values is under 10%. In addition to Nusselt number values, the experimental heat transfer rate at 2C discharge rate under 3.6 m/s and 4/6 m/s air inlet velocity

is also compared with empirical heat transfer rate. As can be seen in Figure , the experimental heat transfer rate (Q-Exp) is correlated with empirical heat transfer (Q-emp) and percentage variation is under 10%. The experimental results of heat transfer are also fit with polynomial curve and the value of coefficient of determination (R^2) value for each polynomial fit at 3.6 m/s and 4.6 m/s is indicated in the figures and its value in all cases is above 0.9 which indicates a good fit. The polynomial fitted curve of experimental results is well in trend with empirical results. The average temperature rise in free convection is compared with temperature rise of 32650 cells in literature of research work done by Scott Mathewson title "Experimental Measurements of $LiFePO_4$ Battery Thermal Characteristics" [85], [210] where discharge process was started at 20°C as compared to present research work 30°C. The comparative analysis (see Figure 3.20) showed same trend in temperature increase with deviation mainly due to difference in initial temperature at start of the discharge process.

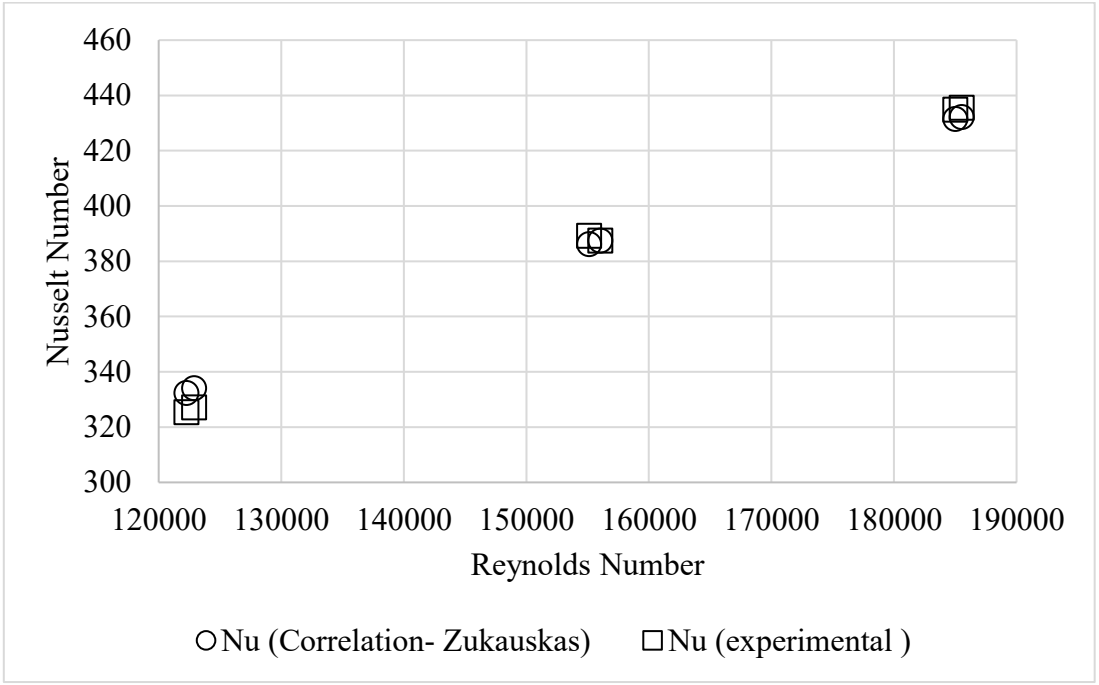

Figure 3.16: Nusselt number values based on correlation and experimental data at 1C discharge rate

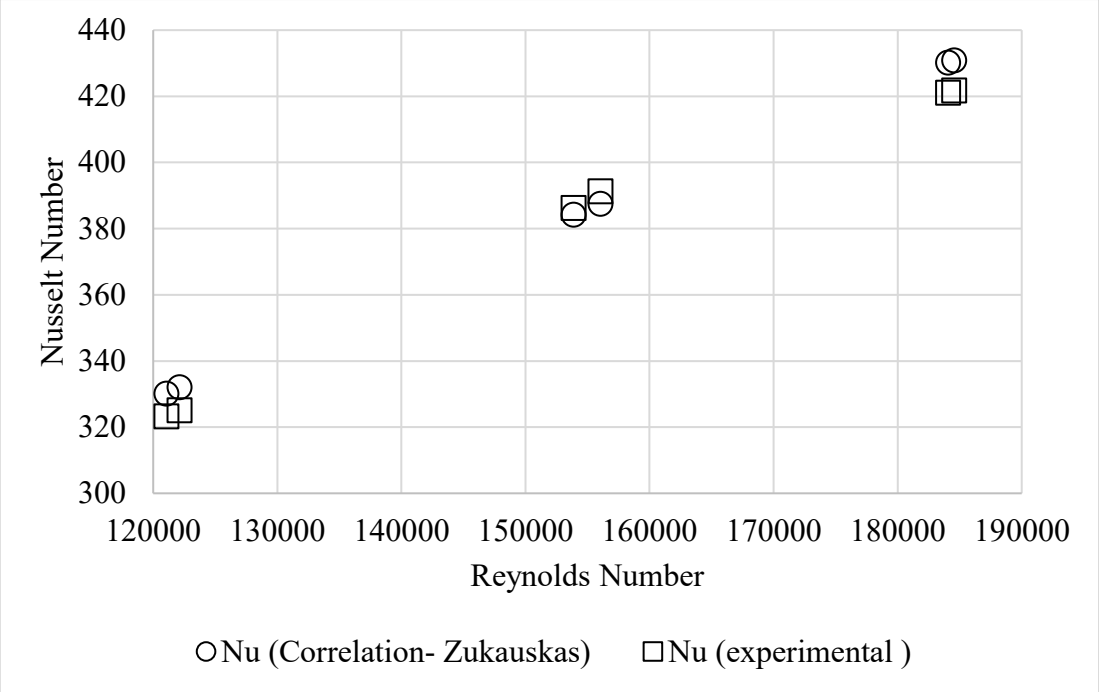

Figure 3.17: Nusselt number values based on correlation and experimental data at 2C discharge rate

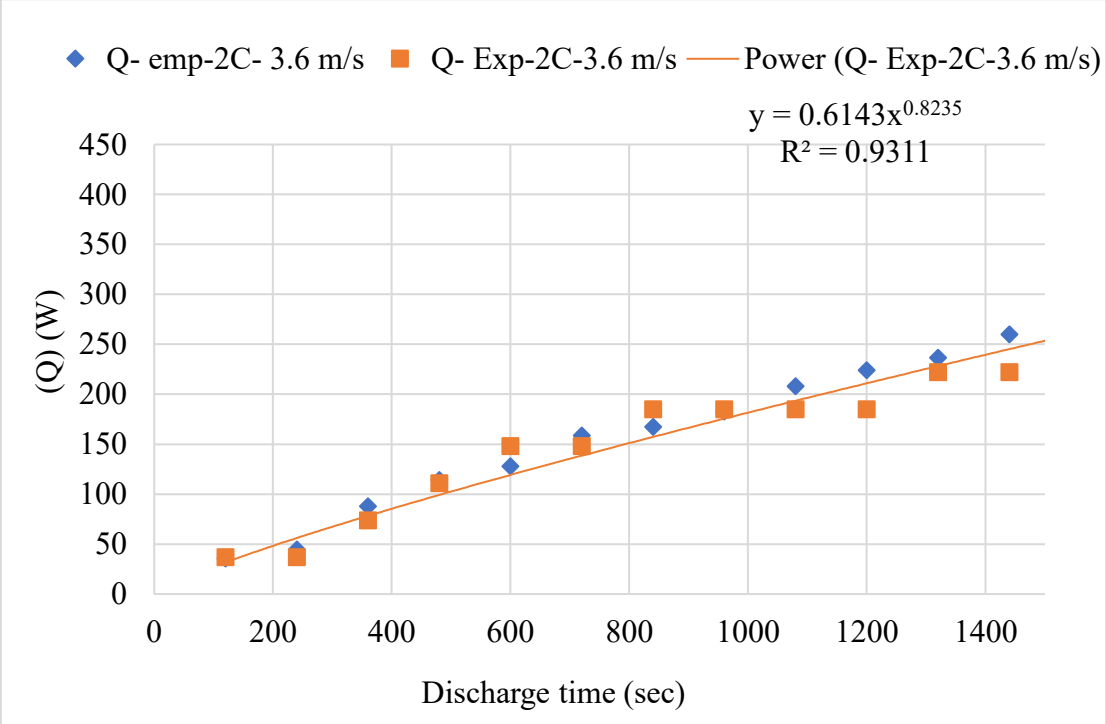

Figure 3.18: Convective heat transfer rate at 2C discharge rate and 3.6 m/s air inlet velocity

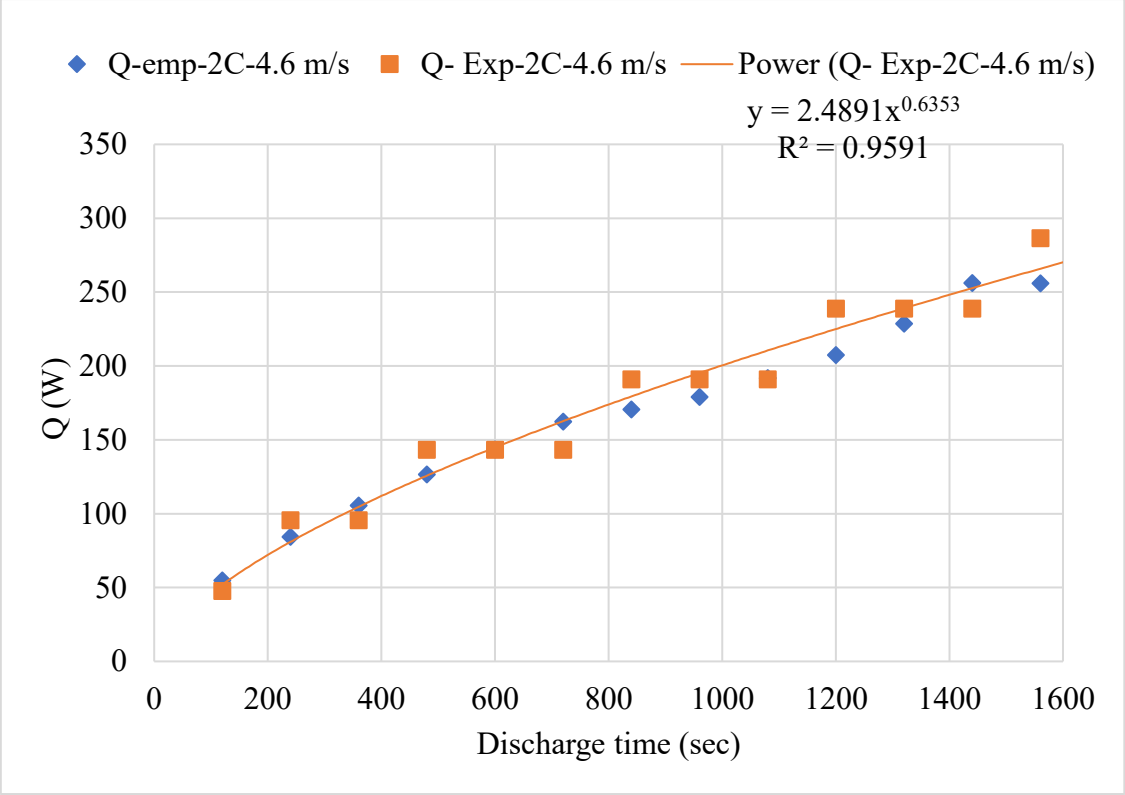

Figure 3.19: Convective heat transfer rate at 2C discharge rate and 4.6 m/s air inlet velocity

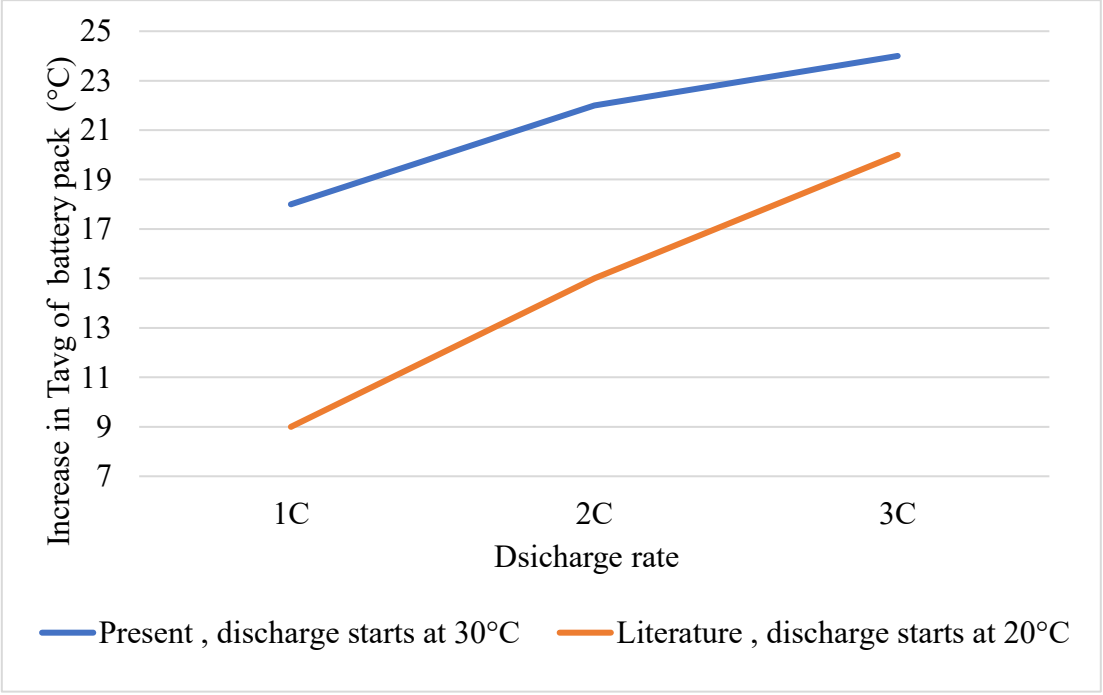

Figure 3.20: Comparative analysis of temperature rise under free convection at 1C, 2C and 3C discharge rates

Chapter 4 Results and Discussion

The results of experimental analysis are presented in this chapter, and results are arranged as per objectives of the research. The experimental data collected include dependent variables and independent variables. The dependent variables studied under experimental investigation are:

1. Peak surface temperature battery cells (T_{max})
2. Average temperature of battery pack (T_{avg})
3. Temperature uniformity or homogeneity inside battery pack (ΔT)

The independent variables in the experimental investigation are varied to study their effect on dependent variables. The selected independent variables are:

1. C-rate
2. Air inlet velocity in forced convection
3. Interspacing between cells

Four different types of battery thermal management systems were fabricated for the research work. These are denoted as:

1. Free convection cooled battery pack is fabricated with 2 mm interspacing, and it is denoted as BTMS-FR. Here the batteries are only cooled with free convective currents of air.
2. Forced convection based battery cooling system. Here forced air is used as a cooling medium. This battery thermal management system is denoted as BTMS-FO.
3. The third battery pack was like second one i.e. BTMS-FO as two different interspacing were tested for forced convection i.e. 2 mm and 4mm. The battery pack has 4 mm interspacing between cells. It is denoted as BTMS-FO-4mm
4. The fourth battery pack and cooling system was fabricated with heat pipes insertions between cells. The heat pipes installed between rows of cells are cooled by forced convection (air). The system is hybrid of heat pipe and air cooling. It is denoted as BTMS-HP.

The first objective of research is related with analysing the performance of free convection and forced convection based battery cooling system (BTMS-FR and BMMS-FO). The second objective introspect the change in performance of cooling with interspacing increase in forced convection based cooling system (BMTS-FO). The third objective of present research is to conduct comparative analysis of heat pipe based hybrid battery cooling system with free and forced convection based battery cooling systems. The overall experimentation at different level of independent variables is presented in Figure 4.1.

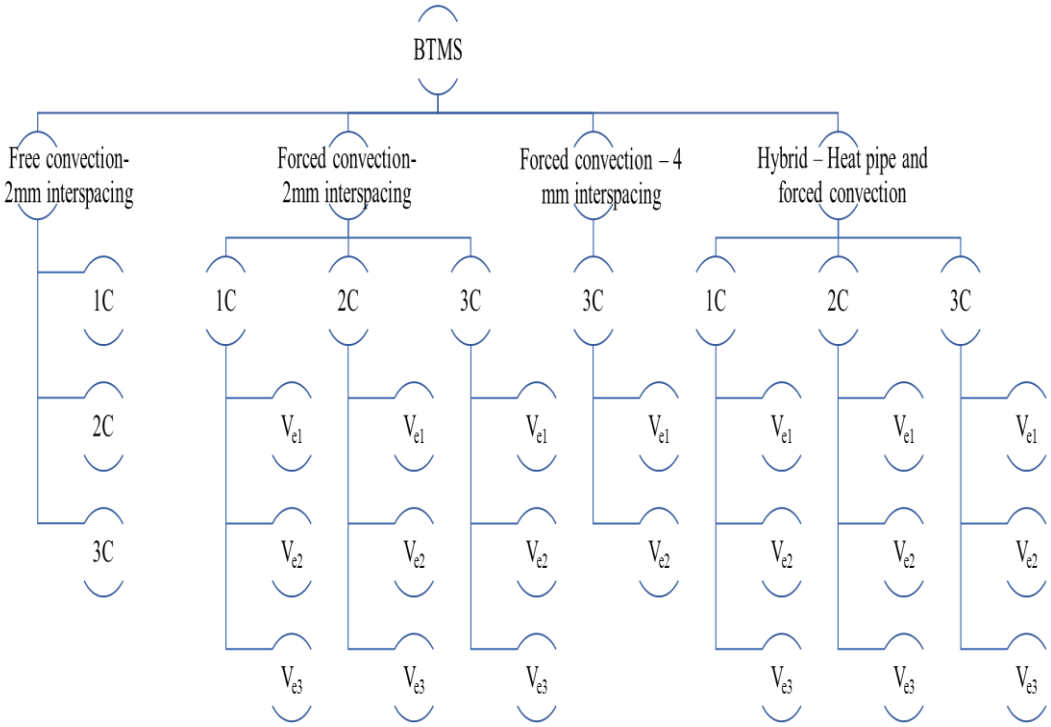

Figure 4.1: Design of experimentation- levels of independent variables

4.1 Objective 1: To analyse the effect of temperature distribution inside Li-ion battery pack at varying discharging rates for base case BTMS-woHP (convection air-cooling without heat pipe).

The base case battery thermal management is cooling system which are used for comparative analysis with heat pipe based hybrid battery thermal management system. Two different BTMS are considered as base case. They are free convection based BTMS (BTMS-FR) and forced convection based BTMS (BTMS-FO) A comparative analysis of the performance of forced convection cooling (BTMS-FO) and free convection cooling (BTMS-FR) was conducted with

respect to hybrid heat pipe based BTMS (BTMS-HP). Before starting experiment, all cells of the battery pack were tested for voltage, and it was about 3.2 V for each cell with only 5% variation from nominal voltage allowed. Two different battery packs were fabricated for objective 1, one for free convection (battery pack 1) with 2 mm interspacing between cells and other for forced convection (battery pack 2) with 2 mm interspacing between cells. The results are presented for both battery packs.

4.1.1 Battery pack 1- Base case BTMS-FR with 2 mm interspacing

Three different cases were taken:

1. Battery pack discharged at 1C, and cut-off voltage was kept at 22 V.
2. Battery pack discharged at 2C, and cut-off voltage was kept at 22 V.
3. Battery pack discharged at 3C, and cut-off voltage was kept at 22 V.

The battery pack was discharged at 1C, 2C and 3C rates. The cut-off voltage was kept at 22 V. The battery pack initial voltage reading was measured with help of digital multi-meter. Twelve LFP cells connected in series and voltage reading across the battery pack was 39.5 V. Cells were exposed to environment and ambient air temperature was 29˚C, Typical discharge curves related to 1C, 2C and 3C rates are shown in Figure 4.2. The cut-off voltage of 22 V was achieved after discharging battery for 46 minutes and 20 seconds in 1C, for 27 minutes and 50 seconds in 2C and for 17 minutes and 40 seconds in 3C.

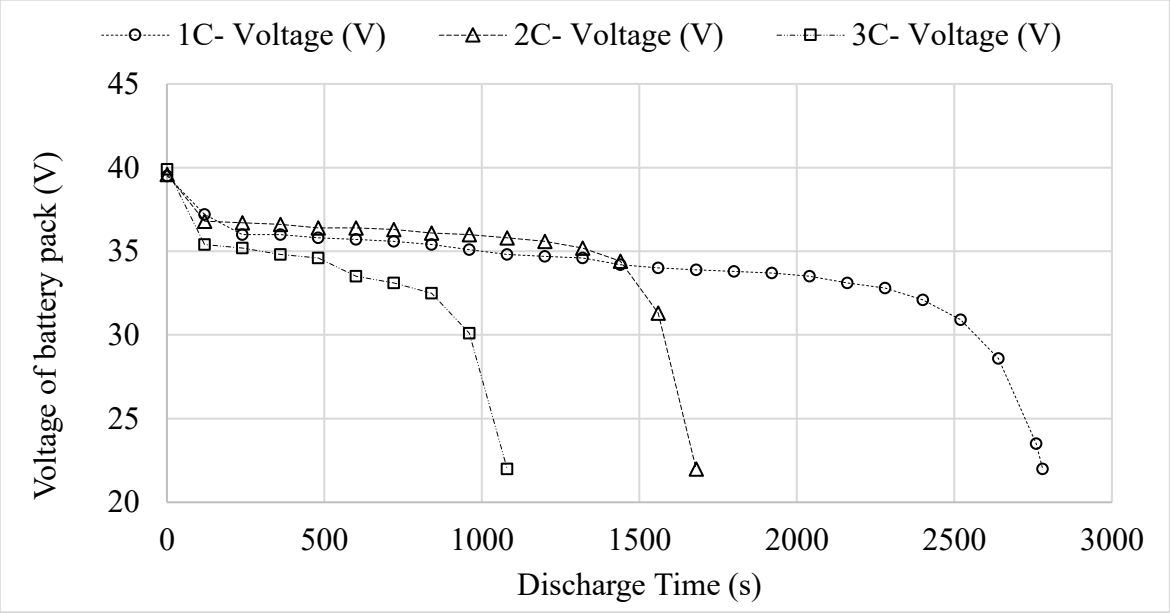

Figure 4.2: Discharge curves at 1C, 2C and 3C discharge rates

The temperature measurements were done at time interval of 120 seconds. Following important parameters were calculated from temperature readings of each thermocouple placed on battery cells.

4.1.1.1 Average temperature (T_{avg}) of battery pack during discharge process.

$$Tavg = \frac{\sum \text{temperature of battery cells at particular time}}{\text{number of battery cells}} \quad (4.1)$$

The average temperature variations of battery pack during discharge process at 1C, 2C and 3C rates can be seen in Figure 4.3. The average temperature of battery pack at 3C rate is higher than 1C and 2C. This is because the batteries are discharged in shorter interval of time at 3C rate, and this leads to more internal heat generation which thereby raises the temperature of batteries. The increase in average temperature of battery pack is 33% and 26% higher at 3C and 2C rates respectively as compared to 1C discharge rate .

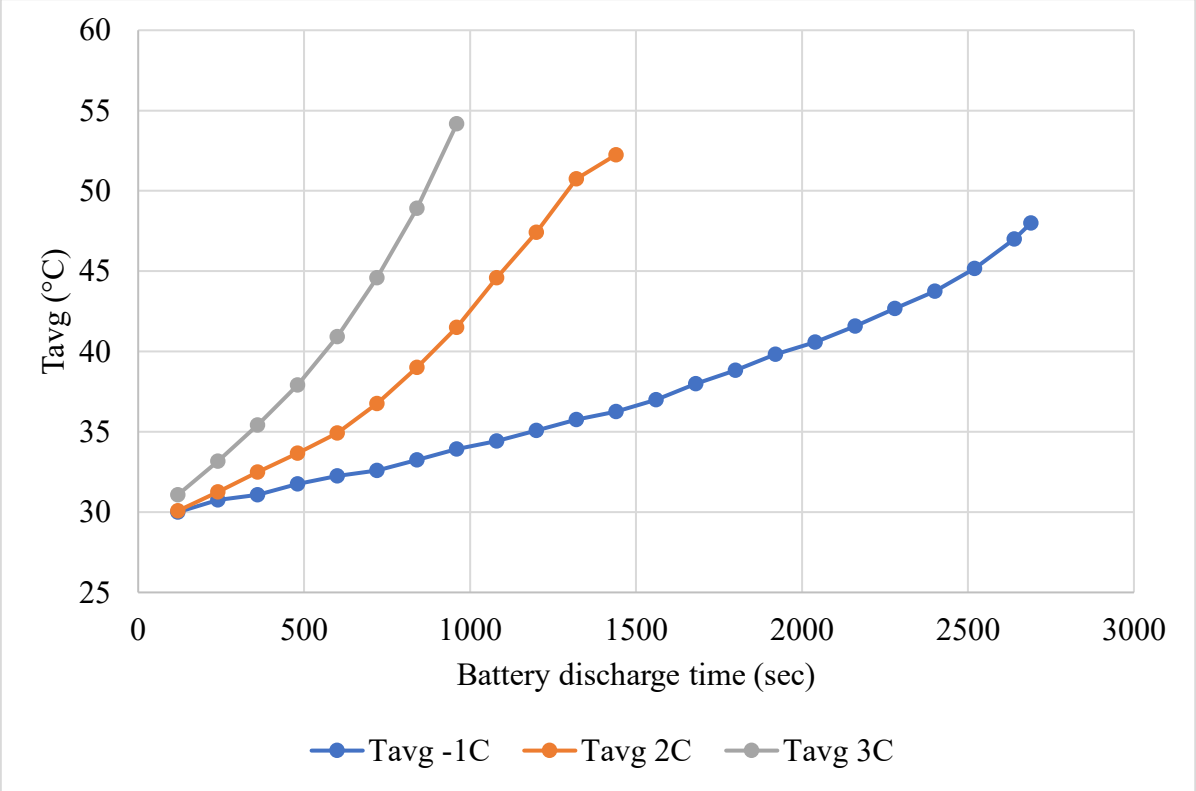

Figure 4.3:Average temperature of battery pack under free convection (BTMS-FR) during 1C, 2C and 3C discharge rates

As can be seen in the Figure 4.4, at the end of discharge process, the difference between recorded temperature at 3C and 2C rate are respectively 6.2°C and 4.3°C higher as compared to 1C rate. In terms of percentage, the average temperature of battery pack at the end of discharge process at 3C and 2C are respectively 33% and 26% higher than average temperature of battery pack at 1C discharge rate.

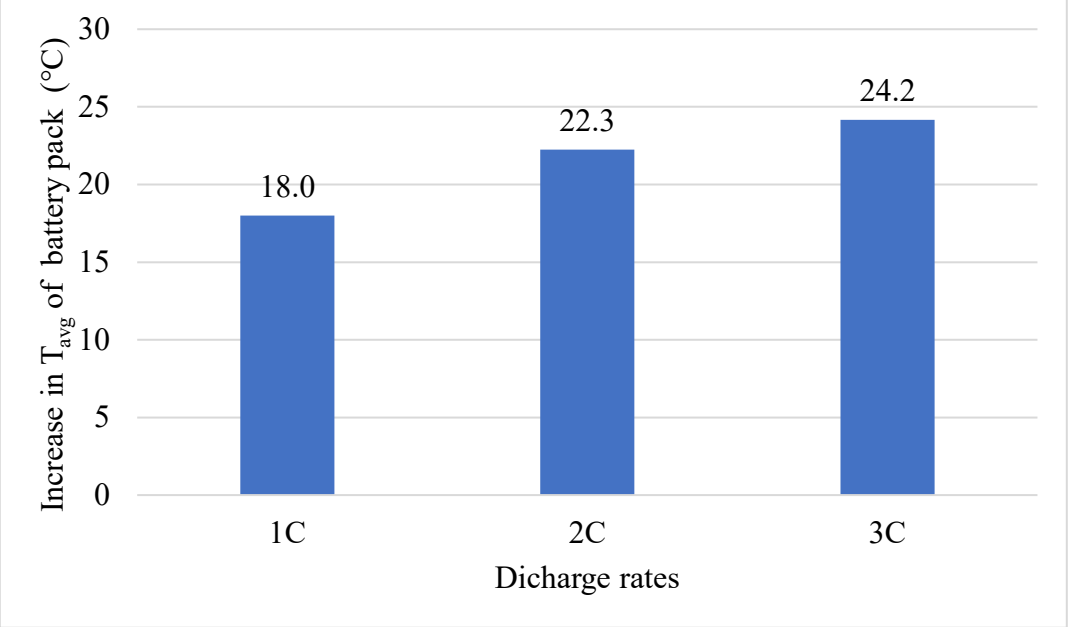

Figure 4.4:Increase in average temperature of battery pack under free convection (BTMS-FR) at 1C, 2C and 3C discharge rate

4.1.1.2 Peak temperature (T_{max}) of each cell at the end of discharge process.

The peak temperature of each cell during discharge process was recorded. The cells in the battery pack are numbered from 1 to 12 as shown in Figure 4.6. The peak temperature of each cell in the battery pack is shown in Figure 4.5. The results indicate that the mid-cells i.e. cell 6 and cell 7 (see Figure 4.6) are more critical as they have higher peak temperature even above 55°C while peak temperature of other cells falls within the range of 45°C to 55°C. This is because these two middle cells (cell 6 and cell 7) have limited space available for free convection as they are surrounded by other cells and because of that the free convective currents are not effective for middle cells.

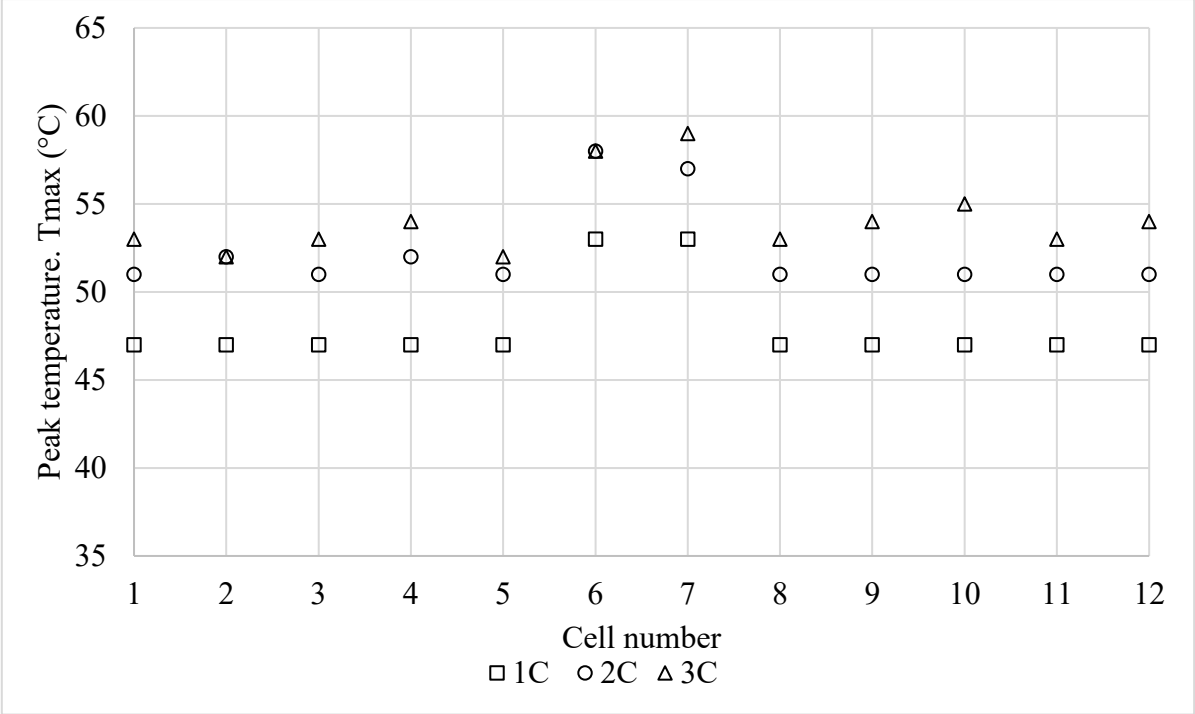

Figure 4.5:Peak cell temperature at the end of discharge process -1C, 2C and 3C - for battery pack under free convection

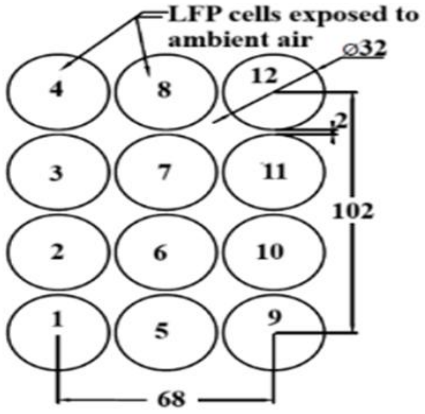

Figure 4.6:Arrangement of cells in battery pack under free convection

4.1.1.3 Temperature uniformity or homogeneity (ΔT) of battery pack.

At time during discharge process, the temperature uniformity is measured by taking difference between temperatures of cell with maximum temperature and cell with minimum temperature.

$$\Delta T = (T_{max} - T_{min}) \quad (4.2)$$

The temperature uniformity inside the pack is prime factor which decide battery pack unbalanced degradation. If certain cells are at higher temperature during the discharge as compared to other cells, these cells will degrade faster. As shown in Figure 4.5, related to peak temperature, middle cells 6 and 7 are critical. But to get an idea of overall uniformity of temperature in the battery pack, ΔT values were considered during discharge process (See Figure 4.7). The temperature non-homogeneity or non-uniformity increase as discharge rate is increased. This shows that the cells which are having higher peak temperature become more stressed with increasing discharge rate. Overall ΔT values at the end of discharge process is shown in Figure 4.8. There is no difference in ΔT at 2C and 3C discharge rate, although as can be seen in Figure 4.7, the rate of increase in ΔT is higher for 3C rate because discharge process interval at 3C is shorter than 2C. The rise of peak temperature and non-uniformity of temperature in short interval make cells highly vulnerable to failure at higher discharge rates. The 1°C reduction in ΔT at 1C rate is very important as each degree drop toward temperature uniformity increase overall battery pack life. The ideal limit and acceptable limit of ΔT are 5°C and 8°C. As can be seen in Figure 4.8, although ΔT value exceeded ideal limit in free convection but it was able to maintain temperature uniformity with acceptable limit of 8°C.

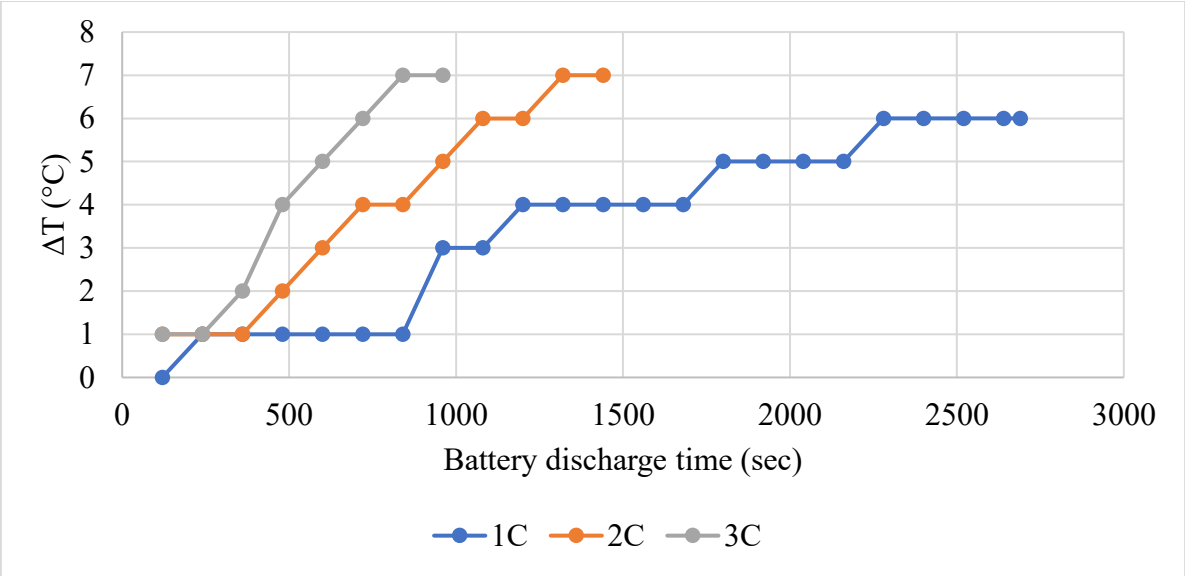

Figure 4.7:Temperature uniformity variation inside battery pack during discharge process under free convection (BTMS-FR) at 1C, 2C and 3C

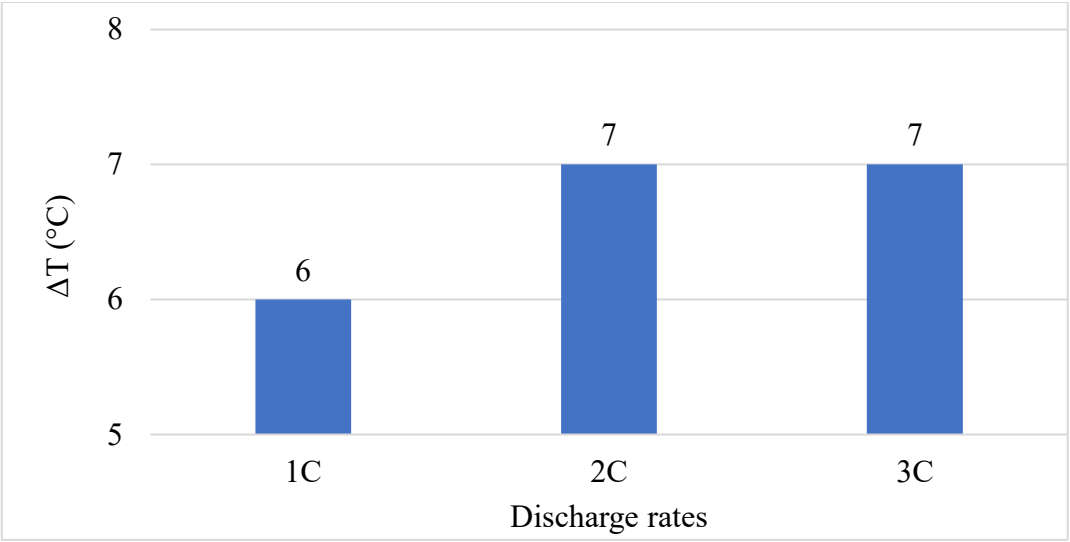

Figure 4.8: Maximum temperature non-uniformity in battery pack at end of discharge process under free convection (BTMS-FR) at 1C, 2C and 3C

4.1.1.4 Heat transfer coefficient (h) and convective heat transfer (Q)

The heat transfer coefficient is calculated from the Nusselt number values as given in Eq. 4.3.

$$Nu = \frac{hL_c}{k} \tag{4.3}$$

Where h is heat transfer coefficient in W/m^2K, k is thermal conductivity W/mK in and L_c characteristic length (i.e., height of cell). For calculation purpose, height of cell is taken as 63 mm as 2 mm remain inside spacer and is not exposed to ambient air. Assuming cylinder cell case as equivalent to vertical plate, Nusselt number is calculated by relation as suggested by Churchill and Chu [211] over entire range of Rayleigh number (Ra_L) under free convection.

$$Nu = \left\{0.825 + \frac{0.387\ Ra_L^{1/6}}{\left[1+ (0.492/Pr)^{9/16}\right]^{8/27}}\right\} \tag{4.4}$$

$$Ra_L = \frac{g\,\beta\,(T_s - T_\infty)L_c^3\,Pr}{\nu^2} \tag{4.5}$$

Where g is acceleration due to gravity in m/sec^2, β is coefficient of volume expansion, T_s is average surface temperature of battery pack in degree Celsius, T_∞ is ambient temperature in degree Celsius, ν is kinematic viscosity in m^2/sec and Pr is Prandtl number. All properties of air are evaluated at Film temperature (T_f). The coefficient of volume expansion is evaluated by assuming air as ideal gas.

$$\beta = \frac{1}{T_f} \text{ (for ideal gas)} \quad (4.6)$$

$$T_f = \frac{T_s + T_\infty}{2} \quad (4.7)$$

The heat transfer coefficient values are well within establish range of heat transfer coefficient available as available literature references for free convection [212]. The range for h for free air convection is 2.5 to 25 W/m^{2}K [212].

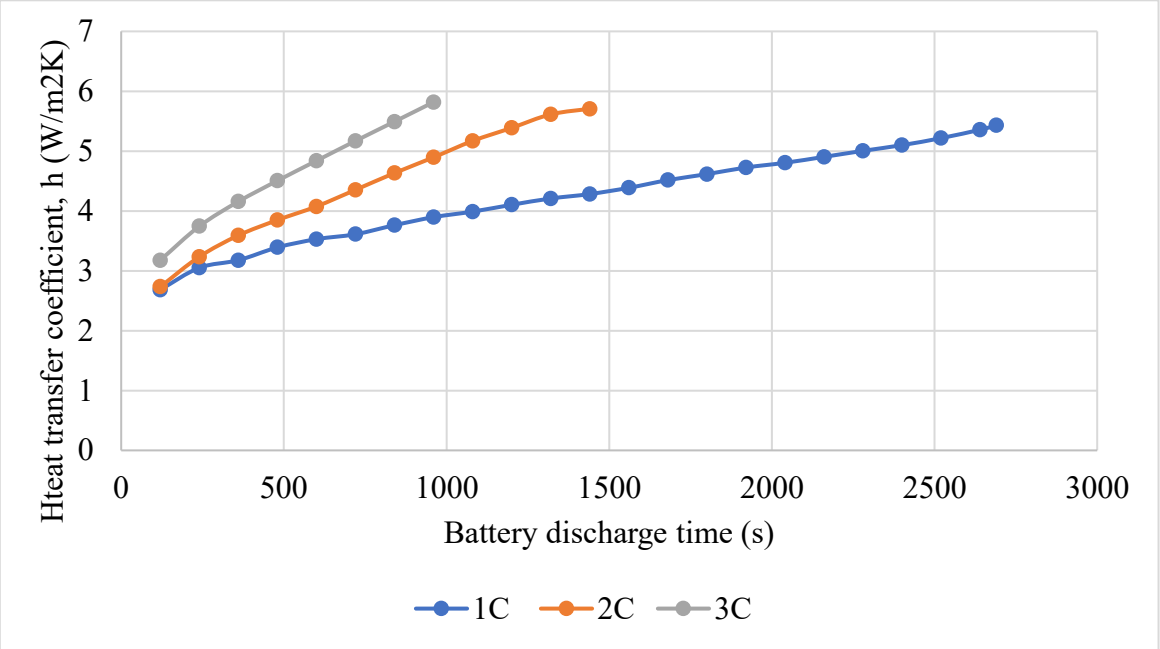

Figure 4.9: Heat transfer coefficient values at 1C, 2C and 3C discharge rate under free convection

The heat transfer rate during discharge process was calculated by using Newton's law of cooling.

$$Q_{conv} = hA_s(T_s - T_\infty) \quad (4.8)$$

Where A_s is the total surface area of all battery cells in m^2. The heat transfer during discharge process at 1C, 2C and 3C is shown in Figure 4.10.

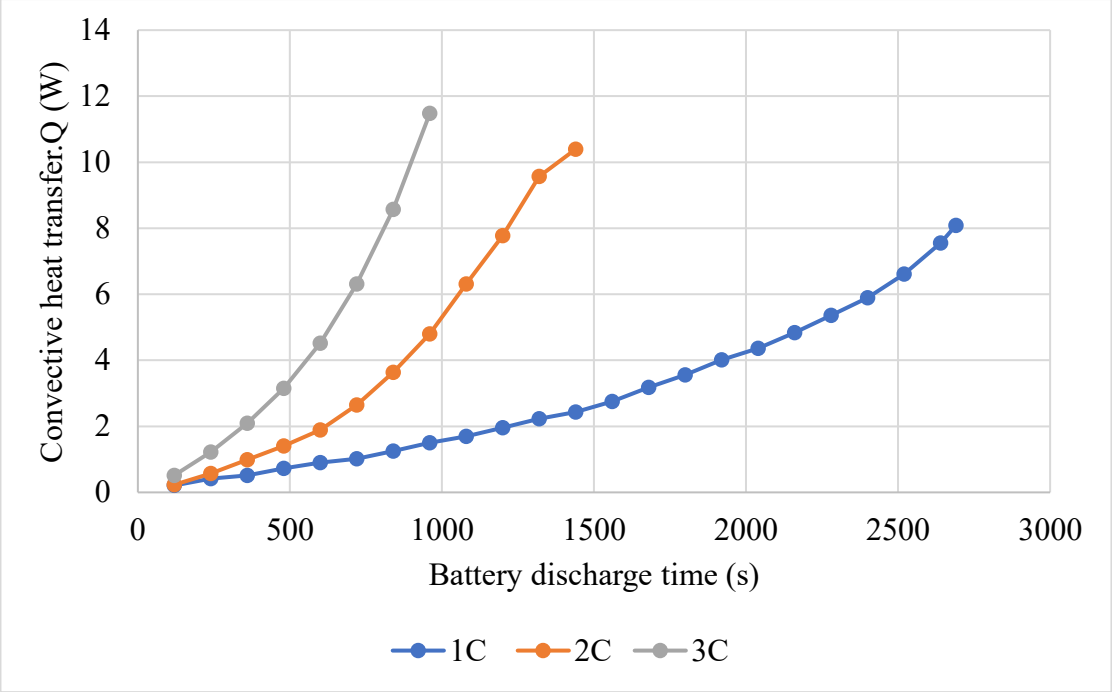

Figure 4.10: Convective heat transfer at 1C, 2C and 3C for battery pack under free convection (BTMS-FR)

4.1.2 Battery pack 2- Battery pack under forced convection with 2 mm interspacing (BTMS-FO)

The battery pack fabricated for forced convection initially has 2 mm as interspacing between cells. Based on other two independent variables i.e. discharge rate and air inlet velocity; nine different cases were taken for forced convection based BTMS (BTMS-FO). They are:

i. Battery pack discharged at 1C when inlet air velocity is V_{e1}, and cut-off voltage was kept at 22 V.
ii. Battery pack discharged at 2C when inlet air velocity is V_{e1}, and cut-off voltage was kept at 22 V.
iii. Battery pack discharged at 3C when inlet air velocity is V_{e1}, and cut-off voltage was kept at 22 V.
iv. Battery pack discharged at 1C when inlet air velocity is V_{e2}, and cut-off voltage was kept at 22 V.
v. Battery pack discharged at 2C when inlet air velocity is V_{e2}, and cut-off voltage was kept at 22 V.

vi. Battery pack discharged at 3C when inlet air velocity is V_{e2}, and cut-off voltage was kept at 22 V.
vii. Battery pack discharged at 1C when inlet air velocity is V_{e3}, and cut-off voltage was kept at 22 V.
viii. Battery pack discharged at 2C when inlet air velocity is V_{e3}, and cut-off voltage was kept at 22 V.
ix. Battery pack discharged at 3C when inlet air velocity is V_{e3}, and cut-off voltage was kept at 22 V.

Battery pack was discharged at 1C, 2C and 3C under forced convection air-cooling. Average temperature, peak temperature and temperature uniformity are the key parameters measured during experimentation. Other than these, convective heat transfer coefficient and heat transfer rate are also calculated. Based on discharge rate and inlet air velocity, there are nine cases for forced convection (BTMS-FO) when interspacing is 2 mm. The experimentation was conducted at different combination of discharge rate and air inlet velocity.

4.1.2.1 Average temperature inside battery pack during discharge process.

The average temperature of battery pack is calculated as given in section 4.1 for free convection. The variation of average temperature at 1C, 2C and 3C under varying air inlet velocity can be seen in Figure 4.11, Figure 4.12 and Figure 4.13 respectively. The results showed that with increase in air inlet velocity there is only 1% to 6% reduction in average temperature of battery. The variation of average temperature at different air inlet velocities under varying discharge rate is also presented. As compared to changing air inlet velocity, the variation in discharge rate significantly affects the average temperature (see Figure 4.14, Figure 4.15 and Figure 4.16). There is 37% to 39% increase in average temperature at 3C rate as compared to 1C rate at varying air inlet velocity. The results indicate that discharge rate is more significant factor than air velocity in average temperature control but to achieve higher acceleration and power, the batteries must be discharged at higher rates. So, limiting discharge rate is not a solution for temperature control. As per acceptable threshold limit, the temperature of li-ion cells should be below 50°C. The BTMS-FO was able to achieve this target, and, in all cases, it was observed that average temperature of battery pack was within acceptable limit of operation. The average temperature does not give complete information about condition of each cell, so peak

temperature is more important parameter than average temperature for studying operating condition of each cell of battery pack.

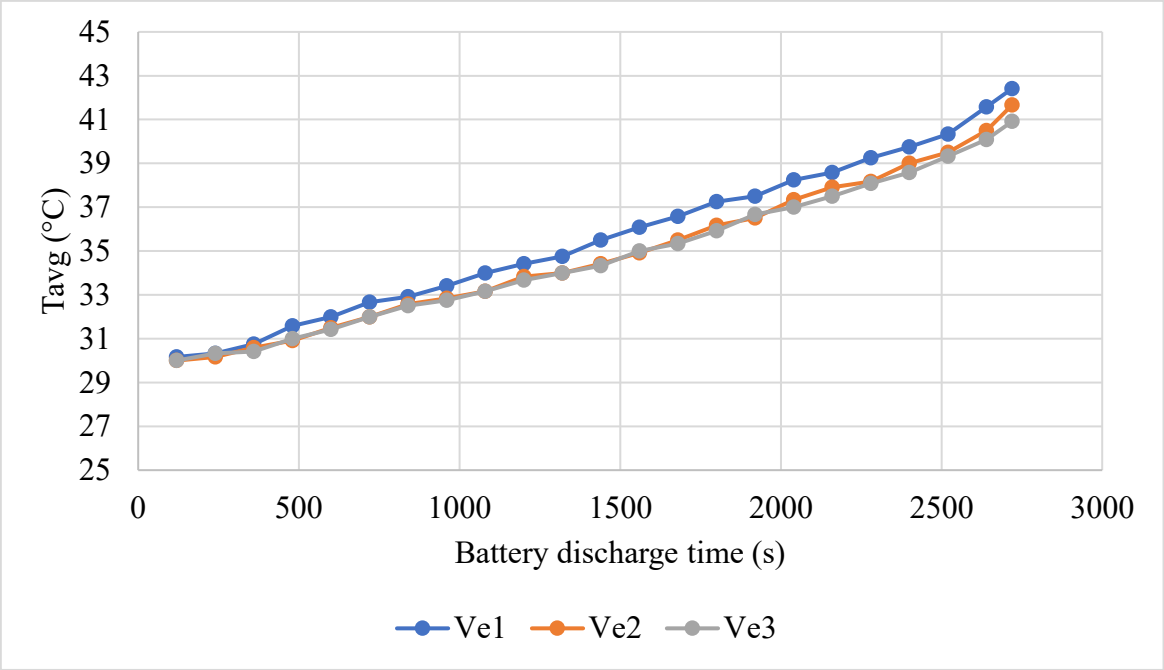

Figure 4.11: Average temperature of battery pack at varying air inlet velocity under forced convection (BTMS-FO) at 1C discharge rate

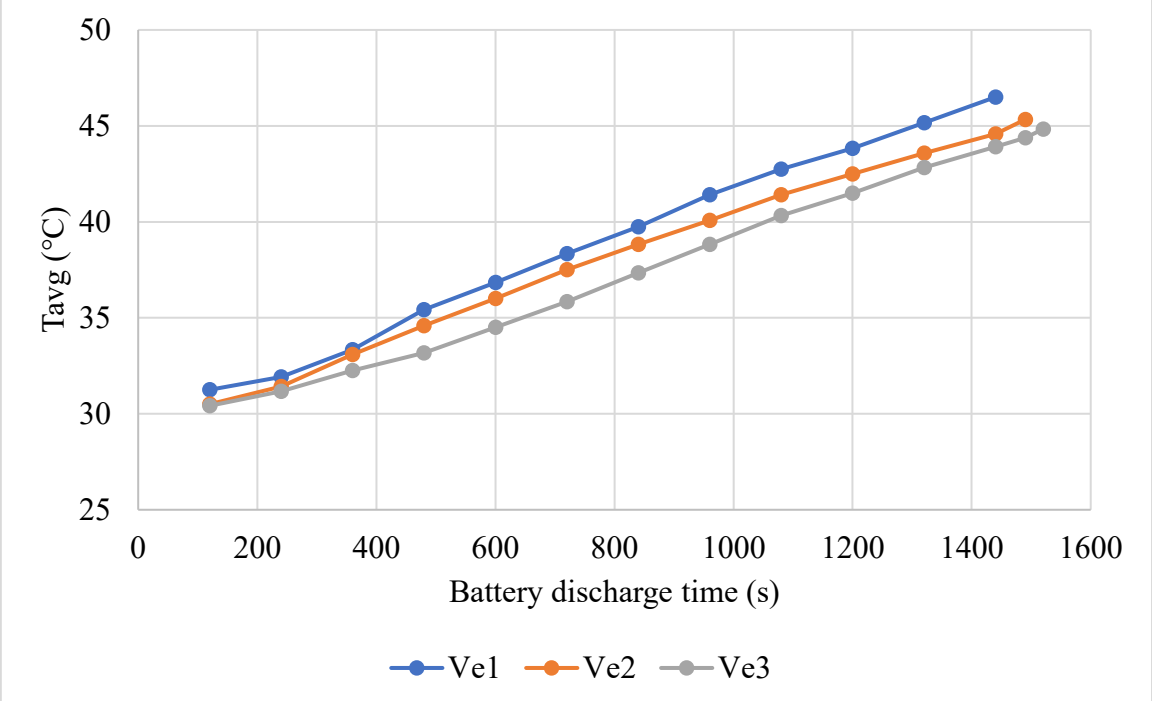

Figure 4.12: Average temperature of battery pack at varying air inlet velocity under forced convection (BTMS-FO) at 2C discharge rate

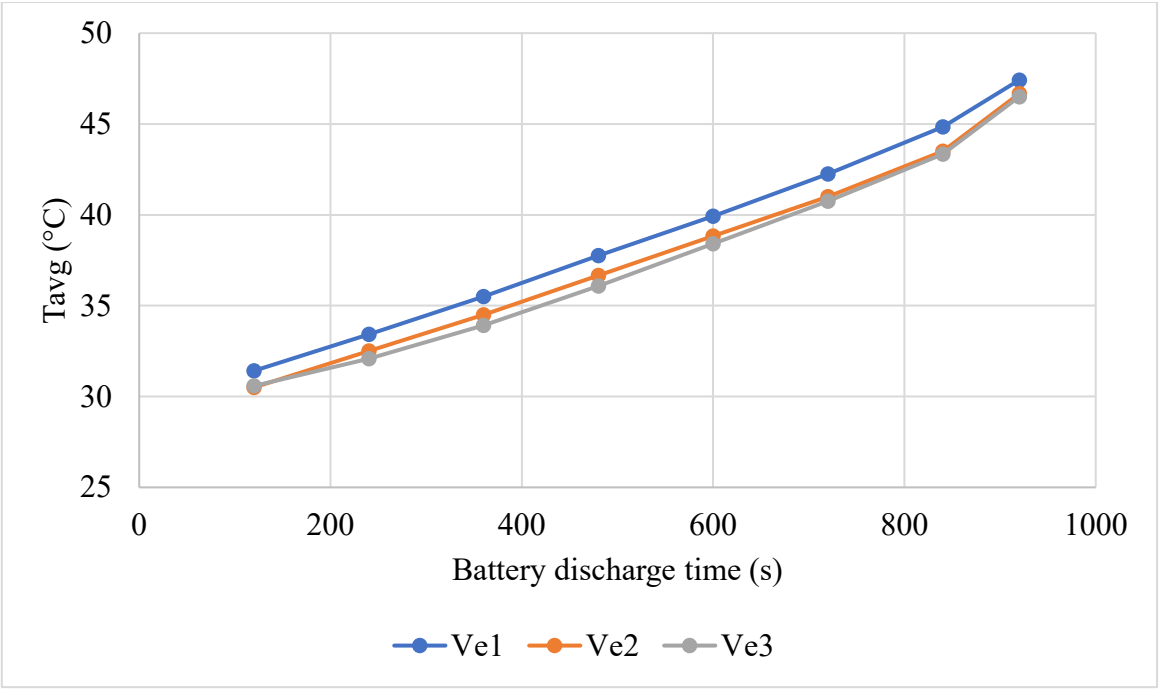

Figure 4.13: Average temperature of battery pack at varying air inlet velocity under forced convection (BTMS-FO) at 3C discharge rate

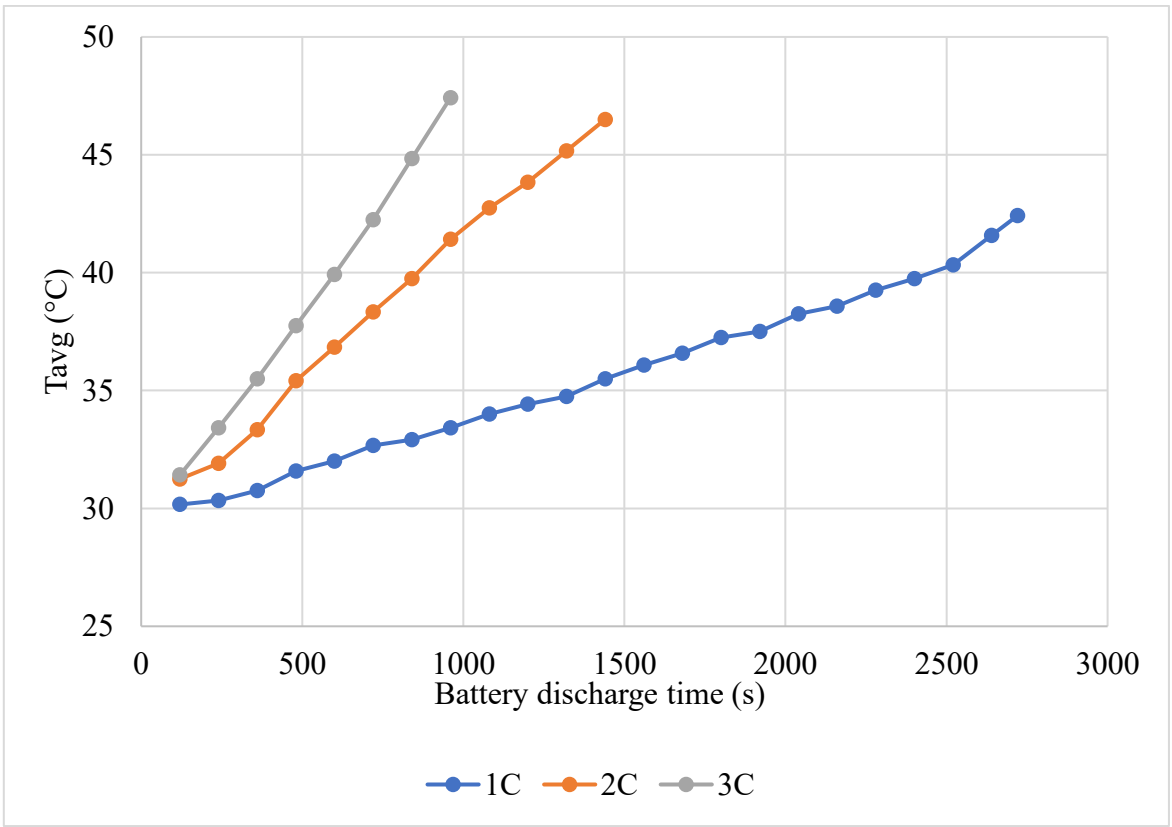

Figure 4.14: Average temperature of battery pack at inlet air velocity 3.6 m/s (Ve1) when discharge rates were 1C, 2C and 3C for BTMS- FO (forced convection)

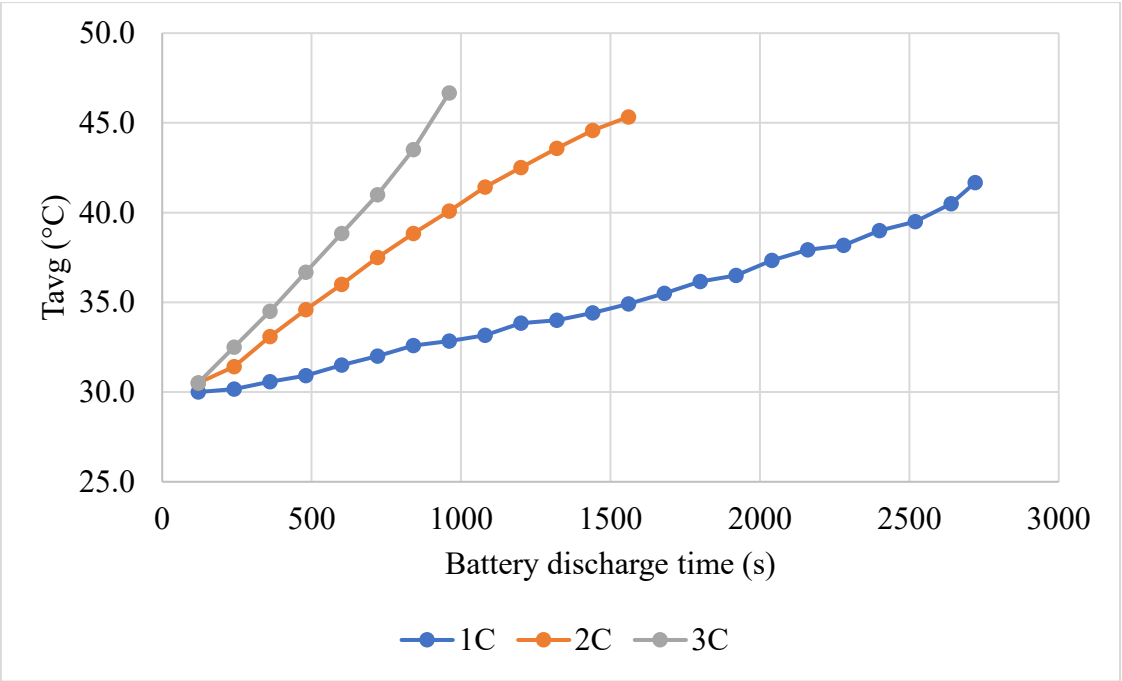

Figure 4.15: Average temperature of battery pack at inlet air velocity 4.6 m/s (Ve2) when discharge rates were 1C, 2C and 3C for BTMS- FO (forced convection)

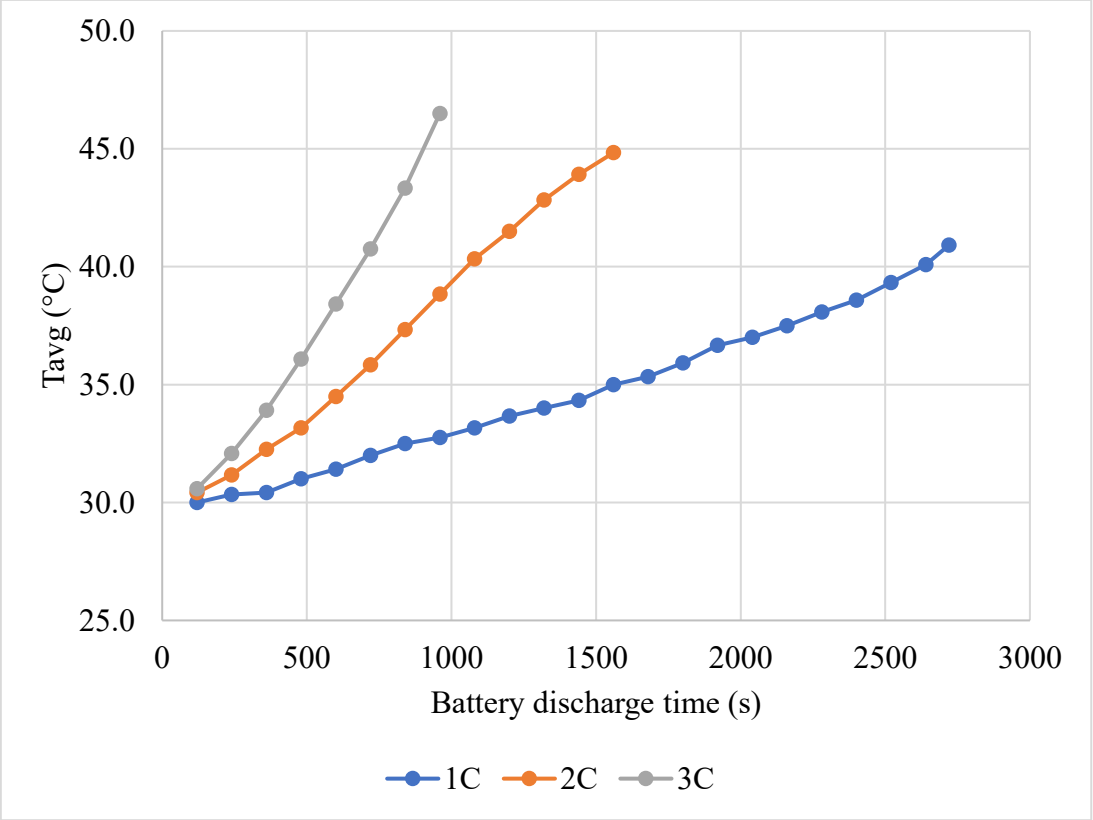

Figure 4.16: Average temperature of battery pack at inlet air velocity 5.5 m/s (Ve3) when discharge rates were 1C, 2C and 3C for BTMS- FO (forced convection)

4.1.2.2 Maximum (Peak) temperature of each cell

The cells reached their peak temperature usually at the end of discharge process as during discharge process more internal heat gets accumulated inside the cells thereby raising the temperature of the cells. As like average temperature, the results are presented at varying discharge rate and at varying air inlet velocity. The Figure 4.17, Figure 4.18 and Figure 4.19 shows the peak temperature of each cell at discharge rate of 1C, 2C and 3C respectively under varying air inlet velocities. The results showed that the cells in last row i.e. cell number 9, 10, 11 and 12 are at much higher temperature than other cells. Row wise temperature distribution also indicate that front row of cells is cooled much more efficiently than other two rows of cells. The results presented in Figure 4.20, Figure 4.21 and Figure 4.22 shows the cell-wise peak temperature of cells at air inlet velocity Ve1 (3.6 m/s), Ve2 (4.6 m/s) and Ve3 (5.5 m/s) under varying discharge rates. The peak temperature distribution at different air velocities also remained same with critical cells being 9, 10, 11 and 12 (last row). The higher peak temperatures were observed at higher discharge rates and at lower air inlet velocities. This being due to the reason that more energy is converted to heat at higher discharge rate as conversion efficiency decreases as discharge rate is increased. The increase in average temperature of battery pack is 33% and 26% higher at 3C and 2C rates respectively as compared to 1C discharge rate. The peak temperature of cells 9, 10, 11 and 12 exceeded beyond acceptable limit of 50°C. These cells are critical cells in the battery as they are under stress, and they may fail earlier as compared to other cells of battery pack. The flow pattern in forced convection is the main reason for non-uniform cooling of cells. The parameter to take care is design of battery pack. The present design being a rectangular layout has inherent limitation as air heat carried by air as it flows through the system reduces due to reduced temperature difference between heated surface and air. The peak temperature across the system creates non-uniformity of temperature and this results in unbalanced cells where some cells fail earlier due to excessive degradation.

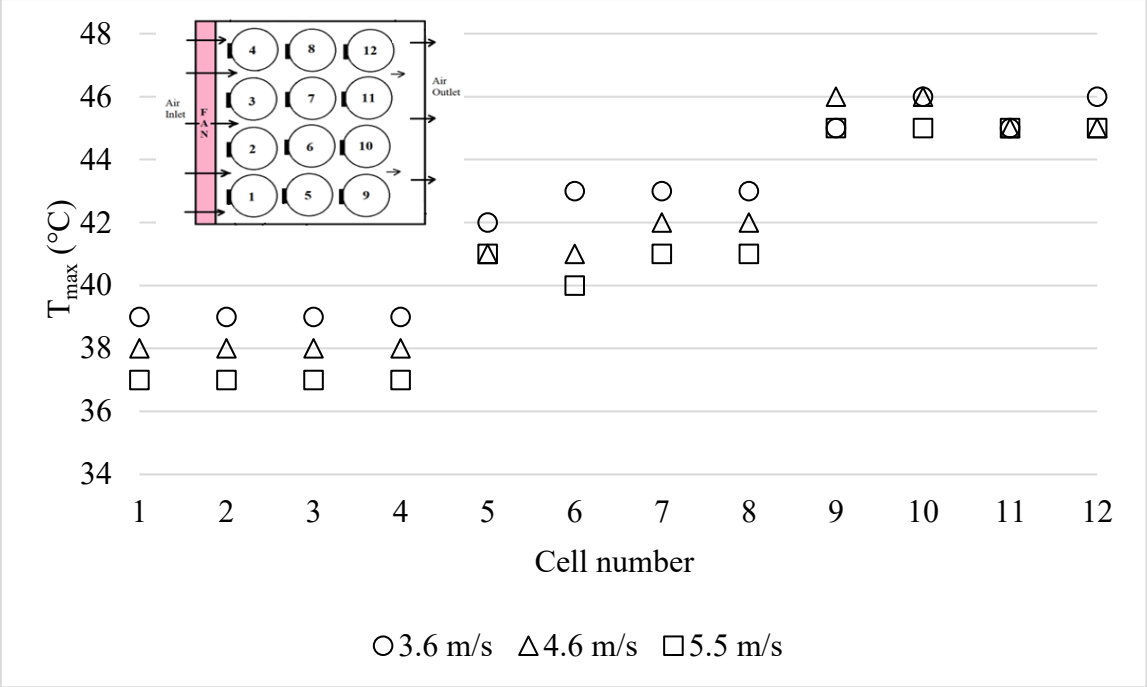

Figure 4.17: Peak temperature of cells at varying air inlet velocity at 1C discharge rate under forced convection (BTMS-FO)

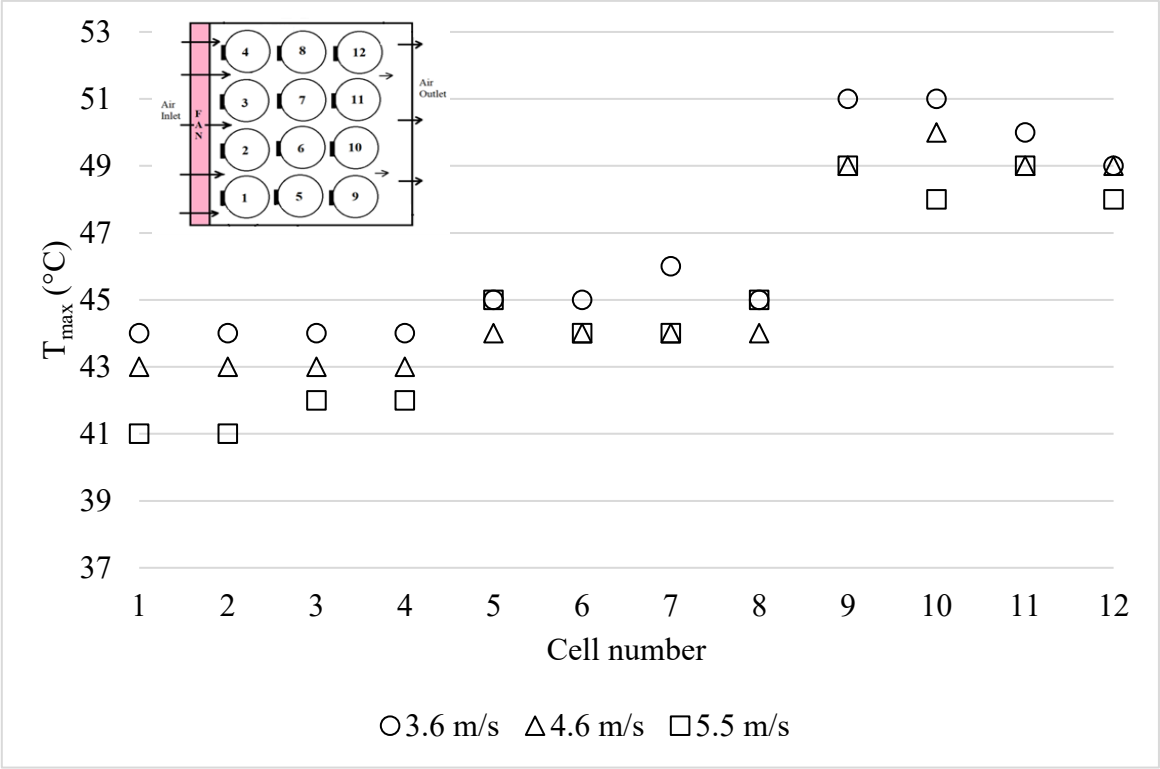

Figure 4.18: Peak temperature of cells at varying air inlet velocity at 2C discharge rate under forced convection (BTMS-FO)

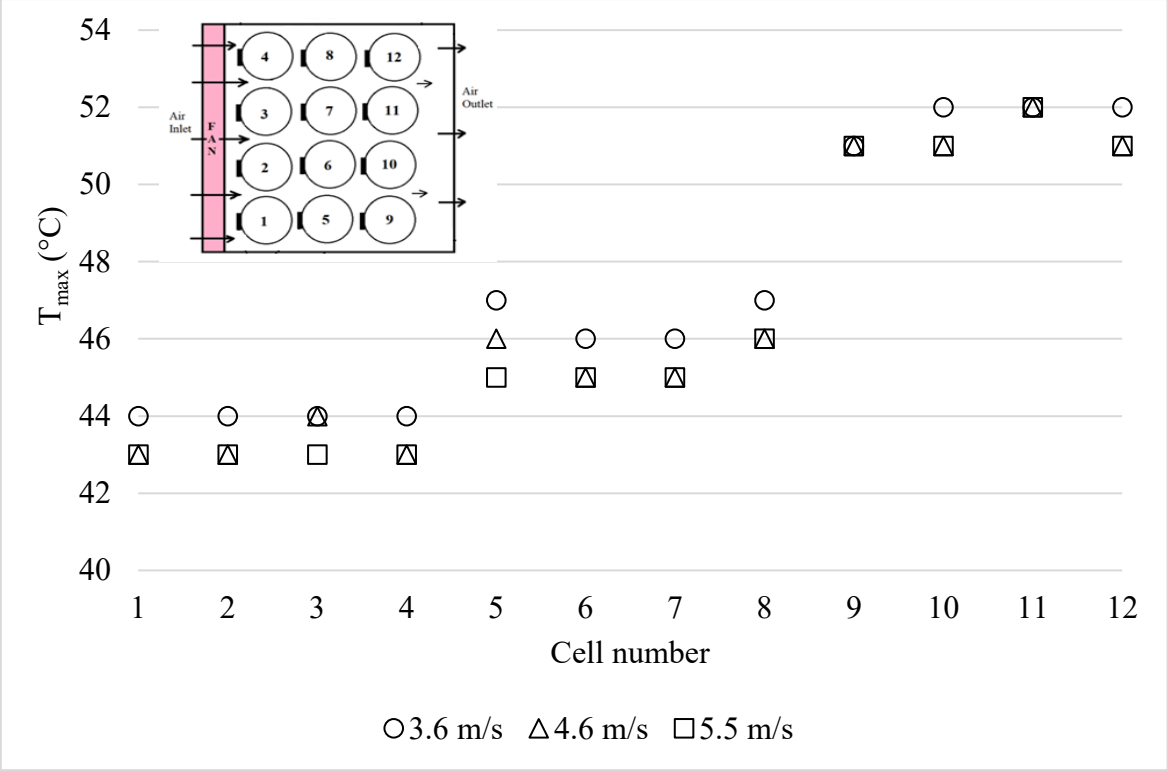

Figure 4.19: Peak temperature of cells at varying air inlet velocity at 3C discharge rate under forced convection (BTMS-FO)

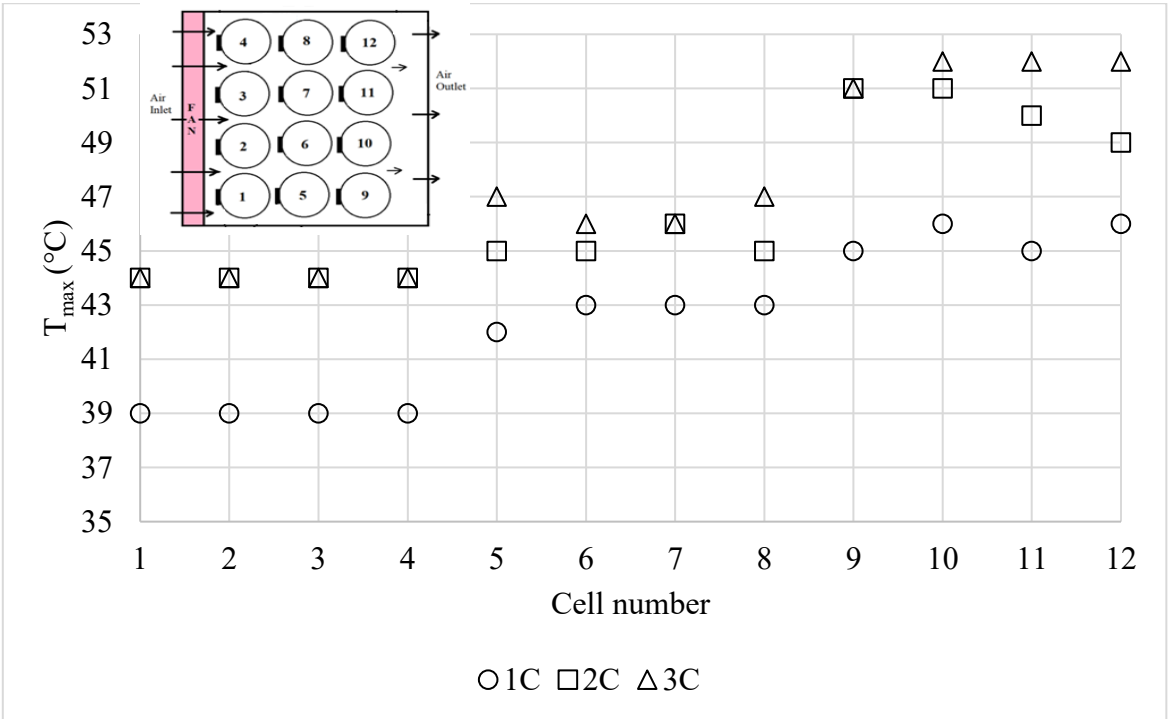

Figure 4.20: Peak temperature of cells at varying discharge rate when air inlet velocity is 3.6 m/s (Ve1) under forced convection (BTMS-FO)

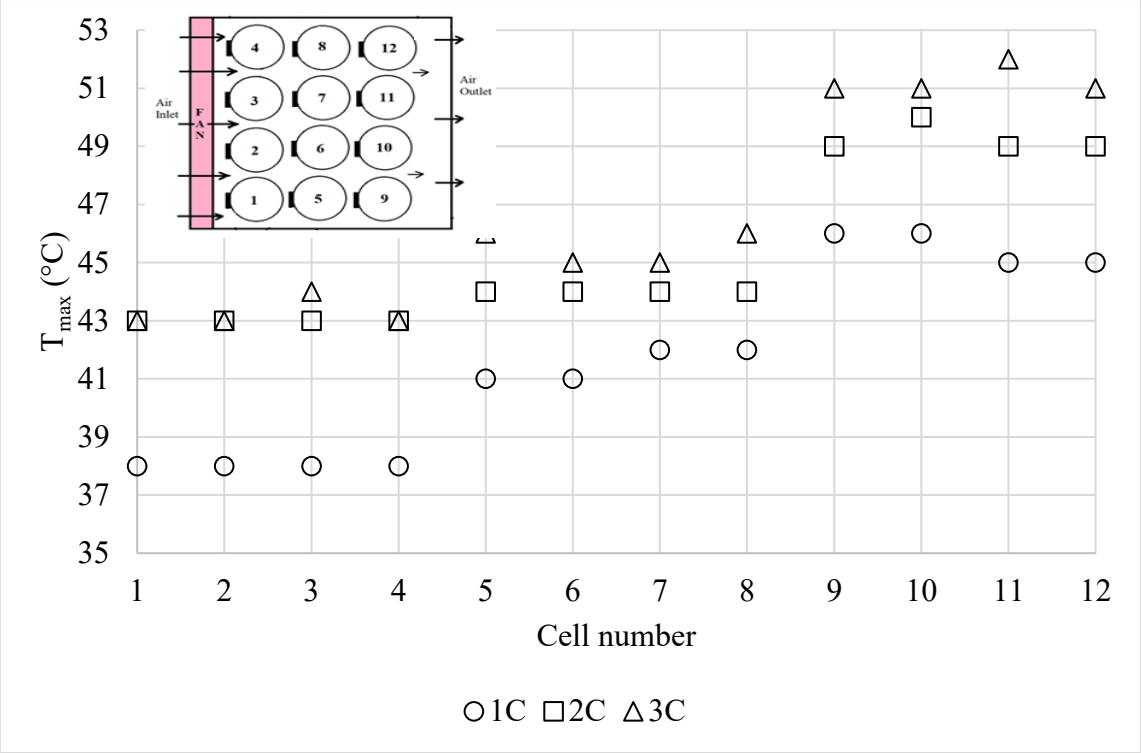

Figure 4.21: Peak temperature of cells at varying discharge rate when air inlet velocity is 4.6 m/s (Ve2) under forced convection (BTMS-FO)

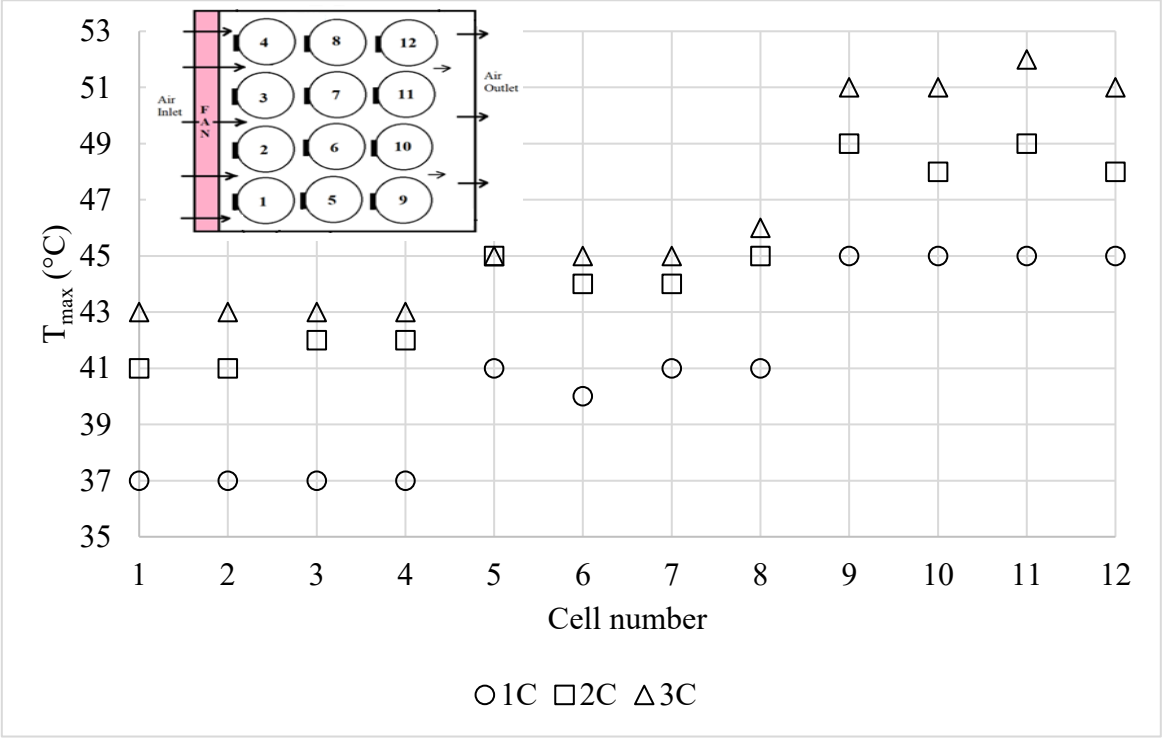

Figure 4.22: Peak temperature of cells at varying discharge rate when air inlet velocity is 5.5 m/s (Ve3) under forced convection (BTMS-FO)

4.1.2.3 Temperature uniformity (ΔT) inside battery pack during discharge

The temperature uniformity of the cells during discharge process for 1C, 2C and 3C discharge rates at varying air inlet velocity are presented in Figure 4.23, Figure 4.24 and Figure 4.25 respectively. The results showed that increase in air inlet velocity has adverse effect on temperature uniformity of the battery pack. At higher air inlet velocities of 5.5 m/s and 4.6 m/s, the ΔT values are higher than at 3.6 m/s. The incremental increase in ΔT during discharge are also presented in bar charts (Figure 4.26, Figure 4.27 and Figure 4.28) and it shows that combination higher air inlet velocity and higher discharge rate have multiplying effect on ΔT. Although the value of ΔT at 4.6 m/s and 5.5 m/s air velocity is same at 1C, 2C and 3C but the rate at which ΔT rise is higher at 5.5 m/s air velocity as compared to 4.6 m/s. The higher the value of ΔT, the greater the non-uniformity of temperature in the battery. The non-uniformity is mainly produced by variation in cells temperature distribution. It is critical to control this non-uniformity within 5°C ideally. The results at varying discharge rate and air inlet velocity are combined in Figure 4.29. The ideal value of 5°C is not maintained by forced convection based BTMS and even at higher discharge rate and air inlet velocity non-uniformity exceeds acceptable limit of 8°C.

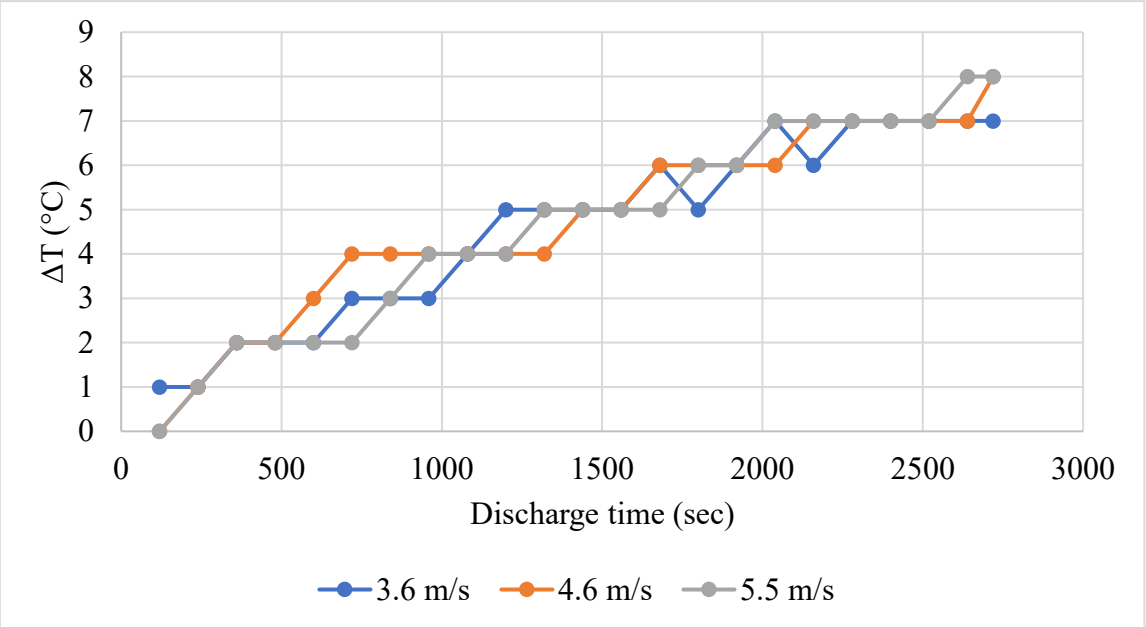

Figure 4.23: Temperature uniformity variation during discharge process at 1C rate at varying air inlet velocity under forced convection (BTMS-FO)

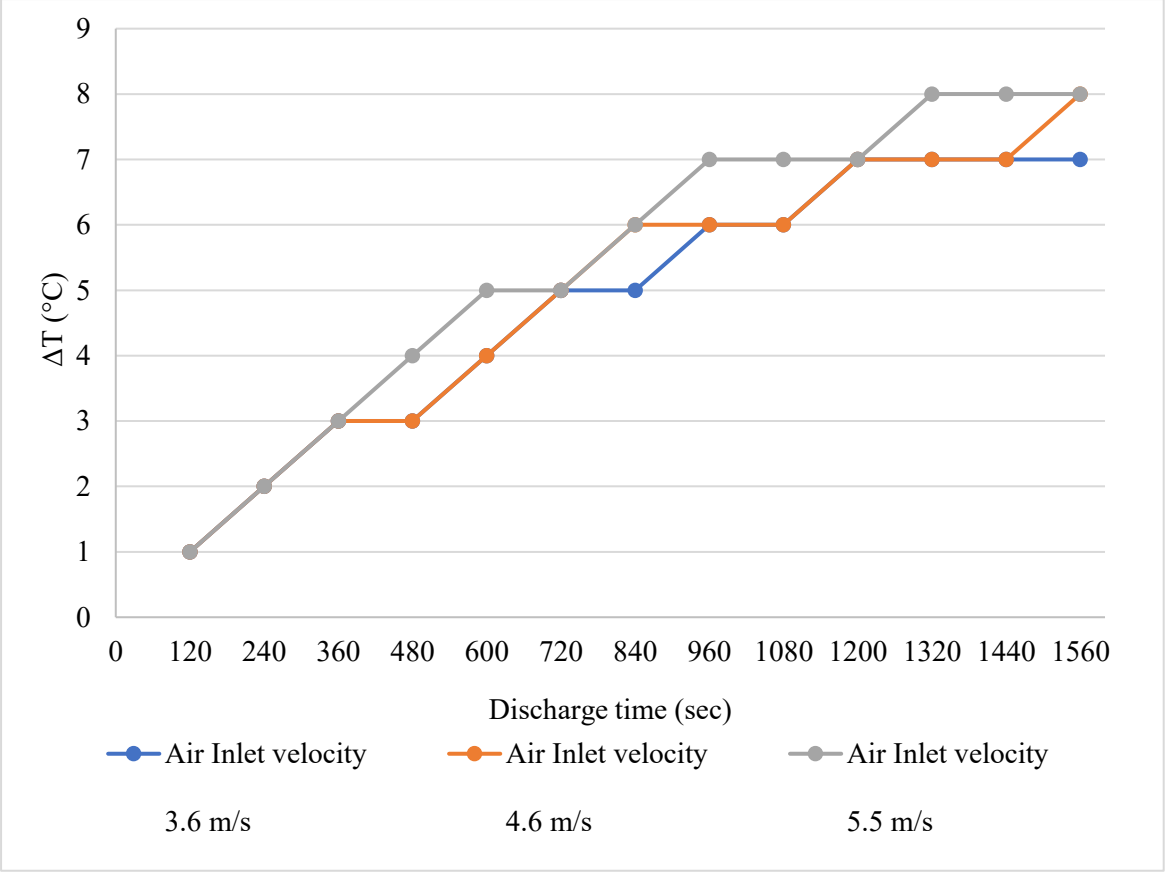

Figure 4.24: Temperature uniformity variation during discharge process at 2C rate at varying air inlet velocity under forced convection (BTMS-FO)

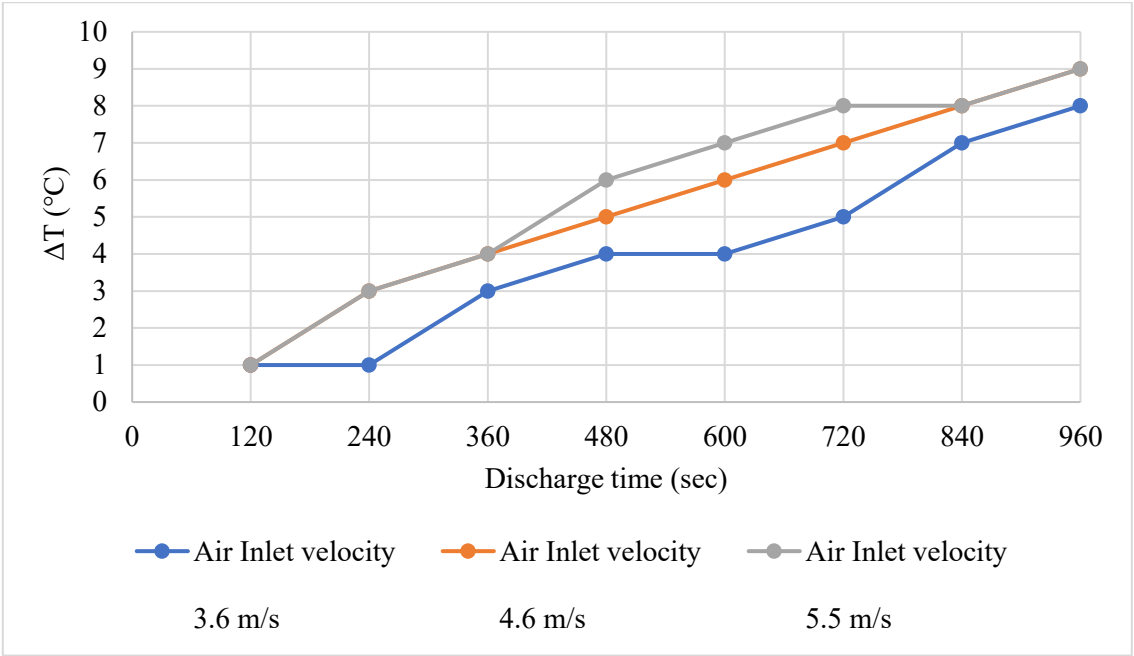

Figure 4.25: Temperature uniformity variation during discharge process at 3C rate at varying air inlet velocity under forced convection (BTMS-FO)

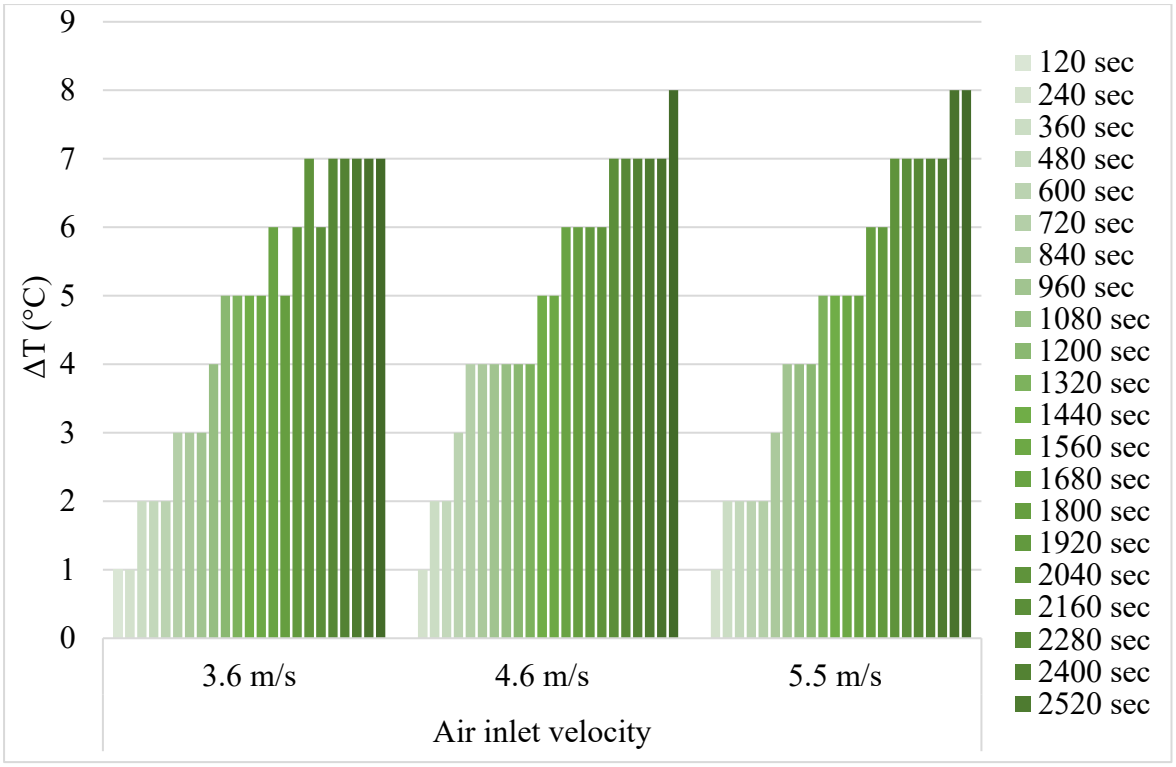

Figure 4.26: The temperature non-uniformity changes during discharge process at 1C rate at three air velocities (Ve1,Ve2 and Ve3)

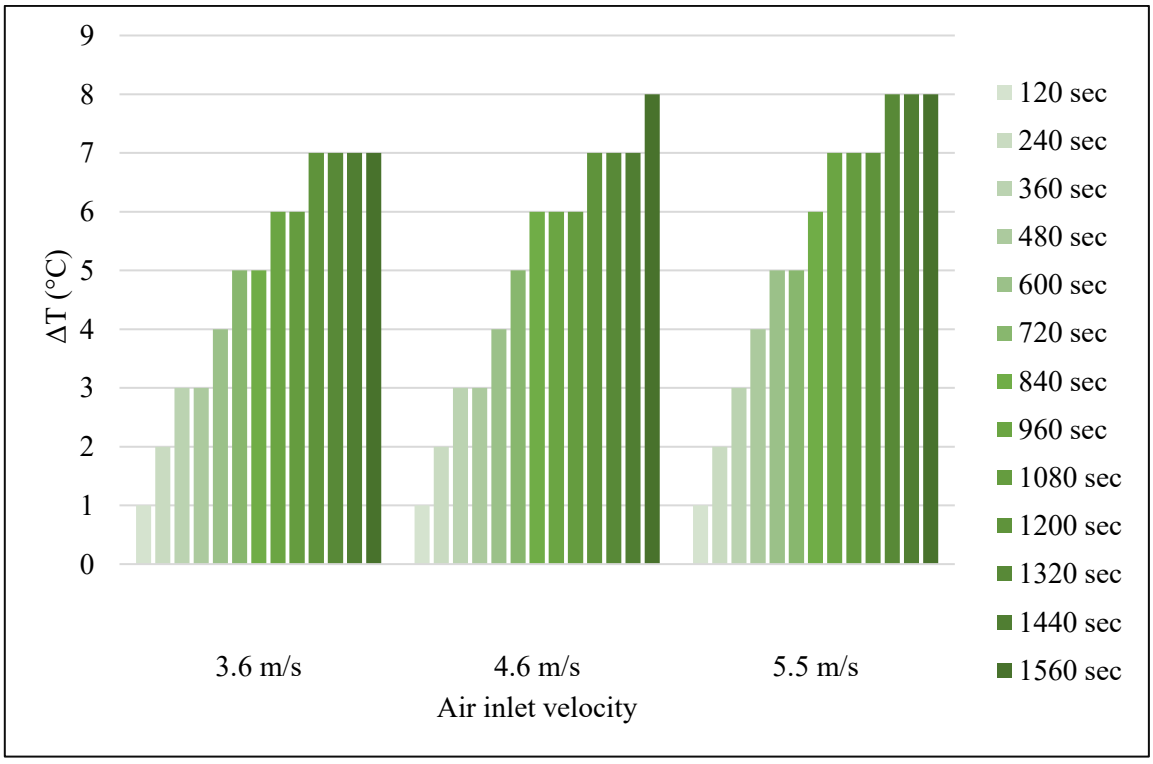

Figure 4.27: The temperature non-uniformity changes during discharge process at 2C rate at three air velocities (Ve1,Ve2 and Ve3)

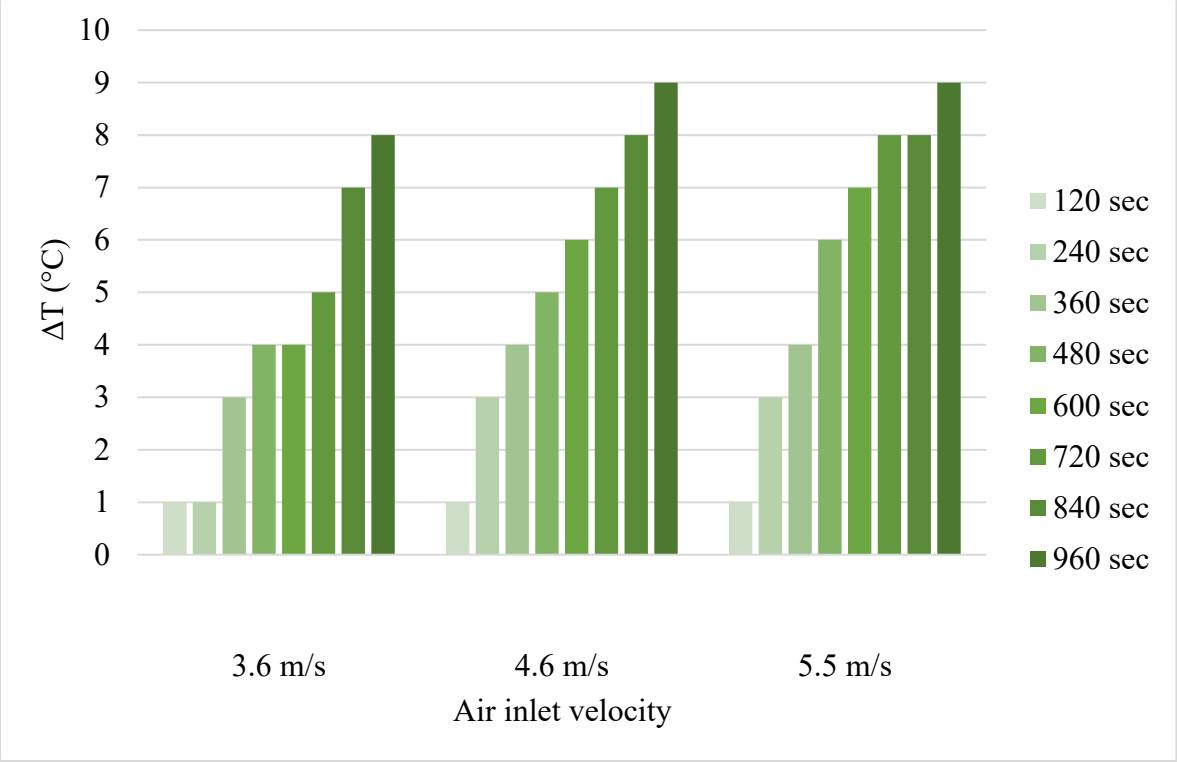

Figure 4.28:The temperature non-uniformity changes during discharge process at 3C rate at three air velocities (Ve1,Ve2 and Ve3)

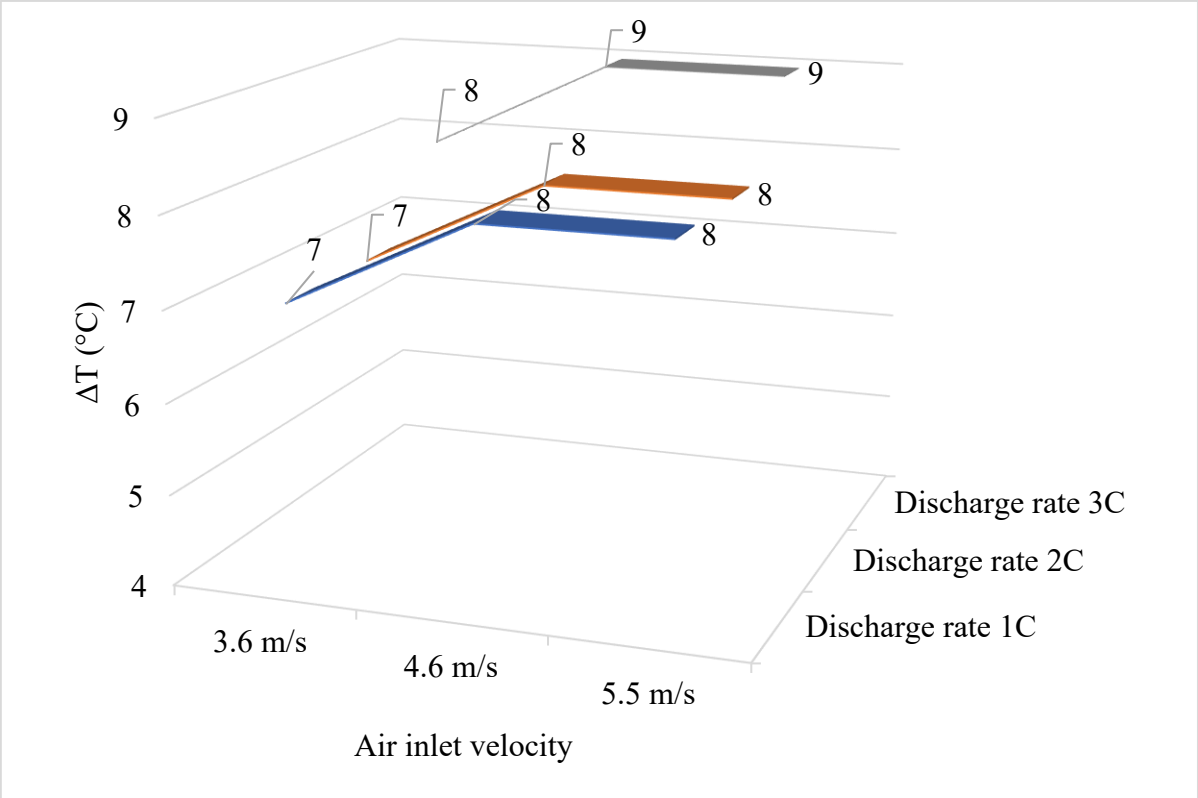

Figure 4.29: The comparative results of non-uniformity at varying discharge rates and air inlet velocity

4.1.2.4 Convective heat transfer

The heat transfer coefficient and convective heat transfer rate were calculated as indicated in Chapter 3. The heat transfer coefficient varies between 250 to 360 W/m^{2}K, with higher values being observed at higher air velocity. The Figure 4.30, Figure 4.31 and Figure 4.32 shows convective heat transfer at 1C, 2C and 3C discharge rates respectively under varying air velocities. It can be observed that increase in air velocity increases convective heat transfer between cell and air. The convective heat transfer rate is highest at 3C rate for respective air velocity. This is because at higher discharge rate, the surface temperature of cells is also high and thus higher convective heat transfer rates are achieved at higher discharge rates. Figure 4.33 clearly indicate that higher inlet air velocity and higher discharge rate results in higher convective heat transfer rate. But as earlier discussed for temperature uniformity and peak temperature, the higher value of discharge and air velocity adversely affect temperature uniformity and results in higher peak temperature. A better design of alternative to conventional forced convection is required if we want to use full potential of higher air velocities while operating battery pack at high discharge rates.

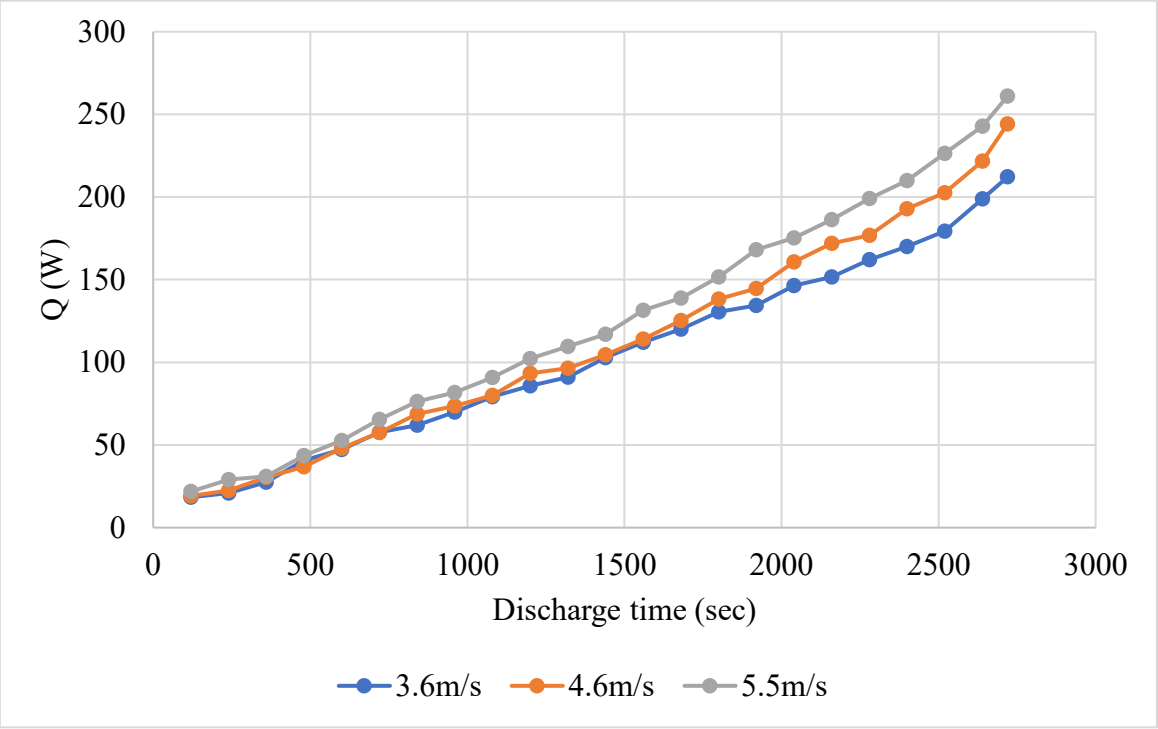

Figure 4.30: Convective heat transfer rate at varying inlet air velocities under 1C discharge rate

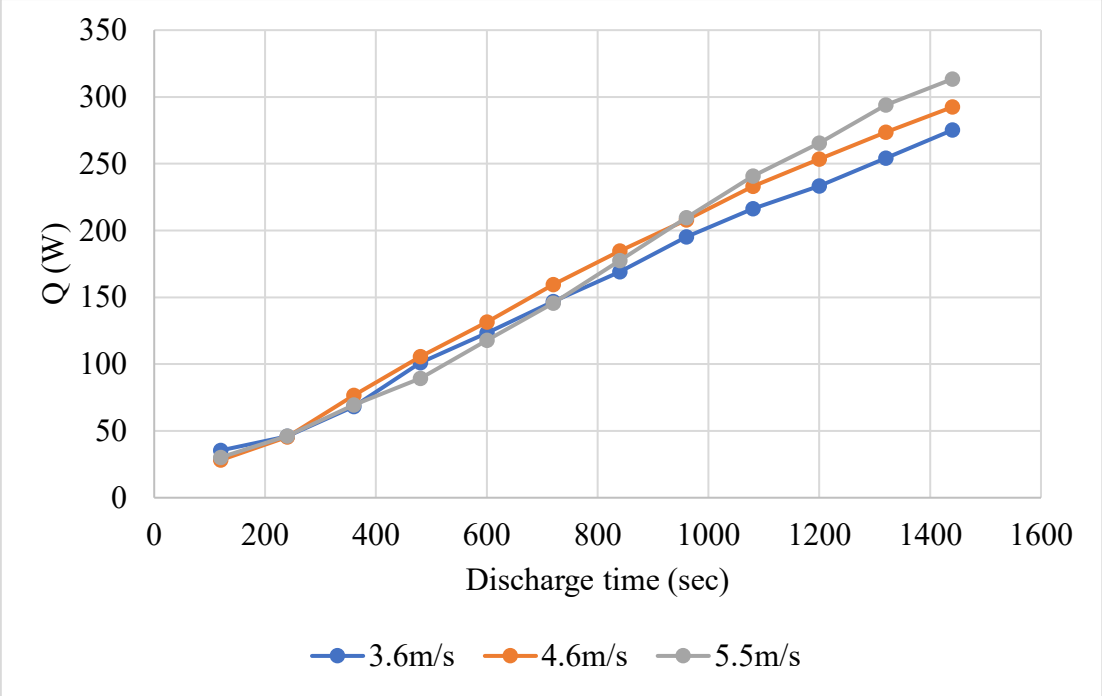

Figure 4.31: Convective heat transfer rate at varying inlet air velocities under 2C discharge rate

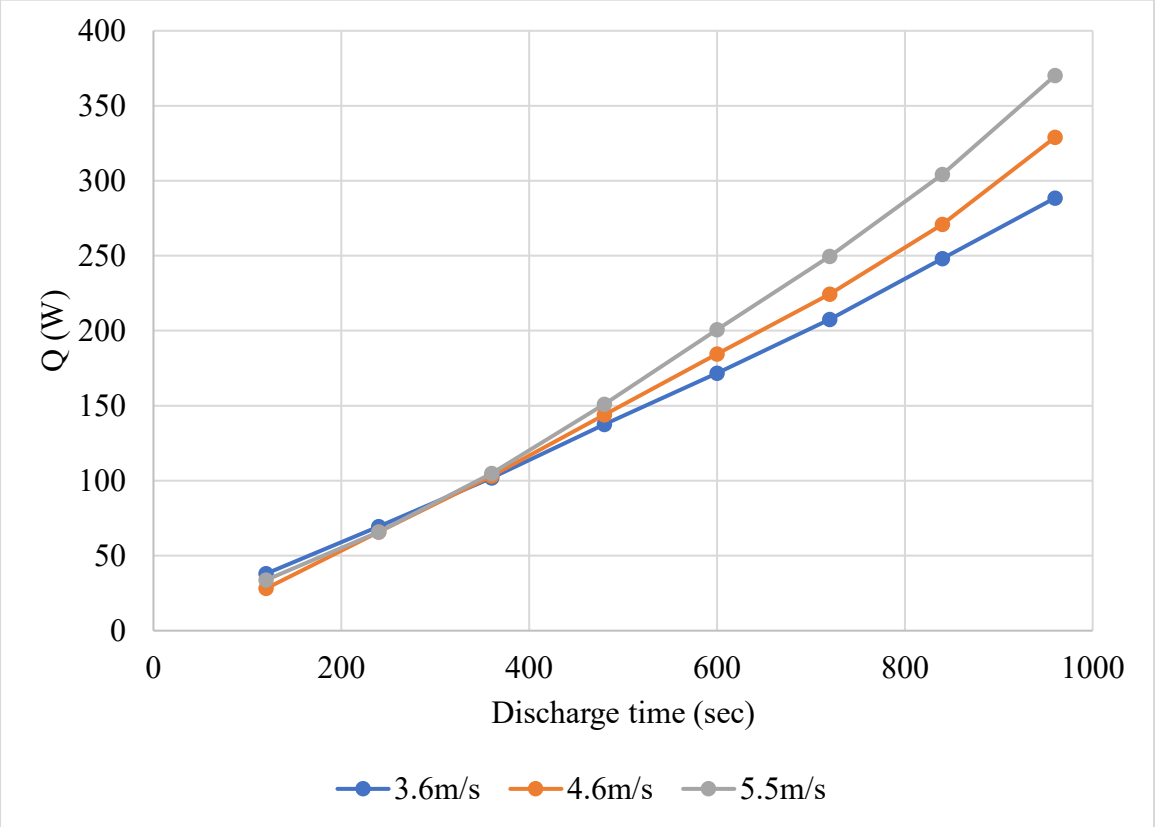

Figure 4.32: Convective heat transfer rate at varying inlet air velocities under 3C discharge rate

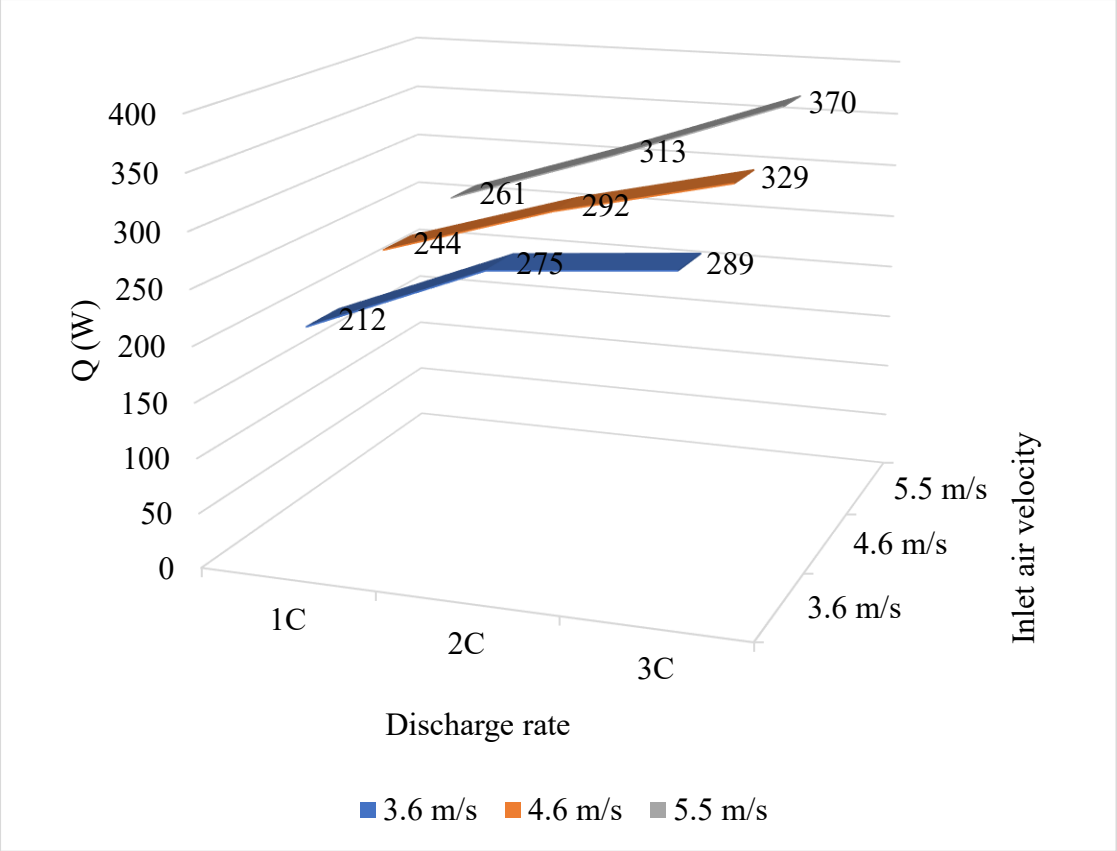

Figure 4.33: Convective heat transfer under forced convection (BTMS-FO) at varying combination of discharge rate and inlet air velocity

4.2 Objective 2: To study the effect of interspacing between battery cells on cooling performance of the base case BTMS-woHP at different operating conditions.

The change in interspacing may affect the cooling performance of the BTMS as with it air flow pattern also changes. The base case forced convection (BTMS-FO) has 2 mm interspacing between cells in both transverse and longitudinal direction. To study how temperature distribution varies inside battery with increase in interspacing, a different battery pack was fabricated with 4 mm interspacing. This is the third battery pack fabrication for research work, and it is denoted as BTMS-FO-4mm. Comparative data was collected for BTMS-FO and BTMS-FO-4mm and three different parameters studied were average temperature, peak temperature and temperature uniformity. The experimentation was conducted at two levels of air inlet velocity (Ve2 and Ve3) and one level of discharge rate (3C). This was done because in the results for BTMS-FR and BTMS-FO, it can be clearly seen that cells are more stressed at 3C rate (higher discharge values), and major non-uniformity of temperature was observed at

higher air inlet velocities. So, it is better to compare results between 2mm and 4mm interspacing at extreme values of discharge rate and air inlet velocities. The average temperature results are presented in Figure 4.34 and Figure 4.35 and it can be observed that there is no significant change in average temperature (T_{avg}) of battery with change in interspacing between cells. The peak temperature (T_{max}) of each cell is recorded during discharge process and data is presented in Figure 4.36. The results indicated that peak temperature of last row cells is still higher than front row cells. There no such significant difference in peak temperature at 2mm and 4 mm interspacing. When cells are placed far apart, the turbulence in flow is reduced which affects the flow near surface. The turbulence in flow enhances the air flow around cell geometry thereby increasing convective heat transfer rate. Increasing interspacing has no positive effect on temperature uniformity as can be seen in Figure 4.37. The increased interspacing also increases the size of battery pack with no significant positive impact on other parameters.

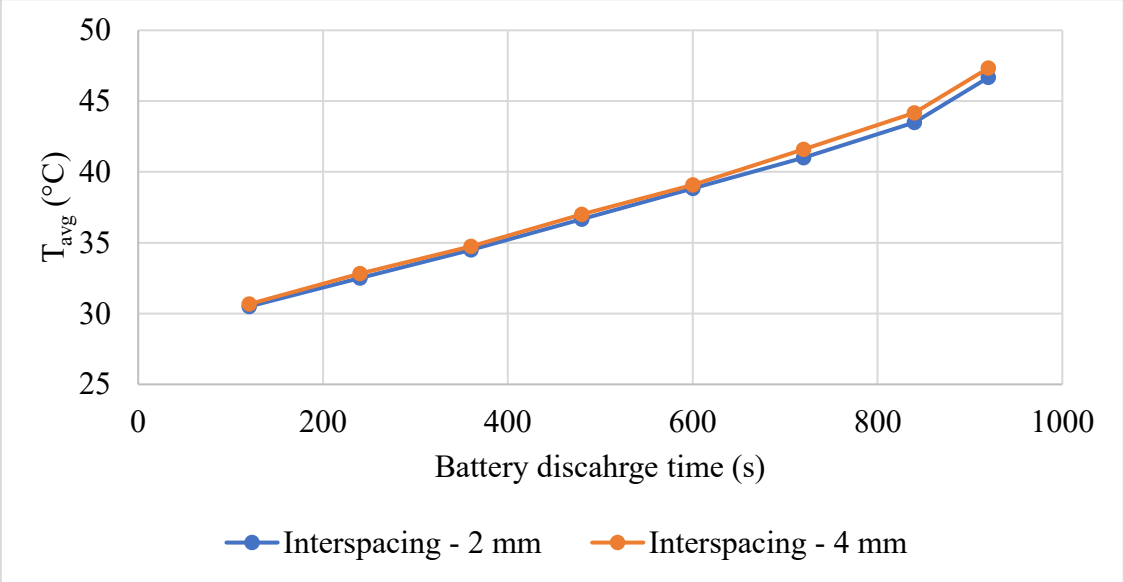

Figure 4.34: Effect of change in interspacing on average temperature of battery pack under forced convection at air inlet velocity 4.6 m/s at 3C discharge rate

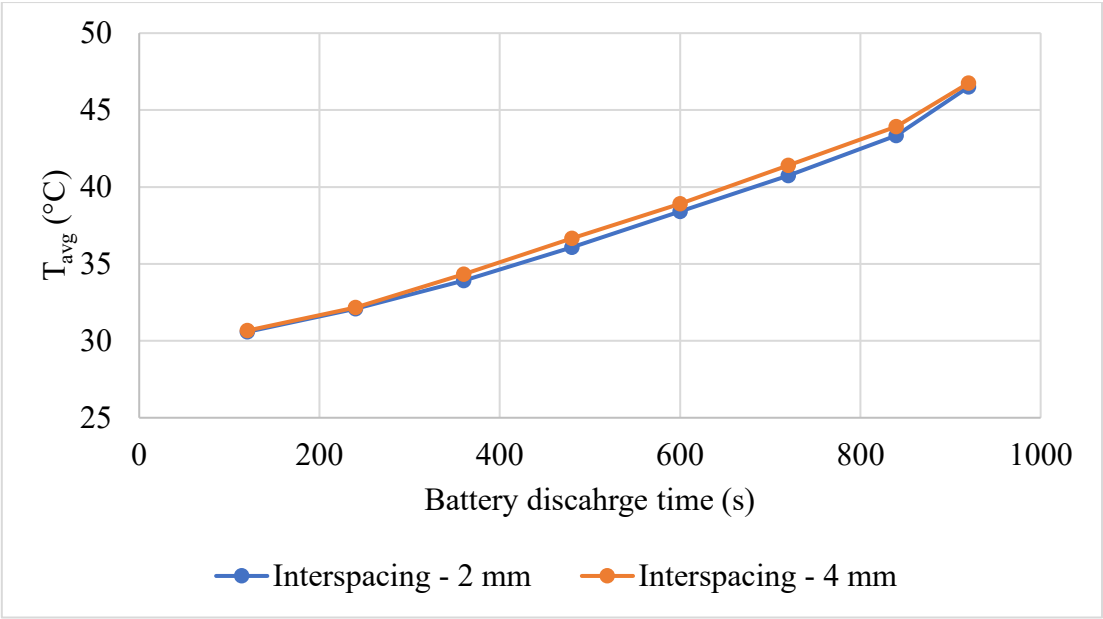

Figure 4.35: Effect of change in interspacing on average temperature of battery pack under forced convection at air inlet velocity 5.5 m/s at 3C discharge rate

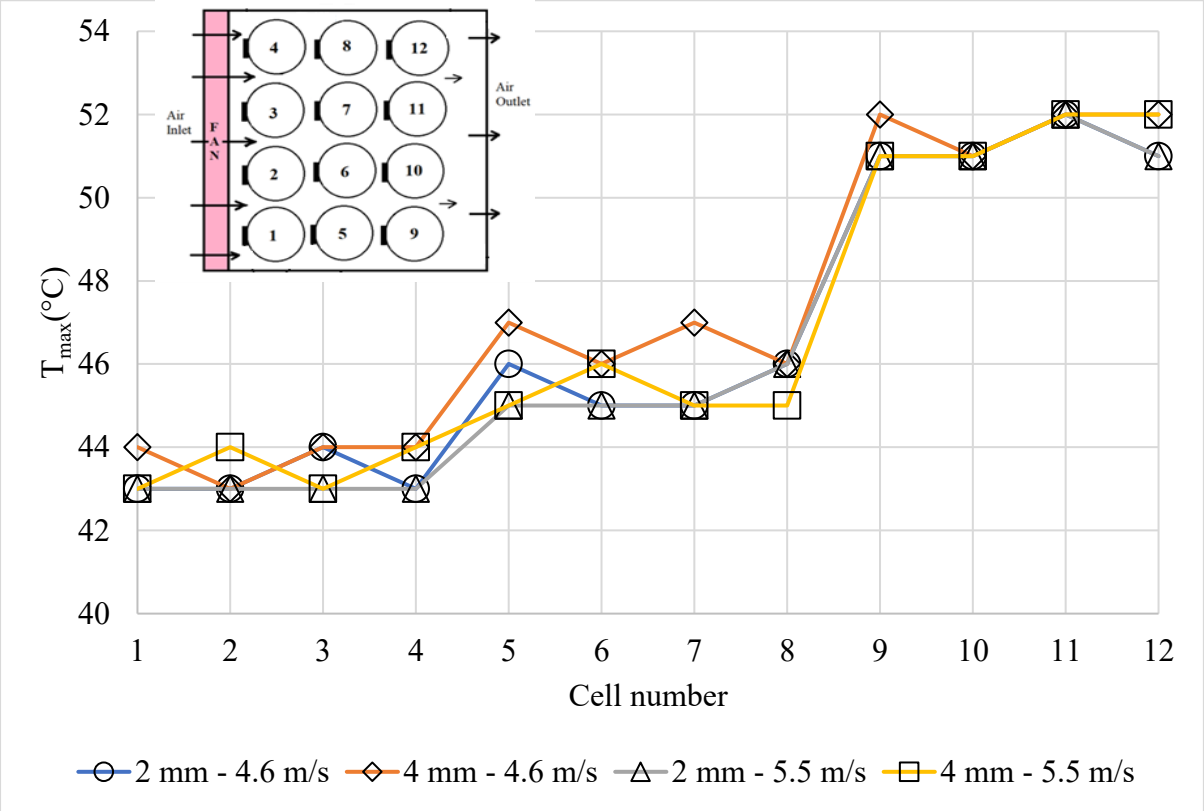

Figure 4.36: Effect of change in interspacing on peak temperature of cells at 4.6 m/s and 5.5 m/s air inlet velocity at 3C discharge rate

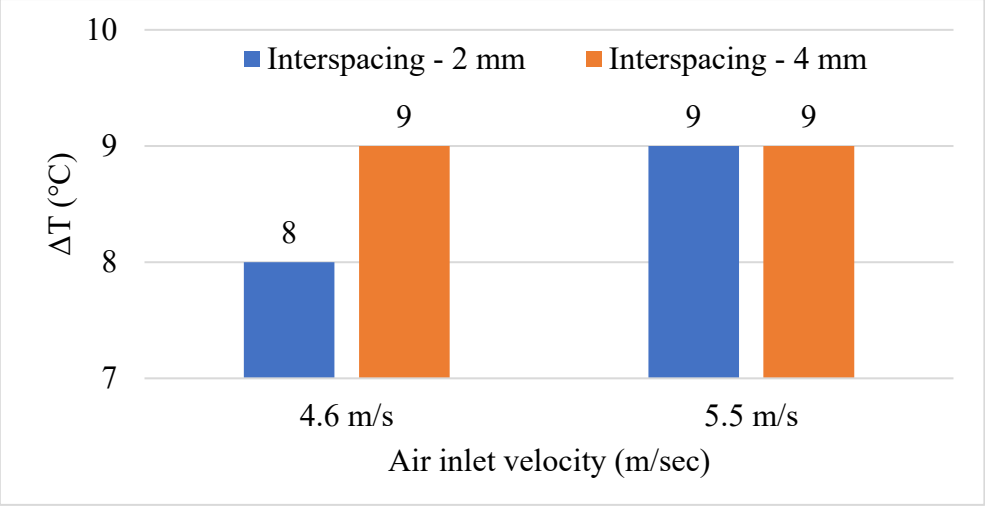

Figure 4.37:Effect of change in interspacing on maximum temperature difference within battery pack at end of discharge process at 3C rate

4.3 Objective 3: To evaluate the effect of heat pipe insertion and cooling performance of hybrid BTMS (heat pipe + air-cooling) at varying discharging rates and airflow rates.

The results discussed in the subsection 4.1 and 4.2 of this chapter were related to BTMS-woHP cooling systems. The heat pipe insertion on performance of battery cooling under forced convection is presented in this section. The battery pack fabricated (Battery pack 4) with heat pipe insertions has 2mm interspacing and experimentation was conducted under varying discharge rate and air inlet velocity. Based on combination of C-rate and air inlet velocity, six different cases were taken:

i. Battery pack discharged at 1C when inlet air velocity is Ve1, and cut-off voltage was kept at 22 V.
ii. Battery pack discharged at 2C when inlet air velocity is Ve1, and cut-off voltage was kept at 22 V.
iii. Battery pack discharged at 3C when inlet air velocity is Ve1, and cut-off voltage was kept at 22 V. (results pending)
iv. Battery pack discharged at 1C when inlet air velocity is Ve2, and cut-off voltage was kept at 22 V.
v. Battery pack discharged at 2C when inlet air velocity is Ve2, and cut-off voltage was kept at 22 V.

vi. Battery pack discharged at 3C when inlet air velocity is Ve2, and cut-off voltage was kept at 22 V.
vii. Battery pack discharged at 1C when inlet air velocity is Ve3, and cut-off voltage was kept at 22 V.
viii. Battery pack discharged at 2C when inlet air velocity is Ve3, and cut-off voltage was kept at 22 V.
ix. Battery pack discharged at 3C when inlet air velocity is Ve3, and cut-off voltage was kept at 22 V.

Three important dependent parameters were observed and recorded under experimentation. They are average temperature, peak temperature and temperature uniformity.

4.3.1 Average temperature inside battery pack during discharge process (T_{avg})

The average temperature results are presented considering two main parameters: discharge rate and air inlet velocity. Figure 4.38 to Figure 4.43 present the results at constant discharge rates of 1C, 2C and 3C and Figure 4.44 to Figure 4.49 present results at constant air velocities of 3.6m/s (Ve1), 4.6 m/s (Ve2) and 5.5 m/s (Ve3) respectively under varying discharge rates. The effect of air inlet velocity on average temperature is not much significant as compared to effect of discharge rate. The results and trend of results is much like forced convection based BTMS (BTMS-FO) i.e. the higher the discharge rate, higher is the average temperature of battery pack. Increasing air velocity although reduced average temperature but it is not that much significant drop. As can be seen in Figure 4.39, Figure 4.41 and Figure 4.43, the average temperature only reduces by 1°C at 1C, 1.9°C at 2C and 1.1°C at 3C when velocity is increased from 3.6 m/s to 5.5 m/s. This shows that there no trend or specific advantage when higher inlet air velocity is used for battery cooling. When results are analysed at varying discharge under air velocity, the effect of discharge rate on average temperature can be clearly observed with maximum difference between average temperature at 3C and 1C being 6.1°C (at 3.6 m/s air velocity). The heat pipe based hybrid system (BTMS-HP) was able to maintain average temperature below acceptable temperature of 50°C and it performs better than conventional free and forced convection.

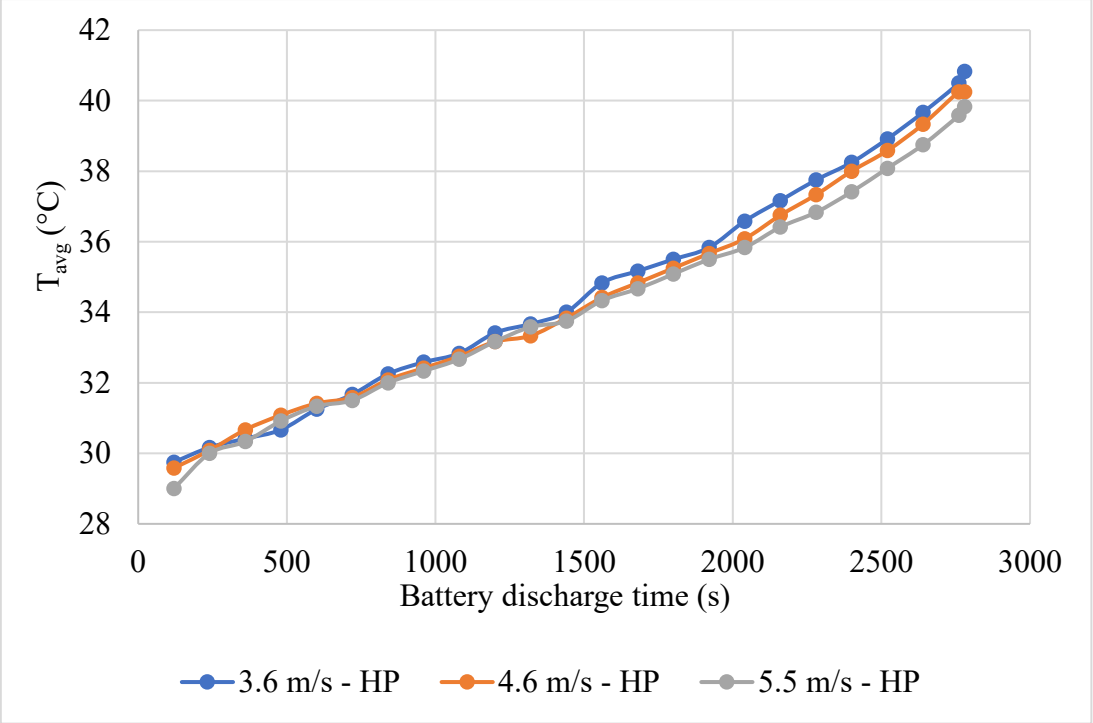

Figure 4.38: Average temperature of battery pack under with heat pipe (HP) forced convection cooling at 1C discharge rate

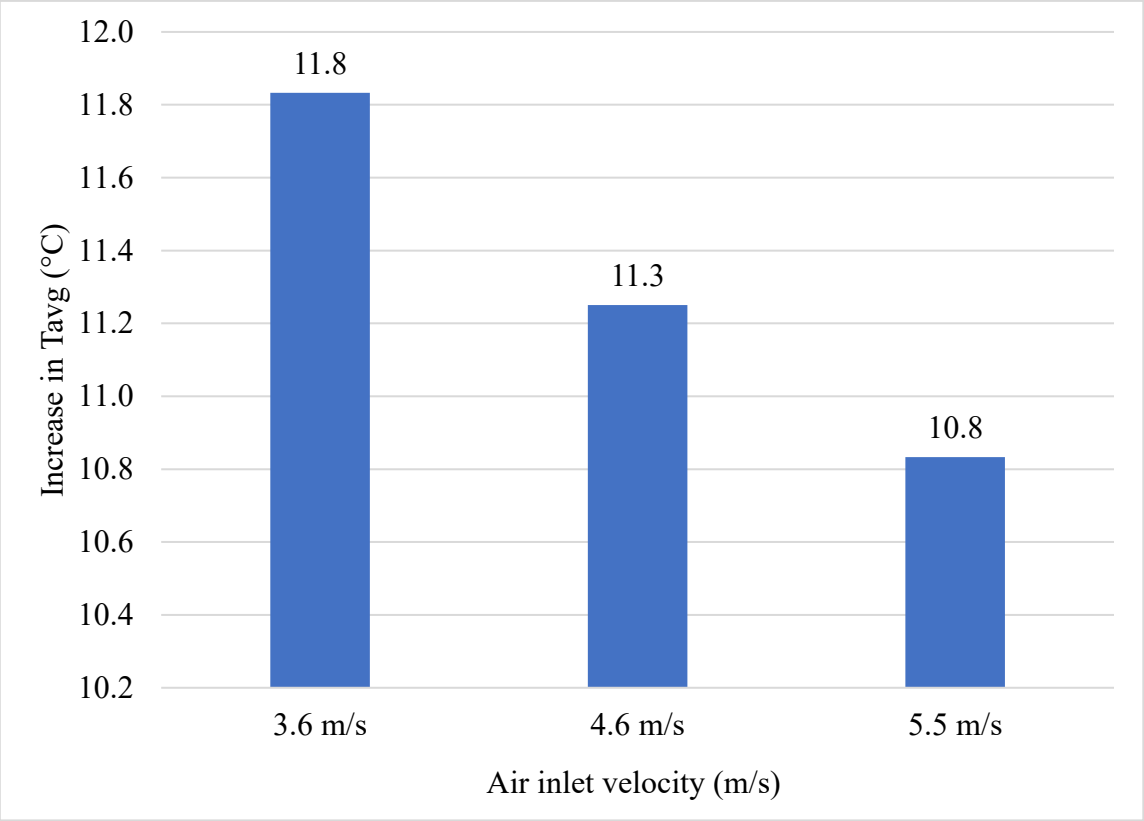

Figure 4.39: Increase in average temperature of battery pack at 1C rate - with heat pipe (HP) forced convection cooling

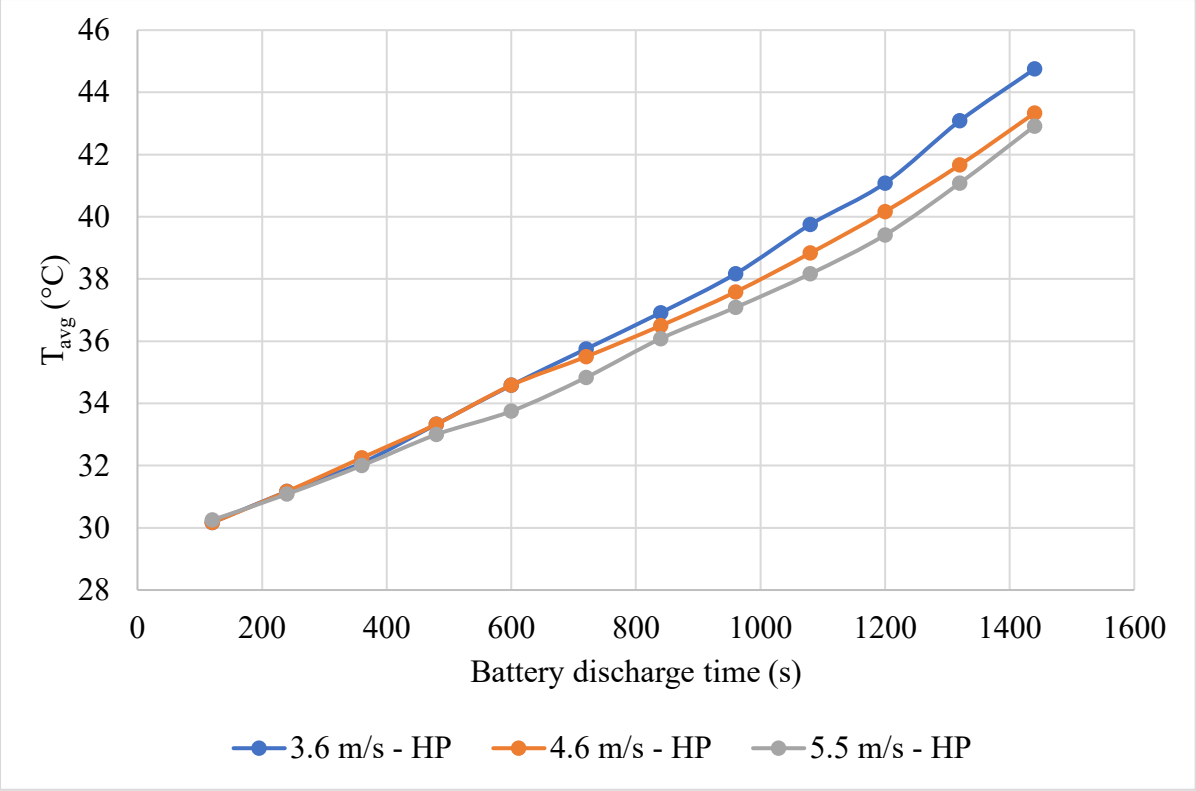

Figure 4.40: Average temperature of battery pack under with heat pipe (HP) forced convection cooling at 2C discharge rate

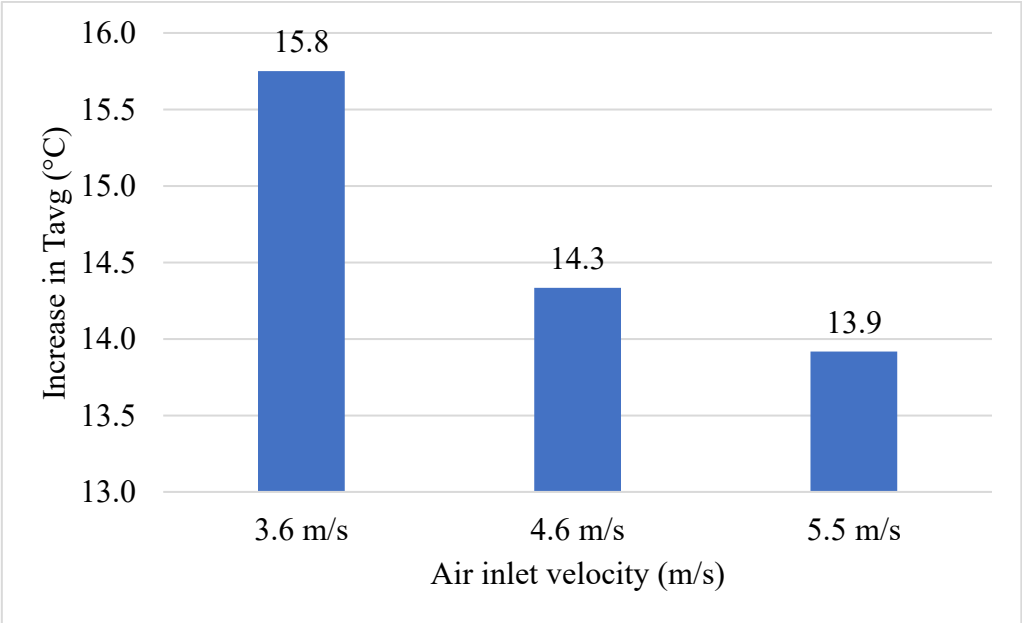

Figure 4.41:Increase in average temperature of battery pack at 2C rate - with heat pipe (HP) forced convection cooling

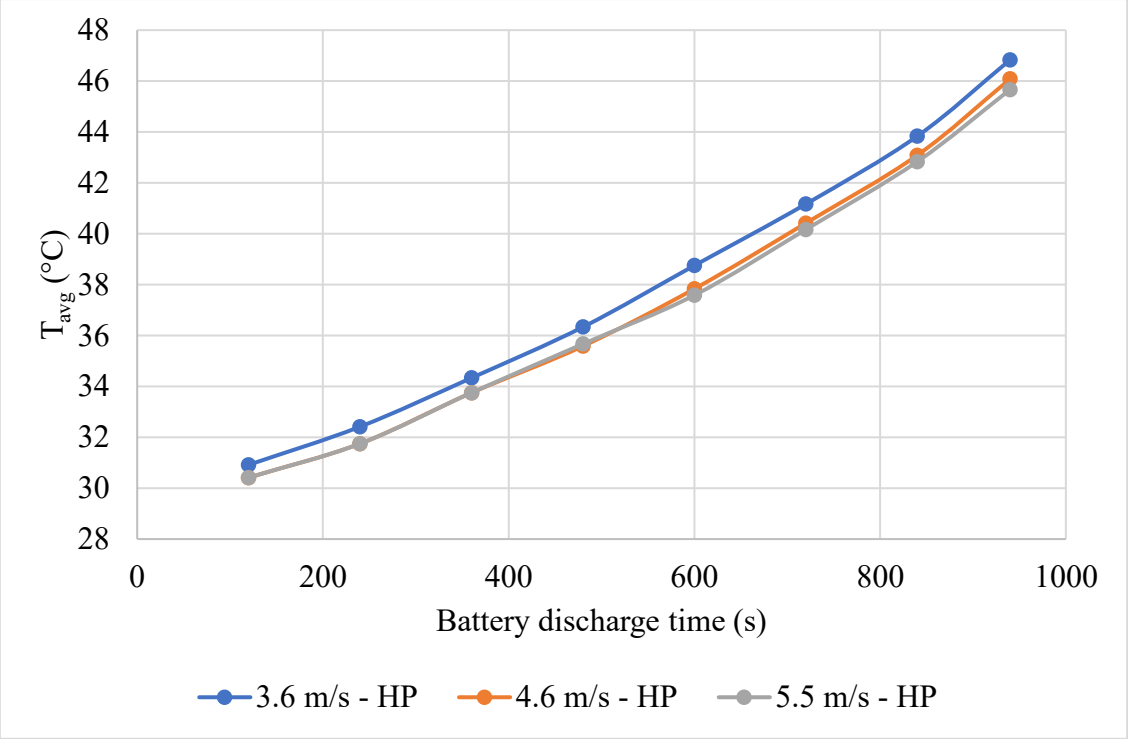

Figure 4.42: Average temperature of battery pack under with heat pipe (HP) forced convection cooling at 3C discharge rate

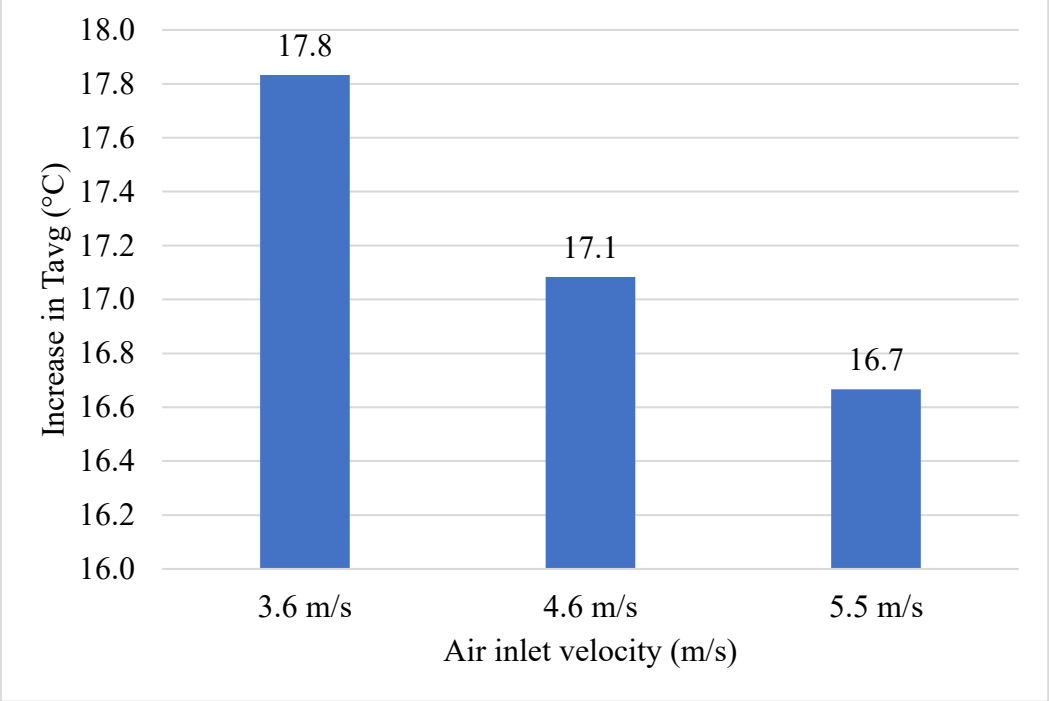

Figure 4.43: Increase in average temperature of battery pack at 3C rate - with heat pipe (HP) forced convection cooling

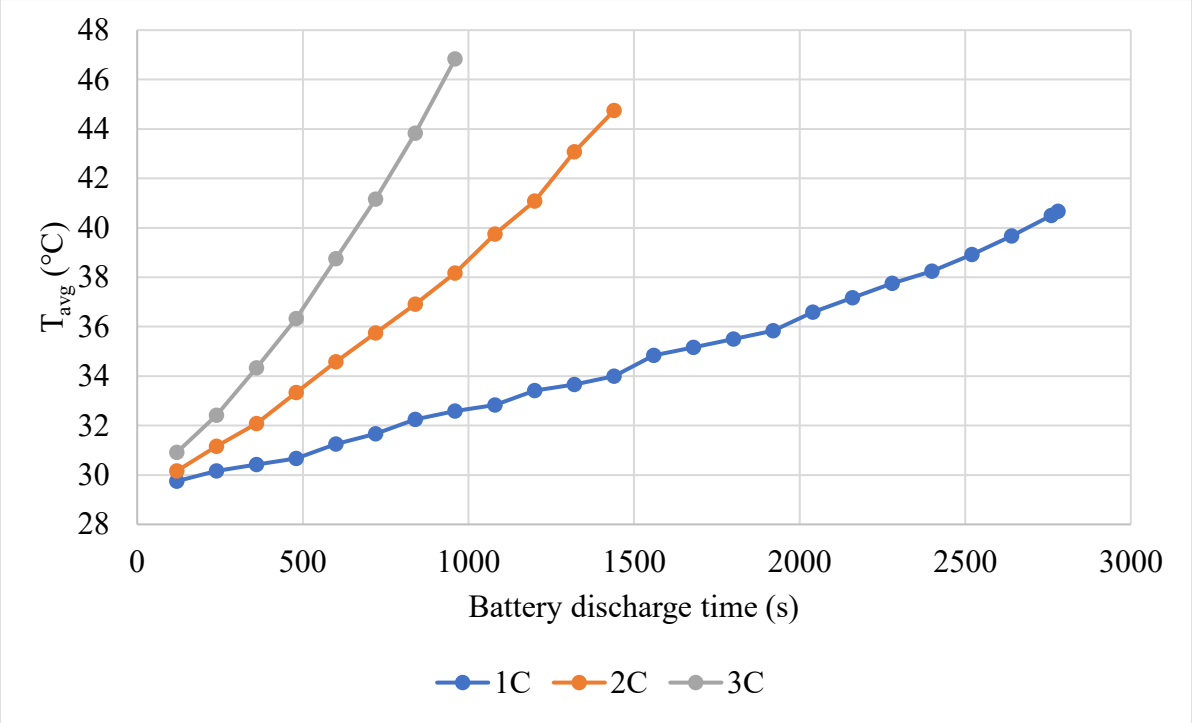

Figure 4.44: Average temperature of battery pack at inlet air velocity 3.6 m/s when discharge rates were 1C, 2C and 3C for BTMS- with Heat Pipe- forced convection

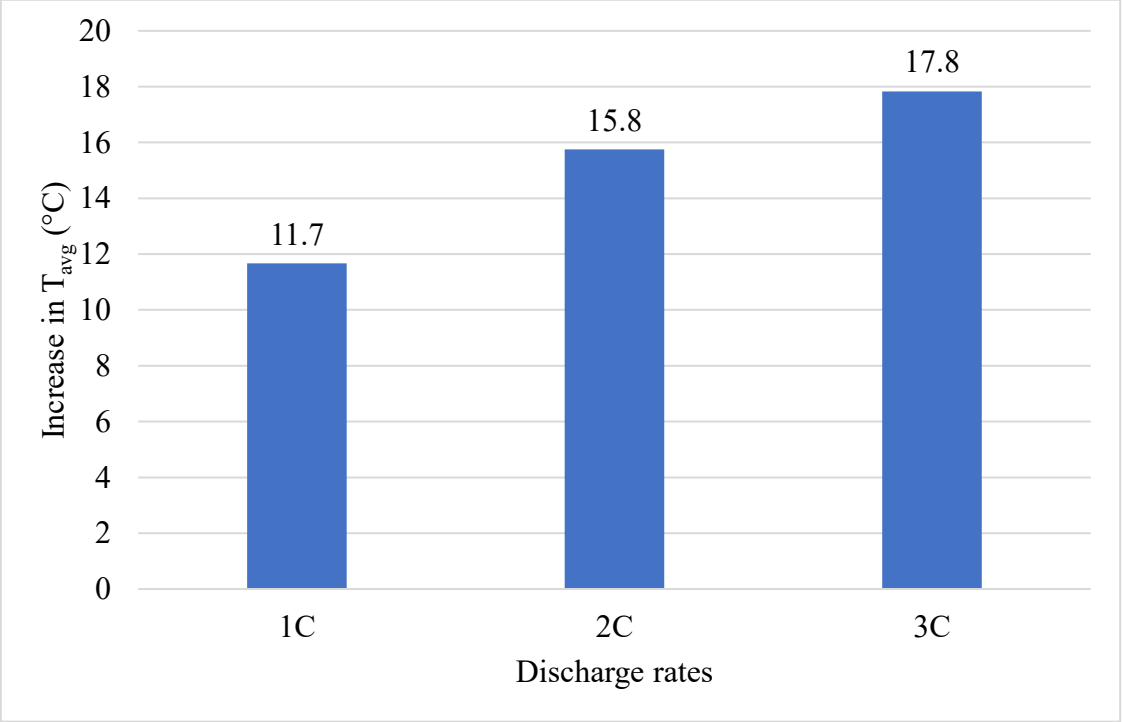

Figure 4.45: Increase in average temperature of battery when air inlet velocity is 3.6 m/s at different discharge rates:1C, 2C and 3C -with heat pipe-forced convection

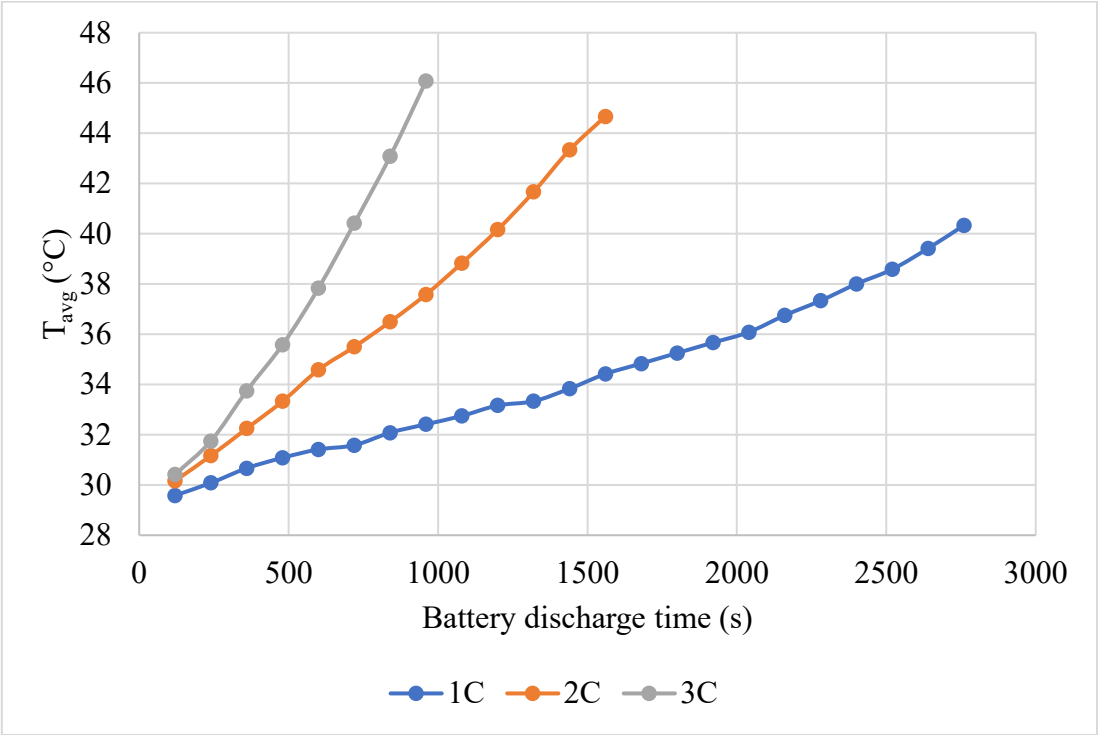

Figure 4.46: Average temperature of battery pack at inlet air velocity 4.6 m/s when discharge rates were 1C, 2C and 3C for BTMS- with Heat Pipe- forced convection

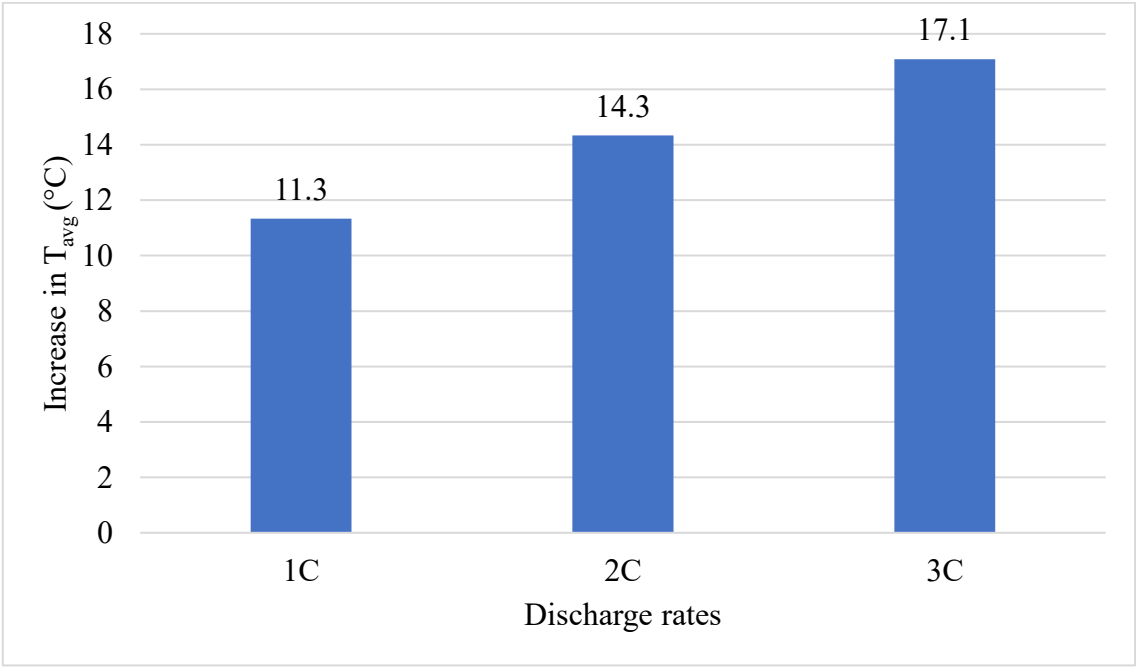

Figure 4.47: Increase in average temperature of battery when air inlet velocity is 4.6 m/s at different discharge rates:1C, 2C and 3C -with heat pipe-forced convection

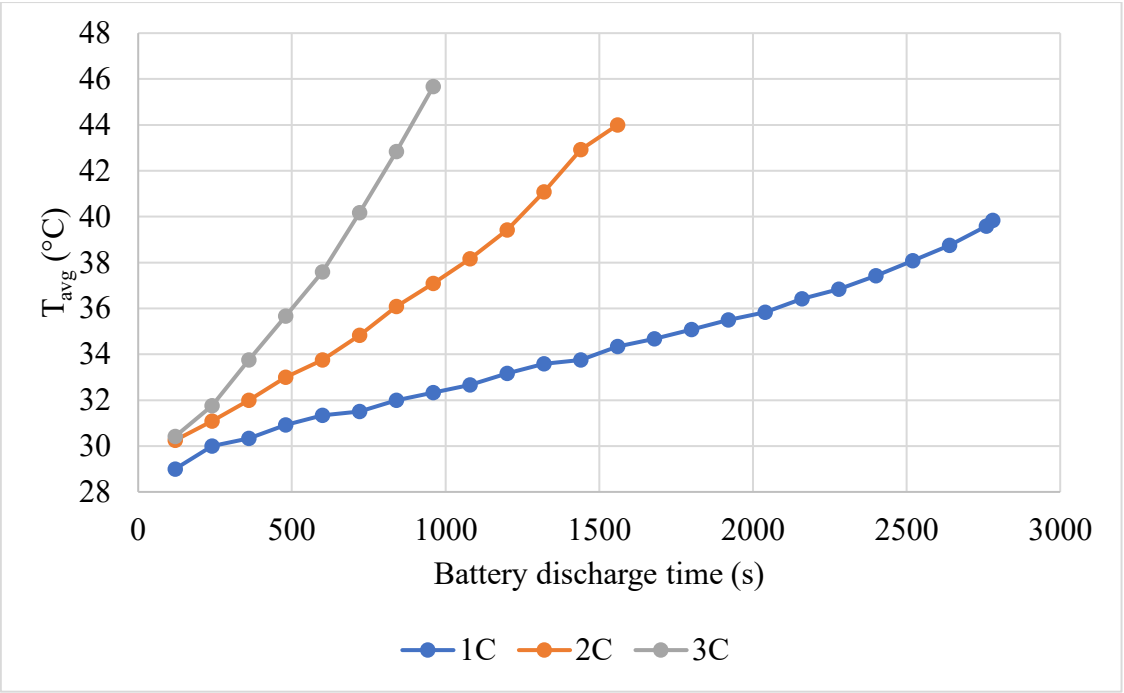

Figure 4.48: Average temperature of battery pack at inlet air velocity 5.5 m/s when discharge rates were 1C, 2C and 3C for BTMS- with Heat Pipe- forced convection

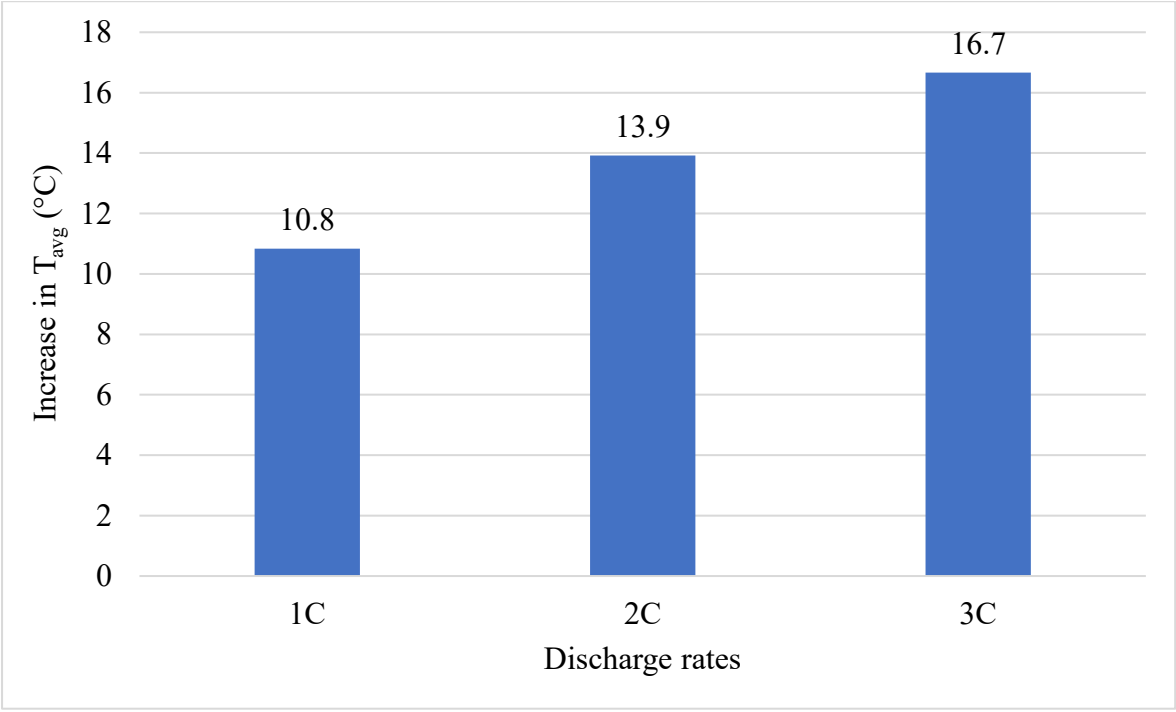

Figure 4.49: Increase in average temperature of battery when air inlet velocity is 5.5 m/s at different discharge rates:1C, 2C and 3C -with heat pipe-forced convection

4.3.2 Maximum (peak) temperature of each cell at end of discharge process (T_{max})

In the battery pack, the peak temperature reached by each cell is different as shown in the cases of free and forced convection cooling systems. In heat pipe based hybrid BTMS (BTMS-HP), peak temperature of each cell is recorded, the results indicate that the front row (cell 1,2,3 and 4) are at much lower temperature than last row cells (9,10,11 and 12). This non-uniformity of temperature was also observed in forced convection cooling without heat pipe (BTMS-FO). Figure 4.50, Figure 4.51 and Figure 4.52 respectively present results of peak temperature at 1C, 2C and 3C discharge rates respectively under varying air inlet velocity. It can be concluded from the results that increase in air inlet velocity has positive effect on battery cooling in case of BTMS-HP. Figure 4.53, Figure 4.54 and Figure 4.55, respectively shows the effect of discharge rate on peak temperature respectively at 3.6m/s, 4.6m/s and 5.5m/s air inlet velocities. The peak temperature at 1C discharge rate is much lower as compared to 2C and 3C rates. This is because for the same capacity, the discharge time for 1C is 60 minutes , while for 2C and 3C it is 30 minutes and 20 minutes respectively. So peak temperature in 2C and 3C are closer as compared to 1C. It can be observed from the results that peak temperature remains below 50°C in all cases of BTMS-HP.

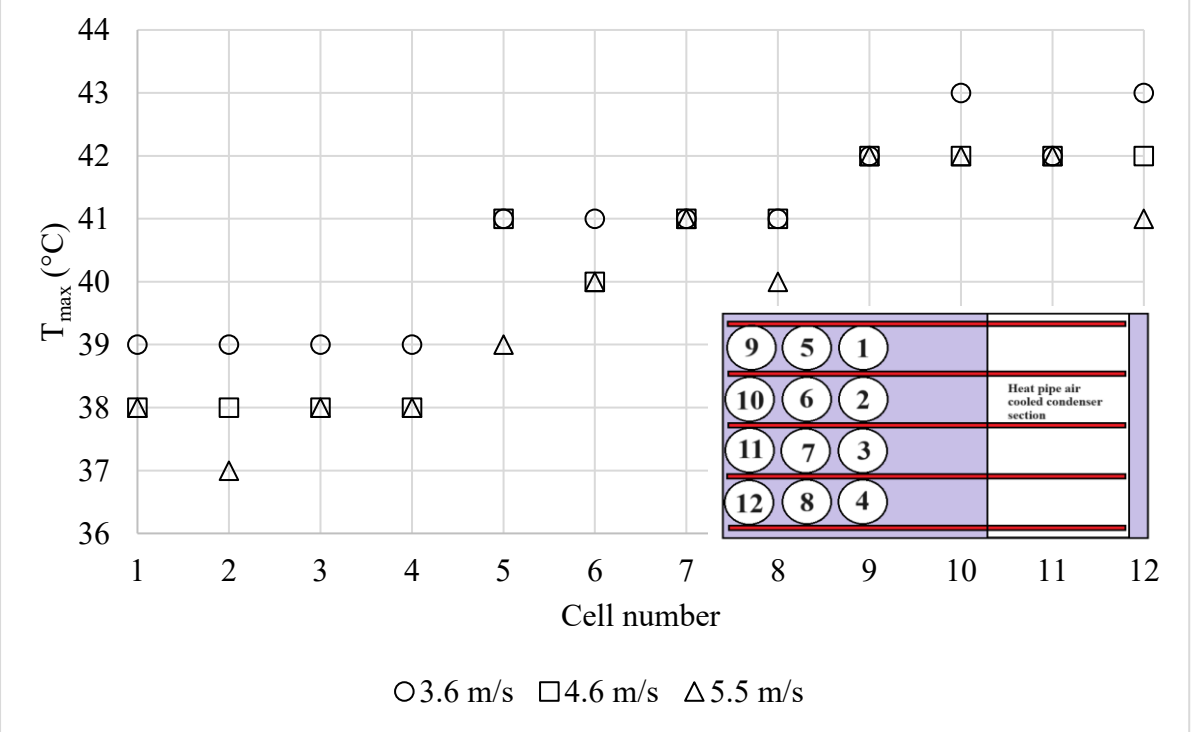

Figure 4.50; Peak temperature of cells at varying air inlet velocity when discharged at 1C-forced convection with heat pipe

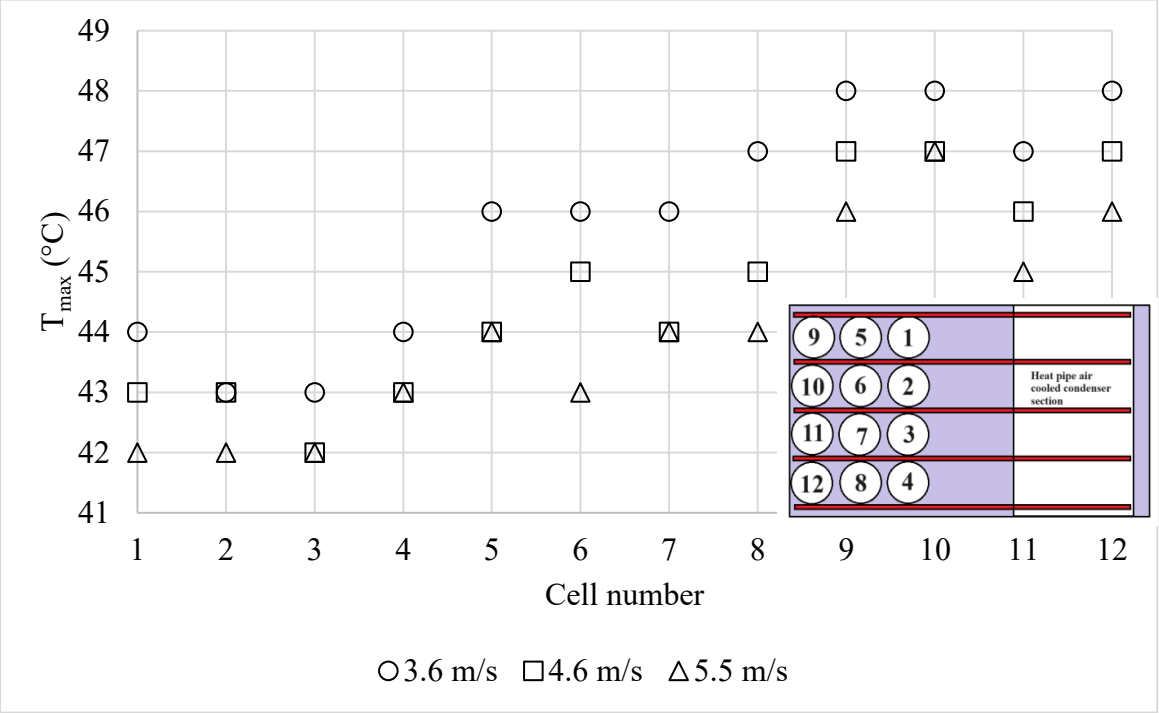

Figure 4.51: Peak temperature of cells at varying air inlet velocity when discharged at 2C-forced convection with heat pipe

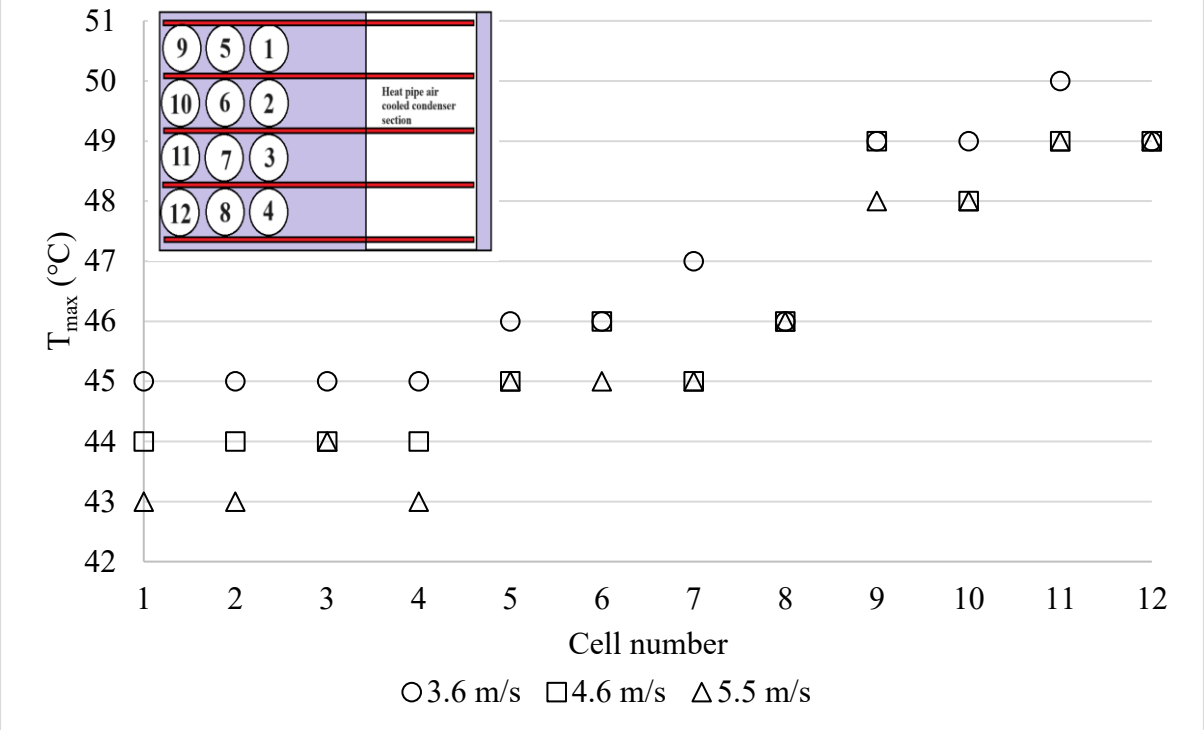

Figure 4.52: Peak temperature of cells at varying air inlet velocity when discharged at 3C-forced convection with heat pipe

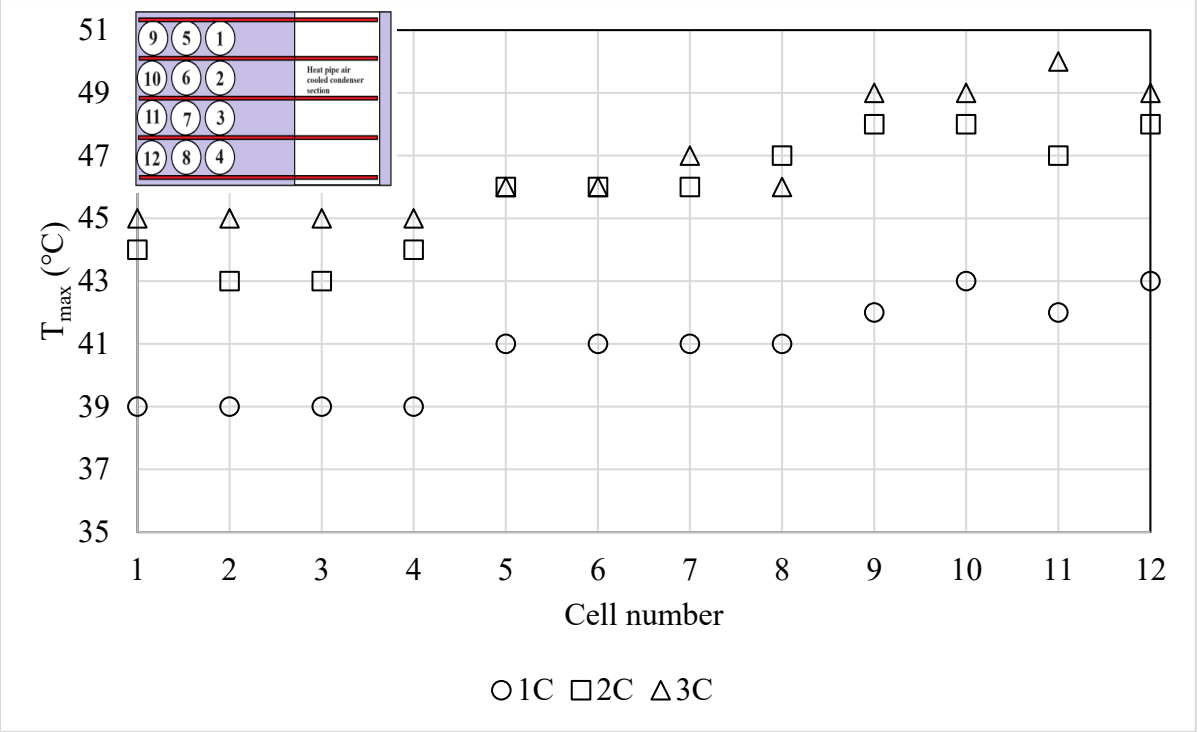

Figure 4.53: Peak temperature of cells at varying discharge rates when inlet air velocity is 3.6 m/s -forced convection with heat pipe

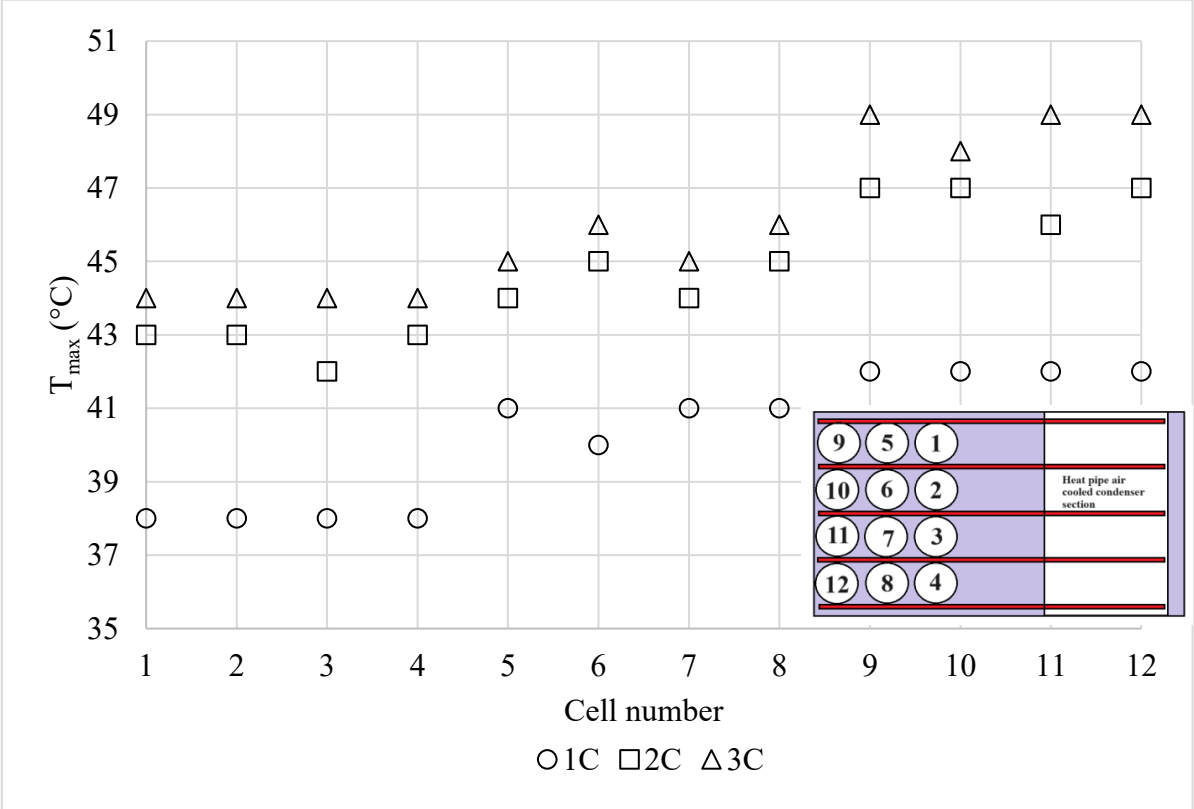

Figure 4.54: Peak temperature of cells at varying discharge rates when inlet air velocity is 4.6 m/s -forced convection with heat pipe

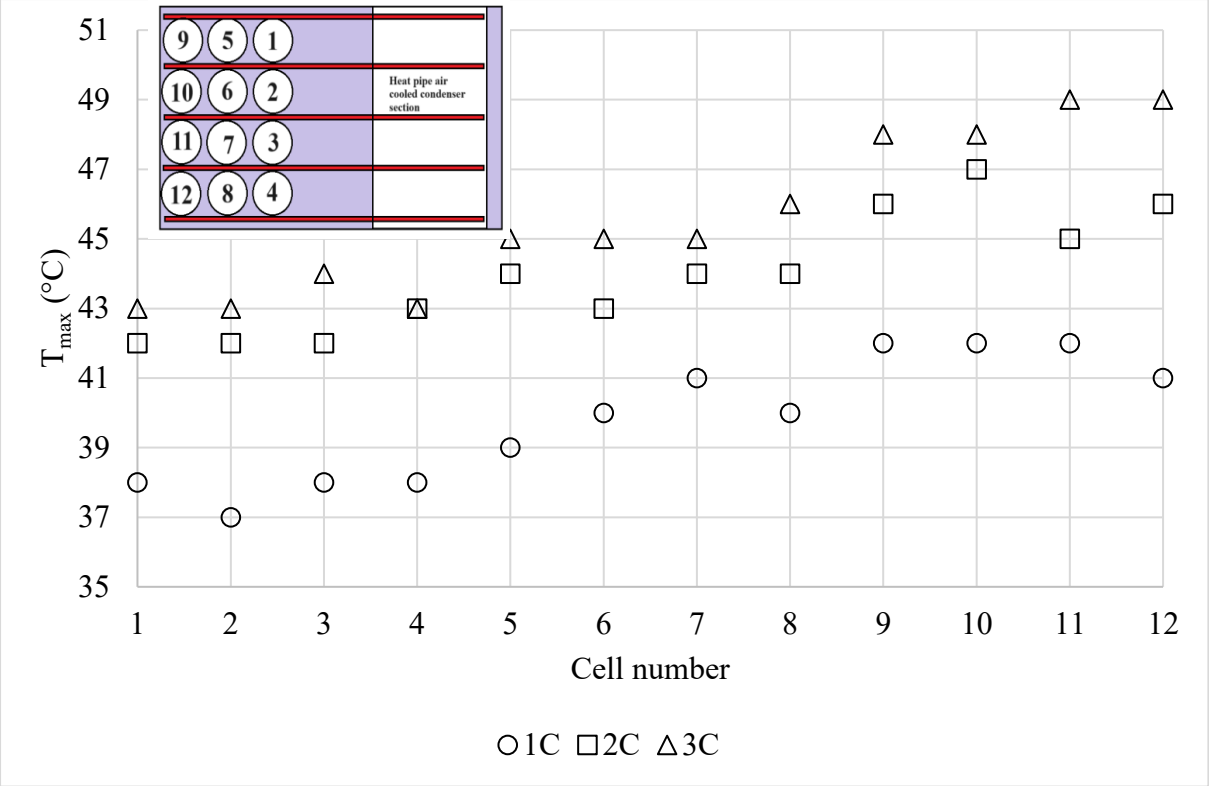

Figure 4.55: Peak temperature of cells at varying discharge rates when inlet air velocity is 5.5 m/s -forced convection with heat pipe

4.3.3 Temperature uniformity or homogeneity (ΔT) inside battery pack during discharge process

The temperature uniformity values observed in case of heat pipe based BTMS are better as compared to conventional forced convection. The BTMS-HP was able to maintain temperature uniformity within battery pack under ideal limit of 5°C in all cases (varying discharge rate and inlet air velocity) except one case where discharge rate is 3C and inlet air velocity is 5.5 m/s (see Figure 4.56, Figure 4.57 and Figure 4.58). In that one case, still the hybrid system maintains temperature uniformity within acceptable limit. Incremental increase in ΔT is also presented in bar charts for 1C, 2C and 3C respectively in Figure 4.59, Figure 4.60 and Figure 4.61. Although the process to discharge battery at 3C takes only 20 minutes and compared to 60 minutes for 1C and 30 minutes for 2C, but value and the slope of rise in ΔT at 3C is higher as compared to 2C and 1C discharge rates. This is due to the fact as same capacity of battery is discharge in shorted span of time, more heat is accumulated in the battery which results higher inner and surface temperature of battery cells. As can be seen in Figure 4.62, lower air velocities

and lower discharge rate are better for temperature uniformity. The same trend was also present in conventional forced cooling (BTMS-FO) but values of ΔT were much higher as compared to heat pipes based cooling system (BTMS-HP).

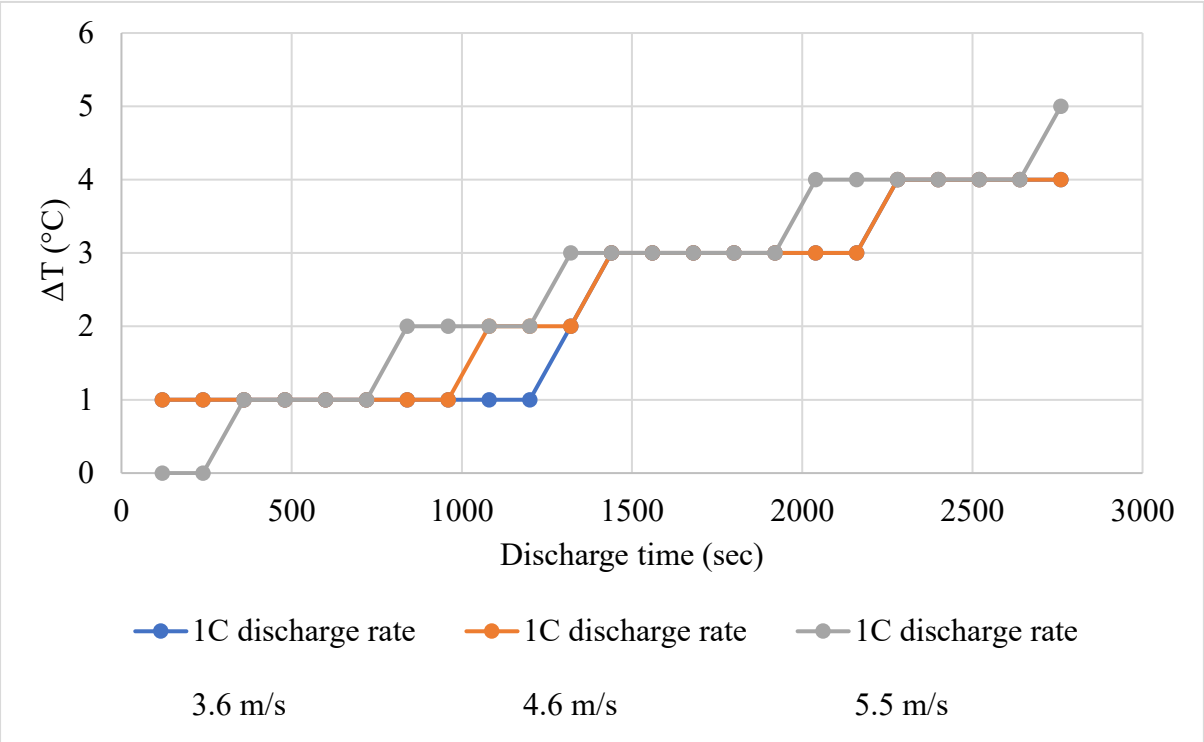

Figure 4.56: Temperature uniformity variation during discharge process at 1C discharge rate at varying air inlet velocity under heat pipe assisted forced convection

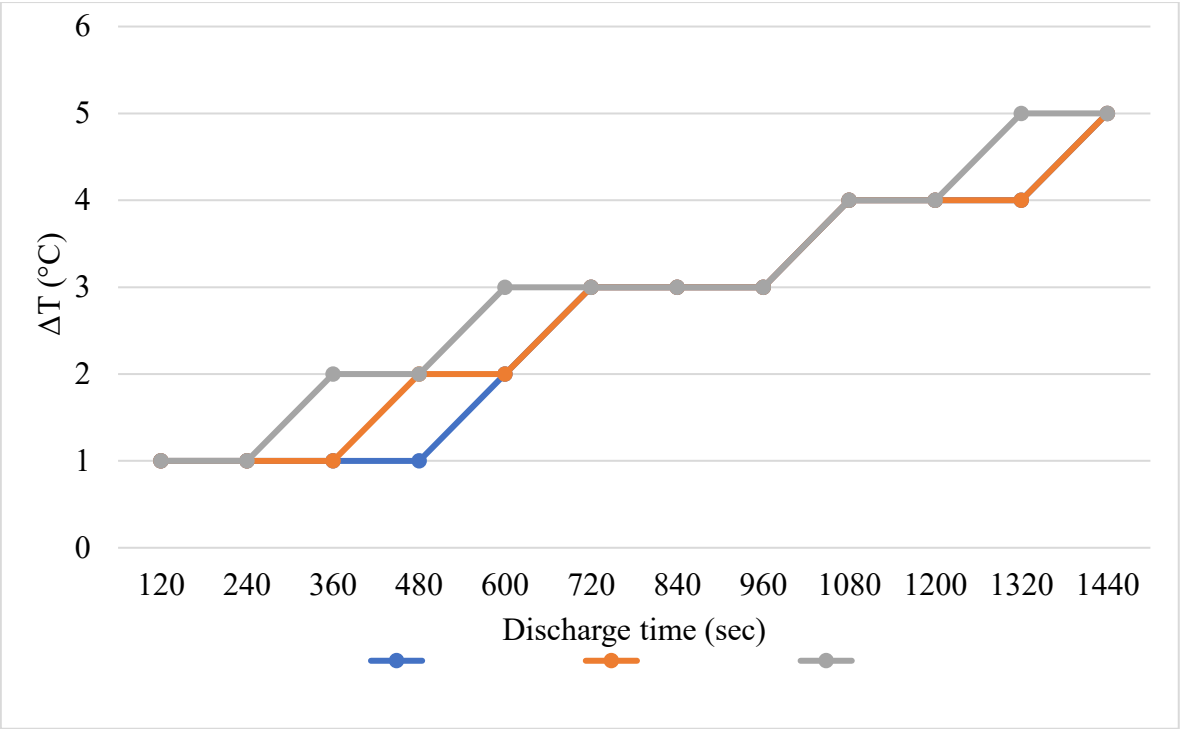

Figure 4.57: Temperature uniformity variation during discharge process at 2C discharge rate at varying air inlet velocity under heat pipe assisted forced convection

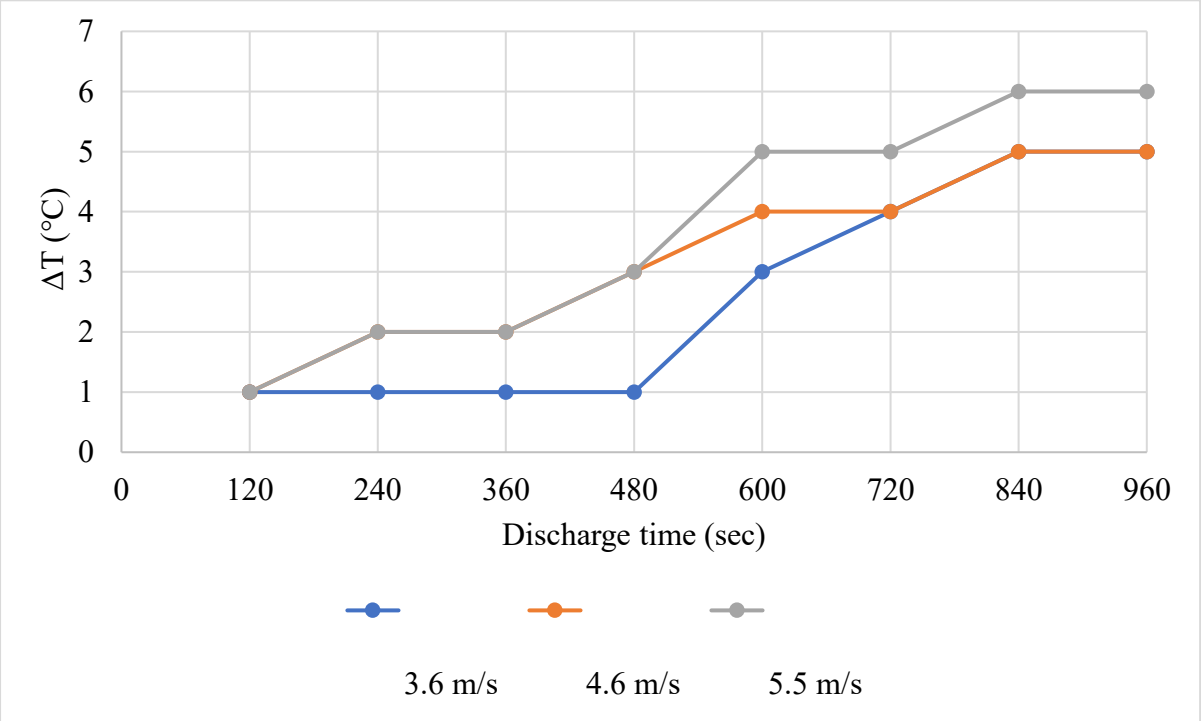

Figure 4.58: Temperature uniformity variation during discharge process at 3C discharge rate at varying air inlet velocity under heat pipe assisted forced convection

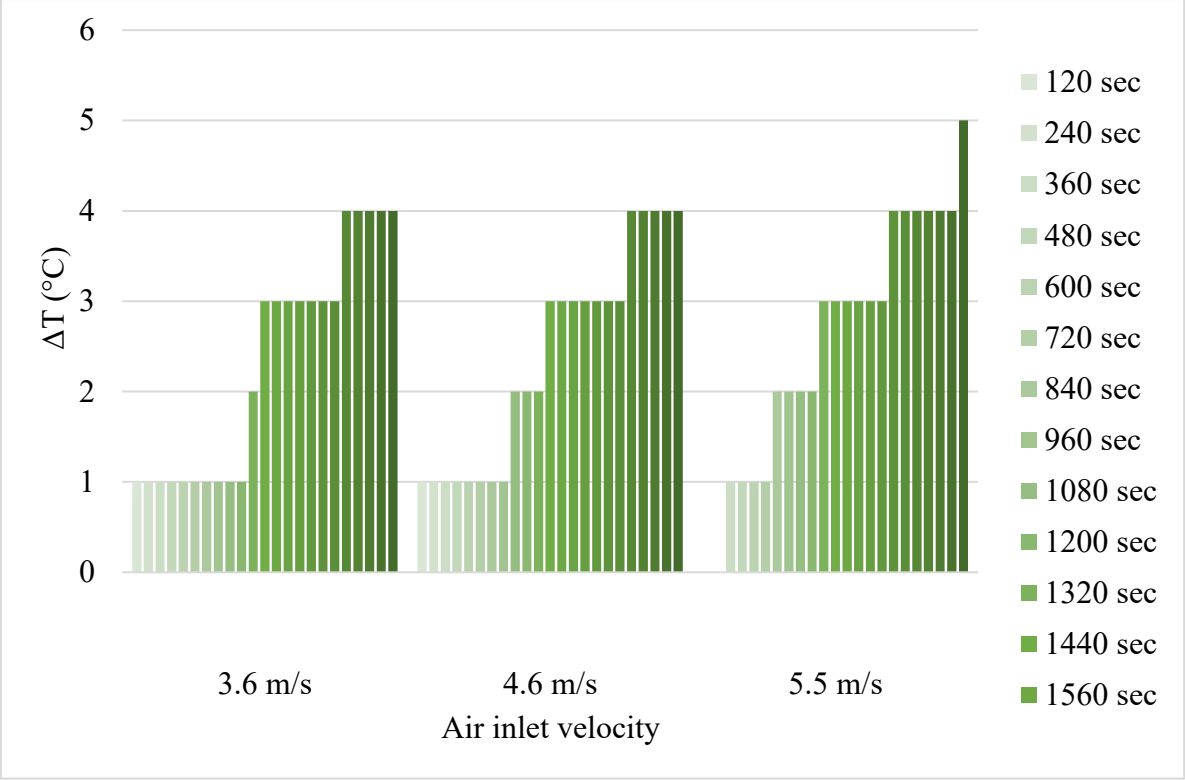

Figure 4.59: Temperature uniformity variation during discharge process at 1C discharge rate at varying air inlet velocity under heat pipe assisted forced convection

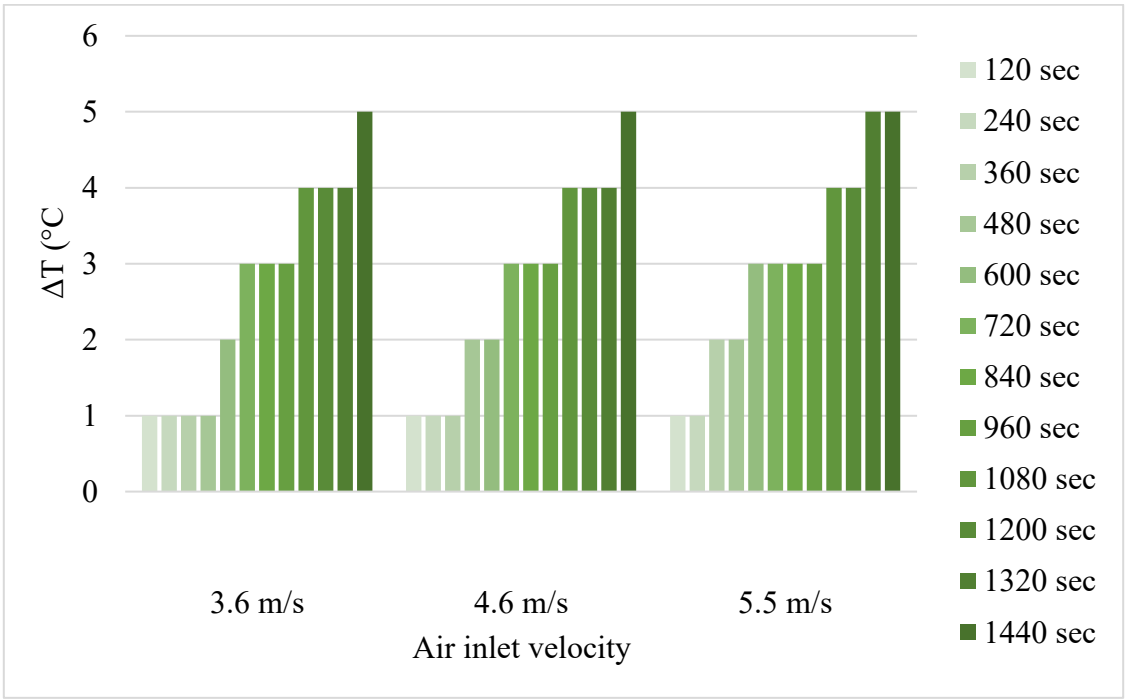

Figure 4.60: Temperature uniformity variation during discharge process at 2C discharge rate at varying air inlet velocity under heat pipe assisted forced convection

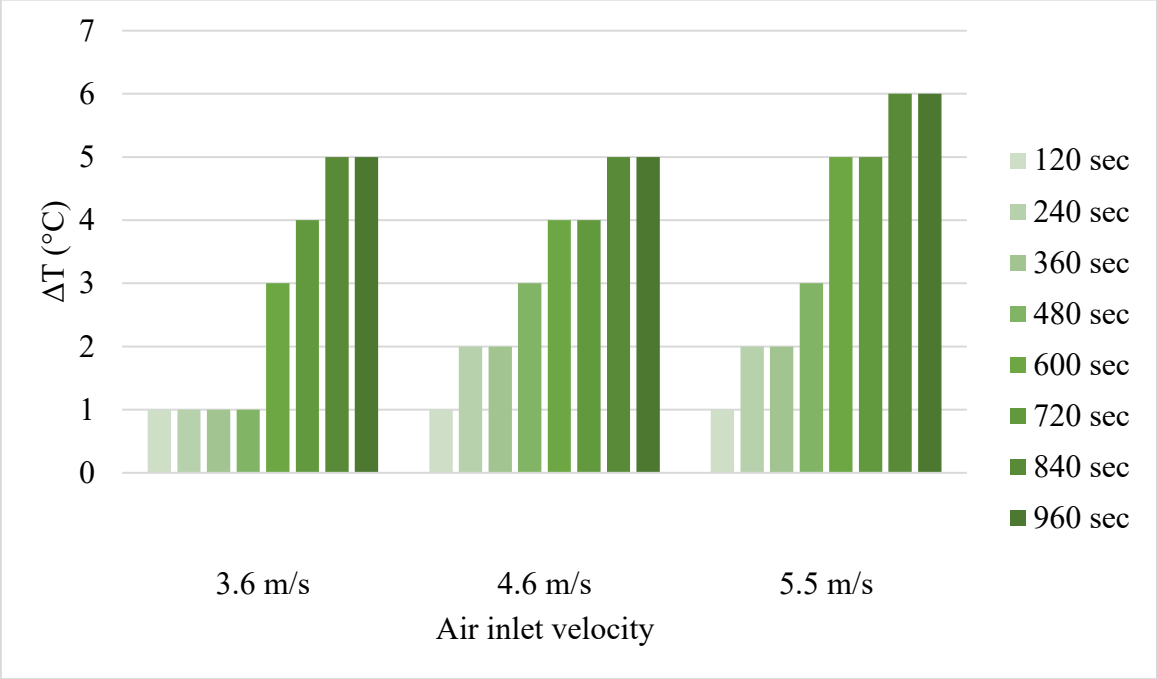

Figure 4.61: Temperature uniformity variation during discharge process at 3C discharge rate at varying air inlet velocity under heat pipe assisted forced convection

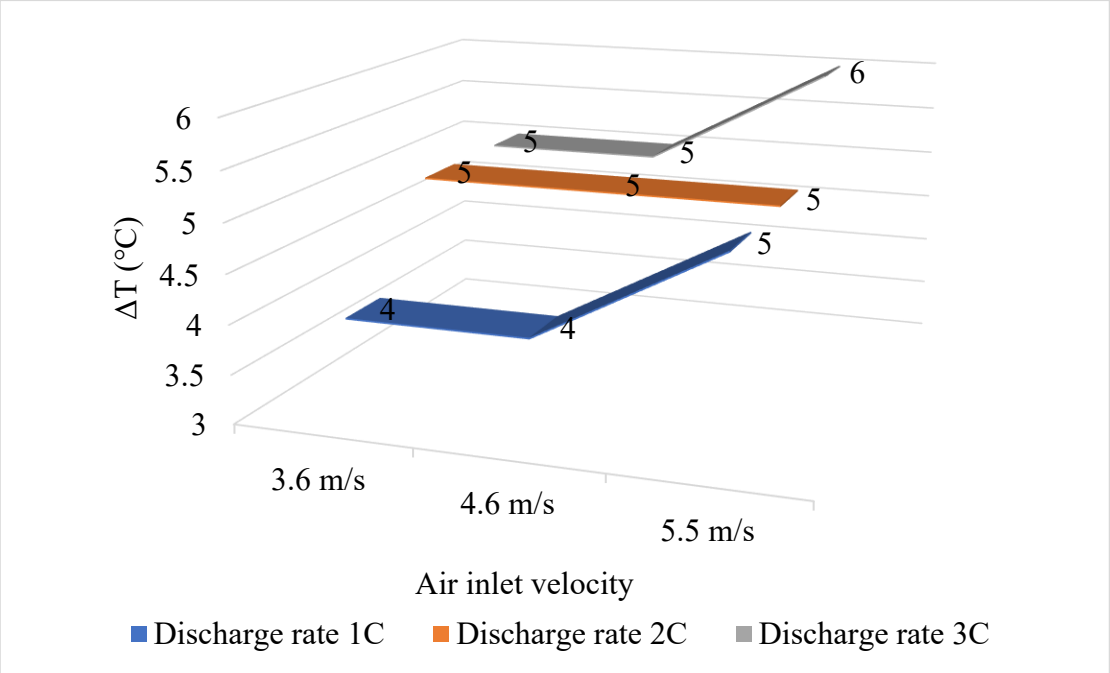

Figure 4.62: Temperature uniformity in battery pack after discharge process at varying discharge rates and air inlet velocity-heat pipe with forced convection

4.4 Comparative analysis of results: Temperature uniformity, Average temperature of battery pack and Peak temperature

(i) Generally, the temperature uniformity should be maintained within 5˚C. In present study, we are assuming the value of 5˚C as ideal ΔT value. An acceptable value of temperature uniformity is taken as 8˚C in present research. The acceptable temperature uniformity threshold for 32650 $LiFePO_4$ (LFP) cells is raised to 8 °C, in contrast to the commonly cited 5 °C threshold applied to 18650 high-energy-density Li-ion cells. The rationale behind this adjustment lies primarily in the intrinsic characteristics of LFP chemistry and the larger 32650 format. Unlike 18650 cells, which have higher energy density and greater susceptibility to thermal runaway, LFP cells possess a lower specific energy and are much more stable. This stability provides a higher tolerance against localized overheating and reduces the likelihood of catastrophic failure under moderate thermal non-uniformity. Additionally, 32650 cells have a larger size and higher thermal mass, which makes them inherently less sensitive to small temperature gradients across the module. In such cells, an 8 °C deviation does not significantly accelerate degradation mechanisms such as lithium plating or uneven SEI growth, compared to high-energy-density cells where even minor non-uniformity can rapidly affect cycle life. Several prior studies have shown that LFP batteries can sustain acceptable electrochemical performance and safety margins even with slightly relaxed thermal constraints, which supports the justification of a higher threshold in this case. It must be highlighted, however, that this choice of 8 °C as the permissible temperature uniformity criterion is adopted solely for the purpose of this investigation and should not be generalized as a universal design standard. Actual threshold values may vary depending on cell chemistry, format, application requirements, and manufacturer guidelines, and further empirical validation under different operating scenarios would be necessary before establishing any standardized limit. If temperature difference within battery pack has risen above 8˚C, in experimental study, that system is considered as a failure due to non-uniformity of temperature across battery pack as it will led to degradation of some cells at higher rate as compared to other cells. This may put excessive stress on some cells which may even lead to total failure or even explosion of battery pack. It can be observed from the results (Figure 4.63) that heat pipe based BTMS and free convection based BTMS were able to maintain temperature uniformity within 8˚C at all three discharge rates i.e., 1C, 2C and 3C. The forced convection based

BTMS (BMTS-FO) even failed in limiting temperature uniformity with acceptable limit of 8°C. Higher inlet air velocity and higher discharge rates have adverse effect on BTMS-FO. The adverse effect of increased air velocity is also observed in heat pipe based BTMS (BTMS-HP), but its severity was low as compared to forced convection. The value of ΔT exceeds 8˚C for such cases where inlet air inlet velocity or discharge rate is high for BTMS-FO. The results indicate that inlet air velocity flow pattern plays significant role in maintaining temperature uniformity. The inherent limitation of rectangular design and coolant flow pattern from inlet to outlet make forced convection unsuitable for keeping temperature uniformity within ideal or acceptable limits.

(ii) The analysis of average temperature of battery pack during discharge process for free, forced and heat assisted forced convection is presented in Figure 4.64. The average temperature should be maintained below 50˚C. The free convection cooling (BTMS-FR) could not limit the temperature of battery pack below 50°C at higher discharge rates of 2C and 3C. BTMS-FR and BTMS-HP both were successful in maintaining average temperature of battery pack below 50°C. It can be observed from the results that increased air velocity slightly improve or reduce temperature of battery pack. Higher discharge rate has adverse effect on average temperature of battery pack. Hybrid heat pipe based cooling system (BTMS-HP) performed better compared to conventional free and forced convection cooling.

(iii) Peak temperature (T_{max}) has a significant role in defining life cycle of battery cell. During discharge process, highest peak temperature values were observed in free convection (BTMS-FR). As can be seen in Figure 4.65, the BTMS-FR and BTMS-FO both failed in maintaining peak temperature of cells below 50°C. The critical cells in BTMS-FR and BTMS-FO are located at different locations in the battery pack. In BTMS-FR, critical cells having higher peak temperature were mid cells while in BTMS-FO, the critical cells were last row cells with higher peak temperature values. The cells that are higher temperature as compared to other were at risk of earlier failure and may be led to fire hazards. BTMS-HP performance was better in keeping battery pack within acceptable limits. It was observed that higher air velocity has positive effect on peak temperature but the drop in peak temperature is only 1°C to 2°C.

The increase in temperature of battery pack during discharge process is present in Figure 4.66. It is observed that increase in temperature as lowest for BTMS-HP at 1C discharge and 5.5m/s air velocity while it was highest for BTMS-FR at 3C.

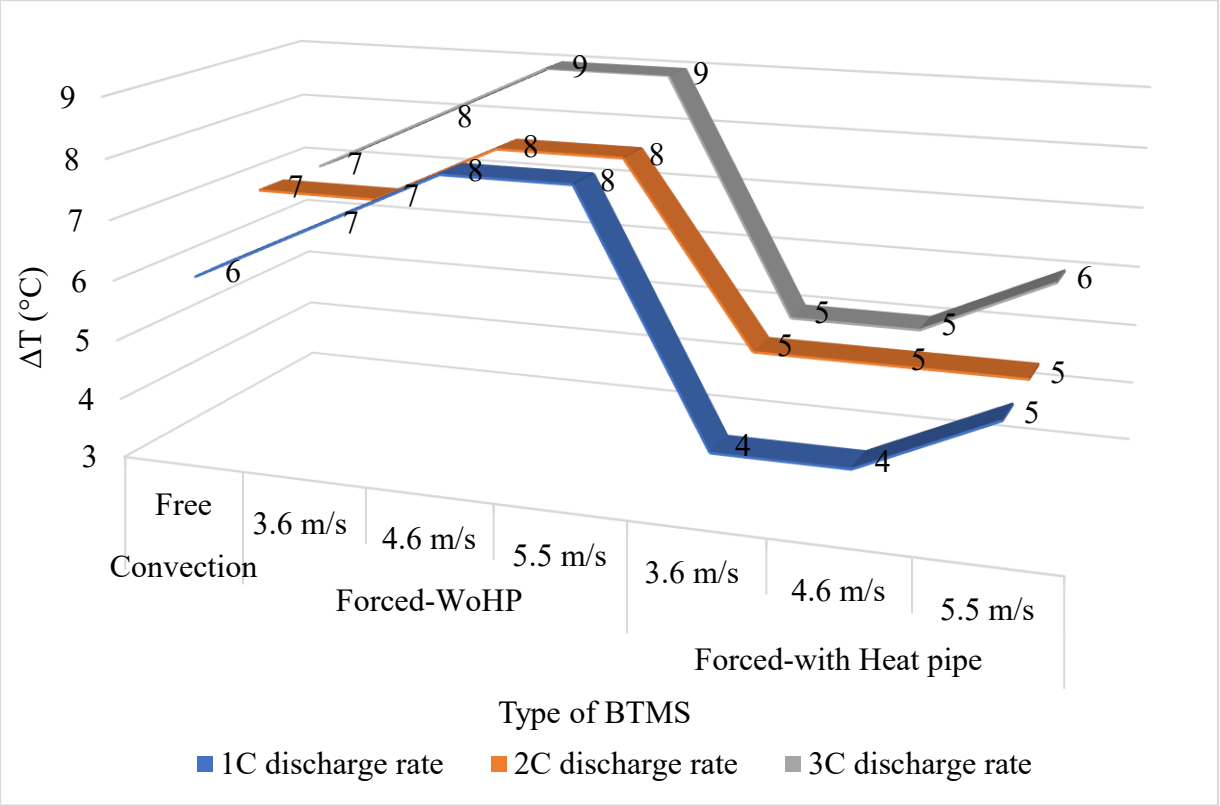

Figure 4.63:Comparative analysis of temperature uniformity in free convection (BTMS-FR), forced convection without heap pipe (BTMS-FO) and forced convection with heat pipe (BTMS-HP) in terms of maximum temperature difference (ΔT) in the battery pack at end of discharge process

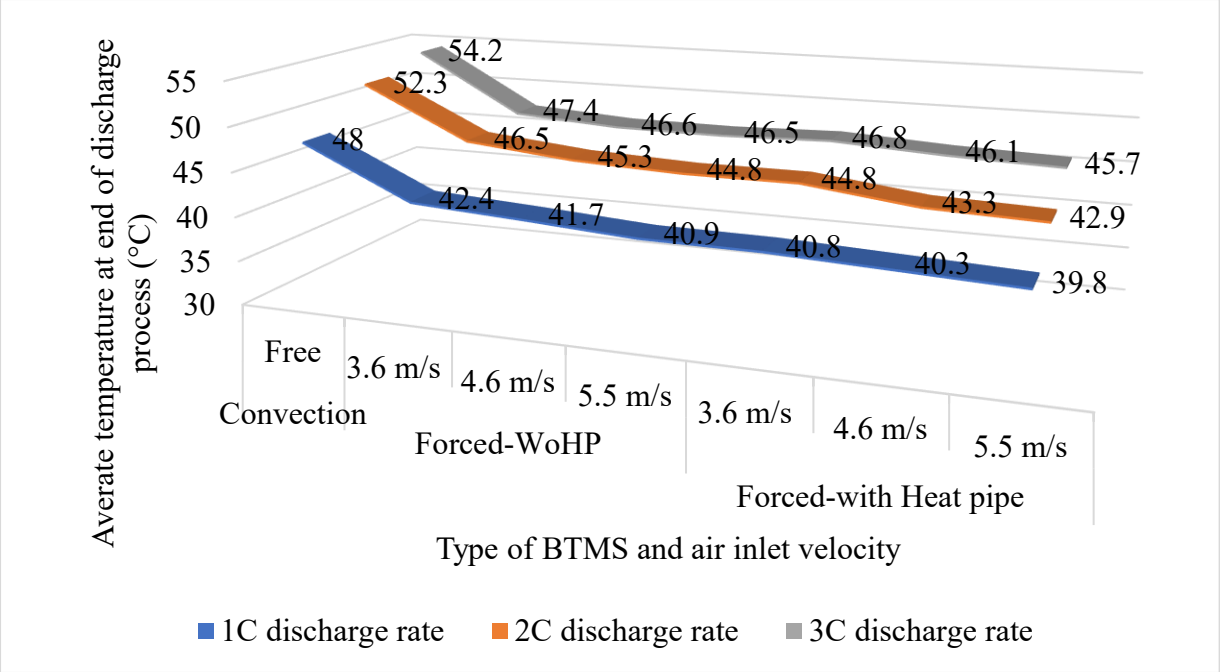

Figure 4.64: Comparative analysis of average temperature in free convection (BTMS-FR), forced convection without heap pipe (BTMS-FO) and forced convection with heat pipe (BTMS-HP) of the battery pack at end of discharge process

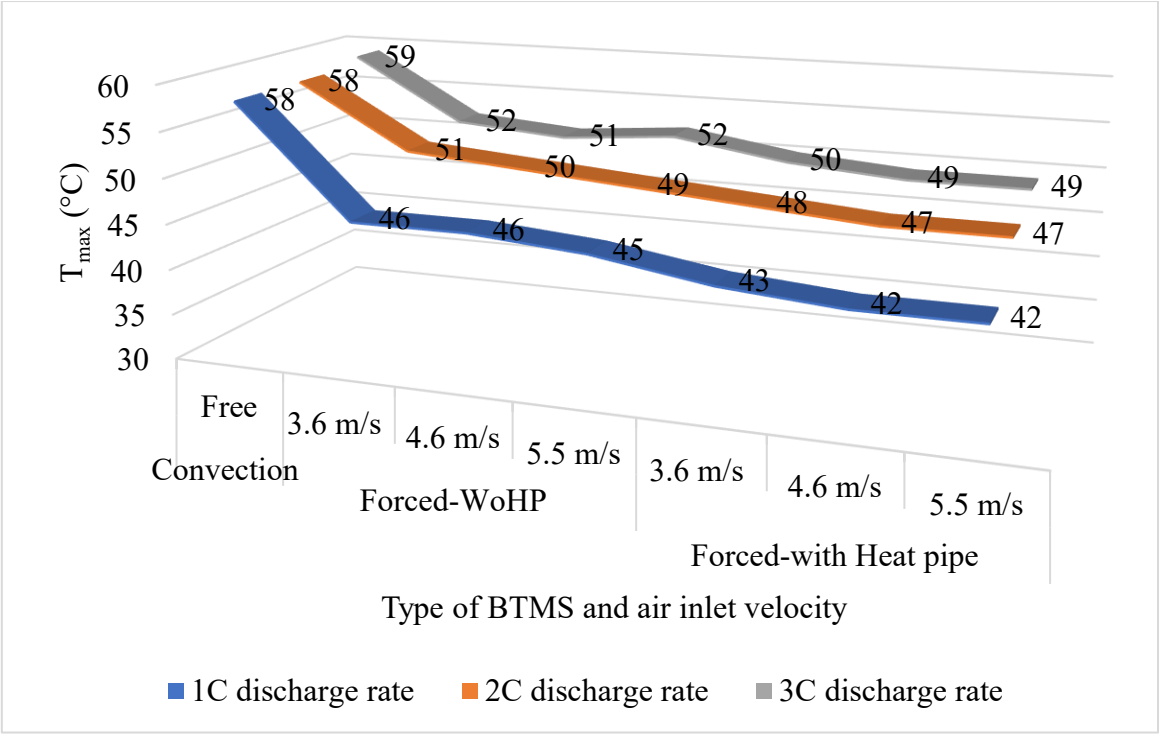

Figure 4.65: Comparative analysis of peak temperature in free convection (BTMS-FR), forced convection without heap pipe (BTMS-FO) and forced convection with heat pipe (BTMS-HP) of the battery pack at end of discharge process

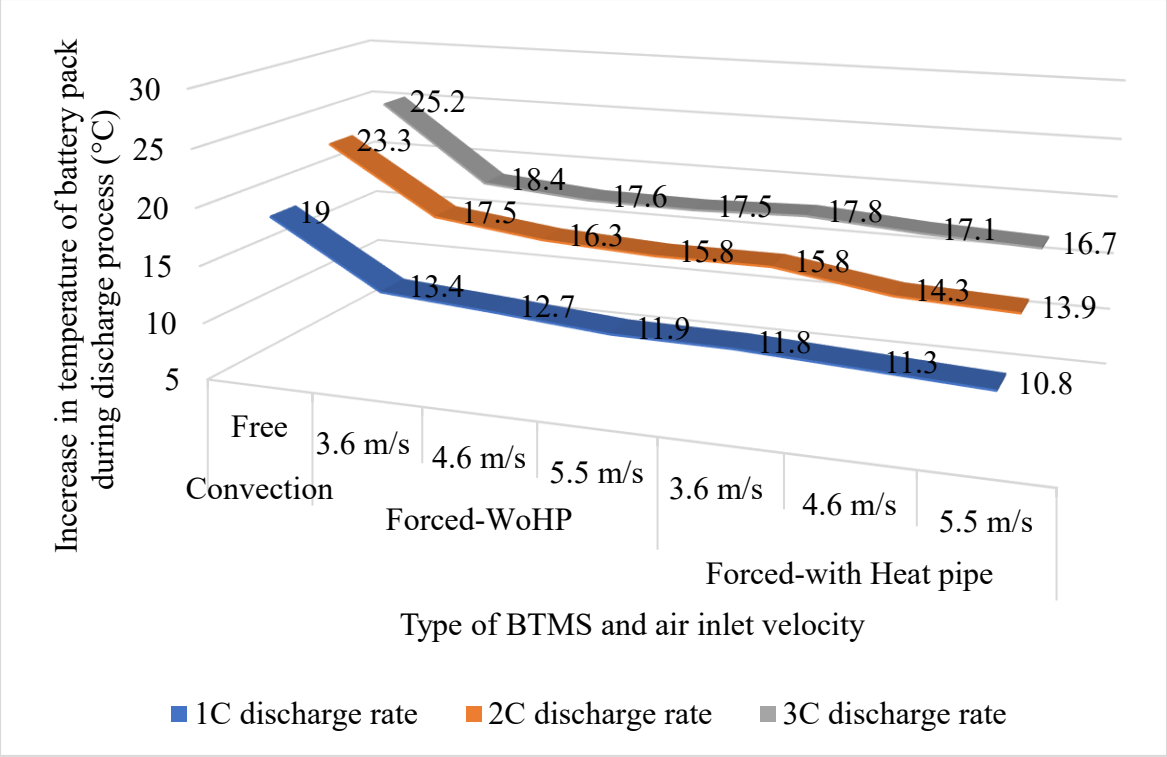

Figure 4.66: Comparative analysis of temperature increase in free convection (BTMS-FR), forced convection without heap pipe (BTMS-FO) and forced convection with heat pipe (BTMS-HP) of the battery pack during the discharge process at 1C, 2C and 3C

Summary and Conclusion

In present research work, experimental analysis of conventional free convection and forced convection based BTMS were conduction to study their limitations in terms of three main parameters: Average temperature of battery pack, Peak temperature of cells and Temperature homogeneity or uniformity in the battery pack. To stimulate acceleration and cruising situations, battery packs were discharge at varying C rates (1C, 2C and 3C). The effect of variations in discharge rate, inlet air velocity and cell interspacing on the performance of BTMS (free and forced) were analysed by discharging battery pack under varying conditions or combinations of these three parameters. A flat heat pipe based BTMS is fabricated by keeping in mind the limitations and observations of conventional BTMS systems. The experimental investigations were carried out to analyse the enhancement in the performance of conventional forced air-cooling system by insertion of heat pipes. A comparative analysis in terms of peak temperature, temperature uniformity and average temperature of free convection, forced convection and hybrid heat pipe assisted cooling systems were conducted to study the impact of heat pipe insertion on the performance of BTMS. The summarized results in terms of threshold limits can be seen in Table 5.1. The results showed that out of the eleven cases of convectional forced air cooling, six failed in keeping parameters within acceptable limits. The failures were mainly at higher air inlet velocities as at higher velocities front cells are cooled at higher rate thereby increasing non-uniformity of temperature within battery pack. This non-uniformity of temperature within battery pack was reduced when heat pipes were inserted, and improvement in both peak temperature and temperature uniformity along with average temperature was observed from experimental analysis. The following conclusions can be drawn from the results:

- The free convection based BTMS (BTMS-FR) was although able to maintain temperature uniformity within acceptable limit of 8°C in the battery pack but the peak temperature of cells and average temperature of battery pack were not within acceptable limits of 50°C.
- The conventional forced convection cooling (BTMS-FO) was successful in maintaining peak temperature and temperature uniformity within acceptable limits in about 45 percent of test cases. The control of peak temperature was better at higher air velocity, but temperature was more uniform at lower air velocity and discharge rate. The main

limitation of forced convection was that it could not maintain temperature uniformity in majority of the cases within acceptable limit. This was because the front row cells were cooled by fresh incoming air at much higher rate as compared to last row cells. This flow pattern of air created problem where cells of each row have different peak temperature range which thereby reduced uniformity of temperature within battery pack.

- Both free and forced convection based BTMS without heat pipe cannot control temperature uniformity within ideal limit of 5˚C. Hybrid BTMS kept temperature homogeneity within ideal limit in majority of cases.
- The critical cells were found in conventional free and forced convection. In free convection, the center or mid cells (6, 7) are critical in free convection while the cells in the last row (9, 10, 11 and 12) are critical in forced convection and hybrid system.
- The flat heat pipe based BTMS (hybrid system) was able to control peak temperature and temperature uniformity within acceptable limits. The success rate in maintaining peak, average and temperature uniformity within acceptable limits in hybrid heat pipe assisted battery thermal system was 100 percent. The reduction in peak temperature ranges from 2°C to 4°C and 10°C to 16°C as compared to forced and free convection respectively. This reduction may not seem much but even a 1°C drop in temperature effect battery life significantly.
- Free convection performs better in terms of temperature homogeneity and forced convection based BTMS performs better in terms of peak temperature and average temperature of battery pack. Hybrid system, being combination of heat pipe and forced convection kept both temperature homogeneity and peak temperature within limits.
- Increasing air inlet velocity in forced convection is not significant in keeping peak temperature and temperature homogeneity within acceptable limits, although average temperature of battery pack reduces at elevated air inlet velocities.
- Increasing interspacing from 2mm to 4mm in forced convection does not significantly improve results. The average temperature and peak temperature were higher at 4 mm interspacing as compared to 2 mm interspacing.
- The main benefit of heat pipe addition was in terms of temperature uniformity. The heat pipe assisted cooling was able to restrict maximum temperature difference within battery pipe to optimum level of 5°C in majority of cases. This was not possible with

conventional forced convection and values were as high as 9°C. Higher values promote early degradation of a few cells which reduce overall battery pack life.

- It was observed during experimentation that higher air velocities are although advantageous in reducing peak temperature of battery cells, but higher air velocity has adverse effect on temperature uniformity.
- The results showed that higher discharge rates are highly correlated with higher peak temperature of battery cell. At higher discharge heat loss by cell increase at much higher rate as compared to lower discharge rates.
- The heat transfer rate in free convection BTMS much lower than forced convection BTMS. This results in higher temperature rise in free convection. The higher temperature during experimentation resulted in failure of one cell due to electrolyte leakage.
- Silicon carbide (SiC) is used as filler material in heat pipe based BTMS. The SiC used seemed to have worked well as temperature control in BTMS-HP was better as compared to conventional system.

Key quantified findings are as follows:

1. Free convection (BTMS-FR):
    - Maintained ΔT within the acceptable 8°C threshold in 100% of cases but ideal threshold of 5°C is not maintained.
    - However, failed to keep $T_{max} \leq 50°C$ in most cases, with peak values exceeding 55°C at 3C.
    - Average pack temperature was also 3–5°C higher than acceptable limits.

2. Forced convection (BTMS-FO):
    - Successfully maintained $Tmax \leq 50°C$ and acceptable $\Delta T \leq 8°C$ in only ~45% of cases.
    - At high inlet air velocities (>3 m/s), T_{max} dropped by 5–7°C, but ΔT worsened to as high as 9°C, due to front-row overcooling vs. rear-row heating.
    - Increasing interspacing from 2 mm to 4 mm increased T_{max} by ~2–3°C and raised T_{avg}, showing limited benefit.

3. Hybrid heat pipe–assisted BTMS (BTMS-HP):

- Maintained all three performance parameters (Tavg ≤ 50°C, Tmax ≤ 50 °C, ΔT ≤ 8°C) in 100% of test cases. ΔT ≤ 5°C (ideal) is also maintained is most of the cases.
- Reduced T_{max} by 10–16°C vs. free convection and by 2–4°C vs. forced convection.
- Reduced ΔT to ≤ 5°C in most cases, compared to values up to 9°C in forced convection.
- Achieved reductions of:
    - $T_{max:}$ up to 16°C (29% improvement),
    - ΔT: up to 44% improvement,
    - T_{avg}: lowered by 3–6°C compared to baseline.
    -

4. Critical cell locations:
    - In free convection, central cells (6–7) recorded T_{max}.
    - In forced convection, rear cells (9–12) reached T_{max}, with ΔT between rows up to 9°C.
    - Hybrid system successfully suppressed temperature gradients to ≤ 5°C.

5. Discharge rate effect:
    - At 3C, T_{max} exceeded 55°C in free convection and 51°C in forced convection, while hybrid system restricted T_{max} to <48°C.
    - ΔT increased with higher C-rates in convectional systems but was effectively contained by heat pipes.

Heat pipes are utilized in various high end electronic components but their use in electrical vehicles is still a challenge. This passive system of heat extraction when combined with active cooling systems can overcome certain inherent limitations of active systems and enhance their performance. The hybrid system presented in the present research was mainly designed to compare convectional and heat pipe-assisted hybrid system of cooling in simplest way possible. Their practical utilization in EVs is still under research. The future work would be to modify and use present heat pipe assisted system with liquid cooling which may further enhance performance of heat pipe assisted thermal management system. Research work may also be taken to further improve the design by addition of extended surfaces, changing battery pack geometry and design and by using better inter filler materials. Present research work was initiated to study the limitations of convectional cooling systems and at the same time developing an alternative approach to conventional cooling which may minimize limitations of conventional systems.

Table 5.1: Summarized results indicating ability of battery thermal management systems to keep peak temperature and temperature uniformity within ideal and acceptable threshold limits

BTMS type along with C rate, air velocity and interspacing	(PT) Threshold limits of Peak temperature		(TU) Threshold limits of Temperature uniformity		BTMS performance in terms of acceptable limit (PT) ∩ (TU)
	Ideal (I)	Acceptable (A)	Ideal (I)	Acceptable (A)	PT-A ∩ TU-A
	(T ≤40˚C)	(T ≤ 50˚C)	(ΔT ≤ 5˚C)	(ΔT ≤ 8˚C)	
Free 1C, 2mm	fail	fail	fail	success	fail
Free 2C, 2mm	fail	fail	fail	success	fail
Free 3C,2mm	fail	fail	fail	success	fail
Forced Ve1,1C,2mm	fail	success	fail	success	success
Forced Ve2,1C,2mm	fail	success	fail	success	success
Forced Ve3,1C,2mm	fail	success	fail	success	success
Forced Ve1,2C,2mm	fail	fail	fail	success	fail
Forced Ve2,2C,2mm	fail	success	fail	success	success
Forced Ve3,2C,2mm	fail	success	fail	success	success
Forced Ve1,3C,2mm	fail	fail	fail	success	fail

Forced Ve2,3C,2mm	fail	fail	fail	fail	fail
Forced Ve3,3C,2mm	fail	fail	fail	fail	fail
Forced Ve2,3C,4mm	fail	fail	fail	fail	fail
Forced Ve3,3C,4mm	fail	fail	fail	fail	fail
Hybrid: HP Ve1,1C	fail	success	success	success	success
Hybrid: HP Ve2-1C	fail	success	success	success	success
Hybrid: HP Ve3-1C	fail	success	success	success	success
Hybrid: HP Ve1-2C	fail	success	success	success	success
Hybrid: HP Ve2-2C	fail	success	success	success	success
Hybrid: HP Ve3-2C	fail	success	success	success	success
Hybrid: HP V1-3C	fail	success	success	success	success
Hybrid: HP V2-3C	fail	success	success	success	success
Hybrid: HP V3-3C	fail	success	fail	success	success

The present study successfully demonstrated the potential of free convection, forced convection, and hybrid flat heat pipe–assisted BTMS in controlling the thermal behaviour of battery packs under varying discharge rates and operating conditions. While the hybrid configuration clearly outperformed the conventional systems in terms of peak temperature

reduction and temperature uniformity, certain limitations remain that must be considered before extending the findings to practical electric vehicle applications.

A key concern lies in the scalability of the tested BTMS to full-scale EV battery systems. The experiments were carried out on a relatively small pack, whereas commercial EV modules often consist of hundreds of cells with complex geometries and tightly packed arrangements. Integrating heat pipes or hybrid structures into such modules may present significant design challenges, including increased weight, spatial constraints, and higher system cost. Furthermore, ensuring uniform airflow distribution in large-scale modules is inherently more difficult, which could limit the direct applicability of the proposed system without further optimization.

Another critical factor is the long-term operational reliability of the BTMS. Heat pipes, while effective in passive heat transfer, are prone to performance degradation over extended thermal cycling, mechanical vibrations, and orientation changes that are common in automotive environments. The filler material (e.g., SiC) and sealing integrity of the heat pipes also require long-term testing under realistic driving conditions to validate durability. Similarly, continuous exposure to dust, humidity, and varying ambient conditions can influence the effectiveness of both convection-based and hybrid systems.

Therefore, while the hybrid BTMS tested in this study shows promising improvements in temperature management at the laboratory scale, its practical deployment in real EV systems would require further investigation. Future research should focus on large-scale pack integration, long-duration cycling tests, vibration and orientation studies, and cost–benefit analysis to assess both the technical feasibility and economic viability of heat pipe–assisted BTMS for electric vehicles.

Bibliography

[1] IEA, "Tracking Transport 2020," 2020. [Online]. Available: https://www.iea.org/reports/tracking-transport-2020

[2] Siddharth Sinha and Madhav Sharma, "Decarbonising transport: Redefining mobility policies in India," *The Indian Express Pvt Ltd*, pp. 1–3, Jun. 23, 2021.

[3] Z. Rao and S. Wang, "A review of power battery thermal energy management," *Renewable and Sustainable Energy Reviews*, vol. 15, no. 9, pp. 4554–4571, 2011, doi: https://doi.org/10.1016/j.rser.2011.07.096.

[4] X. M. Xu and R. He, "Review on the heat dissipation performance of battery pack with different structures and operation conditions," *Renewable and Sustainable Energy Reviews*, vol. 29, pp. 301–315, 2014, doi: https://doi.org/10.1016/j.rser.2013.08.057.

[5] L. Ungurean, G. Cârstoiu, M. V Micea, and V. Groza, "Battery state of health estimation: a structured review of models, methods and commercial devices," *Int J Energy Res*, vol. 41, no. 2, pp. 151–181, 2017, doi: https://doi.org/10.1002/er.3598.

[6] M. M. Kabir and D. E. Demirocak, "Degradation mechanisms in Li-ion batteries: a state-of-the-art review," *Int J Energy Res*, vol. 41, no. 14, pp. 1963–1986, 2017, doi: https://doi.org/10.1002/er.3762.

[7] R. Zhao, S. Zhang, J. Liu, and J. Gu, "A review of thermal performance improving methods of lithium ion battery: Electrode modification and thermal management system," *J Power Sources*, vol. 299, pp. 557–577, 2015, doi: https://doi.org/10.1016/j.jpowsour.2015.09.001.

[8] G. Nagasubramanian, "Electrical characteristics of 18650 Li-ion cells at low temperatures," *J Appl Electrochem*, vol. 31, no. 1, pp. 99–104, 2001, doi: 10.1023/A:1004113825283.

[9] M. Broussely, J. P. Planchat, G. Rigobert, D. Virey, and G. Sarre, "Lithium-ion batteries for electric vehicles: performances of 100 Ah cells," *J Power Sources*, vol. 68, no. 1, pp. 8–12, 1997, doi: https://doi.org/10.1016/S0378-7753(96)02544-X.

[10] "Front Matter," in *Thermal Management of Electric Vehicle Battery Systems*, John Wiley & Sons, Ltd, 2017, pp. i–xvii. doi: https://doi.org/10.1002/9781118900239.fmatter.

[11] V. Etacheri, R. Marom, R. Elazari, G. Salitra, and D. Aurbach, "Challenges in the development of advanced Li-ion batteries: a review," *Energy Environ. Sci.*, vol. 4, no. 9, pp. 3243–3262, 2011, doi: 10.1039/C1EE01598B.

[12] Y. Ye, L. H. Saw, Y. Shi, and A. A. O. Tay, "Numerical analyses on optimizing a heat pipe thermal management system for lithium-ion batteries during fast charging," *Appl Therm Eng*, vol. 86, pp. 281–291, 2015, doi: https://doi.org/10.1016/j.applthermaleng.2015.04.066.

[13] N. Javani, I. Dincer, G. F. Naterer, and B. S. Yilbas, "Heat transfer and thermal management with PCMs in a Li-ion battery cell for electric vehicles," *Int J Heat Mass Transf*, vol. 72, pp. 690–703, 2014, doi: https://doi.org/10.1016/j.ijheatmasstransfer.2013.12.076.

[14] M. Al-Zareer, I. Dincer, and M. A. Rosen, "A novel phase change based cooling system for prismatic lithium ion batteries," *International Journal of Refrigeration*, vol. 86, pp. 203–217, 2018, doi: https://doi.org/10.1016/j.ijrefrig.2017.12.005.

[15] L. H. Saw, Y. Ye, A. A. O. Tay, W. T. Chong, S. H. Kuan, and M. C. Yew, "Computational fluid dynamic and thermal analysis of Lithium-ion battery pack with air cooling," *Appl Energy*, vol. 177, pp. 783–792, 2016, doi: https://doi.org/10.1016/j.apenergy.2016.05.122.

[16] L. Fan, J. M. Khodadadi, and A. A. Pesaran, "A parametric study on thermal management of an air-cooled lithium-ion battery module for plug-in hybrid electric vehicles," *J Power Sources*, vol. 238, pp. 301–312, 2013, doi: https://doi.org/10.1016/j.jpowsour.2013.03.050.

[17] T.-H. Tran, S. Harmand, B. Desmet, and S. Filangi, "Experimental investigation on the feasibility of heat pipe cooling for HEV/EV lithium-ion battery," *Appl Therm Eng*, vol. 63, no. 2, pp. 551–558, 2014, doi: https://doi.org/10.1016/j.applthermaleng.2013.11.048.

[18] N. Terada *et al.*, "Development of lithium batteries for energy storage and EV applications," *J Power Sources*, vol. 100, pp. 80–92, 2001, doi: 10.1016/S0378-7753(01)00885-0.

[19] H. Fathabadi, “High thermal performance lithium-ion battery pack including hybrid active–passive thermal management system for using in hybrid/electric vehicles,” *Energy*, vol. 70, pp. 529–538, 2014, doi: https://doi.org/10.1016/j.energy.2014.04.046.

[20] Herath KM, *Basics of Electric Vehicles Design and Function*, vol. 820233. ©2013 Volkswagen Group of America, Inc., 2013.

[21] J. Y. Yong, V. K. Ramachandaramurthy, K. M. Tan, and N. Mithulananthan, “A review on the state-of-the-art technologies of electric vehicle, its impacts and prospects,” *Renewable and Sustainable Energy Reviews*, vol. 49, pp. 365–385, 2015, doi: https://doi.org/10.1016/j.rser.2015.04.130.

[22] U. Helmolt Rittmar von and Eberle, “Fuel Cell Vehicles: Fundamentals, System Efficiencies, Technology Development, and Demonstration Projects,” in *Hydrogen Technology: Mobile and Portable Applications*, A. Léon, Ed., Berlin, Heidelberg: Springer Berlin Heidelberg, 2008, pp. 273–290. doi: 10.1007/978-3-540-69925-5_9.

[23] L. Lu, X. Han, J. Li, J. Hua, and M. Ouyang, “A review on the key issues for lithium-ion battery management in electric vehicles,” *J Power Sources*, vol. 226, pp. 272–288, 2013, doi: https://doi.org/10.1016/j.jpowsour.2012.10.060.

[24] D. B. Richardson, “Electric vehicles and the electric grid: A review of modeling approaches, Impacts, and renewable energy integration,” *Renewable and Sustainable Energy Reviews*, vol. 19, pp. 247–254, 2013, doi: https://doi.org/10.1016/j.rser.2012.11.042.

[25] L. Lu, X. Han, J. Li, J. Hua, and M. Ouyang, “A review on the key issues for lithium-ion battery management in electric vehicles,” *J Power Sources*, vol. 226, pp. 272–288, 2013, doi: https://doi.org/10.1016/j.jpowsour.2012.10.060.

[26] M. Mohamed, R. Garnett, M. Ferguson, and P. Kanaroglou, “Electric Buses: A Review of Alternative Powertrains,” *Renewable and Sustainable Energy Reviews*, vol. 62, Mar. 2016, doi: 10.1016/j.rser.2016.05.019.

[27] L. Lu, X. Han, J. Li, J. Hua, and M. Ouyang, “A review on the key issues for lithium-ion battery management in electric vehicles,” *J Power Sources*, vol. 226, pp. 272–288, 2013, doi: https://doi.org/10.1016/j.jpowsour.2012.10.060.

[28] S. Muniamuthu, S. Arjun, M. Jalapathy, S. Harikrishnan, and A. Vignesh, “Review on Electric Vehicles,” *International Journal of Mechanical and Production Engineering Research and Development*, vol. 8, pp. 557–566, Mar. 2018, doi: 10.24247/ijmperdapr201865.

[29] A. Tourani, P. White, and P. Ivey, “Analysis of electric and thermal behaviour of lithium-ion cells in realistic driving cycles,” *J Power Sources*, vol. 268, pp. 301–314, 2014, doi: https://doi.org/10.1016/j.jpowsour.2014.06.010.

[30] C. L. Heth, “Energy on demand: A brief history of the development of the battery,” 2019. [Online]. Available: https://api.semanticscholar.org/CorpusID:210137368

[31] F. Rahmawati, L. Yuliati, I. S. Alaih, and F. R. Putri, “Carbon rod of zinc-carbon primary battery waste as a substrate for CdS and TiO2 photocatalyst layer for visible light driven photocatalytic hydrogen production,” *J Environ Chem Eng*, vol. 5, no. 3, pp. 2251–2258, 2017, doi: https://doi.org/10.1016/j.jece.2017.04.032.

[32] T. Wulandari, D. Fawcett, S. B. Majumder, and G. E. J. Poinern, “Lithium-based batteries, history, current status, challenges, and future perspectives,” *Battery Energy*, vol. 2, no. 6, p. 20230030, 2023, doi: https://doi.org/10.1002/bte2.20230030.

[33] J. B. Goodenough and K.-S. Park, “The Li-Ion Rechargeable Battery: A Perspective,” *J Am Chem Soc*, vol. 135, no. 4, pp. 1167–1176, 2013, doi: 10.1021/ja3091438.

[34] P. Ruetschi, F. Meli, and J. Desilvestro, “Nickel-metal hydride batteries. The preferred batteries of the future?,” *J Power Sources*, vol. 57, no. 1, pp. 85–91, 1995, doi: https://doi.org/10.1016/0378-7753(95)02248-1.

[35] P. Bernard and M. Lippert, “Chapter 14 - Nickel–Cadmium and Nickel–Metal Hydride Battery Energy Storage,” in *Electrochemical Energy Storage for Renewable Sources and Grid Balancing*, P. T. Moseley and J. Garche, Eds., Amsterdam: Elsevier, 2015, pp. 223–251. doi: https://doi.org/10.1016/B978-0-444-62616-5.00014-0.

[36] “32055806 (1)”.

[37] “30991665”.

[38] R. Zhao, S. Zhang, J. Liu, and J. Gu, “A review of thermal performance improving methods of lithium ion battery: Electrode modification and thermal management system,”

J Power Sources, vol. 299, pp. 557–577, 2015, doi: https://doi.org/10.1016/j.jpowsour.2015.09.001.

[39] Y. Ding, Z. P. Cano, A. Yu, J. Lu, and Z. Chen, "Automotive Li-Ion Batteries: Current Status and Future Perspectives," *Electrochemical Energy Reviews*, vol. 2, no. 1, pp. 1–28, 2019, doi: 10.1007/s41918-018-0022-z.

[40] D. Lin, Y. Liu, and Y. Cui, "Reviving the lithium metal anode for high-energy batteries," *Nat Nanotechnol*, vol. 12, no. 3, pp. 194–206, 2017, doi: 10.1038/nnano.2017.16.

[41] U. Köhler, J. Kümpers, and M. Ullrich, "High performance nickel-metal hydride and lithium-ion batteries," *J Power Sources*, vol. 105, no. 2, pp. 139–144, 2002, doi: https://doi.org/10.1016/S0378-7753(01)00932-6.

[42] B. S. A. W. L. I. P. HUAT, "THERMAL MANAGEMENT OF ELECTRIC VEHICLE BATTERY PACKS," 2014.

[43] K. T. Chau, Y. S. Wong, and C. C. Chan, "An overview of energy sources for electric vehicles," *Energy Convers Manag*, vol. 40, no. 10, pp. 1021–1039, 1999, doi: https://doi.org/10.1016/S0196-8904(99)00021-7.

[44] O. E. Rojas and M. A. Khan, "A review on electrical and mechanical performance parameters in lithium-ion battery packs," *J Clean Prod*, vol. 378, p. 134381, 2022, doi: https://doi.org/10.1016/j.jclepro.2022.134381.

[45] T. Horiba, K. Hironaka, T. Matsumura, T. Kai, M. Koseki, and Y. Muranaka, "Manganese type lithium ion battery for pure and hybrid electric vehicles," *J Power Sources*, vol. 97–98, pp. 719–721, 2001, doi: https://doi.org/10.1016/S0378-7753(01)00599-7.

[46] M. Majima, S. Ujiie, E. Yagasaki, K. Koyama, and S. Inazawa, "Development of long life lithium ion battery for power storage," *J Power Sources*, vol. 101, no. 1, pp. 53–59, 2001, doi: https://doi.org/10.1016/S0378-7753(01)00554-7.

[47] N. Terada *et al.*, "Development of lithium batteries for energy storage and EV applications," *J Power Sources*, vol. 100, no. 1, pp. 80–92, 2001, doi: https://doi.org/10.1016/S0378-7753(01)00885-0.

[48] E. Baker, H. Chon, and J. Keisler, “Battery technology for electric and hybrid vehicles: Expert views about prospects for advancement,” *Technol Forecast Soc Change*, vol. 77, no. 7, pp. 1139–1146, 2010, doi: https://doi.org/10.1016/j.techfore.2010.02.005.

[49] N. Omar *et al.*, “Lithium iron phosphate based battery – Assessment of the aging parameters and development of cycle life model,” *Appl Energy*, vol. 113, pp. 1575–1585, 2014, doi: https://doi.org/10.1016/j.apenergy.2013.09.003.

[50] T. Sasaki, Y. Ukyo, and P. Novák, “Memory effect in a lithium-ion battery,” *Nat Mater*, vol. 12, Mar. 2013, doi: 10.1038/nmat3623.

[51] S. Dhameja, “1 - Electric Vehicle Batteries,” in *Electric Vehicle Battery Systems*, S. Dhameja, Ed., Woburn: Newnes, 2002, pp. 1–21. doi: https://doi.org/10.1016/B978-075069916-7/50001-7.

[52] “Andreas” “Dinger” *et al.*, “Batteries for Electric cars: Challenges, Opportunities, and the Outlook to 2020,” Dec. 2009.

[53] T. Ohzuku and R. J. Brodd, “An overview of positive-electrode materials for advanced lithium-ion batteries,” *J Power Sources*, vol. 174, no. 2, pp. 449–456, 2007, doi: https://doi.org/10.1016/j.jpowsour.2007.06.154.

[54] W. A. van Schalkwijk and B. Scrosati, Eds., *Advances in Lithium-Ion Batteries*. Boston, MA: Springer US, 2002. doi: 10.1007/b113788.

[55] “M” “Yoshio,” “R J.” “Brodd,” and “Akiya” “Kozawa,” *Lithium-Ion Batteries*. New York, NY: Springer New York, 2009. doi: 10.1007/978-0-387-34445-4.

[56] Barrie Lawson, “https://www.mpoweruk.com/chemistries.htm,” The Electropaedia.

[57] S. Kainat, J. Anwer, A. Hamid, N. Gull, and S. M. Khan, “Electrolytes in Lithium-Ion Batteries: Advancements in the Era of Twenties (2020’s),” *Mater Chem Phys*, vol. 313, p. 128796, 2024, doi: https://doi.org/10.1016/j.matchemphys.2023.128796.

[58] P. Vyroubal, T. Kazda, J. Maxa, and J. Vondrák, “Analysis of Temperature Field in Lithium Ion Battery by Discharging,” *ECS Trans*, vol. 70, pp. 269–273, Mar. 2015, doi: 10.1149/07001.0269ecst.

[59] S. Panchal, “Experimental investigation and modeling of lithium-ion battery cells and packs for electric vehicles,” 2016. [Online]. Available: https://api.semanticscholar.org/CorpusID:139252334

[60] J. Warner, “Chapter 7 - Lithium-Ion and Other Cell Chemistries,” in *The Handbook of Lithium-Ion Battery Pack Design*, J. Warner, Ed., Amsterdam: Elsevier, 2015, pp. 65–89. doi: https://doi.org/10.1016/B978-0-12-801456-1.00007-5.

[61] I. Buchmann, “Batteries in a Portable World: A Handbook on Rechargeable Batteries for Non-Engineers,” 2011. [Online]. Available: https://api.semanticscholar.org/CorpusID:107040936

[62] P. N. Halimah, S. Rahardian, and B. Budiman, “Battery Cells for Electric Vehicles,” *International Journal of Sustainable Transportation Technology*, vol. 2, pp. 54–57, Mar. 2019, doi: 10.31427/IJSTT.2019.2.2.3.

[63] C. Iclodean, B. Varga, N. Burnete, D. Cimerdean, and B. Jurchiş, “Comparison of Different Battery Types for Electric Vehicles,” *IOP Conf Ser Mater Sci Eng*, vol. 252, no. 1, p. 12058, Oct. 2017, doi: 10.1088/1757-899X/252/1/012058.

[64] V. and A. Md. J. N. and S. D. and R. M. A. and J. B. and S. A. and V. P. S. and M. T. D. Gopinadh Sumol V. and Anoopkumar, “Lithium-Ion Pouch Cells: An Overview,” in *Energy Harvesting and Storage: Fundamentals and Materials*, A. and S. P. P. Jayaraj M. K. and Antony, Ed., Singapore: Springer Nature Singapore, 2022, pp. 209–224. doi: 10.1007/978-981-19-4526-7_7.

[65] Y. Inui, Y. Kobayashi, Y. Watanabe, Y. Watase, and Y. Kitamura, “Simulation of temperature distribution in cylindrical and prismatic lithium ion secondary batteries,” *Energy Convers Manag*, vol. 48, no. 7, pp. 2103–2109, 2007, doi: https://doi.org/10.1016/j.enconman.2006.12.012.

[66] Y. Chen *et al.*, “A review of lithium-ion battery safety concerns: The issues, strategies, and testing standards,” *Journal of Energy Chemistry*, vol. 59, pp. 83–99, 2021, doi: https://doi.org/10.1016/j.jechem.2020.10.017.

[67] M. Winter, B. Barnett, and K. Xu, “Before Li Ion Batteries,” *Chem Rev*, vol. 118, no. 23, pp. 11433–11456, Dec. 2018, doi: 10.1021/acs.chemrev.8b00422.

[68] A. A. Pesaran and S. D. Burch, “Thermal Performance of EV and HEV Battery Modules and Packs,” 1997. [Online]. Available: https://api.semanticscholar.org/CorpusID:14839818

[69] V. G. Choudhari, D. A. S. Dhoble, and T. M. Sathe, “A review on effect of heat generation and various thermal management systems for lithium ion battery used for electric vehicle,” *J Energy Storage*, vol. 32, p. 101729, 2020, doi: https://doi.org/10.1016/j.est.2020.101729.

[70] M. Balasundaram, V. Ramar, C. Yap, Lu Li, A. A. O. Tay, and Palani Balaya, “Heat loss distribution: Impedance and thermal loss analyses in LiFePO4/graphite 18650 electrochemical cell,” *J Power Sources*, vol. 328, pp. 413–421, 2016, doi: https://doi.org/10.1016/j.jpowsour.2016.08.045.

[71] R. Zhao, J. Gu, and J. Liu, “An investigation on the significance of reversible heat to the thermal behavior of lithium ion battery through simulations,” *J Power Sources*, vol. 266, pp. 422–432, 2014, doi: https://doi.org/10.1016/j.jpowsour.2014.05.034.

[72] K. Jalkanen, T. Aho, and K. Vuorilehto, “Entropy change effects on the thermal behavior of a LiFePO4/graphite lithium-ion cell at different states of charge,” *J Power Sources*, vol. 243, pp. 354–360, 2013, doi: https://doi.org/10.1016/j.jpowsour.2013.05.199.

[73] Y. Chen and J. W. Evans, “Three-Dimensional Thermal Modeling of Lithium-Polymer Batteries under Galvanostatic Discharge and Dynamic Power Profile,” *J Electrochem Soc*, vol. 141, no. 11, p. 2947, Nov. 1994, doi: 10.1149/1.2059263.

[74] C. R. Pals and J. Newman, “Thermal Modeling of the Lithium/Polymer Battery: II . Temperature Profiles in a Cell Stack,” *J Electrochem Soc*, vol. 142, no. 10, p. 3282, Oct. 1995, doi: 10.1149/1.2049975.

[75] B. L. McKinney, G. L. Wierschem, and E. N. Mrotek, “Thermal Management of Lead-Acid Batteries for Electric Vehicles,” *SAE Transactions*, vol. 92, pp. 839–845, 1983, [Online]. Available: http://www.jstor.org/stable/44644417

[76] K. Smith and C.-Y. Wang, “Power and thermal characterization of a lithium-ion battery pack for hybrid-electric vehicles,” *J Power Sources*, vol. 160, no. 1, pp. 662–673, 2006, doi: https://doi.org/10.1016/j.jpowsour.2006.01.038.

[77] C. Park and A. K. Jaura, “Dynamic Thermal Model of Li-Ion Battery for Predictive Behavior in Hybrid and Fuel Cell Vehicles,” Jun. 2003. doi: 10.4271/2003-01-2286.

[78] W. B. Gu and C. Y. Wang, “Thermal-Electrochemical Modeling of Battery Systems,” *J Electrochem Soc*, vol. 147, no. 8, p. 2910, Aug. 2000, doi: 10.1149/1.1393625.

[79] G. Liu, M. Ouyang, L. Lu, L. Jianqiu, and X. Han, “Analysis of the heat generation of lithium-ion battery during charging and discharging considering different influencing factors,” *J Therm Anal Calorim*, vol. 116, Apr. 2014, doi: 10.1007/s10973-013-3599-9.

[80] R. Spotnitz and J. Franklin, “Abuse behavior of high-power, lithium-ion cells,” *J Power Sources*, vol. 113, no. 1, pp. 81–100, 2003, doi: https://doi.org/10.1016/S0378-7753(02)00488-3.

[81] X. Feng, M. Ouyang, X. Liu, L. Lu, Y. Xia, and X. He, “Thermal runaway mechanism of lithium ion battery for electric vehicles: A review,” *Energy Storage Mater*, vol. 10, pp. 246–267, 2018, doi: https://doi.org/10.1016/j.ensm.2017.05.013.

[82] P. T. Coman, S. Rayman, and R. E. White, “A lumped model of venting during thermal runaway in a cylindrical Lithium Cobalt Oxide lithium-ion cell,” *J Power Sources*, vol. 307, pp. 56–62, 2016, doi: https://doi.org/10.1016/j.jpowsour.2015.12.088.

[83] P. Ramadass, B. Haran, R. White, and B. N. Popov, “Capacity fade of Sony 18650 cells cycled at elevated temperatures: Part II. Capacity fade analysis,” *J Power Sources*, vol. 112, no. 2, pp. 614–620, 2002, doi: https://doi.org/10.1016/S0378-7753(02)00473-1.

[84] T. M. Bandhauer, S. Garimella, and T. F. Fuller, “A Critical Review of Thermal Issues in Lithium-Ion Batteries,” *J Electrochem Soc*, vol. 158, no. 3, p. R1, Jan. 2011, doi: 10.1149/1.3515880.

[85] S. Panchal, S. Mathewson, R. Fraser, R. Culham, and M. Fowler, “Experimental Measurements of Thermal Characteristics of LiFePO4 Battery,” *SAE Technical Papers*, vol. 2015, Apr. 2015, doi: 10.4271/2015-01-1189.

[86] H. Budde-Meiwes *et al.*, “A review of current automotive battery technology and future prospects,” *Proceedings of the Institution of Mechanical Engineers, Part D: Journal of Automobile Engineering*, vol. 227, no. 5, pp. 761–776, 2013, doi: 10.1177/0954407013485567.

[87] J. Kim, J. Oh, and H. Lee, “Review on battery thermal management system for electric vehicles,” *Appl Therm Eng*, vol. 149, pp. 192–212, 2019, doi: https://doi.org/10.1016/j.applthermaleng.2018.12.020.

[88] L. Li, F. Dababneh, and J. Zhao, “Cost-effective supply chain for electric vehicle battery remanufacturing,” *Appl Energy*, vol. 226, pp. 277–286, 2018, doi: https://doi.org/10.1016/j.apenergy.2018.05.115.

[89] T. Waldmann, R.-G. Scurtu, K. Richter, and M. Wohlfahrt-Mehrens, “18650 vs. 21700 Li-ion cells – A direct comparison of electrochemical, thermal, and geometrical properties,” *J Power Sources*, vol. 472, p. 228614, 2020, doi: https://doi.org/10.1016/j.jpowsour.2020.228614.

[90] Y.-W. Chang, C.-H. Cheng, J.-C. Wang, and S.-L. Chen, “Heat pipe for cooling of electronic equipment,” *Energy Convers Manag*, vol. 49, no. 11, pp. 3398–3404, 2008, doi: https://doi.org/10.1016/j.enconman.2008.05.002.

[91] R. Zhao, S. Zhang, J. Liu, and J. Gu, “A review of thermal performance improving methods of lithium ion battery: Electrode modification and thermal management system,” *J Power Sources*, vol. 299, pp. 557–577, 2015, doi: 10.1016/j.jpowsour.2015.09.001.

[92] M. Bernagozzi, A. Georgoulas, N. Miché, and M. Marengo, “Heat pipes in battery thermal management systems for electric vehicles: A critical review,” Jan. 25, 2023, *Elsevier Ltd*. doi: 10.1016/j.applthermaleng.2022.119495.

[93] L. Ghadbeigi, B. Day, K. Lundgren, and T. D. Sparks, “Cold temperature performance of phase change material based battery thermal management systems,” *Energy Reports*, vol. 4, pp. 303–307, 2018, doi: https://doi.org/10.1016/j.egyr.2018.04.001.

[94] C. von Lüders *et al.*, “Lithium plating in lithium-ion batteries investigated by voltage relaxation and in situ neutron diffraction,” *J Power Sources*, vol. 342, pp. 17–23, 2017, doi: https://doi.org/10.1016/j.jpowsour.2016.12.032.

[95] Chester G. Motloch, Jon P. Christophersen, and Jeffrey R. Belt, “High-Power Battery Testing Procedures and Analytical Methodologies for HEV’s,” *SAE Technical Paper 2002-01-1950*, 2002.

[96] M. R. Giuliano, A. K. Prasad, and S. G. Advani, “Experimental study of an air-cooled thermal management system for high capacity lithium–titanate batteries,” *J Power*

Sources, vol. 216, pp. 345–352, 2012, doi: https://doi.org/10.1016/j.jpowsour.2012.05.074.

[97] W. Li *et al.*, "A Comprehensive Approach for the Clustering of Similar-Performance Cells for the Design of a Lithium-Ion Battery Module for Electric Vehicles," *Engineering*, vol. 5, no. 4, pp. 795–802, 2019, doi: https://doi.org/10.1016/j.eng.2019.07.005.

[98] A. A. Pesaran, "Battery thermal models for hybrid vehicle simulations," *J Power Sources*, vol. 110, no. 2, pp. 377–382, 2002, doi: https://doi.org/10.1016/S0378-7753(02)00200-8.

[99] R. Matthé, L. Turner, and H. Mettlach, "VOLTEC Battery System for Electric Vehicle with Extended Range," *SAE Int J Engines*, vol. 4, pp. 1944–1962, 2011, [Online]. Available: https://api.semanticscholar.org/CorpusID:111278450

[100] P. Qin, M. Liao, D. Zhang, Y. Liu, J. Sun, and Q. Wang, "Experimental and numerical study on a novel hybrid battery thermal management system integrated forced-air convection and phase change material," *Energy Convers Manag*, vol. 195, pp. 1371–1381, 2019, doi: https://doi.org/10.1016/j.enconman.2019.05.084.

[101] J. Lin, X. Liu, S. Li, C. Zhang, and S. Yang, "A review on recent progress, challenges and perspective of battery thermal management system," *Int J Heat Mass Transf*, vol. 167, p. 120834, 2021, doi: https://doi.org/10.1016/j.ijheatmasstransfer.2020.120834.

[102] F. Bahiraei, A. Fartaj, and G.-A. Nazri, "Electrochemical-thermal Modeling to Evaluate Active Thermal Management of a Lithium-ion Battery Module," *Electrochim Acta*, vol. 254, pp. 59–71, 2017, doi: https://doi.org/10.1016/j.electacta.2017.09.084.

[103] L. H. Saw, Y. Ye, A. A. O. Tay, W. T. Chong, S. H. Kuan, and M. C. Yew, "Computational fluid dynamic and thermal analysis of Lithium-ion battery pack with air cooling," *Appl Energy*, vol. 177, pp. 783–792, 2016, doi: https://doi.org/10.1016/j.apenergy.2016.05.122.

[104] T.-H. Tran, S. Harmand, B. Desmet, and S. Filangi, "Experimental investigation on the feasibility of heat pipe cooling for HEV/EV lithium-ion battery," *Appl Therm Eng*, vol. 63, no. 2, pp. 551–558, 2014, doi: https://doi.org/10.1016/j.applthermaleng.2013.11.048.

[105] Y. Ye, Y. Shi, L. H. Saw, and A. A. O. Tay, “Performance assessment and optimization of a heat pipe thermal management system for fast charging lithium ion battery packs,” *Int J Heat Mass Transf*, vol. 92, pp. 893–903, 2016, doi: https://doi.org/10.1016/j.ijheatmasstransfer.2015.09.052.

[106] J. Cen, Z. Li, and F. Jiang, “Experimental investigation on using the electric vehicle air conditioning system for lithium-ion battery thermal management,” *Energy for Sustainable Development*, vol. 45, pp. 88–95, 2018, doi: https://doi.org/10.1016/j.esd.2018.05.005.

[107] D. Dan, C. Yao, Y. Zhang, H. Zhang, Z. Zeng, and X. Xu, “Dynamic thermal behavior of micro heat pipe array-air cooling battery thermal management system based on thermal network model,” *Appl Therm Eng*, vol. 162, p. 114183, 2019, doi: https://doi.org/10.1016/j.applthermaleng.2019.114183.

[108] M. Lu, X. Zhang, J. Ji, X. Xu, and Y. Zhang, “Research progress on power battery cooling technology for electric vehicles,” *J Energy Storage*, vol. 27, p. 101155, 2020, doi: https://doi.org/10.1016/j.est.2019.101155.

[109] X. Peng, C. Ma, A. Garg, N. Bao, and X. Liao, “Thermal performance investigation of an air-cooled lithium-ion battery pack considering the inconsistency of battery cells,” *Appl Therm Eng*, vol. 153, pp. 596–603, 2019, doi: https://doi.org/10.1016/j.applthermaleng.2019.03.042.

[110] K. Yu, X. Yang, Y. Cheng, and C. Li, “Thermal analysis and two-directional air flow thermal management for lithium-ion battery pack,” *J Power Sources*, vol. 270, pp. 193–200, 2014, doi: https://doi.org/10.1016/j.jpowsour.2014.07.086.

[111] T. Wang, K. J. Tseng, J. Zhao, and Z. Wei, “Thermal investigation of lithium-ion battery module with different cell arrangement structures and forced air-cooling strategies,” *Appl Energy*, vol. 134, pp. 229–238, 2014, doi: https://doi.org/10.1016/j.apenergy.2014.08.013.

[112] H. Zhou, F. Zhou, Q. Zhang, Q. Wang, and Z. Song, “Thermal management of cylindrical lithium-ion battery based on a liquid cooling method with half-helical duct,” *Appl Therm Eng*, vol. 162, p. 114257, 2019, doi: https://doi.org/10.1016/j.applthermaleng.2019.114257.

[113] Y. Fan, Y. Bao, C. Ling, Y. Chu, X. Tan, and S. Yang, "Experimental study on the thermal management performance of air cooling for high energy density cylindrical lithium-ion batteries," *Appl Therm Eng*, vol. 155, pp. 96–109, 2019, doi: https://doi.org/10.1016/j.applthermaleng.2019.03.157.

[114] K. Chen, S. Wang, M. Song, and L. Chen, "Structure optimization of parallel air-cooled battery thermal management system," *Int J Heat Mass Transf*, vol. 111, pp. 943–952, 2017, doi: https://doi.org/10.1016/j.ijheatmasstransfer.2017.04.026.

[115] N. K. Gupta, A. K. Tiwari, and S. K. Ghosh, "Heat transfer mechanisms in heat pipes using nanofluids – A review," *Exp Therm Fluid Sci*, vol. 90, pp. 84–100, 2018, doi: https://doi.org/10.1016/j.expthermflusci.2017.08.013.

[116] M. Shafahi, V. Bianco, K. Vafai, and O. Manca, "An investigation of the thermal performance of cylindrical heat pipes using nanofluids," *Int J Heat Mass Transf*, vol. 53, no. 1, pp. 376–383, 2010, doi: https://doi.org/10.1016/j.ijheatmasstransfer.2009.09.019.

[117] R. Feng, P. Huang, Z. Tang, Y. He, and Z. Bai, "Experimental and numerical study on the cooling performance of heat pipe assisted composite phase change material-based battery thermal management system," *Energy Convers Manag*, vol. 272, p. 116359, 2022, doi: https://doi.org/10.1016/j.enconman.2022.116359.

[118] H. Behi, M. Ghanbarpour, and M. Behi, "Investigation of PCM-assisted heat pipe for electronic cooling," *Appl Therm Eng*, vol. 127, pp. 1132–1142, 2017, doi: https://doi.org/10.1016/j.applthermaleng.2017.08.109.

[119] T.-H. Tran, S. Harmand, B. Desmet, and S. Filangi, "Experimental investigation on the feasibility of heat pipe cooling for HEV/EV lithium-ion battery," *Appl Therm Eng*, vol. 63, no. 2, pp. 551–558, 2014, doi: https://doi.org/10.1016/j.applthermaleng.2013.11.048.

[120] Z. Rao, S. Wang, M. Wu, Z. Lin, and F. Li, "Experimental investigation on thermal management of electric vehicle battery with heat pipe," *Energy Convers Manag*, vol. 65, pp. 92–97, 2013, doi: https://doi.org/10.1016/j.enconman.2012.08.014.

[121] G. Burban, V. Ayel, A. Alexandre, P. Lagonotte, Y. Bertin, and C. Romestant, "Experimental investigation of a pulsating heat pipe for hybrid vehicle applications," *Appl Therm Eng*, vol. 50, no. 1, pp. 94–103, 2013, doi: https://doi.org/10.1016/j.applthermaleng.2012.05.037.

[122] N. K. Gupta, A. K. Tiwari, and S. K. Ghosh, “Heat transfer mechanisms in heat pipes using nanofluids – A review,” *Exp Therm Fluid Sci*, vol. 90, pp. 84–100, 2018, doi: https://doi.org/10.1016/j.expthermflusci.2017.08.013.

[123] M.-S. Wu, K. H. Liu, Y.-Y. Wang, and C.-C. Wan, “Heat dissipation design for lithium-ion batteries,” *J Power Sources*, vol. 109, no. 1, pp. 160–166, 2002, doi: https://doi.org/10.1016/S0378-7753(02)00048-4.

[124] H. Behi *et al.*, “Thermal management analysis using heat pipe in the high current discharging of lithium-ion battery in electric vehicles,” *J Energy Storage*, vol. 32, p. 101893, 2020, doi: https://doi.org/10.1016/j.est.2020.101893.

[125] D. Worwood *et al.*, “A new approach to the internal thermal management of cylindrical battery cells for automotive applications,” *J Power Sources*, vol. 346, pp. 151–166, 2017, doi: https://doi.org/10.1016/j.jpowsour.2017.02.023.

[126] K. Shah, C. McKee, D. Chalise, and A. Jain, “Experimental and numerical investigation of core cooling of Li-ion cells using heat pipes,” *Energy*, vol. 113, pp. 852–860, 2016, doi: https://doi.org/10.1016/j.energy.2016.07.076.

[127] Y. Gan, J. Wang, J. Liang, Z. Huang, and M. Hu, “Development of thermal equivalent circuit model of heat pipe-based thermal management system for a battery module with cylindrical cells,” *Appl Therm Eng*, vol. 164, p. 114523, 2020, doi: https://doi.org/10.1016/j.applthermaleng.2019.114523.

[128] H. Behi *et al.*, “A new concept of thermal management system in Li-ion battery using air cooling and heat pipe for electric vehicles,” *Appl Therm Eng*, vol. 174, p. 115280, 2020, doi: https://doi.org/10.1016/j.applthermaleng.2020.115280.

[129] W. Zhang, J. Qiu, X. Yin, and D. Wang, “A novel heat pipe assisted separation type battery thermal management system based on phase change material,” *Appl Therm Eng*, vol. 165, p. 114571, 2020, doi: https://doi.org/10.1016/j.applthermaleng.2019.114571.

[130] R. Zhao, J. Gu, and J. Liu, “An experimental study of heat pipe thermal management system with wet cooling method for lithium ion batteries,” *J Power Sources*, vol. 273, pp. 1089–1097, 2015, doi: https://doi.org/10.1016/j.jpowsour.2014.10.007.

[131] A. Pesaran, “Battery Thermal Management in EVs and HEVs: Issues and Solutions,” *Battery Man*, vol. 43, Apr. 2001.

[132] T. Heckenberg, *Li-ion battery cooling: more than just another cooling task*. Technical Press Day, 2009.

[133] A. Pesaran, "Battery Thermal Management in EVs and HEVs: Issues and Solutions," *Battery Man*, vol. 43, 2001.

[134] J. Warner, "Chapter 10 - Thermal Management," in *The Handbook of Lithium-Ion Battery Pack Design*, J. Warner, Ed., Amsterdam: Elsevier, 2015, pp. 115–130. doi: https://doi.org/10.1016/B978-0-12-801456-1.00010-5.

[135] Z. An, L. Jia, Y. Ding, C. Dang, and X. Li, "A review on lithium-ion power battery thermal management technologies and thermal safety," *Journal of Thermal Science*, vol. 26, no. 5, pp. 391–412, 2017, doi: 10.1007/s11630-017-0955-2.

[136] J. Liu, H. Chen, S. Huang, Y. Jiao, and M. Chen, "Recent Progress and Prospects in Liquid Cooling Thermal Management System for Lithium-Ion Batteries," *Batteries*, vol. 9, no. 8, 2023, doi: 10.3390/batteries9080400.

[137] Y. Deng *et al.*, "Effects of different coolants and cooling strategies on the cooling performance of the power lithium ion battery system: A review," *Appl Therm Eng*, vol. 142, pp. 10–29, 2018, doi: https://doi.org/10.1016/j.applthermaleng.2018.06.043.

[138] C. Liu *et al.*, "Phase Change Materials Application in Battery Thermal Management System: A Review," *Materials*, vol. 13, no. 20, 2020, doi: 10.3390/ma13204622.

[139] A. Wazeer, A. Das, C. Abeykoon, A. Sinha, and A. Karmakar, "Phase change materials for battery thermal management of electric and hybrid vehicles: A review," *Energy Nexus*, vol. 7, p. 100131, 2022, doi: https://doi.org/10.1016/j.nexus.2022.100131.

[140] Z. Ling *et al.*, "Review on thermal management systems using phase change materials for electronic components, Li-ion batteries and photovoltaic modules," *Renewable and Sustainable Energy Reviews*, vol. 31, pp. 427–438, 2014, doi: https://doi.org/10.1016/j.rser.2013.12.017.

[141] Z. Rao and S. Wang, "A review of power battery thermal energy management," *Renewable and Sustainable Energy Reviews*, vol. 15, no. 9, pp. 4554–4571, 2011, doi: https://doi.org/10.1016/j.rser.2011.07.096.

[142] V. H. Johnson, A. A. Pesaran, and T. Sack, “Temperature-Dependent Battery Models for High-Power Lithium-Ion Batteries,” 2001. [Online]. Available: https://api.semanticscholar.org/CorpusID:110111874

[143] W. He, G. Zhang, X. Zhang, J. Ji, G. Li, and X. Zhao, “Recent development and application of thermoelectric generator and cooler,” *Appl Energy*, vol. 143, pp. 1–25, 2015, doi: https://doi.org/10.1016/j.apenergy.2014.12.075.

[144] Y. Wang, H. Zhang, H. Hao, and H. Li, “Performance assessment and parametric study of a hybrid system consisting of an alkali metal thermoelectric converter and an absorption refrigerator,” *Energy Convers Manag*, vol. 188, pp. 346–353, 2019, doi: https://doi.org/10.1016/j.enconman.2019.03.064.

[145] H. H. Saber, S. A. AlShehri, and W. Maref, “Performance optimization of cascaded and non-cascaded thermoelectric devices for cooling computer chips,” *Energy Convers Manag*, vol. 191, pp. 174–192, 2019, doi: https://doi.org/10.1016/j.enconman.2019.04.028.

[146] M. Lu, X. Zhang, J. Ji, X. Xu, and Y. Zhang, “Research progress on power battery cooling technology for electric vehicles,” *J Energy Storage*, vol. 27, p. 101155, 2020, doi: https://doi.org/10.1016/j.est.2019.101155.

[147] B. Zohuri, *Heat pipe design and technology: Modern applications for practical thermal management, second edition*. 2016. doi: 10.1007/978-3-319-29841-2.

[148] G. M. Grover, T. P. Cotter, and G. F. Erickson, “Structures of Very High Thermal Conductance,” *J Appl Phys*, vol. 35, pp. 1990–1991, 1964, [Online]. Available: https://api.semanticscholar.org/CorpusID:121338942

[149] M. Mochizuki, T. Nguyen, K. Mashiko, S. Yuji, T. A. Nguyen, and V. Wuttijumnong, “A REVIEW OF HEAT PIPE APPLICATION INCLUDING NEW OPPORTUNITIES,” 2011. [Online]. Available: https://api.semanticscholar.org/CorpusID:55009637

[150] J. Bohdansky, C. A. Busse, and G. M. Grover, “THE USE OF A NEW HEAT REMOVAL SYSTEM IN SPACE THERMIONIC POWER SUPPLIES,” 1965. [Online]. Available: https://api.semanticscholar.org/CorpusID:107495499

[151] L. L. Vasiliev, “Heat pipes in modern heat exchangers,” *Appl Therm Eng*, vol. 25, no. 1, pp. 1–19, 2005, doi: https://doi.org/10.1016/j.applthermaleng.2003.12.004.

[152] Y. Ye, Y. Shi, L. H. Saw, and A. A. O. Tay, “Performance assessment and optimization of a heat pipe thermal management system for fast charging lithium ion battery packs,” *Int J Heat Mass Transf*, vol. 92, pp. 893–903, 2016, doi: https://doi.org/10.1016/j.ijheatmasstransfer.2015.09.052.

[153] Y. Ye, L. H. Saw, Y. Shi, and A. A. O. Tay, “Numerical analyses on optimizing a heat pipe thermal management system for lithium-ion batteries during fast charging,” *Appl Therm Eng*, vol. 86, pp. 281–291, 2015, doi: https://doi.org/10.1016/j.applthermaleng.2015.04.066.

[154] T.-H. Tran, S. Harmand, and B. Sahut, “Experimental investigation on heat pipe cooling for Hybrid Electric Vehicle and Electric Vehicle lithium-ion battery,” *J Power Sources*, vol. 265, pp. 262–272, 2014, doi: https://doi.org/10.1016/j.jpowsour.2014.04.130.

[155] H. Jouhara, A. Chauhan, T. Nannou, S. Almahmoud, B. Delpech, and L. C. Wrobel, “Heat pipe based systems - Advances and applications,” *Energy*, vol. 128, pp. 729–754, 2017, doi: https://doi.org/10.1016/j.energy.2017.04.028.

[156] B. Zohuri, *Heat Pipe Design and Technology*. Cham: Springer International Publishing, 2016. doi: 10.1007/978-3-319-29841-2.

[157] P. DUNN and D. A. REAY, “Introduction,” in *Heat Pipes (Third Edition)*, Third Edition., P. DUNN and D. A. REAY, Eds., Oxford: Pergamon, 1982, pp. 1–6. doi: https://doi.org/10.1016/B978-0-08-029355-4.50006-1.

[158] B. D. Marcus, “Theory and design of variable conductance heat pipes,” 1972. [Online]. Available: https://api.semanticscholar.org/CorpusID:106798219

[159] H. Behi *et al.*, “Heat pipe air-cooled thermal management system for lithium-ion batteries: High power applications,” *Appl Therm Eng*, vol. 183, p. 116240, 2021, doi: https://doi.org/10.1016/j.applthermaleng.2020.116240.

[160] J. Jose and T. Kumar Hotta, “A comprehensive review of heat pipe: Its types, incorporation techniques, methods of analysis and applications,” *Thermal Science and Engineering Progress*, vol. 42, p. 101860, 2023, doi: https://doi.org/10.1016/j.tsep.2023.101860.

[161] J. Warner, “Chapter 10 - Thermal Management,” in *The Handbook of Lithium-Ion Battery Pack Design*, J. Warner, Ed., Amsterdam: Elsevier, 2015, pp. 115–130. doi: https://doi.org/10.1016/B978-0-12-801456-1.00010-5.

[162] M. Bernagozzi, A. Georgoulas, N. Miché, and M. Marengo, “Heat pipes in battery thermal management systems for electric vehicles: A critical review,” *Appl Therm Eng*, vol. 219, p. 119495, 2023, doi: https://doi.org/10.1016/j.applthermaleng.2022.119495.

[163] V. Wickramaratne, “BATTERY THERMAL MANAGEMENT SYSTEM (Formula Student),” 2017. doi: 10.13140/RG.2.2.13379.71203.

[164] M. Singh and R. Jilte, “Development of experimental facility for testing battery thermal management system of electrical vehicles,” *Mater Today Proc*, vol. 72, pp. 1917–1924, 2023, doi: https://doi.org/10.1016/j.matpr.2022.10.154.

[165] B. S. A. W. L. I. P. HUAT, “THERMAL MANAGEMENT OF ELECTRIC VEHICLE BATTERY PACKS,” 2014.

[166] Z. Rao and S. Wang, “A review of power battery thermal energy management,” *Renewable and Sustainable Energy Reviews*, vol. 15, no. 9, pp. 4554–4571, 2011, doi: https://doi.org/10.1016/j.rser.2011.07.096.

[167] J. Jaguemont and J. Van Mierlo, “A comprehensive review of future thermal management systems for battery-electrified vehicles,” *J Energy Storage*, vol. 31, p. 101551, 2020, doi: https://doi.org/10.1016/j.est.2020.101551.

[168] G. Xia, L. Cao, and G. Bi, “A review on battery thermal management in electric vehicle application,” *J Power Sources*, vol. 367, pp. 90–105, 2017, doi: https://doi.org/10.1016/j.jpowsour.2017.09.046.

[169] J. Kim, J. Oh, and H. Lee, “Review on battery thermal management system for electric vehicles,” *Appl Therm Eng*, vol. 149, pp. 192–212, 2019, doi: https://doi.org/10.1016/j.applthermaleng.2018.12.020.

[170] Y.-C. Weng, H.-P. Cho, C.-C. Chang, and S.-L. Chen, “Heat pipe with PCM for electronic cooling,” *Appl Energy*, vol. 88, no. 5, pp. 1825–1833, 2011, doi: https://doi.org/10.1016/j.apenergy.2010.12.004.

[171] K. Shah, C. McKee, D. Chalise, and A. Jain, “Experimental and numerical investigation of core cooling of Li-ion cells using heat pipes,” *Energy*, vol. 113, pp. 852–860, 2016, doi: https://doi.org/10.1016/j.energy.2016.07.076.

[172] X. Yuan, A. Tang, C. Shan, Z. Liu, and J. Li, “Experimental investigation on thermal performance of a battery liquid cooling structure coupled with heat pipe,” *J Energy Storage*, vol. 32, p. 101984, 2020, doi: https://doi.org/10.1016/j.est.2020.101984.

[173] H. J. Strumpf, “Ceramic heat pipes for high-temperature heat recovery,” *Journal of Heat Recovery Systems*, vol. 2, no. 2, pp. 189–199, 1982, doi: https://doi.org/10.1016/0198-7593(82)90046-7.

[174] P. Ramadass, B. Haran, R. White, and B. N. Popov, “Capacity fade of Sony 18650 cells cycled at elevated temperatures: Part II. Capacity fade analysis,” *J Power Sources*, vol. 112, no. 2, pp. 614–620, 2002, doi: https://doi.org/10.1016/S0378-7753(02)00473-1.

[175] Y. Xuan, Y. Hong, and Q. Li, “Investigation on transient behaviors of flat plate heat pipes,” *Exp Therm Fluid Sci*, vol. 28, no. 2, pp. 249–255, 2004, doi: https://doi.org/10.1016/S0894-1777(03)00047-5.

[176] K. Amine, J. Liu, and I. Belharouak, “High-temperature storage and cycling of C-LiFePO4/graphite Li-ion cells,” *Electrochem commun*, vol. 7, no. 7, pp. 669–673, 2005, doi: https://doi.org/10.1016/j.elecom.2005.04.018.

[177] W. Kong, H. Li, X. Huang, and L. Chen, “Gas evolution behaviors for several cathode materials in lithium-ion batteries,” *J Power Sources*, vol. 142, no. 1, pp. 285–291, 2005, doi: https://doi.org/10.1016/j.jpowsour.2004.10.008.

[178] C. W. Robak, T. L. Bergman, and A. Faghri, “Enhancement of latent heat energy storage using embedded heat pipes,” *Int J Heat Mass Transf*, vol. 54, no. 15, pp. 3476–3484, 2011, doi: https://doi.org/10.1016/j.ijheatmasstransfer.2011.03.038.

[179] A. Greco, D. Cao, X. Jiang, and H. Yang, “A theoretical and computational study of lithium-ion battery thermal management for electric vehicles using heat pipes,” *J Power Sources*, vol. 257, pp. 344–355, 2014, doi: 10.1016/j.jpowsour.2014.02.004.

[180] R. Zhao, J. Gu, and J. Liu, “An experimental study of heat pipe thermal management system with wet cooling method for lithium ion batteries,” *J Power Sources*, vol. 273, pp. 1089–1097, 2015, doi: https://doi.org/10.1016/j.jpowsour.2014.10.007.

[181] W. Yuan, Z. Yan, Z. Tan, W. Chen, and Y. Tang, “Heat-pipe-based thermal management and temperature characteristics of Li-ion batteries,” *Can J Chem Eng*, vol. 94, 2016, doi: 10.1002/cjce.22566.

[182] N. Putra, B. Ariantara, and R. Pamungkas, “Experimental investigation on performance of lithium-ion battery thermal management system using flat plate loop heat pipe for electric vehicle application,” *Appl Therm Eng*, vol. 99, 2016, doi: 10.1016/j.applthermaleng.2016.01.123.

[183] K. Chen, S. Wang, M. Song, and L. Chen, “Configuration optimization of battery pack in parallel air-cooled battery thermal management system using an optimization strategy,” *Appl Therm Eng*, vol. 123, pp. 177–186, 2017, doi: https://doi.org/10.1016/j.applthermaleng.2017.05.060.

[184] J. Smith, R. Singh, M. Hinterberger, and M. Mochizuki, “Battery thermal management system for electric vehicle using heat pipes,” *International Journal of Thermal Sciences*, vol. 134, pp. 517–529, 2018, doi: 10.1016/j.ijthermalsci.2018.08.022.

[185] S. Hong, X. Zhang, K. Chen, and S. Wang, “Design of flow configuration for parallel air-cooled battery thermal management system with secondary vent,” *Int J Heat Mass Transf*, vol. 116, pp. 1204–1212, 2018, doi: 10.1016/j.ijheatmasstransfer.2017.09.092.

[186] J. Liang, Y. Gan, and Y. Li, “Investigation on the thermal performance of a battery thermal management system using heat pipe under different ambient temperatures,” *Energy Convers Manag*, vol. 155, pp. 1–9, 2018, doi: https://doi.org/10.1016/j.enconman.2017.10.063.

[187] M. Amin, B. Ariantara, N. Putra, A. Sandi, and N. Abdullah, “Thermal Management of Electric Vehicle Batteries Using Heat Pipe and Phase Change Materials,” *E3S Web of Conferences*, vol. 67, p. 3034, 2018, doi: 10.1051/e3sconf/20186703034.

[188] Z. Jiang and Z. Qu, “Lithium-ion battery thermal management using heat pipe and phase change material during discharge-charge cycle: A comprehensive numerical study,” *Appl Energy*, vol. 242, pp. 378–392, 2019, doi: 10.1016/j.apenergy.2019.03.043.

[189] A. Wei, J. Qu, H. Qiu, C. Wang, and G. Cao, “Heat transfer characteristics of plug-in oscillating heat pipe with binary-fluid mixtures for electric vehicle battery thermal

management," *Int J Heat Mass Transf*, vol. 135, pp. 746–760, 2019, doi: https://doi.org/10.1016/j.ijheatmasstransfer.2019.02.021.

[190] J. Wang, Y. Gan, J. Liang, M. Tan, and Y. Li, "Sensitivity analysis of factors influencing a heat pipe-based thermal management system for a battery module with cylindrical cells," *Appl Therm Eng*, vol. 151, pp. 475–485, 2019, doi: https://doi.org/10.1016/j.applthermaleng.2019.02.036.

[191] S. Lei, Y. Shi, and G. Chen, "Heat-pipe based spray-cooling thermal management system for lithium-ion battery: Experimental study and optimization," *Int J Heat Mass Transf*, vol. 163, p. 120494, 2020, doi: https://doi.org/10.1016/j.ijheatmasstransfer.2020.120494.

[192] M. Suresh Patil, J.-H. Seo, and M.-Y. Lee, "A novel dielectric fluid immersion cooling technology for Li-ion battery thermal management," *Energy Convers Manag*, vol. 229, p. 113715, 2021, doi: https://doi.org/10.1016/j.enconman.2020.113715.

[193] D. N. J. Vipul. M. P. Milan Vachhani Kalpak R. Sagar and H. B. Mehta, "Cooling hybrid/electric vehicle battery module: exploring the thermal potential of single evaporator Loop heat Pipe," *Energy Sources, Part A: Recovery, Utilization, and Environmental Effects*, vol. 46, no. 1, pp. 689–705, 2024, doi: 10.1080/15567036.2023.2289555.

[194] A. Burkitbay, D. Weragoda, F. Ciampa, K. H. Lo, and G. Tian, "A Numerical and Experimental Investigation on a Gravity-Assisted Heat-Pipe-Based Battery Thermal Management System for a Cylindrical Battery," *Batteries*, vol. 9, p. 456, May 2023, doi: 10.3390/batteries9090456.

[195] Q. G. Z. H. H. H. Shengshi Wang Tianshi Zhang and J. Yao, "Performance simulation of L-shaped heat pipe and air coupled cooling process for ternary lithium battery module," *Engineering Applications of Computational Fluid Mechanics*, vol. 18, no. 1, p. 2301058, 2024, doi: 10.1080/19942060.2023.2301058.

[196] S. Patil, P. Damle, P. Meshram, and N. Salunke, "Optimizing Thermal Management in Electric Battery Packs through Heat Pipe-Based Systems and Aluminum Sleeve Integration," *International Journal of Mechanical Engineering*, vol. 11, no. 8, pp. 122–133, Aug. 2024, doi: 10.14445/23488360/IJME-V11I8P114.

[197] F. Zhu, Y. Wang, Y. Xie, H. Chen, and Y. Zhang, “Analysis on battery thermal management system based on flat heat pipe at high discharging rate,” *Appl Therm Eng*, vol. 254, p. 123798, Oct. 2024, doi: 10.1016/j.applthermaleng.2024.123798.

[198] H. Lu, K. Kadirgama, and M. M. Noor, “Experimental Study on a Hybrid Battery Thermal Management System Combining Oscillating Heat Pipe and Liquid Cooling,” *Frontiers in Heat and Mass Transfer*, vol. 23, no. 1, pp. 299–324, 2025, doi: 10.32604/fhmt.2024.059871.

[199] S. Maalej, I. Saad, A. Hamdani, R. Cherif, R. Msaddek, and M. C. Zaghdoudi, “Electric Vehicle Battery Thermal Management Using Hybrid Heat Pipe-Cold Plate Cooling System,” *EPJ Web Conf*, vol. 330, p. 06010, Jun. 2025, doi: 10.1051/epjconf/202533006010.

[200] J. A. Sanguesa, V. Torres-Sanz, P. Garrido, F. J. Martinez, and J. M. Marquez-Barja, “A Review on Electric Vehicles: Technologies and Challenges,” *Smart Cities*, vol. 4, no. 1, pp. 372–404, 2021, doi: 10.3390/smartcities4010022.

[201] R. M. Salgado, F. Danzi, J. E. Oliveira, A. El-Azab, P. P. Camanho, and M. H. Braga, “The Latest Trends in Electric Vehicles Batteries,” *Molecules*, vol. 26, no. 11, 2021, doi: 10.3390/molecules26113188.

[202] N. Faezaa, S. Toha, N. Azubir, N. Ishak, M. K. Hassan, and B. S. Ksm Kader Ibrahim, “Simplified Heat Generation Model for Lithium ion battery used in Electric Vehicle,” *IOP Conf Ser Mater Sci Eng*, vol. 53, p. 12014, Jan. 2013, doi: 10.1088/1757-899X/53/1/012014.

[203] R. Moffat, “Uncertainty analysis,” 2020, pp. 45–80. doi: 10.1201/9781003067948-2.

[204] M. Al-Zareer, I. Dincer, and M. A. Rosen, “Performance assessment of a new hydrogen cooled prismatic battery pack arrangement for hydrogen hybrid electric vehicles,” *Energy Convers Manag*, vol. 173, pp. 303–319, 2018, doi: https://doi.org/10.1016/j.enconman.2018.07.072.

[205] J. Day, M. Traum, and S. Boetcher, “Laminar Natural Convection From Isothermal Vertical Cylinders: A Revisit to a Classical Subject,” in *Journal of Heat Transfer*, Aug. 2011. doi: 10.1115/AJTEC2011-44552.

[206] T. Cebeci, “Laminar-free-convective-heat transfer from the outer surface of a vertical slender circular cylinder,” 1974. [Online]. Available: https://api.semanticscholar.org/CorpusID:140140090

[207] E. M. Sparrow and J. L. Gregg, “Laminar-Free-Convection Heat Transfer From the Outer Surface of a Vertical Circular Cylinder,” *J Fluids Eng*, vol. 78, no. 8, pp. 1823–1828, Nov. 1956, doi: 10.1115/1.4014194.

[208] A. Žukauskas, “Heat Transfer from Tubes in Crossflow,” vol. 8, J. P. Hartnett and T. F. Irvine, Eds., in Advances in Heat Transfer, vol. 8. , Elsevier, 1972, pp. 93–160. doi: https://doi.org/10.1016/S0065-2717(08)70038-8.

[209] Y. Cengel, “Heat Transfer : A Practical Approach / Y.A. Çengel.,” Sep. 2003.

[210] S. Mathewson, “Experimental Measurements of LiFePO 4 Battery Thermal Characteristics,” 2014.

[211] S. W. Churchill and H. H. S. Chu, “Correlating equations for laminar and turbulent free convection from a horizontal cylinder,” *Int J Heat Mass Transf*, vol. 18, no. 9, pp. 1049–1053, 1975, doi: https://doi.org/10.1016/0017-9310(75)90222-7.

[212] P. Kosky, R. Balmer, W. Keat, and G. Wise, “Chapter 12 - Mechanical Engineering,” in *Exploring Engineering (Third Edition)*, Third Edition., P. Kosky, R. Balmer, W. Keat, and G. Wise, Eds., Boston: Academic Press, 2013, pp. 259–281. doi: https://doi.org/10.1016/B978-0-12-415891-7.00012-1.

Index

Appendix A: Discharge data tables: Free convection

Appendix Table 1-A: Temperature measurement in free convection at 1C discharge rate

Discharge time (in seconds)	Temperature (°C)												
	Cell 1	Cel l2	Cel l3	Cel l4	Cel l5	Cell 6	Cell 7	Cell 8	Cell 9	Cell 10	Cell 11	Cell 12	Ambient
120	30	30	30	30	30	30	30	30	30	30	30	30	29
240	31	31	30	31	31	31	31	31	31	30	31	30	29
360	31	31	31	31	31	32	31	31	31	31	31	31	29
480	32	32	32	32	32	32	32	32	32	31	31	31	29
600	32	32	33	32	32	33	33	32	32	32	32	32	29
720	33	33	33	32	33	33	33	33	32	32	32	32	29
840	33	33	34	33	33	34	34	33	33	33	33	33	29
960	34	34	34	33	34	35	36	34	34	33	33	33	29
1080	34	34	34	34	34	36	37	34	34	34	34	34	29
1200	35	35	35	34	35	37	38	35	35	34	34	34	29
1320	35	35	37	35	35	38	39	35	35	35	35	35	29
1440	36	36	37	35	36	39	39	36	36	35	35	35	29
1560	36	37	38	36	36	40	40	37	36	36	36	36	29
1680	37	38	39	37	37	41	41	38	37	37	37	37	29
1800	38	39	40	38	38	42	42	39	38	38	37	37	29
1920	39	40	41	39	39	43	43	40	39	39	38	38	29
2040	39	40	41	40	40	44	44	41	40	40	39	39	29
2160	40	41	42	41	41	45	45	42	41	41	40	40	29
2280	41	42	43	42	42	46	47	43	42	42	41	41	29
2400	42	43	44	43	43	48	48	44	43	43	42	42	29
2520	44	44	45	44	44	50	50	45	44	44	44	44	29
2640	46	46	46	46	46	52	52	46	46	46	46	46	29
2690	47	47	47	47	47	53	53	47	47	47	47	47	29

Appendix Table 2 -A: Temperature measurement in free convection at 2C discharge rate

Discharge time (in seconds)	Temperature (°C)												
	Cell 1	Cel l2	Cel l3	Cel l4	Cel l5	Cell 6	Cell 7	Cell 8	Cell 9	Cell 10	Cell 11	Cell 12	Ambient
120	30	30	30	30	30	31	30	30	30	30	30	30	29
240	31	31	31	31	31	32	32	31	32	31	31	31	29
360	33	33	33	32	32	33	33	32	33	32	32	32	29
480	34	34	34	34	33	35	34	33	34	33	33	33	29
600	35	35	36	35	34	37	36	34	35	34	34	34	29
720	37	37	38	36	36	39	38	35	36	37	36	36	29
840	39	39	39	38	38	42	41	38	38	39	39	38	29
960	42	42	41	41	40	45	44	40	40	41	41	41	29
1080	44	44	44	43	43	48	49	44	43	45	44	44	29
1200	47	46	47	46	46	52	52	46	46	47	47	47	29
1320	50	50	50	50	49	56	56	49	49	50	50	50	29
1340	51	52	51	52	51	58	57	51	51	51	51	51	29

Appendix Table 3 -A: Temperature measurement in free convection at 3C discharge rate

Discharge time (in seconds)	Temperature (°C)												
	Cell 1	Cel l2	Cell 3	Cell 4	Cell 5	Cell 6	Cell 7	Cell 8	Cell 9	Cell 10	Cell 11	Cell 12	Ambient
120	31	31	31	31	31	31	32	31	31	31	31	31	29
240	33	33	33	33	33	34	34	33	33	33	33	33	29
360	35	35	35	36	35	36	37	35	35	35	36	35	29
480	37	37	37	38	38	40	41	37	38	37	38	37	29
600	40	40	40	41	40	44	45	40	40	40	41	40	29
720	44	43	44	45	44	48	49	44	43	43	44	44	29
840	48	47	48	49	48	53	54	48	48	47	48	49	29
920	53	52	53	54	52	58	59	53	54	55	53	54	29

Appendix B: Discharge data tables: Forced convection

Appendix Table 4-B: Temperature measurement in forced convection at 1C discharge rate and 3.6 m/s air inlet velocity

Discharge time (in seconds)	Temperature (°C)													
	Cell 1	Cell 2	Cell 3	Cell 4	Cell 5	Cell 6	Cell 7	Cell 8	Cell 9	Cell 10	Cell 11	Cell 12	In-Air	Out-Air
120	30	30	30	30	30	30	30	30	30	31	31	30	29	29
240	30	30	30	30	30	30	30	30	31	31	31	31	29	29
360	30	30	30	30	31	30	31	31	31	32	32	31	29	29
480	31	31	31	31	31	31	32	32	32	33	32	32	29	30
600	31	31	31	32	31	32	32	32	33	33	33	33	29	30
720	31	31	31	32	32	33	33	33	34	34	34	34	29	31
840	32	31	32	32	33	33	33	33	34	34	34	34	29	31
960	32	32	32	32	33	34	33	33	35	35	35	35	29	31
1080	32	32	32	32	34	34	34	34	36	36	36	36	29	31
1200	33	33	33	32	34	34	34	34	36	37	37	36	29	31
1320	33	33	33	32	34	35	34	35	37	37	37	37	29	32
1440	33	33	34	33	35	36	35	36	37	38	38	38	29	32
1560	34	34	34	34	35	36	36	36	38	38	39	39	29	32
1680	34	34	34	34	36	37	36	37	39	39	39	40	29	32
1800	35	35	35	35	37	37	37	37	39	40	40	40	29	33
1920	35	35	35	35	37	38	37	37	40	40	40	41	29	33
2040	35	36	36	36	38	38	37	38	41	41	41	42	29	33
2160	36	36	36	36	38	38	38	38	41	42	42	42	29	33
2280	36	36	36	36	39	39	39	39	42	43	43	43	29	34
2400	37	37	37	37	39	39	39	39	43	44	43	43	29	34
2520	37	37	37	37	40	41	40	40	43	44	44	44	29	34
2640	38	38	38	38	42	42	42	42	44	45	45	45	29	35
2720	39	39	39	39	42	43	43	43	45	46	45	46	29	35

Appendix Table 5 -B: Temperature measurement in forced convection at 1C discharge rate and 4.6 m/s air inlet velocity

Discharge time (in seconds)	Temperature (°C)													
	Cell 1	Cell 2	Cell 3	Cell 4	Cell 5	Cell 6	Cell 7	Cell 8	Cell 9	Cell 10	Cell 11	Cell 12	In-Air	Out-Air
120	30	30	30	30	30	30	30	30	30	30	30	30	29	29
240	30	30	30	30	30	30	30	30	31	30	31	30	29	29
360	30	30	30	30	31	30	31	30	31	31	32	31	29	29
480	30	30	30	30	31	31	31	31	31	32	32	32	29	29
600	30	30	30	30	32	31	32	32	33	33	33	32	29	30
720	30	31	30	31	32	31	32	32	34	34	34	33	29	30
840	31	31	31	31	32	32	32	33	34	35	35	34	29	30
960	31	31	31	31	33	32	33	33	35	35	35	34	29	30
1080	32	32	32	31	33	32	33	33	35	35	35	35	29	30
1200	32	32	32	32	34	33	34	34	36	36	36	35	29	31
1320	32	32	32	32	34	34	34	34	36	36	36	36	29	31
1440	33	32	32	33	34	34	34	35	37	36	37	36	29	31
1560	33	33	33	33	34	34	34	35	38	37	38	37	29	31
1680	33	33	33	34	34	35	35	36	38	38	39	38	29	32
1800	34	34	34	34	35	35	36	36	39	39	40	38	29	32
1920	34	34	34	34	35	36	36	36	40	40	40	39	29	32
2040	35	35	35	35	36	36	37	37	40	41	41	40	29	32
2160	35	35	35	35	37	37	38	38	41	41	42	41	29	32
2280	35	36	35	35	37	37	38	38	41	42	42	42	29	33
2400	36	36	36	36	38	38	39	39	42	43	43	42	29	33
2520	36	36	36	36	39	39	40	40	43	43	43	43	29	33
2640	37	37	37	37	40	40	41	41	44	44	44	44	29	34
2720	38	38	38	38	41	41	42	42	46	46	45	45	29	34

Appendix Table 6-B: Temperature measurement in forced convection at 1C discharge rate and 5.5 m/s air inlet velocity

Discharge time (in seconds)	Temperature (°C)													
	Cell 1	Cell 2	Cell 3	Cell 4	Cell 5	Cell 6	Cell 7	Cell 8	Cell 9	Cell 10	Cell 11	Cell 12	In-Air	Out-Air
120	30	30	30	30	30	30	30	30	30	30	30	30	29	29
240	30	30	30	30	30	30	30	30	31	31	31	31	29	29
360	30	30	30	30	30	30	30	30	31	32	31	31	29	29
480	30	30	30	30	31	31	31	31	32	32	32	32	29	29
600	31	31	31	31	31	31	31	31	32	33	32	32	29	30
720	31	31	31	31	32	32	32	32	33	33	33	33	29	30
840	31	31	31	31	32	32	33	33	34	34	34	34	29	30
960	32	31	31	31	32	33	33	33	34	34	35	34	29	30
1080	32	32	31	32	33	33	34	33	34	34	35	35	29	30
1200	32	32	32	32	33	33	34	34	35	35	36	36	29	31
1320	32	32	32	32	33	33	35	34	36	36	36	37	29	31
1440	33	32	32	32	34	34	35	35	36	36	36	37	29	31
1560	33	33	33	33	34	34	36	35	37	37	37	38	29	31
1680	33	33	33	33	35	35	36	36	37	37	38	38	29	32
1800	34	34	33	33	35	35	37	36	38	38	39	39	29	32
1920	34	34	34	34	36	36	37	37	39	39	40	40	29	32
2040	35	34	34	34	36	36	38	37	39	39	41	41	29	32
2160	34	35	35	34	37	37	38	38	40	40	41	41	29	32
2280	35	35	35	35	37	37	39	38	41	41	42	42	29	33
2400	35	35	36	35	38	38	39	39	42	42	42	42	29	33
2520	36	36	36	36	39	38	40	39	43	43	43	43	29	33
2640	36	37	36	37	40	39	40	40	44	44	44	44	29	34
2770	37	37	37	37	41	40	41	41	45	45	45	45	29	34

Appendix Table 7 -B: Temperature measurement in forced convection at 2C discharge rate and 3.6 m/s air inlet velocity

Discharge time (in seconds)	Temperature (°C)													
	Cell 1	Cell 2	Cell 3	Cell 4	Cell 5	Cell 6	Cell 7	Cell 8	Cell 9	Cell 10	Cell 11	Cell 12	In-Air	Out-Air
120	31	31	31	31	31	31	31	32	31	32	31	32	29	30
240	31	31	31	31	32	32	32	32	33	33	32	33	29	30
360	32	32	32	32	33	34	33	34	35	34	35	34	29	31
480	34	34	34	35	35	35	35	35	37	37	37	37	29	32
600	35	35	35	35	36	36	37	37	39	39	39	39	29	33
720	36	37	36	37	37	37	38	38	41	41	41	41	29	33
840	38	38	38	38	38	38	39	39	43	42	43	43	29	34
960	39	39	39	39	40	40	41	41	45	45	45	44	29	34
1080	40	41	40	40	42	42	42	43	46	46	46	45	29	35
1200	41	42	41	41	42	42	43	44	48	47	48	47	29	35
1320	42	43	42	42	44	44	45	45	49	49	49	48	29	36
1440	44	44	44	44	45	45	46	45	51	51	50	49	29	36

Appendix Table 8 -B: Temperature measurement in forced convection at 2C discharge rate and 4.6 m/s air inlet velocity

Discharge time (in seconds)	Temperature (°C)													
	Cell 1	Cell 2	Cell 3	Cell 4	Cell 5	Cell 6	Cell 7	Cell 8	Cell 9	Cell 10	Cell 11	Cell 12	In-Air	Out-Air
120	30	30	30	31	30	30	31	30	31	31	31	31	29	30
240	31	31	31	31	31	31	31	31	32	33	32	32	29	30
360	32	32	32	32	33	33	33	33	34	35	34	34	29	31
480	33	33	33	33	35	34	35	35	36	36	36	36	29	32
600	34	34	34	34	36	36	36	36	38	38	38	38	29	33
720	35	35	36	35	37	37	38	38	39	40	40	40	29	33
840	36	36	37	36	38	38	39	39	41	42	42	42	29	34
960	38	38	38	37	39	39	40	40	43	43	43	43	29	34
1080	39	39	39	39	40	40	41	41	44	45	45	45	29	34
1200	40	40	40	40	41	41	41	42	46	46	46	47	29	34
1320	41	41	41	41	43	42	42	42	47	48	47	48	29	35
1440	42	42	42	42	44	43	43	43	48	49	48	49	29	35
1490	43	42	43	43	44	44	44	44	49	50	49	49	29	35

Appendix Table 9-B: Temperature measurement in forced convection at 2C discharge rate and 5.5 m/s air inlet velocity

Discharge time (in seconds)	Temperature (°C)													
	Cell 1	Cell 2	Cell 3	Cell 4	Cell 5	Cell 6	Cell 7	Cell 8	Cell 9	Cell 10	Cell 11	Cell 12	In-Air	Out-Air
120	30	30	30	30	31	30	30	30	31	31	31	31	29	30
240	30	31	30	31	31	31	31	31	32	32	32	32	29	30
360	31	32	31	31	32	32	32	32	34	33	33	34	29	31
480	31	32	32	32	33	34	33	33	35	34	34	35	29	32
600	32	33	32	33	34	35	35	34	37	36	36	37	29	32
720	33	35	34	34	36	36	36	36	38	37	37	38	29	33
840	34	36	36	35	37	38	37	38	40	39	39	39	29	34
960	35	37	37	36	39	39	38	39	42	42	42	40	29	34
1080	37	38	38	37	40	40	40	41	44	43	44	42	29	34
1200	38	39	39	39	41	41	41	42	45	44	45	44	29	35
1320	39	40	40	40	43	42	42	43	47	45	47	46	29	35
1440	40	41	41	41	44	43	43	44	48	47	48	47	29	36
1520	41	41	42	42	45	44	44	45	49	48	49	48	29	36

Appendix Table 10-B: Temperature measurement in forced convection at 3C discharge rate and 3.6 m/s air inlet velocity

Discharge time (in seconds)	Temperature (°C)													
	Cell 1	Cell 2	Cell 3	Cell 4	Cell 5	Cell 6	Cell 7	Cell 8	Cell 9	Cell 10	Cell 11	Cell 12	In-Air	Out-Air
120	31	31	31	31	31	31	31	32	32	32	32	32	29	30
240	33	33	33	33	33	33	33	34	34	34	34	34	29	31
360	34	35	35	35	35	35	35	36	37	37	36	36	29	32
480	36	36	37	37	37	37	37	38	40	40	39	39	29	33
600	38	38	39	39	39	39	39	40	42	42	42	42	29	34
720	40	40	41	41	41	41	41	42	45	45	45	45	29	35
840	42	42	43	43	44	43	44	44	48	49	48	48	29	36
960	44	44	44	44	47	46	46	47	51	52	52	52	29	37

Appendix Table １１-B: Temperature measurement in forced convection at 3C discharge rate and 4.6 m/s air inlet velocity

Discharge time (in seconds)	Temperature (°C)													
	Cell 1	Cell 2	Cell 3	Cell 4	Cell 5	Cell 6	Cell 7	Cell 8	Cell 9	Cell 10	Cell 11	Cell 12	In-Air	Out-Air
120	30	30	30	30	31	30	30	31	31	31	31	31	29	30
240	31	32	32	31	33	33	32	33	33	33	33	34	29	30
360	33	33	33	33	35	35	34	34	36	35	36	37	29	31
480	35	36	35	34	37	37	36	35	39	38	39	39	29	32
600	37	37	37	37	38	38	38	37	42	41	43	41	29	33
720	39	39	39	38	40	40	40	40	44	44	45	44	29	34
840	41	41	41	40	43	42	42	43	48	46	48	47	29	35
960	43	43	44	43	46	45	45	46	51	51	52	51	29	36

Appendix Table １２-B: Temperature measurement in forced convection at 3C discharge rate and 5.5 m/s air inlet velocity

Discharge time (in seconds)	Temperature (°C)													
	Cell 1	Cell 2	Cell 3	Cell 4	Cell 5	Cell 6	Cell 7	Cell 8	Cell 9	Cell 10	Cell 11	Cell 12	In-Air	Out-Air
120	30	30	30	30	31	30	31	31	31	31	31	31	29	29
240	31	31	31	31	32	32	32	32	33	33	33	34	29	30
360	33	32	32	33	33	34	34	34	35	35	36	36	29	31
480	35	34	33	34	35	36	36	36	38	38	39	39	29	32
600	37	36	35	36	37	38	38	38	41	41	42	42	29	33
720	39	38	37	38	39	40	40	40	44	44	45	45	29	34
840	41	40	40	40	42	42	42	43	47	47	48	48	29	35
960	44	42	43	43	45	46	45	46	51	51	51	51	29	36

Appendix C: Discharge data tables: Hybrid (Heat pipe and Forced convection)

Appendix Table １３-C: Temperature measurement in heat pipe assisted forced convection cooling at 1C discharge rate and 3.6 m/s air inlet velocity

Discharge time (in seconds)	Temperature (°C)												
	Cell 1	Cell 2	Cell 3	Cell 4	Cell 5	Cell 6	Cell 7	Cell 8	Cell 9	Cell 10	Cell 11	Cell 12	In-Air
120	30	29	29	29	30	30	30	30	30	30	30	30	29
240	30	30	30	30	30	30	30	30	31	30	30	31	29
360	30	30	30	30	31	30	31	30	31	31	30	31	29
480	31	30	30	30	31	31	31	30	31	31	31	31	29
600	31	31	31	31	31	31	31	31	32	32	31	32	29
720	31	31	31	31	32	32	32	32	32	32	32	32	29
840	32	32	32	32	32	32	32	32	32	33	33	33	29
960	32	32	32	32	33	33	33	32	33	33	33	33	29
1080	32	33	32	33	33	33	33	33	33	33	33	33	29
1200	33	33	33	33	33	34	33	33	34	34	34	34	29
1320	33	33	33	33	34	34	34	34	34	34	34	34	29
1440	33	34	34	33	34	34	34	34	35	34	34	35	29
1560	34	34	34	34	35	35	35	35	35	35	35	37	29
1680	34	34	34	34	35	36	35	35	36	37	36	36	29
1800	34	34	34	34	36	36	36	36	36	37	36	37	29
1920	34	35	35	34	36	36	36	36	37	37	37	37	29
2040	35	35	35	35	37	37	37	37	38	38	37	38	29
2160	36	36	36	36	37	37	37	37	38	39	38	39	29
2280	36	36	37	36	38	38	38	38	39	39	39	39	29
2400	37	36	37	37	38	39	38	39	39	40	39	40	29
2520	37	37	38	37	39	39	39	39	40	41	40	41	29
2640	38	38	38	38	39	40	39	40	41	42	41	42	29
2760	39	39	39	39	40	41	40	40	42	43	42	42	29
2780	39	39	39	39	41	41	41	41	42	43	42	43	29

Appendix Table １４-C: Temperature measurement in heat pipe assisted forced convection cooling at 1C discharge rate and 4.6 m/s air inlet velocity at 29°C ambient temperature

Discharge time (in seconds)	Temperature (°C)											
	Cell 1	Cell 2	Cell 3	Cell 4	Cell 5	Cell 6	Cell 7	Cell 8	Cell 9	Cell 10	Cell 11	Cell 12
120	29	30	29	30	29	30	30	29	30	29	30	30
240	30	30	30	30	30	30	30	30	30	31	30	30
360	30	31	30	31	30	31	31	30	31	31	31	31
480	31	31	31	31	31	31	31	31	31	31	32	31
600	31	31	31	31	31	31	32	31	32	32	32	32
720	31	31	31	31	31	32	32	32	32	32	32	32
840	32	32	32	32	32	32	32	32	32	33	32	32
960	32	32	32	32	32	32	33	33	33	33	32	33
1080	32	32	32	32	32	33	33	34	33	34	33	33
1200	32	32	33	33	33	33	33	34	34	34	33	34
1320	33	32	33	33	33	33	33	34	34	34	34	34
1440	33	32	33	33	33	34	34	35	35	35	34	35
1560	33	33	34	34	34	34	35	35	35	35	35	36
1680	34	33	34	34	34	35	35	36	36	36	35	36
1800	34	34	34	34	35	35	36	36	36	36	36	37
1920	34	34	35	34	35	36	36	37	37	37	36	37
2040	35	34	35	35	36	36	37	37	37	37	37	37
2160	35	35	36	35	36	37	37	38	38	38	38	38
2280	36	35	36	36	37	37	38	38	39	39	39	38
2400	36	36	37	36	38	38	39	39	39	39	39	40
2520	37	36	37	37	39	38	40	39	40	40	40	40
2640	37	37	38	37	40	39	40	40	41	41	41	41
2760	38	38	38	38	41	40	41	41	42	42	42	42
2810	38	38	38	38	41	40	41	41	42	42	42	42

Appendix Table １５-C: Temperature measurement in heat pipe assisted forced convection cooling at 1C discharge rate and 5.5 m/s air inlet velocity at 29°C ambient temperature

Discharge time (in seconds)	Temperature (°C)											
	Cell 1	Cell 2	Cell 3	Cell 4	Cell 5	Cell 6	Cell 7	Cell 8	Cell 9	Cell 10	Cell 11	Cell 12
120	29	29	29	29	29	29	29	29	29	29	29	29
240	30	30	30	30	30	30	30	30	30	30	30	30
360	30	30	30	30	30	30	31	30	30	31	31	31
480	31	31	30	31	31	31	31	31	31	31	31	31
600	31	31	31	31	31	31	32	31	31	32	32	32
720	31	31	31	31	31	31	32	32	32	32	32	32
840	32	31	31	32	32	32	32	32	32	33	33	32
960	32	32	31	32	32	32	33	32	33	33	33	33
1080	32	32	32	32	32	32	33	33	33	34	34	33
1200	33	32	32	33	33	33	33	33	34	34	34	34
1320	33	33	32	33	33	33	34	34	34	35	35	34
1440	33	33	32	33	33	33	34	34	35	35	35	35
1560	33	33	33	34	34	34	34	35	35	36	36	35
1680	34	33	33	34	34	34	35	35	36	36	36	36
1800	34	34	34	34	34	34	35	36	36	37	37	36
1920	34	34	34	34	35	35	36	36	37	37	37	37
2040	34	34	34	35	35	35	36	37	37	38	38	37
2160	35	35	34	35	36	36	37	37	38	38	38	38
2280	35	35	35	36	36	36	37	38	38	39	39	38
2400	35	36	36	36	37	37	38	38	39	39	39	39
2520	36	36	36	37	37	38	39	39	39	40	40	40
2640	37	37	37	37	38	39	40	39	40	40	41	40
2760	37	37	38	38	39	40	41	40	41	41	42	41
2810	38	37	38	38	39	40	41	40	42	42	42	41

Appendix Table １６-C: Temperature measurement in heat pipe assisted forced convection cooling at 2C discharge rate and 3.6 m/s air inlet velocity at 29°C ambient temperature

Discharge time (in seconds)	Temperature (°C)											
	Cell 1	Cell 2	Cell 3	Cell 4	Cell 5	Cell 6	Cell 7	Cell 8	Cell 9	Cell 10	Cell 11	Cell 12
120	30	30	30	30	30	30	30	30	31	30	31	30
240	31	31	31	31	31	31	31	31	32	31	32	31
360	32	32	32	32	32	32	32	32	32	32	33	32
480	33	33	33	33	33	33	33	33	34	34	34	34
600	34	34	34	34	34	34	34	34	35	36	36	36
720	35	35	35	35	35	35	35	35	36	38	38	37
840	36	36	36	36	36	36	36	36	38	39	39	39
960	37	37	37	37	37	38	37	38	40	40	40	40
1080	38	38	38	38	39	40	39	40	42	42	42	41
1200	39	39	39	39	41	41	41	42	43	43	43	43
1320	41	41	41	41	43	43	43	44	45	45	45	45
1440	43	42	42	42	45	45	45	46	47	47	46	47
1480	44	43	43	44	46	46	46	47	48	48	47	48

Appendix Table １７-C: Temperature measurement in heat pipe assisted forced convection cooling at 2C discharge rate and 4.6 m/s air inlet velocity at 29°C ambient temperature

Discharge time (in seconds)	Temperature (°C)											
	Cell 1	Cell 2	Cell 3	Cell 4	Cell 5	Cell 6	Cell 7	Cell 8	Cell 9	Cell 10	Cell 11	Cell 12
120	30	30	30	30	30	30	30	30	31	30	30	31
240	31	31	31	31	31	31	31	31	32	31	31	32
360	32	32	32	32	32	32	32	32	33	32	33	33
480	33	33	33	33	33	33	33	33	35	33	34	34
600	34	34	34	34	35	35	34	35	36	34	35	35
720	35	35	34	35	36	36	35	36	37	35	36	36
840	36	36	35	36	37	37	36	37	38	36	37	37
960	37	37	36	37	38	38	37	38	39	37	39	38
1080	38	38	37	38	39	39	38	39	40	39	41	40
1200	39	40	38	39	40	40	40	40	41	41	42	42
1320	40	41	40	40	41	42	42	41	43	43	43	44
1440	42	42	41	42	42	44	43	43	45	45	45	46
1480	43	43	42	43	44	45	44	45	47	47	46	47

Appendix Table １８-C: Temperature measurement in heat pipe assisted forced convection cooling at 2C discharge rate and 5.5 m/s air inlet velocity at 29°C ambient temperature

Discharge time (in seconds)	Temperature (°C)											
	Cell 1	Cell 2	Cell 3	Cell 4	Cell 5	Cell 6	Cell 7	Cell 8	Cell 9	Cell 10	Cell 11	Cell 12
120	30	30	30	30	30	30	30	30	31	30	30	31
240	31	31	31	31	31	31	31	31	32	31	31	32
360	32	32	32	32	32	32	32	32	33	32	33	33
480	33	33	33	33	33	33	33	33	35	33	34	34
600	34	34	34	34	35	35	34	35	36	34	35	35
720	35	35	34	35	36	36	35	36	37	35	36	36
840	36	36	35	36	37	37	36	37	38	36	37	37
960	37	37	36	37	38	38	37	38	39	37	39	38
1080	38	38	37	38	39	39	38	39	40	39	41	40
1200	39	40	38	39	40	40	40	40	41	41	42	42
1320	40	41	40	40	41	42	42	41	43	43	43	44
1440	42	42	41	42	42	44	43	43	45	45	45	46
1480	43	43	42	43	44	45	44	45	47	47	46	47

Appendix Table １９-C: Temperature measurement in heat pipe assisted forced convection cooling at 3C discharge rate and 3.6 m/s air inlet velocity at 29°C ambient temperature

Discharge time (in seconds)	Temperature (°C)											
	Cell 1	Cell 2	Cell 3	Cell 4	Cell 5	Cell 6	Cell 7	Cell 8	Cell 9	Cell 10	Cell 11	Cell 12
120	30	31	31	31	31	31	31	31	31	31	31	31
240	32	32	32	32	32	32	32	33	33	33	33	33
360	34	34	34	34	34	34	34	34	35	35	35	35
480	36	36	36	36	36	36	36	36	37	37	37	37
600	38	38	38	38	38	38	38	38	40	40	41	40
720	40	40	40	40	40	40	40	41	43	43	44	43
840	42	42	42	42	43	43	43	44	46	46	47	46
960	45	45	45	45	46	46	47	46	49	49	50	49

Appendix Table 20-C: Temperature measurement in heat pipe assisted forced convection cooling at 3C discharge rate and 4.6 m/s air inlet velocity at 29°C ambient temperature

Discharge time (in seconds)	Temperature (°C)											
	Cell 1	Cell 2	Cell 3	Cell 4	Cell 5	Cell 6	Cell 7	Cell 8	Cell 9	Cell 10	Cell 11	Cell 12
120	30	30	30	30	30	30	30	31	31	31	31	31
240	31	31	31	31	31	31	31	32	33	33	33	33
360	33	33	33	33	33	33	33	34	35	35	35	35
480	34	35	35	34	35	35	35	36	37	37	37	37
600	36	37	37	36	37	37	37	38	40	39	40	40
720	39	39	39	39	39	40	39	40	43	42	43	43
840	41	41	41	41	42	43	42	43	46	45	46	46
960	44	44	44	44	45	46	45	46	49	48	49	49

Appendix Table 21-C: Temperature measurement in heat pipe assisted forced convection cooling at 3C discharge rate and 5.5 m/s air inlet velocity at 29°C ambient temperature

Discharge time (in seconds)	Temperature (°C)											
	Cell 1	Cell 2	Cell 3	Cell 4	Cell 5	Cell 6	Cell 7	Cell 8	Cell 9	Cell 10	Cell 11	Cell 12
120	30	30	30	30	30	30	31	30	31	31	31	31
240	31	31	31	31	31	31	32	32	32	33	33	33
360	33	33	33	33	33	33	34	34	34	35	35	35
480	34	34	34	34	36	36	37	36	36	37	37	37
600	36	35	35	35	38	38	39	38	39	39	39	40
720	38	38	38	38	40	40	41	40	42	42	42	43
840	40	40	41	40	43	42	43	43	45	45	46	46
960	43	43	44	43	45	45	45	46	48	48	49	49

List of Publications

Sr. No.	Journal indexing	Status	Journal Name	Title of the Paper
1	Scopus	Published	Journal of Advanced Research in Fluid Mechanics and Thermal Sciences	Experimental Investigation of Temperature Homogeneity and Peak Temperature in a Battery Pack of Cylindrical Li-ion Cells Under Free and Forced Convection
2	Scopus	Accepted	Internation Journal of Renewable Energy Research (IJRER)	Experimental Investigation of Novel Thin Aluminum Flat Heat Pipe Assisted Battery Thermal Management System for Cylindrical Lithium-ion Battery of Electrical Vehicles

List of Conferences

Sr.No.	Status	Journal Name	Title of the Paper
1	Published	Materials Today Proceedings	Development of Experimental Facility for Testing Battery Thermal Management System of Electrical Vehicles
2	Presentation certificate	International conference on recent advances in energy and material for sustainable development (RAEM-2023)	Experimental Investigation of Temperature Homogeneity and Peak Temperature in a Battery Pack of Cylindrical Li-ion Cells Under Free and Forced Convection
3	Presentation certificate (Published in Materials Today Proceedings)	2nd International conference & exposition on advances in mechanical engineering	Development of Experimental Facility for Testing Battery Thermal Management System of Electrical Vehicles